

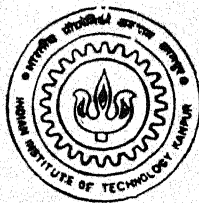
Entered
✓

08/05/65

MODELING OF MULTICOMPONENT FUEL DROPLET COMBUSTION

by

SNEHANSU MANDAL



DEPARTMENT OF MECHANICAL ENGINEERING
INDIAN INSTITUTE OF TECHNOLOGY KANPUR

MAY, 1995

TH
ME/1995/D
M 3/2m

ME

1995

D

MAN

MOD

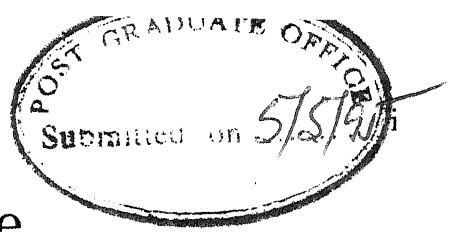
MODELING OF MULTICOMPONENT FUEL DROPLET COMBUSTION

*A Thesis Submitted
For The Partial Fulfilment
for the Degree of*
DOCTOR OF PHILOSOPHY

by
SNEHANSU MANDAL

to the
**DEPARTMENT OF MECHANICAL ENGINEERING
INDIAN INSTITUTE OF TECHNOLOGY KANPUR
MAY, 1995**

DEDICATED TO MY SPIRITUAL MASTER
HIS HOLINESS BHAKTI SWARUP DAMODAR SWAMI
AND
MY PARENTS



Certificate

It is to certify that the work contained in the thesis entitled " Modeling of Multicomponent Fuel Droplet Combustion ". by Snehansu Mandal has been carried out under my supervision and that this work has not been submitted elsewhere for a degree.

May, 1995

Keshav Kant
5.5.95

(Dr. Keshav Kant)

Associate Professor,

Department of Mechanical Engineering,

Indian Institute of Technology, Kanpur.

Acknowledgement

I am very much indebted to Dr. Keshav Kant for his inspiring and valuable guidance during the period of this work. I have learnt innumerable things from him which will help me in my future work. I also express my deep gratitude towards Dr. T. Sundararajan for his great help in modeling the present combustion problem. I am very much thankful to Dr. G. Biswas, Dr. P. N. Kaul and Dr. M. Prasad for their valuable suggestions. A number of discussions with Dr. Dipankar Sanyal helped me to clear my idea regarding combustion. His thesis has helped me a lot in preparing the manuscript for the present work. I am also thankful to Dr. V.C.V. Rao for his valuable help regarding the work on adaptive grid generation part. I express my deep feelings towards my parents. Without their inspiration this work could not have been finished. Timely help from Arun (C F D lab) helped me a lot to organise this thesis. So many discussions with Sita Nath at various stages helped me to put my work in proper shape and perspective. I am very much thankful to my friends, in particular, Mishraji, Japesh, Paritosh, Rupa Manohar, Debu, Santanu, Giri, Mama, Rangan, Manab and Sunu for giving me inspiration.

May, 1995

(Snehansu Mandal)

Synopsis

Combustion of fuel is a highly complex phenomena involving interactive heat, momentum and mass transfer processes both inside and outside each individual droplet. It becomes even more complex when the fuel is multicomponent by nature. An understanding of the combustion process is very much needed for it's wide industrial applications. The present study deals with the analysis of a laminar multicomponent single droplet fuel burning in a quiescent atmosphere. The spray is assumed to be very dilute so that a droplet is not influenced by the presence of the neighbouring droplets. The effect of radiation, sorret and Dufour effects are neglected. The properties of both gas and liquid phases are assumed to be constant in general. However, later on, for one of the cases variable specific heat for the gas phase was also considered. There is no internal circulation or flow in the liquid droplet due to the absence of any external flow. The Raoult's law and the Clausius-Clapeyron relations are used for coupling the liquid and gas phase concentrations at the liquid-vapour interface. Micro-explosion is neglected. The stationary coordinate system is transformed in such a way that the droplet surface is always maintained at $r=1$. This converts moving boundary problem into a fixed boundary problem. However, due to this transformation, a convective term appears in the liquid phase heat and mass transfer equations. At the droplet center, radially symmetric boundary conditions are applied for

both heat and mass transfer equations. At the droplet surface ($r=1$), the overall mass conservation relation, gas-side flux balance relation for each of the species, liquid-side flux balance relation for each fuel, heat flux balance relation and the Clausius-Clapeyron relation for phase equilibrium at interface are applied for both boundary conditions as well as for retrieving the coupling parameters. The far boundary conditions for the solution domain are assumed to be at far stream conditions. The gas phase properties are assumed to be same as those of free stream conditions. The study is carried out in two parts.

In the first part, semi-analytical solution has been developed for the spherico-symmetric burning of binary fuel droplets. The gas phase is assumed to be quasi-steady. Thin flame combustion, unit Lewis number (for all gas species) are taken to be valid. For rendering the liquid phase equations to be solved semi-analytically, the convective term, which appears in the liquid phase transport equations due to the coordinate transformation and which takes into account the surface regression rate, is neglected. The highly non-linear reaction term is eliminated by using Schvab-Zeldovich variables and then the quasi-steady gas phase equations are solved analytically for $1 < r < r_f$ and $r_f < r < r_\infty$. Liquid phase transient energy and species equations are solved in infinite series form using 100 terms. The liquid phase and the gas phase equations are solved in a sequential manner through an iterative scheme. The liquid phase transient equations are solved analytically

in space and numerically in time direction. Thus, the name 'semi-analytical' appears. The semi-analytical solution is compared with the finite difference solution of the same governing differential equations and excellent agreement (upto 4 places of decimals) is observed between them. It was found that the semi-analytical solution was about 10 times faster than the numerical solution. For the finite difference procedure, using a uniform mesh size, it had become necessary to use atleast a mesh size of $1/1000$ within the droplet for achieving a good match with the analytical results. Ignition and extinction can not be analysed by this model.

Results are presented for combinations of n-heptane, n-octane and dodecane fuels. While presenting the results, certain salient features are highlighted. The time history of mass-fraction and temperature profiles of heptane-dodecane droplet for the liquid phase are presented. Transient variation of the important surface parameters such as mass-gasification rate, surface temperature, square of the diameter, fractional mass-gasification rate etc. are also looked into. These results show the existence of two $d^2 - law$ periods as shown by experiments. A transition zone exists between the two $d^2 - law$ periods. An initial transition also exists. This initial transient and the intermediate transition zone are characterised by vigorous droplet heating which can not be neglected. The effect of initial mass-fraction combination and volatility differential on the transient nature of multicomponent fuel burning is also presented. As the initial mass-fraction of the more volatile fuel is

gradually increased, the first $d^2 - law$ period becomes more prominent and the second $d^2 - law$ period gradually decreases. As the volatility differential between the two fuels is increased progressively, the transition zone becomes sharper, and the difference of the two $d^2 - law$ periods becomes progressively more distinct.

In the second part, full transient heat and mass transfer equations for both gas and liquid phases are solved numerically. Finite rate flame chemistry is used to analyse the nature of the flame. In addition to this, dissociation of products at high temperature near the flame zone is also included. Finite difference method is used to solve the liquid phase equations by implicit scheme in the time direction. Galerkin Weighted Residual Method is used to discretize the gas phase transport equations. Both liquid and gas phase discretized equations are solved by TDM algorithm. The gas phase solution for the present combustion system contains regions in which variables exhibit high spatial activity resulting in sharp peaks. For such cases, these high activity regions need to be resolved adaptively for ensuring efficient solution to the problem. Therefore, an adaptive grid generation technique is used. It is effected statistically by equidistributing a positive weight function in such a way that the local discretization errors are minimized. Both the gas and liquid phases are solved iteratively in time direction to trace out the entire burning history of the droplet. The present model can analyse both the transient phenomena namely ignition and extinction in detail with high

efficiency.

The coupling parameters for the liquid and the gas phases are the evaporation velocity (u_d), heat flux rate coming from the gas phase to liquid phase (H_l) and the fractional mass gasification rate (ϵ_i). Initially, these parameters are guessed. Based on these guess values, both liquid and gas phase solutions are obtained, from which new values of the coupling parameters are obtained and checked for convergence.

Initially, at a given time, a coarse grid is chosen as a guess, and for this guess, a unique solution for the entire domain is reached by iteration. Then based on the solution obtained, total discretization error is checked against global tolerance limit. If it exceeds the latter, fresh grid is adapted according to the local error distributions. This loop, for a given time, is repeated until the optimum grid distribution is reached. Thus the solution proceeds in time direction. The adaptive grid algorithm is tested against a known analytical solution. It showed excellent agreement.

In this part of the thesis, a full numerical model is developed for the case of a transient multicomponent single droplet burning in an otherwise quiescent atmosphere. An adaptive grid generation technique is used based on the equidistribution of a positive weight function such that the local discretization error is minimised. This adaptive grid generation technique helps to record accurately the flame structure as well as the position and movement of the flame. This study gives a critical analysis of how a diffusion flame

around the liquid droplet develops during the ignition period, how it moves away from the droplet, how it moves towards the droplet and finally, how it is extinguished. The study reveals that the flame zone is initially established very near the droplet surface and then as the chemical reaction gathers momentum, the flame temperature rises very fast and almost instantaneously reaches it's peak temperature. Simultaneously, the flame moves and at the same time expands towards the droplet surface in search of fuel vapour for sustaining the enhanced chemical reaction at the flame. As the flame moves and expands towards the droplet surface, the temperature gradient at the surface becomes very high as a result of which the droplet surface is heated up very fast and the surface temperature approaches the boiling point of the more volatile fuel. So, the fuel starts evaporating vigorously. For this high evaporation rate, the flame starts moving away from the droplet surface due to fuel vapour accumulation. But as the burning proceeds, the droplet volume becomes progressively smaller for which the overall mass-gasification rate gradually falls. Therefore, fuel vapour accumulation between the droplet surface and the flame becomes progressively lesser. So, the flame then becomes steady maintaining a fixed distance from the droplet centre. Finally, towards the end of burning, the flame moves back towards the droplet surface almost instantaneously.

The flame exists till the droplet becomes very small. The total burning time for a heptane-hexadecane droplet for 0.9-0.1 initial mass fraction combination is about 0.0658048 s. Ignition becomes complete within 0.003s and extinction takes about 260 μ s. Results show that the pre-ignition period, initial transient (ignition period), first $d^2 - law$ period, 2nd transient (transition), second $d^2 - law$ period and extinction cover approximately 2.28 %, 2.28 %, 35.6 %, 19.5 %, 40 % and 0.36 % respectively of the total burning time. This study brings out the two $d^2 - law$ periods quite explicitly. The multicomponent feature of burning is predominant when the volatility differential of the two components is high, and also, when the initial liquid side mass fraction of the more volatile fuel is around 0.9. Results show that the flame is not thick. Comparison shows that the surface regression rate is neither too high nor too low. Therefore, we can neither neglect the effect of surface regression, nor can we assume the batch distillation model to be valid. Gas phase dissociation, taking gas phase specific heat to be variable and fuel vapour accumulation are all important considerations and they should not be ignored. Through parametric study of important parameters such as \hat{D} , D , \hat{C}_p , C_p , it is found that the total burning time as well as other burning characteristics are very much sensitive to the property values being used. Comparison of the quasi-steady model proposed in this thesis, it is observed that the quasi-steady assumption of the gas phase is quite reasonable barring the initial transient and the final extinction. The present theoretical

results shows very good agreement with the experimental results available in literature for heptane fuel burning under zero gravity condition with normal ambient conditions. The comparison with the experimental results available for the burning of heptane-hexadecane fuel with 0.7-0.3 initial liquid side mass fraction combination, the agreement is quite satisfactory considering the fact that the present model deals with spherically symmetric combustion whereas, experiments were performed on freely falling droplets under natural convection conditions. These experiments show three periods, the two periods correspond to the preferential gasification of the two fuels and the third period corresponds to the short sudden intermediate transition in between during which vigorous droplet heating takes place. The present model also exhibits three dominant zones, two d^2 - law periods separated by a transition zone which exhibit a gradual change. The present model does not include the effect of thermal expansion for the liquid phase which may cause this deviation between the theoretical and experimental results.

Contents

1	Introduction	1
1.1	Preface	2
1.2	Literature Survey	4
1.2.1	Single Component Fuel	5
1.2.2	Multicomponent Fuel	18
1.2.3	Adaptive Grid Generation	22
1.3	Scope of Present Study	24
2	General Formulation For Multicomponent Combustion	26
2.1	Introduction	27
2.2	Liquid Phase and Gas Phase Transport	27
2.3	Derivation of General Conservation Equations	30
2.3.1	Species Conservation Equations	30
2.3.2	Overall Mass Conservation Equations	32
2.3.3	Momentum Conservation Equations	32
2.3.4	Energy Conservation Equations	34

2.4	Modeling for Multicomponent Fuel Droplet Combustion	37
2.4.1	Liquid Phase	37
2.4.2	Gas Phase	38
2.4.3	Boundary Conditions	40
2.4.4	Initial Conditions	45
2.4.5	Non-dimensionalization	46
2.5	Thermo-chemistry	49
2.5.1	Heat of Reaction	49
2.5.2	Chemical Kinetics	50
2.5.3	Dissociation Reactions	52
2.6	Closure	53
3	Semi Analytical Solution	54
3.1	Introduction	55
3.2	Mathematical Formulation	56
3.3	Analytical Solutions	62
3.3.1	Gas-Phase	62
3.3.2	Liquid-Phase	64
3.4	Numerical Evaluation	69
3.5	Results and Discussions	70
3.5.1	Transient Features of Multicomponent Combustion . .	70
3.5.2	Effects of Volatility Differential	75
3.5.3	Effects of Initial Mass Fraction	79

3.5.4	Comparison with Earlier Work	79
3.6	Conclusions	79
4	Numerical Solution Using Adaptive Grid Generation	81
4.1	Introduction	82
4.2	Liquid Phase Transport Equations	83
4.3	Gas Phase Transport Equations	83
4.4	Boundary and Initial Conditions	84
4.5	Calculation of Heat of Reaction	86
4.6	Finite Difference Method of Solution for Liquid phase	88
4.6.1	Domain Discretization	88
4.6.2	Algebraic Equations	89
4.6.3	Discretization of Boundary Conditions	91
4.7	Finite Element Method of Solution for Gas Phase	94
4.7.1	Domain Discretization	94
4.7.2	Finite Element Formulation for the Gas Phase	95
4.8	Iterative Scheme for the entire Solution Procedure	100
4.9	Processing of Parameters after each Time-step	101
4.10	Adaptive Grid Generation	104
4.10.1	Introduction	104
4.10.2	Formulation for Adaptive Grid Generation	104
4.10.3	Testing of Adaptive Grid Algorithm	106
4.10.4	Results of the Test Problem	109

4.11 Closure	113
5 Results and Discussions	114
5.1 Introduction	115
5.2 Surface Parameters	115
5.3 Liquid-Side Mass-Fraction and Temperature Profiles	122
5.4 Gas-Side Mass-Fraction and Temperature Profiles	127
5.5 Effect of Initial Mass-fraction Variation on Surface Parameters	134
5.6 Effect of Volatility-Differential on Burning Characteristics . .	139
5.7 Comparison of Analytical Models	144
5.8 Gas Phase Dissociation	149
5.9 Effect of Ambient Temperature	153
5.10 Variable Specific Heat for the Gas Phase	157
5.11 Gas Side Diffusion Coefficient	161
5.12 Liquid Side Diffusion Coefficient	163
5.13 Comparison with the Semi Analytical Model	167
5.14 Comparison with Earlier Work	169
5.15 Conclusions	177
5.16 Recommendation of Further Study	180
5.17 Contribution to Knowledge	180
Reference	182

List of Figures

2.1	Flow configuration for spherically symmetric droplet combustion	28
3.1	Time history of liquid side mass fraction and temperature profiles	71
3.2	Transient variation of surface temperature, evaporation velocity, volumetric mass gasification rate, surface mass fraction and fractional mass gasification rate	73
3.3	Effect of volatility differential on the transient variations of square of the diameter, surface temperature, fractional mass gasification rate, volumetric mass gasification rate and surface mass fraction	77
3.4	Effect of initial mass fraction on the transient variations of square of the diameter, surface temperature, fractional mass gasification rate, volumetric mass gasification rate and surface mass fraction	80
3.5	Comparison of predicted surface mass fraction of Shaw, 1990 and of normalised burning rate with earlier work of Law and Law, 1982	80

4.1	Flow chart for the overall numerical scheme	102
4.2	Flow chart for adaptive grid generation	107
4.3	Evolution of grids at a given time starting with only two elements	110
4.4	Evolution of grids at a given time starting with only thirty elements	111
4.5	Evolution of grids at different times	112
5.1	Transient variation of different surface parameters for heptane- hexadecane fuel burningi with $\hat{Y}_{in,f1} = 0.9$	121
5.2	Time history of mass-fraction profiles for heptane inside the fuel droplet for heptane-hexadecane burningi with $\hat{Y}_{in,f1} = 0.9$.	125
5.3	Time history of liquid side temperature profiles for heptane inside the fuel droplet for heptane-hexadecane burningi with $\hat{Y}_{in,f1} = 0.9$	126
5.4	Evolution of gas side temperature profiles and transient vari- ation of flame position and flame stand-off-ratio for heptane- hexadecane burningi with $\hat{Y}_{in,f1} = 0.9$	131
5.5	Evolution of gas-phase mass-fraction profiles for heptane and oxidiser for heptane-hexadecane burningi with $\hat{Y}_{in,f1} = 0.9$. . .	132
5.6	Evolution of gas-phase mass-fraction profiles for hexadecane and oxidiser for heptane-hexadecane burningi with $\hat{Y}_{in,f1} = 0.9$	133

5.7	Effect of initial mass-fraction on the transient variation of surface temperature, vol. mass gasification rate, droplet heating and heat available for evaporation	136
5.8	Effect of initial mass-fraction on the transient variation of liquid and gas phase surface mass-fractions of heptane, gas phase surface mass-fraction of dodecane and fractional mass gasification rate of heptane	137
5.9	Effect of initial mass-fraction on the transient variation of flame position, flame stand-off-ratio and square of the diameter	138
5.10	Effect of volatility-differential on the transient variation of surface temperature, vol. mass gasification rate and droplet heating	141
5.11	Effect of volatility-differential on the transient variation of liquid and gas phase surface mass-fractions of heptane, gas phase surface mass-fraction of dodecane and fractional mass gasification rate of heptane	142
5.12	Effect of volatility-differential on the transient variation of flame position, flame stand-off-ratio and square of the diameter	143
5.13	Comparison among the quasi steady model (i), the model which neglects the effect of surface regression (ii) and the present numerical model (iii) for liquid and gas phase surface mass-fractions of heptane, fractional mass gasification rate of heptane and gas phase surface mass-fraction of dodecane . . .	146

5.14 Comparison among the quasi steady model (i), the model which neglects the effect of surface regression (ii) and the present numerical model (iii) for droplet heating, surface temperature, dsquare of the diameter and vol. mass gasification rate	147
5.15 Comparison among the quasi steady model (i), the model which neglects the effect of surface regression (ii) and the present numerical model (iii) for flame position and flame stand-off-ratio	148
5.16 Effect of gas phase dissociation on the transient variation of flame temperature, flame position and flame stand-off-ratio . .	150
5.17 Effect of gas phase dissociation on the transient variation of droplet heating, heat available for evaporation, surface temperature, vol. mass gasification rate and square of the diameter	151
5.18 Effect of gas phase dissociation on the transient variation of liquid and gas phase surface mass-fractions of heptane, fractional mass gasification rate of heptane and gas phase surface mass-fraction of dodecane	152
5.19 Effect of ambient temperature on the transient variation of flame temperature, droplet heating, surface temperature, vol. mass gasification rate and square of the diameter	155

5.20	Effect of ambient temperature on the transient variation of liquid and gas phase surface mass-fractions of heptane, fractional mass gasification rate of heptane and gas phase surface mass-fraction of dodecane	156
5.21	Effect of variable specific heat as well as different values of constant specific heat on the transient variation of flame temperature, heat coming from the gas phase, droplet heating and heat available for evaporation	158
5.22	Effect of variable specific heat as well as different values of constant specific heat on the transient variation of surface temperature, vol. mass gasification rate, flame position, flame stand-off-ratio, liquid phase surface mass-fractions of heptane, and square of the diameter	160
5.23	Effect of gas phase mass diffusion coefficient on the transient variation of liquid phase surface mass-fractions of heptane, surface temperature, droplet heating, heat available for evaporation and square of the diameter	162
5.24	Effect of liquid side mass diffusion coefficient on the transient variation of square of the diameter, liquid phase surface mass-fractions of heptane, fractional mass gasification rate of heptane, surface temperature	164

5.25	Effect of liquid side mass diffusion coefficient on the transient variation of droplet heating, heat available for evaporation, vol. mass gasification rate, flame position, and flame stand-off-ratio	165
5.26	Time history of liquid side mass-fraction profiles for heptane	166
5.27	Comparison of the semi-analytical model with two cases of the numerical model where for one case, the effect of surface regression is neglected and for the other case, the effect of surface regression is considered	168
5.28	Comparison of the present model with the experimental results of Okazima and Kumagai (1975) and Wang et al. (1984) for the burning of heptane fuel	168
5.29	Comparison with the experimental work of Okazima and Kumagai (1975) for	172
5.30	Comparison with the experimental results of Wang et al. (1984) for heptane-hexadecane fuel burning with 0.7-0.3 initial mass-fraction combination	174

List of Tables

3.1	variation of flame stand off ratio with time	74
-----	--	----

List of Symbols

Symbols

C_p	specific heat at constant pressure;
D	coefficient of binary diffusion;
E	activation energy; elemental error;
G	group combustion number;
G_1	Schvab Zeldovich variable;
G_2	Schvab Zeldovich variable;
H	Schvab Zeldovich variable; heat flux;
\underline{I}	unit vector;
K	Arrhenius rate constant; equilibrium rate constant for a given reaction;
L	latent heat evaporation of fuel;
Le	Lewis number;
M	molecular weight; number of reacting species as in eqn. 2.75; specification of chemical species;
N	linear shape functions; number of elements; number of chemical species;
P	pressure;
Pr	Prandtle number;
\dot{Q}	rate of heat generation;
R	weighted residue integrated over a given domain;
R_u	universal gas constant;
Re	Reynolds number;
Sc	Schmidt number;
T	temperature;
V	voumetric mass gasification rate;
\underline{V}	diffusion velocity;

W	molecular weight;
X	mole fraction;
Y	mass fraction;
$-\Delta h$	heat of reaction;
d	droplet diameter;
e	specific internal energy;
	ratio of maximum grid length to minimum grid length;
	element number;
\underline{f}	body force;
\underline{g}	gravitational force;
g_{mass}	global mass matrix;
g_{con}	global conductivity matrix;
g_{gen}	global generation vector;
h	specific enthalpy;
h^0	heat of formation at the reference temperature T^0 ;
\underline{j}	mass diffusive flux;
\dot{m}	mass flux;
\underline{n}	species flux;
\underline{q}	heat flux due to conduction;
r	spherical radial coordinate;
	droplet radius;
	flame position;
t	time;
u_d	evaporation velocity;
\hat{u}_d	droplet radius regression rate;
\underline{v}	mass average velocity;
v	volume;
x	x-direction;
y	y-direction;
z	z-direction;
ρ	density;

$\dot{\omega}$	rate of generation of species i;
η	coefficient of dynamic viscosity;
σ	standard deviation;
$\underline{\underline{\sigma}}$	stress tensor;
α	factor used in equation 2.76;
	thermal diffusion coefficient;
	scaling constant for mass fraction;
ϵ	fractional mass gasification rate;
ν	stoichiometric coefficients;
	order of reaction;
ξ	local coordinate;
θ	polar angle;
ϕ	azimuthal angle;
δ	exponent to be used in radial step size variation;
λ	conductivity;
μ	mean;

Subscripts

b	boiling point;
d	droplet;
e	element;
ev	evaporation;
f	flame;
f1	fuel1;
f2	fuel2;
g	gas phase;
i	species;
in	initial condition;
m	used to denote x-direction;
max	maximum value;
min	minimum value;

n	normal; used to denote y-direction;
l	used to denote z-direction; liquid;
p	product;
r	radial direction;
s	surface;
T	temperature;
x	x-direction; oxidiser;
y	y-direction;
z	z-direction;
θ	polar direction;
ϕ	azimuthal direction;
∞	at infinity;

Superscripts

0	pure state;
/	for reactants;
//	for products; non-dimensional;
e	element;
K	reference for time step;

Diacriticals

^	liquid side;
-	approximate numerical solution

Chapter 1

Introduction

1.1 Preface

Combustion has become very important and relevant to the present day civilization, specially when, the rate of energy consumption is growing alarmingly, day by day, due to progressive technological development. The modern day society can not survive even for a moment without energy. Life has become very fast. In order to meet this extremely high demand, a progressively large variety of fuels are being used. So far, fossil fuels namely coal and petroleum have been used extensively, but because of relatively easy handling and transportation, the use of the latter i.e. petroleum has been on the increase. Therefore, research on gasification, finite rate flame chemistry, flame-movement tracking, dynamics of liquid and gas phases, dissociation due to high temperature of fuel droplets etc. have become very important as far as both practical and fundamental research in energy and combustion science is concerned. These studies have lead to modelling of practical combustion situations, and their verification with experiments which have revealed various burning characteristics. Desired objectives in the combustion research have been to establish design criteria for efficient and stable combustors, determine the heat transfer rates to combustion chamber surfaces and examine the formation of pollutants such as soot, unburnt hydrocarbons, oxides of nitrogen and carbon. While many studies are purely experimental, an underlying theme has always been to develop predictive models for spray combustion processes in order to reduce the cost of development by cut and try methods.

Fundamentally, droplet combustion involves chemically reacting multicomponent two-phase flows with phase change. It involves complex physical and chemical phenomena, such as, heat, mass and momentum transfer processes in gas and liquid phases and their coupling at the interface. Kinetic effects are also important, specially, for critical phenomena such as ignition and extinction. In typical combustors, it is found that the gas temperatures are rather high and the gas is far from a fuel-vapor-saturated state so that regression rates of the liquid-gas interface are high.

The fuels are sprayed into the combustion chamber through the injectors. Injectors are

classified into two major categories (Faeth,1977): (1) pressure atomization, where only the liquid passes through the injector; and (2) twin fluid injection, where atomization of the liquid is accelerated by flow of a high velocity gas through the injector passage.

Injectors take care that drop sizes are properly distributed. It's properties are characterised by the angle of spray and by it's ability to produce spray structures with full cones and hollow cones.

In pressure atomization, the atomization is achieved through pressure drop in an orifice and in twin fluid injection system, one fluid is blasted through another. There are many steps in between leading to the final atomization. They are break-up of primary jet, break-up of secondary droplet and collision between droplets. These sequences lead to an evolving distribution of drop sizes and velocities which are normally measured some distance away from the injector. Spray characterization is generally carried out under cold conditions, but there are factors that influence this characterization. Thus, exact description of the velocity, shape and size of the fully atomized droplets become very difficult to estimate and we must be satisfied with average spray characteristics(Mellor et al., 1970).

The fuels may be either mixed with or kept separate from the oxidiser before it is injected into the combustion chamber. When they are thoroughly mixed before being injected, the resulting flame is known as a pre-mixed flame. It moves at a characteristic flame speed. This type of flame is observed in the stabilization of spray flames on flame holders, rocket engine combustion, and the development of deflagration and detonation waves in spray fields. Burgoyne and Cohen(1954) inferred through their classical experiment on pre-mixed flame combustion that when drop sizes are less than 10 microns, the resulting flame speeds are not very different from the pure gas case. But when the droplet size was increased, the flame speed decreased due to the time required to evaporate the fuel. Williams(1965) agreed with this theory. Mizutani(1973) pointed out that the burning velocities, at a fixed overall fuel-air ratio, are increased due to the presence of drops in the gaseous fuels. It also extends the region of stable burning to leaner overall mixture ratios.

A diffusion flame occurs when the fuel(s) and the oxidiser are kept separate before injection. After injection of the fuel, evaporation, diffusion of one species into another and chemical reaction between the fuel vapor and the oxidant give rise to a luminous diffusion flame around the droplets. Diffusion flame can exist as a part of pre-mixed spray in the sense that the spray is injected from a single point into an air stream and the combustion process proceeds simultaneously with the mixing process. This happens because diffusion flames can surround each droplet. Burke and Schuman(1965) described the simplest type of diffusion flame. For such a case, the concentration of all species becomes zero at the flame. This enables the flame position to be determined as a function of distance from the source(Williams, 1965). Bilger(1976) dealt with more practical situation where reaction between fuel and oxidiser did not take place at a fixed radial position rather, there was a broad region of overlap of the fuel and the oxidiser concentrations. The diffusion flame is automatically taken care of depending upon the availability of relative fuel and oxidiser. For such cases, a lot of pollutants, such as oxides of nitrogen, are produced due to very high reaction rate and high flame temperature. For pre-mixed flame, this control can be achieved by controlling the mixing of fuel and air. Thus, generation of high temperature at flame, and correspondingly, formation of hazardous oxides can be avoided for a premixed flame, though this mixing needs a high level of sophistication. But the pre-mixing causes danger of undesirable burning and explosion which makes this mode of combustion practically still unviable and in most of the industrial combustors, diffusion flame combustion mode is used.

1.2 Literature Survey

Combustion phenomenon is a very complex process involving a very high degree of non-linearity. So, initially, the study of the combustion process started with simplified models like quasi-steady burning of a single component, individual fuel droplet burning in a quiescent atmosphere in absence of any external flow. Later, in due course of time, complex-

ities in the modelling were gradually incorporated in order to simulate realistic situations. These are: external convection, droplet heating, transient nature, internal convection, fuel vapour accumulation, finite rate flame chemistry, variable property, micro-explosion, effect of neighbouring droplets, presence of more than one fuel in the liquid phase etc. The present literature survey mainly deals with combustion in the diffusion flame mode relevant to the present study.

1.2.1 Single Component Fuel

(1) Spherically Symmetric Burning

Agafanova et al.(1958), Godsave(1949, 1953, 1950, 1951), Goldsmith and Penner(1954), Spalding(1950, 1953), Varshavskii(1945, 1957, 1962), Wise et al. (1955) and Williams(1972) are the pioneers who first formulated the basic droplet combustion model for an isolated, single-component, quasi-steady droplet burning in a stagnant, oxidising environment. This basic model has become famous by the name 'd-square law model'. It predicts that the surface regression rate of a droplet is proportional to the burning time elapsed. In this model, the chemical reaction rate is assumed to be infinitely fast and thermal diffusion & radiation losses are neglected. This has been shown to be the case except in the case of heavy fuel oils (Probert, 1946 ; Friedman and Churchill, 1965; Wolfhard, and Parker, 1947, 1949). But later many authors questioned the validity of the above d^2 -law model. Krier and Wronkiewicz(1972) showed a general relation (d^n) between surface regression rate and the time elapsed. This relation is based on their experimental observation that the flame stand-off ratio (ratio of flame radius to droplet radius) grows linearly with time. The value of n lies between 1 and 2 when the chemical reaction rate becomes the controlling factor and it equals 2 when diffusion becomes the rate controlling process.

(i) Quasi-Steady Combustion and Infinite Rate Kinetics:

Williams(1960) assumed quasi-steadiness, which implies that soon after the ignition period, the burning reaches steady state condition i.e. the plot of d^2 against time remains

linear after the initial transient. The quasi-steadiness also assumes that the liquid side temperature becomes spatially uniform and invariant with time. This temperature was taken to be the boiling point of the fuel. He also assumed the droplet radius to be fixed. This means that the velocity of the fuel vapour flowing away from the surface is much greater than the surface regression velocity i.e. the effect of surface regression was neglected. The general continuity equation for predicting the burning rate coefficient (defined as the area of the droplet surface regressed per unit time i.e. $\frac{d}{dt}(d^2)$), temperature and composition field surrounding a burning droplet were developed by Hirschfelder et al.(1954). Most analyses are based on constant transport properties. Wise and Agoston(1972) gave a typical and widely accepted solution based on temperature independent transport properties. Solutions depended upon the choice of gas side specific heat, C_p and conductivity, λ . Both conductivity and specific heat were generally calculated at the arithmetic mean or the logarithmic mean of flame temperature and droplet surface temperature.

In practical situations, both temperature and the composition of the gas mixture vary over wide ranges. More sophisticated methods have been used by Sioni and Roblee(1969) and Annamalai et al.(1971). Sioni and Roblee used a computer calculation of λ while, Annamalai et al. used a more accurate analytic type calculation for evaluating conductivity, λ . Temperature dependent expressions for λ and C_p are also used. Goldsmith and Penner(1954) and Faeth and Lazar(1971) assumed linear variations of λ and C_p of the gas mixture with temperature. Kassoy and Williams (1968a,b) and Fendell(1966) have also developed analytic solutions based on singular perturbation technique, allowing for a general transport property variation with temperature and variable Lewis number and have shown their effects on flame temperature, droplet radius and burning rates. They were obtained in terms of asymptotic expansions and are given for the limit of the Damkohler number, which is defined as the ratio of chemical reaction rate to heat conduction rate, approaching infinity. Analytic forms are available for simple temperature dependence(1968b) but for more complex forms, numerical methods have to be used. An alternative diffusion theory of

combustion applicable to the special case of combustion of a liquid hydrogen droplet in still air was given by Varshavskii and Germeier(1967). Brzustowski(1965, 1966) developed a dimensionless form of the quasi-steady droplet combustion theory. Raghunandan and Mukunda (1977) in their quasi-steady analysis considered the variation of specific heat and thermal conductivity as a function of temperature and concentration of various species.

(ii) Finite Rate Kinetics

Very precise theoretical indications of the rate of chemical reaction rates in droplet burning are very difficult to quantify. Brzustowski(1965) pointed out the general restrictions imposed by chemical reaction and also the evaporation rates. Agafanova et al.(1958), Lorell et al.(1956), Tarifa et al.(1962), Williams(1961), and others used a simplified chemical reaction mechanism for their combustion analysis involving finite rate kinetics. For such cases, an overall reaction rate expression is adopted. It is seen that using such an (overall reaction rate) expression, for typical hydrocarbon fuel burning under normal conditions, little error is introduced in the mass burning rate relationship by assuming infinite reaction rate except under certain extreme conditions. Inclusion of finite rate kinetics gives a more realistic information regarding the structure of the flame zone or the reaction zone in the sense that it lies nearer to the droplet surface compared to that indicated by the infinite reaction rate, though the evaporation rate hardly changes. This inclusion also brings down the flame temperature to a more realistic value. Agafanova(1958) first made this realistic consideration which is supported by experimental results [Kumagai and co-workers (1957, 1971, 1975) , Wang et al. (1984) etc.]. These effects are highlighted by Lorell et al. (1956) in their calculation of flame structure. Their numerical results show that the mass burning rate and the location of the flame front are hardly affected by variation in the activation energy(hence, the reaction rate) of the chemical reaction. Bracco(1973) has also used this type of analysis to determine the rate of formation of NO in hydrocarbon droplet flames. Chung and Law(1984) worked with constant, but mutually different gas properties for the two regions across the flame for their quasi-steady

model. They considered finite rate chemical kinetics and has shown that the gas-phase dissociation results in a lower flame temperature. These predictions are in conformity with the earlier analyses of Lorell et al.(1956) and Agafanova et al.(1957).

(iii) Transient Combustion

Experimental results indicate that the heat and mass transfer involved in and around the droplet during its combustion are in a transient state during the major part of the droplet lifetime. Kumagai and Isoda(1957a) were the persons who first tried to solve the transient energy equation. Their analysis considers only gas-phase unsteadiness while neglecting radial convection terms. Spalding(1959), Chervinsky(1969a), Kotake and Okazaki(1969), and Krier and Wronkiewicz(1972) carried out further analyses on solving transient equations. The transient theory of Spalding(1959) makes use of a point source at the origin where the fuel is injected into the field to simulate the burning drop. The radial convective velocity is assumed to be zero. By considering the gas-phase unsteadiness, Spalding (1959) has shown that the flame initially moves away from and later towards the droplet. The transient analysis as well as the results of Chervinsky(1969) constitute a modification of Spalding's work. Williams(1960) discussed the effects of unsteadiness during the pre-ignition period and established the region of validity of the quasi-steady assumption. Parks et al.(1966) gave an account of temperature distribution within the droplet, while Shyn et al.(1972) investigated the liquid phase cracking in a heavy fuel oil during combustion. In all the above cases, time-dependent terms were retained while the analyses were carried out. Kotake and Okazaki(1969) solved an unsteady state model by numerically integrating the equations. However, the spherical symmetry was retained. The equations of species, momentum and energy of the gas surrounding the droplet and that of energy within the droplet were written as the time-dependent differential equations and integrated. Hubbard et al.(1975) pointed out that gas-phase unsteadiness is insignificant in the evaporation process. This gas-phase unsteadiness exists for a very short time. Waldman(1975) and Crespo and Linan(1975) used singular perturbation technique to study

the far-field unsteadiness of the gas phase for unsteady state combustion. Crespo and Linan used the ratio of densities of the ambient gas and the liquid as the small perturbation parameter, while Waldman used the ratio of droplet radius to the characteristic diffusion field length as the small perturbation parameter. Both reveal that the flame initially moves away from the droplet surface and then comes back towards the droplet. This feature was also reported by Kumagai and Isoda(1957) and Kumagai et al.(1971).

(2) Moving Droplets

(i) Low Reynolds Number Flow:

It is seen that in almost all practical situations, droplet burning takes place in an external velocity field. Calculation of the mass burning rate of a droplet in a convective field from fundamental principles would require quite an elaborate numerical scheme.

The first realistic model of combustion in a convective field was put forward by Brzustowski and Natarajan(1966). Essentially, Natarajan and Brzustowski(1966), and Brzustowski and Natarajan(1970) put forward a two-film model. This model assumes a spherical inner stagnant film through which diffusion and conduction occur, while the convective and diffusive mass transfers of the oxidant occur through the outer film. Due to the presence of convection, the oxidiser mass-flux towards the inner film is enhanced and is expressed empirically through dimensionless parameters. It is reported that the augmentation, for free convection, is proportional to $(Gr)^{\frac{1}{4}}$ and for forced convection, it was reported to vary as $(Re^{\frac{1}{2}})$. The evaporation rate was evaluated in terms of droplet surface heat transfer Nusselt number. A more detailed and a more fundamental analysis of droplet combustion in a slow viscous flow was carried out by Fendell et al.(1966). They assumed that the entire flow field was in stokes regime, the internal circulation was zero and the flame was thin. They solved the governing differential equations by singular perturbation technique. They used small values of droplet Reynolds number based on far-stream conditions as the perturbation parameter. The enhancement of burning rate and the distortion of flame due

to external flow field were evaluated. Sangiovanni(1978) used an integral formulation to see the effect of droplet motion. He calculated the thickness of the convective film around the droplet (within which both heat and mass transfer were assumed to be important) by using Ranz and Marshall's (1952) correlation. He used the Green's function technique to evaluate droplet burning rate and flame stand-off ratio. Law and Williams(1972) tried to link the earlier theoretical and experimental analyses. Okazima and Kumagai(1975,1982) conducted a series of experiments to see the burning of both stationary and moving droplets under normal and micro-gravity conditions. It was reported that burning rate enhancement due to droplet motion was insignificant. But, in the micro-gravity experiments, the free-fall height was inadequate. The effect of internal circulation inside the liquid droplet in the creeping flow regime was looked into by Ayyaswamy and co-workers(1983,1986, 1988,1990). Here the effect of radial flow was considered to be dominating. From another study of Sadhal and Ayyaswami(1983), it was observed that the internal circulation within the droplet causes the coldest region to be shifted from the droplet centre to a ring of radius approximately equal to two-third of the droplet radius. This reduces the characteristic diffusion length, but high rate of mass transfer(i.e. high surface regression rate) at the surface reduces internal circulation and may, eventually, cause a reversal of flow. Gogos and Ayyaswamy(1988) cited in their variable property analysis that a reduction of viscosity at higher temperature may also lower the internal circulation. Gogos et al.(1986) showed that the total drag comes from momentum transfer to the droplet due to evaporation. In this work, they accounted for the initial droplet heat up period.

(ii) Intermediate Reynold Number Flow:

For the droplet motion in the intermediate Reynold's number zone, various numerical schemes are used to analyse the typical burning of liquid fuels. This is because in this Reynolds number zone, neither a boundary layer analysis (generally applied for high Re. flow) nor an asymptotic analysis (generally employed for creeping flow regime) can be applied. So, one has to depend only on various elaborate numerical schemes. The works in this

area are, in general, quite recent. Dwyer and Sanders(1984,1986) considered the influence of drag on the deceleration of the droplet while applying the finite volume stream-vorticity function formulation. They took into account the effect of transients in both the phases and used non-orthogonal grids to track down the motion of the shrinking droplet. The drag results deviated from experimental data. Renksizbulnt and Ynen(1983) used steady state correlations and variable thermo-physical properties in their finite difference analysis to calculate drag. Their results indicated close agreement with experiment. Dwyer(1989) analysed an isolated droplet by finite volume method. He used variable property and continuity equation to correct pressure through a direct solver. For solving the transport equations, a predictor-corrector algorithm of the Alternating Direction Implicit (ADI) sweeping type was used. They did not measure drag. Recently, Renksizbulnt and Haywood(1988), Haywood et al.(1989) and Huang and Ayyaswamy(1990) assumed gas-phase quasi-steadiness in their variable property analysis for an evaporating drop. A Lagrangian frame of reference was used for balancing the forces on the droplet. The gas-phase analysis was coupled with the droplet motion. Huang and Ayyaswamy considered the effect of gravitational field. They adapted a hybrid solution scheme like that of Gogos et al.(1986). The SIMPLEC solution procedure developed by Vandoormaal and Raithby(1984) was used by Haywood and co-workers. All these studies of droplet evaporation belonging to the intermediate Reynolds number zone point out that the evaporation drag contributes to only a small fraction of the total drag. This is quite contrasting to the low Reynolds flow situation.

(iii) High Reynolds Number Flow:

It is seen that boundary layer approximations are generally used for studying high Reynolds number(of the order of 100) flow situations. Prakash and Sirignano(1978,1980), Tong and Sirignano(1982a,b) used the boundary layer approximations for their study in high Re. flow regime. Prakash and Sirignano established the existence of boundary layer on either side of the droplet surface with the help of their order of magnitude analysis. They

pointed out that the droplet core resembled Hill spherical vortex and that the gas-phase boundary layer merged with the potential flow. Tong and Sirignano(1983) developed a simplified model for the vaporization of a single component droplet. The model accounts for the liquid-phase internal circulation and axi-symmetric gas-phase convection. The solutions have been obtained by coupling the gas-phase similarity solution to the simplified liquid-phase solution. Gakkhar and Prakash(1990) varied the ambient conditions and studied their effects on burning.

In high Reynolds number flow situations, both for single component and multicomponent fuel droplets, it is noted that the characteristic diffusion length inside the droplet is reduced due to internal circulation. And at the same time, the droplet lifetime is also reduced by a similar scale due to enhanced evaporation rate. So, inspite of enhanced transport rate due to droplet motion, the transient heating remains almost throughout the droplet lifetime.

(3) Interaction Between Spray Droplets

In practical situations, it is found that there are many droplets present in a spray system and the average distance between droplets can become as low as few droplet diameters. So, a typical droplet, in real situation, will not behave as an isolated droplet, rather it will be very much influenced by neighbouring droplets. Basically, there are two kinds of models used for describing the interaction of spray droplets. The first one is the group combustion model introduced by Suzuki and Chiu (1971), and the alternative approach is the discrete droplet burning model or droplet array model. In the latter, a few droplets in a well defined geometry or a large number of droplets in a periodic configuration are examined. The droplet group combustion theory is distinct from the array theory in that a statistical description of droplet spacing, rather than a precise geometrical description, is used. As a matter of fact, group theory can deal with many more droplets than array theory. Array theory gives a detailed field analysis i.e. it gives a more detailed picture of the burning characteristics in the vicinity of a typical droplet whereas, an overall averaging

or collective burning effects of a cloud of droplets is given more stress in the statistical approach of group combustion model. Results of the array theory can be employed as an input to the group combustion approach. The two approaches have relative advantages and disadvantages over each other depending upon different practical situations.

Sirignano (1986) discussed different types of formulations of the governing equations for modelling spray combustion situations. In the two-continua approach where both the gas and the liquid phases are assumed to be co-existing, group combustion model is suitable. He formulated the governing equations in Eulerian frame, Lagrangian frame and discussed their relative advantages and disadvantages. For discrete droplet burning model or the droplet array model, Eulerian description can be used for solving the gas phase, and both Lagrangian description or Eulerian description can be used for solving the liquid phase. Eulerian-Eulerian form is not advantageous when resolution is desired on scale as small as or smaller than the average distance between the droplets. In such situations, Eulerian-Lagrangian form is advantageous. Eulerian form is simple and easy to apply, but the Lagrangian frame can eliminate numerical diffusion, resolve multivalued solution and has the ability to achieve resolution on a scale smaller than the droplet spacing. He also outlined a probabilistic (or, distribution) function approach to analyse spray system. When the scale of resolution is even smaller or finer than to the average droplet spacing, the practical situation becomes probabilistic rather than deterministic, since it is difficult to locate any droplet. In such situations, probabilistic function approach becomes more realistic for modelling.

(i) Discrete Droplet Burning:

In this model, each droplet is considered as a fuel source as well as a heat sink. Twardus and Brzustowski (1977), Brzustowski et al. (1979) and Umemura et al. (1981) employed a bi-spherical coordinate system to facilitate their analysis of the interaction of two burning droplets. Twardus and Brzustowski (1977) did not consider Stefan convection and forced convection. They indicated that two droplets may burn separately only when the ratio of

the distance between droplet centers to the droplet radius is above a certain critical value, otherwise they burn with one single envelope flame. Chigier (1976) has cited experimental evidence that the droplet in combustors rarely burn in an isolated fashion. Rather, a flame envelopes many droplets. Umemura et al.(1981) used a potential flow approximation and Brzustowski et al. (1979) used a Nusselt number correlation to account for the convective effect. All of them noted the decrease of burning rate due to the influence of neighbouring droplets. Umemura et al.(1981) saw that when the two droplets are of different sizes, the smaller droplet is affected more.

Labowsky(1976, 1978, 1980a, 1980b) and Labowsky and Rosner(1978) used a modified superposition principle for solving a situation having simple arrangements of droplet array. Labowsky(1976) used this modified image method to determine vapour density field in arrays of spherically symmetric and isothermal evaporating droplets. In this study, Stefan flow was neglected which enabled the equations to be linear and consequently, method of images or superposition could be applied. Later, Labowsky(1978) included Stefan flow in his analysis, but the equations were reduced to Laplace equations through a suitable transformation. After this, method of superposition could be applied to solve the transformed linear equations. Labowsky (1980b) extended his work (1978) to the case of interacting droplet combustion. He(1980a) also relaxed the isothermal condition of the droplet in his analysis. In the superposition method, an infinite succession of sources and sinks are placed at the image points of the earlier generations and thus, the flow pattern was simulated. Labowsky(1976) proposed an extrapolation formula which enabled to approximate the boundary conditions within 5sources. Labowsky and Rosner (1978) pointed out that the difference in results between a continuous distribution of monopole sources and the discrete distribution of monopole sources becomes insignificant when the number of droplets in the cloud is large. Reduction of burning rate was noted and this became more severe when the number of interacting droplets increased in the system.

Ray and Davis(1980, 1984) have presented a generalised treatment of heat and mass

transport between an assemblage of particles and a surrounding continuum. This analysis is based on the solution of unsteady state diffusive transport equations with unknown point sources located at the centers of the particles. Integral equations matching the boundary conditions at the surface of the particles are used to describe these point sources. They compared their results with Labowsky(1978) quite successfully. This formulation was extended by Merberry et al.(1984) to the case of interacting droplet combustion. The theory is applied to burning droplets of different sizes as well as monodisperse droplets in multi-particle arrays. In their quasi-steady analysis, they developed a simpler solution technique by using a modified Laplace equation with point sources. They provided correction factor by which, burning rate for multiple particle can be retrieved from the burning rate of a single particle. Sangiovanni and Labowsky(1982) found that with decrease in droplet spacing, the burning time of monodisperse droplets in a linear array increased gradually. They initiated the quasi-steady halo model to simulate the transient nature of droplet interaction and suggested only the droplet having overlapping halos could interact directly.

Miyaska and Law (1981) experimented on linear arrays of two and three droplets in low pressure environments. Their, both natural convection and low pressure effects were shown to be negligible. They indicated that the droplet vaporization rate and droplet heating were significantly retarded due to the interaction effect. Their result showed that the superposition calculation for a pair of droplets situated far apart were in qualitative agreement with this study. But when droplets were close to each other, the results deviated significantly. This mismatch was attributed to the longer heat-up period resulting from droplet interaction. Ryan et al.(1990) utilised the group combustion theory which involved a large number of droplets, assumed top hat profiles in the interstitial space between the drops, and accounted for their variation in the radial direction. Their study accounted for the change in transport rate due to proximity of other droplets and found close agreement between the results obtained by group combustion approach and droplet array study. Samson et al.(1978), in their statistical model, established the concept of a screening distance

within the radius of which, the interaction of that droplet was significant.

(ii) Cell Model Approach:

Unit cell model approach due to Happel(1958) and Kuwabara(1959) is yet another powerful technique applied for the hydrodynamic analysis of a multiparticle system. In this approach, a given spray system is assumed to consist of a number of cells which are isolated from each other through suitable boundary conditions at the cell surface. Each of these cells has one droplet at its centre. Thus, by studying one representative cell, one can greatly simplify analysis of practical spray situations. Happel (1958) applied zero shear stress at the cell surface to isolate the cell from the surrounding. Kuwabara (1959) used zero vorticity condition at the cell boundary. Jaiswal (1990) used Happel model in his finite element analysis. In order to study the transient effect, Zung(1967) applied zero mass transfer condition in order to isolate the cell, in his pure mass-transfer analysis. Tishkoff (1979) considered the heat transfer aspect in addition to mass transfer, and applied zero heat flux condition at the cell boundary. Bellan and Cuffel (1983) used spherical cells which were touching each other. The global equations were modified to accommodate the heat and mass transfer that take place in between the cells. Bellan and Harstad (1987a) used a correlation to account for droplet motion and later they(1987b) modified the global conservation equations to account for convection. El-Kaissy and Homsy (1973) used regular perturbation technique while using Happel and Kuwabara models for their analysis. Tal and co-workers (1982, 1983, 1984a, 1984b) used cylindrical cell model to take advantage of the periodic structure of the array. The finite-difference calculations gave excellent agreement with experimental results for drag-coefficients, indicating that drag increased as streamwise and transverse spacings decreased in identical fashion. Tsai and Sterling (1990) used the grid-embedding technique to solve for velocity and temperature field in their cylindrical cell model study. Chen and Tong (1988) predicted stronger influence of droplet interaction for high Reynolds number flow in their three drops-in-cell arrangement study. Whereas, Shuen (1988) in his planar droplet arrays oriented normal to the flow, indicated

that interaction effect became less with increasing Reynolds number. Ramachandran et al.(1987) gave a numerical model to study the transient characteristics of a train of three vertically falling droplets. These results comply with their earlier(1985) experimental data. Ramachandran et al.(1989) used three spheres-in-cell model in their finite element analysis to see heat-transfer and flow effects. Wang (1989) used the above analysis to see interaction effects on vaporizing droplets. Recently, Sanyal and Sundararajan (1991) applied this unit cell approach in their study of quasi-steady, laminar, single component fuel combustion. They considered the droplet to burn in a conceptual spherical cell. They studied this spherical cell by regular perturbation technique in the creeping flow regime and by a full numerical solution using FEM in the intermediate Reynolds number regime. They assumed the cells to be touching each other.

(iii) Group Combustion Model:

Suzuki and Chiu(1971) proposed the first theoretical model on group combustion, followed by experimental studies conducted by many researchers such as McCreath and Chigier (1973), Hayshi and Kumagai (1975), Mizutani et al.(1977) and Khalil and Whitelaw (1977). Suzuki and Chiu (1971) established that when the group combustion number G exceeds a critical value, group combustion mode starts. Chiu and Liu (1977) and Chiu et al.(1983) used the characteristic group combustion number in order to isolate the two basic burning models, namely, the group combustion model and the discrete droplet burning(or, droplet array) model. Nusselt number correlations were used to account for the droplet motion. Depending upon the value of the group combustion number (G), the burning of droplets was categorised as follows:

Discrete droplet burning for $G < 0.01$

Internal group combustion for $0.01 \leq G \leq 1.0$

External group combustion for $1 \leq G \leq 100$

External sheath combustion for $G > 100$

Annamalai and Ramalingam (1987) presented the analysis of a spherically symmetric cloud of particles burning in a quiescent atmosphere in order to study the group combustion behaviour. They predicted results for burning rate and the flame structure as function of G . They found that for char/carbon particles, group flame occurs i.e. the change from discrete droplet burning to the group combustion mode takes place at $G > 5$ while for a cloud of liquid drops, this occurs at $G > 0.1$. So, it is noted that this critical value of G for the liquid drops is one order lower compared to that for the carbon particles. This happens due to the lower burning rate of carbon particles inside the cloud. They established the existence of individual particle combustion, group combustion and sheath combustion. Later, they (1988) performed this study in cylindrical clouds. Lotters(1989) has indicated that the group combustion structure broke down due to various transport processes.

1.2.2 Multicomponent Fuel

It is observed in the practical situations that the fuels used are mostly multicomponent in nature. These fuel constituents have widely different properties. This variation of characteristics within the fuel alters the combustion characteristics as compared to that of the pure liquids. So, in order to simulate the practical situations for fuel burning in a more realistic manner, the study of multicomponent fuel burning is very essential. Therefore, in recent years, significant attention is being given to the burning of multicomponent fuels. Multicomponent droplet burning is more complex than single component fuel combustion due to mass-transfer effects in the liquid phase. The blend of the multicomponent fuel can be of two types: miscible and immiscible. The phase change characteristics of a multicomponent fuel depend upon the extent of miscibility of the constituents. Two simplified models corresponding to batch distillation and mass diffusion limited mode of burning have been developed to look into the multicomponent aspect of combustion. For diffusion limit model, in absence of internal circulation, diffusion is considered to be the only mode of transport inside the liquid droplet. For the batch distillation mode of burning, at any

instant, the most volatile component has the fastest gasification rate relative to its concentration such that the depletion of the constituents from the droplet composition occurs approximately in the sequence of their relative volatilities. The batch distillation mode of burning was initially looked into by Faeth (1970), Newbold and Amundson (1973) and Law (1976). They adopted the batch distillation limit concept and assumed the droplet temperature and composition to be perpetually uniform such that they varied with time only. They did this in order to incorporate the effects of internal circulation.

Based on the diffusion limit model, by numerically integrating the conservation equations, it was shown by Law (1978a), and Landis and Mills (1974) that the evaporation process consisted of an initial transient regime, an intermediate quasi-steady regime and a final volatility-dominated regime. This behaviour was attributed to the high diffusional resistance of the liquid phase.

Law and Law (1982) examined the diffusion-limited quasi-steady regime with the assumption that no changes occurred in the temperature or the mass-fraction profiles on the liquid side. Using an asymptotic analysis, they showed that the fraction of mass-flux leaving the droplet surface for any species was equal to the initial liquid mass-fraction of that species prior to evaporation. Shaw (1990) extended the study of Law and Law (1982), and found that the mass-flux fraction of a species at droplet surface was equal to the volume-averaged mass-fraction within the droplet at that time. Wang et al.(1984) and Nioka and Sato(1986) reported the occurrence of sudden and rapid heating of the droplet after the constant surface regression rate was over. At this point in time, flame moves back towards the droplet surface and the burning rate falls.

Considering a trace amount of low volatility component in the liquid phase, Shaw and Williams (1990) developed an asymptotic analysis for heat and mass transport during the burning of a multicomponent fuel drop. For the entire process, evaporation of the impurity material was neglected. It was indicated by Makino and Law (1988) that as the diameter of the shrinking droplet approached the characteristic mass-diffusion length, the volatility

differential of the constituents became the rate controlling factor and thus the vaporization followed the batch-distillation mode. Law et al.(1977) analysed vaporization of a multi-component droplet in a strong convective gas stream. They demonstrated that boundary layer existed in both liquid and gas phases near the droplet surface over most of the droplet lifetime, and that convection was an important transport mechanism within the droplet. Lara-Urbaneja and Sirignano (1981) found that droplet heating effects were important for most part of the droplet life time ,especially if the boiling points of the components differed widely. They applied similar boundary layer analysis. Basically, they followed the same arguments used in Prakash and Sirignano's single-component droplet study(1980) and extended the analysis to the multicomponent droplet case. The gasification and the burning of the individual components are strongly influenced by the coupled transport processes occurring in the liquid and gas phases. The studies of prakash and Sirignano (1978, 1980) and Lara-Urbaneja and Sirignano (1981)have clarified that when the gasification rate is not too slow, rapid internal circulation can not cause perpetual spatial uniformity throughout the droplet, and therefore, the batch distillation limit can never be approached. The cause is that though the internal circulation is infinite and therefore having perpetual streamwise uniformity, transport in the direction normal to the stream lines is still effected through the slow diffusion process. They have shown that since the reduction in characteristic diffusion and burning time are of the same order even for a highly convective case, the transient mass diffusion should prevail throughout the droplet life time. Tong and Sirignano(1986) studied transient vaporization of a multicomponent droplet in a hot convective environment. They accounted for liquid-phase internal circulation, transient droplet diffusion, and axi-symmetric gas-phase convection in their model. This simplified model is an extension of their previous single-component droplet model(1983).

Very recently, a fully transient numerical study for both the liquid and gas phases was presented by Mawid and Aggarwal (1991) for spherically symmetric multicomponent fuel droplet burning. The authors observed that for certain time intervals, the mass evapo-

ration from the droplet surface was suppressed. They attributed such a trend to vapour accumulation in the gas phase and the high diffusional resistance of the liquid phase.

Micro-Explosion:

It may happen during the course of fuel burning that the droplet surface becomes more concentrated with the less volatile (high boiling point) component while, the droplet core has a higher concentration of the more volatile (lower boiling point) components. Thus the more volatile component in the droplet interior may accumulate substantial amount of superheat beyond it's boiling point. This may start homogeneous nucleation, whose extremely fast gasification rate may lead to sufficient pressure build-up and thus the droplet may eventually fragment, causing what is known as micro-explosion. This phenomenon can best be explained by diffusion-limit model (Law, 1978). They accounted for liquid-phase internal environment. They accounted for liquid-phase internal micro-explosion can be controlled properly, then large-scale mixing can be achieved through spraying and penetration, with some what larger droplets, which is then followed by instantaneous gasification and local mixing through micro-explosion. Law (1978) and Law(1981) pointed out the possibility of increasing the occurrence of micro-explosion by increasing the system pressure. This is attractive for fuel burning in high pressure environments. Law(1981a) pointed out that high pressure may also decrease the possibility of micro-explosion because, at higher pressure, the dynamics of bubble expansion is weakened. Higher pressure also increases internal motion. Thus, the concentration gradient is reduced, reducing the possibility of nucleation. Law et al.(1979) predicted that micro-explosion is favoured in an optimum range of mixture composition. The reason for this is that the more volatile component facilitates homogeneous nucleation while, the less volatile component raises the droplet temperature. This was later experimentally verified by Lasheras et al.(1980,1981). It was experimentally established by Lasheras et al.(1980) that the intensity of micro-explosion for miscible multicomponent droplets was less.

For the case of immiscible fuel undergoing equilibrium evaporation, the partial pressures

of the individual components are independent of the pressure of the other components. Therefore, the surface temperature of the droplet is limited to the boiling point of the more volatile fuel. This was first indicated by Law(1981). By making use of the above property, the surface temperature of the fuel can be suppressed by adding a small quantity of the low boiling point liquid like water. This can reduce pollutant formation as well as incendiary ignition. By adding a small quantity (a few percent) of surfactants to normally immiscible water and oil, a stable emulsion can be established. Cook and Law(1978) showed that the addition of water generally does not exceed 20 percent for smooth engine operations. Water-oil emulsions have been tested in different combustors of diesel engines, gas turbines, and furnaces and boilers (Dryer, 1977). Wheatherford et al.(1979) and Law(1981) has come up with the fact that water/diesel emulsions are fire-safe because upon spillage and incendiary ignition, the initial fire ball will extinguish itself. Lasheras et al.(1979), in their experiment, have shown that the emulsion-droplets explode with much more intensity than those of miscible fuel blends. This takes place due to the presence of larger amount of superheated mass contained by individual micro-droplets of water when the nucleation starts. Lee and Law(1991) have shown that the particles agglomerate into a rigid porous sphere during initial d-square law period in case of gasification for slurry droplets. This was an experimental verification of their own proposition.

Experimental observations by Wang et al.(1984) indicate that two d^2 -law regimes occur during the burning of binary fuel mixtures. After the initial heating, the droplet follows d^2 -law burning for the more volatile fuel until it is nearly depleted. Then rapid droplet heating takes place upto the boiling point of the less volatile fuel, leading to the d^2 -law burning regime of this fuel.

1.2.3 Adaptive Grid Generation

In Modelling environments or situations, where regions of high spatial activity are a function of time, initial boundary value problems mixed with moving adaptive grids are needed to be solved. Several approaches are available. Miller and Miller(1981) used a moving finite

element method. In their method, they expanded the solution in piecewise linear polynomials where both time dependent coefficients of the series and the grid points are unknown functions of time. These quantities were obtained by minimising the partial differential equation's residue in a least square sense. David and Flaherty(1982), in their adaptive finite element method, did not couple together the calculation of the solution and the grid points, but kept them separate. Different approaches or methods were used by Dwyer et al.(1980), Tscharnuter and Winkler(1979) and Bolstad(1982) to solve the above problem. White(1982), in his study, calculated the solution and the grid together by using finite difference method. He generalised the idea of equidistributing the arc-length of the solution of a two point boundary value problem to one-dimensional mixed initial-boundary value problems. Pereyra and Sewell(1975) equidistributed the local truncation error. Apart from Bolstad (1982), all have used methods that use a fixed number of grid-points so that they are concentrated in the regions where the spatial activity of the solution is highest. Essentially, here, positive weight functions are equidistributed over a fixed number of spatial intervals and the positive weight functions are chosen in such a way that it reduces the local discretization error. Either finite element or finite difference approach is used to discretize space in these cases. The weight function may depend on the solution either implicitly or explicitly. In case of implicit dependence, the solution components and the grid are calculated together, where as for explicit dependence, the grid is determined by using a previously calculated solution. Later, Smooke and Koszykowski(1986) developed a fully adaptive method for solving one-dimensional mixed initial boundary value problem. Their method had the capability to change the total number of grid points according to the need, during adaption. In addition, when a fixed number of grid points were enough to accurately describe a solution, the mesh was moved by extrapolating the nodal positions from earlier time levels.

1.3 Scope of Present Study

The present study deals with the analysis of a laminar multicomponent single droplet fuel burning in a stationary atmosphere. The spray is assumed to be very dilute so that the effect of neighbouring droplets on the droplet under consideration is negligibly small. Liquid phase mass diffusion is considered to be the only means for liquid phase mass transport. Liquid phase and gas phase properties are considered to be constants. Effect of radiation is neglected. Equilibrium condition is assumed to be always prevailing at the liquid-gas interface. Therefore, the Raoult's law and Clausius Clapeyron relation hold true at the interface. At the droplet surface, overall mass balance, species flux balance for both liquid and gas sides and heat flux balance are used as boundary conditions to couple the two phases. At the center, radial symmetry is applied as boundary condition. Far stream conditions are assumed to be valid at the outer boundary of the solution domain ($r \rightarrow \infty$). Chapter 2 deals with the above general formulation part where general equations are derived in context of the present problem. The study is carried out in two parts.

In the first part, a semi-analytical solution is sought. The additional assumptions made are the gas phase quasi-steadiness and unity gas phase Lewis number. The effect of surface regression which appears as the convective term in the liquid phase equations is neglected. Thin film approximation as well as Schvab-Zeldovich variables are used to eliminate the non-linear reaction term. A detailed parametric study is attempted to bring out the salient features of the multicomponent fuel burning. The details of the formulation and results and discussion for this first part are presented in chapter 3.

In the second part, the full transient heat and mass transport equations are solved numerically for both the liquid and the gas phases. Finite rate chemistry, gas phase dissociation, use of variable gas phase specific heat are considered to catch finer details. Unity Lewis number for the gas phase has been relaxed. The liquid phase equations are solved by using FDM and the gas phase equations are solved by using FDM. Fixed grid distribution with unequal grid spacing has been used for the liquid phase and adaptive

grid generation technique has been developed to track down the steep flame region in the gas phase. The detailed formulation for this second part is included in chapter 4 and the details of the results and discussion are presented in chapter 5.

Chapter 2

General Formulation For Multicomponent Combustion

2.1 Introduction

Combustion is a highly complex phenomena involving interactive momentum, heat, and mass transport processes both inside and outside of each individual fuel droplet. The complexity of analysis is further enhanced when the fuel droplet is of a multicomponent nature. Very high temperature, smallness of each fuel droplet, unpredictable flame chemistry, complex gas-liquid phase coupling, flame movement, highly transient nature of the process are some of the key features of the combustion phenomena. Moreover the effect of the neighbouring droplets is almost unpredictable. This causes problem in specifying proper boundary conditions. Relative velocity between the droplet and the gas adds to the complexity. In view of such complexities, the complete modelling of spray combustion becomes extremely involved and is the subject matter of the present chapter.

2.2 Liquid Phase and Gas Phase Transport

As soon as the atomised fuel droplets are injected into the combustion chamber, the liquid fuel immediately starts evaporating due to a concentration gradient at the droplet surface. The fuel vapour meets the oxidiser in stoichiometric proportion somewhere near the droplet surface, where ignition takes place. Ignition can be achieved by an ignition stimulus or if the environment is sufficiently hot. At the flame, fuels and oxidiser undergo chemical reaction, as a result of which, intense heat is produced. So, immediately, heat starts flowing from the gas phase to the liquid phase, thereby, effecting rise in droplet temperature and more evaporation of fuel at the surface. Due to the volatility-differential between the species of the liquid droplet, one fuel is preferentially evaporated than the other. This develops concentration gradient within the droplet and, the gradient is maintained throughout the droplet lifetime. Therefore, both heat and mass transport within the droplet are very important for multicomponent fuel droplet burning. Momentum transport inside the liquid droplet is also important because, as soon as the atomised droplets are introduced into the combustion chamber, interfacial shear stress is generated due to the relative motion between

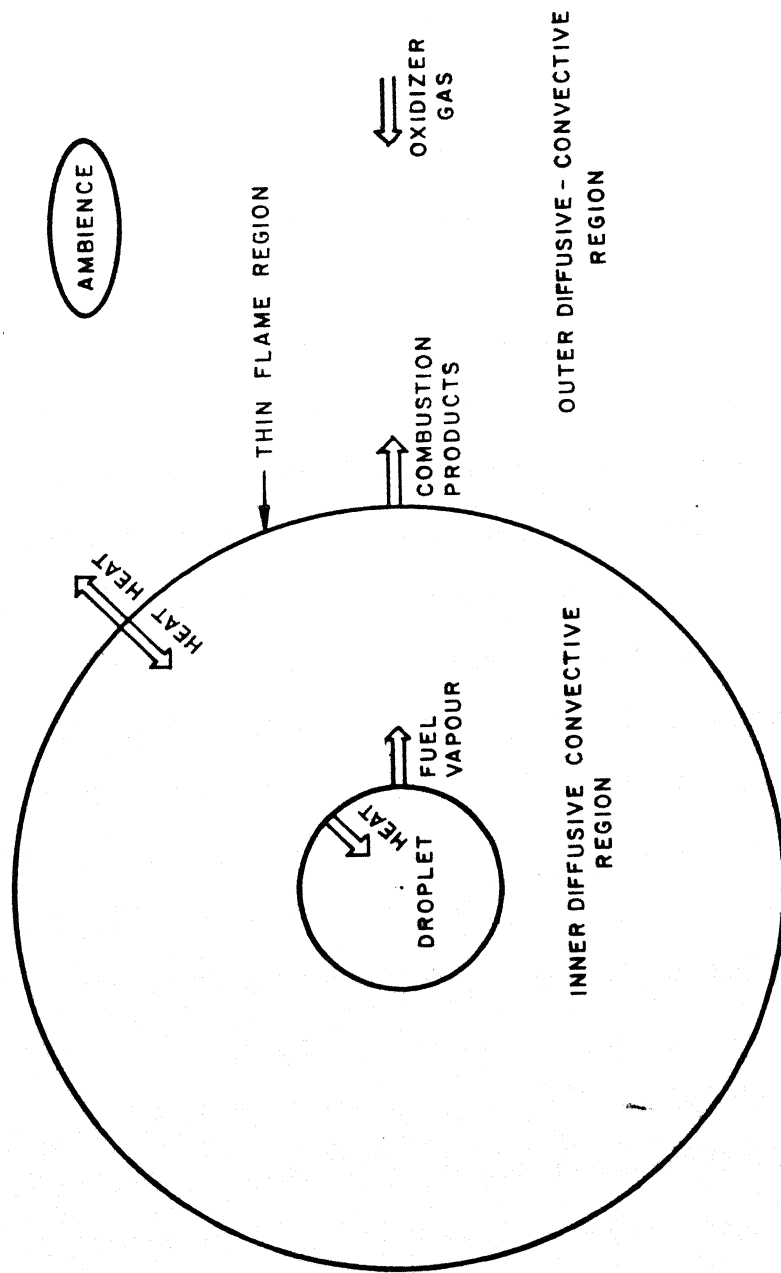


Fig. 21 Flow configuration for spherically symmetric droplet combustion.

the droplets and the gas phase which creates circulatory motion inside the droplet. But the strength of this circulation depends on the Reynolds Number. If the relative velocity between the liquid and gas phase is low, the liquid phase circulation is negligibly small. So, for accurately predicting combustion behaviour, mass, momentum and heat transport phenomena generally become important for the liquid phase.

As a result of chemical reactions at the flame, a number of products like oxides of carbon and nitrogen, water vapour and also many other intermediate species are generated. Infact, there are innumerable steps in between, before the final products are produced. But, a detailed modelling, which includes all the intermediate steps, is impossible because of the complexity of the system as well as due to the lack of complete knowledge of most of the intermediate reactions. In most of the combustion studies, a single step global irreversible reaction is generally used for a given fuel. Dissociation of the products at high temperature is another feature which influences the droplet burning. These dissociation reactions are endothermic in nature. So, it does not allow the flame temperature to rise beyond a certain limit. It is seen that unless the prevailing temperature is quite high, i.e. $R_u T > \text{activation energy } (E_a)$ of the fuel, the molecules cannot take part in chemical reaction. Therefore, the combustion reactions remain frozen in most of the places of the gas phase. Only in a very narrow zone, the molecules are generally, able to penetrate this high activation energy barrier and, therefore, flame exists only in this narrow zone. In this region, reaction kinetics becomes very important and the reaction proceeds to equilibrium at a finite rate. Finite rate flame chemistry is very important in analysing the structure of the flame.

Assumptions of co-existing media are assumed to be valid for deducing the conservation equations for a multicomponent system (both reacting and non-reacting). In this concept, the entire volume is assumed to be accessible to all the components in the mixture. The various chemical species in a diffusing mixture move at different velocities. Let \underline{v}_i denote the velocity of the i^{th} species with respect to stationary coordinate axes. So, for a mixture of N species, the mass-averaged velocity is defined as

$$\underline{v} = \sum_{i=1}^N \underline{v}_i Y_i \quad (2.1)$$

where, $Y_i = \frac{\rho_i}{\rho}$ = mass-fraction of the i^{th} species.

Diffusion velocity, V_i , of the i^{th} species with respect to the mass-average velocity of the mixture (\underline{v}) is defined as

$$V_i = \underline{v}_i - \underline{v} \quad (2.2)$$

The diffusion velocity, V_i , is evaluated from Fick's law of binary diffusion as

$$V_i = -\frac{D \nabla Y_i}{Y_i} \quad (2.3)$$

where, D is the coefficient of binary diffusion. In the above expression, the effect of temperature and pressure gradients as well as that of external forced fields are neglected because, their effect on diffusion velocity are very small compared to the concentration gradient. The diffusion coefficients for liquids are much smaller compared to the low pressure gases owing to the densely packed liquid molecules. **Fick's law** of diffusion can be assumed to be valid for multiphase systems also, if the binary diffusion coefficients of all the pairs of species are equal. This is valid if the molecular weights of all the species are close to each other. This assumption is generally valid for most of the combustion situations. Fick's law of diffusion can also be used for multiphase systems in situations where dilute reactants are present in an almost inert environment. The above equations and relations are generally valid for both gas and liquid phases.

2.3 Derivation of General Conservation Equations

2.3.1 Species Conservation Equations

The species conservation equation for each species, Y_i , can be derived by making a species balance [Kuo, 1986] over an arbitrary differential fluid element of volume $\Delta x \Delta y \Delta z$ in a mixture as

$$\frac{\partial \rho_i}{\partial t} + \frac{\partial \dot{m}_{ix}}{\partial x} + \frac{\partial \dot{m}_{iy}}{\partial y} + \frac{\partial \dot{m}_{iz}}{\partial z} = \dot{\omega}_i \quad (2.4)$$

or, in vector notation,

$$\frac{\partial \rho_i}{\partial t} + \nabla \cdot \dot{\underline{m}}_i = \dot{\omega}_i \quad (2.5)$$

where, ρ is the mixture density, ρ_i is the density of the i^{th} species,

$\frac{\partial \rho_i}{\partial t}$ = rate of change of mass per unit volume of species i ,

$\frac{\partial \dot{m}_{ix}}{\partial x} + \frac{\partial \dot{m}_{iy}}{\partial y} + \frac{\partial \dot{m}_{iz}}{\partial z}$ = net rate of change of mass-flux vector in the 3 directions,

\dot{m}_{ix} , \dot{m}_{iy} and \dot{m}_{iz} are the rectangular components of mass flux vector, $\dot{\underline{m}}_i$ and

$\dot{\omega}_i$ is the rate of production of the species i in kg/m^3s .

Using, $\rho_i = \rho Y_i$, $\underline{v}_i = \underline{V}_i + \underline{v}$,

$$\begin{aligned} \dot{\underline{m}}_i &= \rho_i \underline{v}_i \\ &= \rho Y_i (\underline{V}_i + \underline{v}) \end{aligned} \quad (2.6)$$

Using $\rho_i = \rho Y_i$ and Eqs. 2.5, 2.6, one can write the general conservation equation for the i^{th} species as,

$$\frac{\partial (\rho Y_i)}{\partial t} + \nabla \cdot [\rho Y_i (\underline{V}_i + \underline{v})] = \dot{\omega}_i \quad (2.7)$$

(i) for **liquid phase**, the species conservation equations can be written as,

$$\frac{\partial (\hat{\rho} \hat{Y}_i)}{\partial t} + \nabla \cdot [\hat{\rho} \hat{Y}_i (\hat{\underline{V}}_i + \hat{\underline{v}})] = \hat{\dot{\omega}}_i \quad (2.8)$$

(ii) for **gas phase**, the species conservation equations can be written as,

$$\frac{\partial (\rho Y_i)}{\partial t} + \nabla \cdot [\rho Y_i (\underline{V}_i + \underline{v})] = \dot{\omega}_i \quad (2.9)$$

The symbol, $\hat{}$ stands for liquid phase quantities, and those without this symbol stand for the gas phase quantities.

2.3.2 Overall Mass Conservation Equations

Adding the conservation Eq. 2.5 for all the N species, the general overall mass conservation is obtained as,

$$\sum_{i=1}^N \frac{\partial \rho_i}{\partial t} + \sum_{i=1}^N \nabla \cdot \dot{m}_i = \sum_{i=1}^N \dot{\omega}_i$$

or,

$$\frac{\partial}{\partial t} \sum_{i=1}^N \rho Y_i + \nabla \cdot \sum_{i=1}^N \dot{m}_i = 0$$

or,

$$\frac{\partial \rho}{\partial t} + \nabla \cdot \rho \underline{v} = 0 \quad (2.10)$$

(i) for **liquid phase**, the continuity equation can be written as,

$$\frac{\partial \hat{\rho}}{\partial t} + \nabla \cdot \hat{\rho} \underline{\hat{v}} = 0 \quad (2.11)$$

(ii) for **gas phase**, the continuity equation can be written as,

$$\frac{\partial \rho}{\partial t} + \nabla \cdot \rho \underline{v} = 0 \quad (2.12)$$

2.3.3 Momentum Conservation Equations

Momentum conservation equations can be derived by making momentum balance over a control volume as follows (Kuo, 1986)

$$A = B + C + D \quad (2.13)$$

where, A = rate of increase of momentum inside the control volume (c.v.),

B = Net influx of momentum into the control volume through control surface (c.s.),

C = Net body force on control volume and

D = Net surface force on control surface.

So, the momentum balance can be expressed as in integral form as

$$\begin{aligned} \frac{\partial}{\partial t} \left[\iiint (\rho dv) \underline{v} \right] &= - \iint \underline{v} (\rho \underline{v} \cdot d\underline{A}) + \iiint \underline{x} + \iint \underline{\sigma} \cdot d\underline{A} \\ &= - \iint \rho \underline{v} \underline{v} \cdot d\underline{A} + \iiint \underline{x} dv + \iint \underline{\sigma} \cdot d\underline{A} \\ &= - \iiint (\nabla \cdot \rho \underline{v} \underline{v}) dv + \iiint \underline{x} dv + \iint \underline{\sigma} \cdot d\underline{A} \end{aligned}$$

or,

$$\iiint \left[\frac{\partial}{\partial t} (\rho \underline{v}) + (\underline{\nabla} \cdot \rho \underline{\nabla} \underline{v}) - \underline{\nabla} \cdot \underline{\sigma} - \underline{x} \right] dv = 0$$

where,

$$\underline{x} = \rho \sum_{i=1}^N Y_i \underline{f}_i$$

Therefore,

$$\frac{\partial}{\partial t} (\rho \underline{v}) = - (\underline{\nabla} \cdot \rho \underline{\nabla} \underline{v}) + \underline{\nabla} \cdot \underline{\sigma} + \rho \sum_{i=1}^N Y_i \underline{f}_i$$

or,

$$\frac{\partial}{\partial t} (\rho \underline{v}) + (\underline{\nabla} \cdot \rho \underline{\nabla} \underline{v}) = \underline{\nabla} \cdot \underline{\sigma} + \rho \sum_{i=1}^N Y_i \underline{f}_i \quad (2.14)$$

where, \underline{v} is the velocity vector, ρ is the density, $\underline{\sigma}$ is the total stress tensor, \underline{f}_i is the contribution due to the body force on the i^{th} species and, N is the number of species.

Here,

$$\underline{\nabla} \cdot \underline{\sigma} = -\underline{\nabla} p + \underline{\nabla} \cdot \left[\eta \left(\underline{\nabla} \underline{v} + (\underline{\nabla} \underline{v})^T \right) - \frac{2}{3} (\underline{\nabla} \cdot \underline{v}) \underline{I} \right]$$

Therefore, Eq. 2.14 can be written as

$$\frac{\partial}{\partial t} (\rho \underline{v}) + (\underline{\nabla} \cdot \rho \underline{\nabla} \underline{v}) = \rho \frac{\partial \underline{v}}{\partial t} + \underline{v} \frac{\partial \rho}{\partial t} + \underline{v} (\underline{\nabla} \cdot \rho \underline{v}) + \rho \underline{v} \cdot \underline{\nabla} \underline{v} \quad (2.15)$$

Since,

$$\frac{\partial \rho}{\partial t} + (\underline{\nabla} \cdot \rho \underline{v}) = 0 \quad (\text{from continuity eq. 2.12})$$

Therefore,

$$\rho \frac{\partial \underline{v}}{\partial t} + \rho \underline{v} \cdot \underline{\nabla} \underline{v} = -\underline{\nabla} p + \underline{\nabla} \cdot \left[\eta \left(\underline{\nabla} \underline{v} + (\underline{\nabla} \underline{v})^T \right) - \frac{2}{3} (\underline{\nabla} \cdot \underline{v}) \underline{I} \right] + \rho \sum_{i=1}^N Y_i \underline{f}_i$$

or,

$$\rho \frac{\partial \underline{v}}{\partial t} + \rho \underline{v} \cdot \underline{\nabla} \underline{v} = -\underline{\nabla} p + \underline{\nabla} \cdot \left[\eta \left(\underline{\nabla} \underline{v} + (\underline{\nabla} \underline{v})^T \right) - \frac{2}{3} (\underline{\nabla} \cdot \underline{v}) \underline{I} \right] - \rho \underline{g} \quad (2.16)$$

where, \underline{g} is the gravitational force which acts on the system as body force, η is the dynamic viscosity and, \underline{I} is the unit tensor. For constant ρ and η , the momentum conservation becomes

$$\rho \frac{\partial \underline{v}}{\partial t} + \rho \underline{v} \cdot \underline{\nabla} \underline{v} = -\underline{\nabla} p + \eta \nabla^2 \underline{v} - \rho \underline{g} \quad (2.17)$$

(i) for **liquid phase**, the general momentum conservation equations can be written as,

$$\rho \frac{\partial \hat{v}}{\partial t} + \rho \hat{v} \cdot \nabla \hat{v} = -\nabla \hat{p} + \nabla \cdot \left[\hat{\eta} \left(\nabla \hat{v} + (\nabla \hat{v})^T \right) - \frac{2}{3} (\nabla \cdot \hat{v}) \underline{I} \right] - \hat{\rho} \underline{g} \quad (2.18)$$

(ii) for **gas phase**, the general momentum conservation equations can be written as,

$$\rho \frac{\partial v}{\partial t} + \rho v \cdot \nabla v = -\nabla p + \nabla \cdot \left[\eta \left(\nabla v + (\nabla v)^T \right) - \frac{2}{3} (\nabla \cdot v) \underline{I} \right] - \rho \underline{g} \quad (2.19)$$

2.3.4 Energy Conservation Equations

Starting with the stationary differential volume through which a pure fluid is flowing, the conservation of energy for the fluid contained in the differential volume, can be written as [Kuo, 1986]

$$A = B + C + D + E \quad (2.20)$$

where, A = rate of accumulation of internal and kinetic energy,

B = net rate of influx of internal and kinetic energy by convection,

C = net rate of heat addition due to heat flux by conduction,

D = rate at which heat is added by the heat source and,

E = net rate of work done on the system by the surrounding, which includes the work done by body force and the total surface stress tensor ($\underline{\sigma}$) acting on the boundary of the control volume. So, the energy balance can be written down mathematically as

$$\frac{\partial}{\partial t} (\rho e) = -\nabla \cdot (\rho e \underline{v}) - \nabla \cdot \underline{q} + \dot{Q} + \underline{\sigma} : \nabla \underline{v} + \rho \sum_{i=1}^N Y_i \underline{f}_i \cdot \underline{V}_i \quad (2.21)$$

where, e is the specific internal energy, ρ is the mixture density of the fluid, \underline{v} is the mass-average velocity, \underline{q} is the heat flux due to conduction, \dot{Q} is the rate of heat generation, $\underline{\sigma}$ is the total stress tensor, Y_i is mass-fraction of the i^{th} species, \underline{f}_i is the external body force on the i^{th} species and, \underline{V}_i is the mass-diffusion velocity of the i^{th} species. Here, specific heat, C_p of the overall mixture at constant pressure is defined as

$C_p = \sum_{i=1}^N C_{p,i} Y_i$ and standard heat of formation, h^0 for the overall gas mixture is defined as $h^0 = \sum_{i=1}^N h_i^0 Y_i$ where, $C_{p,i}$ and h_i^0 are the specific heat at constant pressure and the

standard heat of formation at the reference temperature, T^0 respectively for the individual species. In general, the Mach number is well below unity for most of the combustion situations. Therefore, the flow work contribution ($\frac{p}{\rho}$) arising in the energy balance can be neglected. Therefore,

$$\begin{aligned}
 e &= h - \frac{p}{\rho} = \sum_{i=1}^N h_i^0 Y_i \\
 &= \sum_{i=1}^N \left[h_i^0 + \int_{T^0}^T C_{p,i} dT \right] Y_i \\
 &= \sum_{i=1}^N h_i^0 Y_i + \int_{T^0}^T \left(\sum_{i=1}^N C_{p,i} Y_i \right) dT \\
 &= h^0 + \int_{T^0}^T C_p dT
 \end{aligned} \tag{2.22}$$

$\dot{Q} = 0$ as there is no heat generation. Contributions of viscous dissipation and pressure work are also zero unless the Reynold's number for the flow is very high i.e. $\underline{\sigma} : \underline{\nabla} \underline{v} = 0$. The external body force (\underline{f}_i) is only due to gravity.

Therefore,

$$\rho \sum_{i=1}^N Y_i \underline{f}_i = -\rho \underline{g} \sum_{i=1}^N Y_i = -\rho \underline{g}$$

and since,

$$\begin{aligned}
 Y_i \underline{V}_i &= Y_i (\underline{v}_i - \underline{v}), \\
 \sum_{i=1}^N Y_i \underline{V}_i &= \sum_{i=1}^N Y_i \underline{v}_i - \sum_{i=1}^N \underline{v} = \underline{v} - \underline{v} = 0.
 \end{aligned}$$

So,

$$\rho \sum_{i=1}^N Y_i \underline{f}_i \cdot \underline{V}_i = \rho \left[-\underline{g} \cdot \sum_{i=1}^N Y_i \underline{V}_i \right] = 0$$

Now,

$$\begin{aligned}
 \underline{q} &= -\lambda \underline{\nabla} T + \rho \sum_{i=1}^N h_i Y_i \underline{V}_i \\
 &= -\lambda \underline{\nabla} T + \rho \sum_{i=1}^N Y_i \underline{V}_i \left(h_i^0 + \int_{T^0}^T C_{p,i} dT \right)
 \end{aligned} \tag{2.23}$$

The first term in Eq. 2.23 represents the heat flow due to conduction and the second term corresponds to the total enthalpy of all the species per unit area per unit time flowing relative to the mixture. This energy is carried across a surface when the average velocity of the i^{th} species differs from the mass average velocity of the mixture. Using the Eqs. 2.22 and 2.23 and all the above conditions, the Eq. 2.21 for energy balance can be written as

$$\frac{\partial}{\partial t} \left[\rho \left(h^0 + \int_{T^0}^T C_p dT \right) \right] + \underline{\nabla} \cdot \left[\rho \underline{v} \left(h^0 + \int_{T^0}^T C_p dT \right) + \rho \sum_{i=1}^N Y_i \underline{V}_i \left(h_i^0 + \int_{T^0}^T C_{p,i} dT \right) - \lambda \underline{\nabla} T \right] = 0$$

or,

$$\begin{aligned} \frac{\partial}{\partial t} \left[\rho \int_{T^0}^T C_p dT \right] + \underline{\nabla} \cdot \left[\rho \underline{v} \int_{T^0}^T C_p dT + \rho \sum_{i=1}^N Y_i \underline{V}_i \int_{T^0}^T C_{p,i} dT - \lambda \underline{\nabla} T \right] \\ = - \frac{\partial}{\partial t} \left[\rho \sum_{i=1}^N h_i^0 Y_i \right] - \underline{\nabla} \cdot \left[\rho \underline{v} \sum_{i=1}^N h_i^0 Y_i + \rho \sum_{i=1}^N Y_i \underline{V}_i h_i^0 \right] \\ = - \sum_{i=1}^N h_i^0 \left[\frac{\partial}{\partial t} (\rho Y_i) + \underline{\nabla} \cdot (\rho Y_i (\underline{V}_i + \underline{v})) \right] \end{aligned} \quad (2.24)$$

Using species Eq. 2.9, the above equation can be written as

$$\frac{\partial}{\partial t} \left[\rho \int_{T^0}^T C_p dT \right] + \underline{\nabla} \cdot \left[\rho \underline{v} \int_{T^0}^T C_p dT + \rho \sum_{i=1}^N Y_i \underline{V}_i \int_{T^0}^T C_{p,i} dT - \lambda \underline{\nabla} T \right] = - \sum_{i=1}^N h_i^0 \dot{\omega}_i \quad (2.25)$$

Using $C_p = \sum_{i=1}^N C_{p,i} Y_i$, the following simplification can be made:

$$\begin{aligned} \underline{\nabla} \int_{T^0}^T C_p dT &= \underline{\nabla} \int_{T^0}^T \sum_{i=1}^N C_{p,i} Y_i dT \\ &= \int_{T^0}^T \underline{\nabla} \left(\sum_{i=1}^N C_{p,i} Y_i \right) dT + \left(\sum_{i=1}^N C_{p,i} Y_i \right) \underline{\nabla} T \\ &= \left(\sum_{i=1}^N \underline{\nabla} Y_i \right) \int_{T^0}^T C_{p,i} dT + C_p \underline{\nabla} T \end{aligned}$$

or,

$$\sum_{i=1}^N -\underline{\nabla} Y_i \int_{T^0}^T C_{p,i} dT = -\underline{\nabla} \int_{T^0}^T C_p dT + C_p \underline{\nabla} T \quad (2.26)$$

using Fick's law of diffusion (eq.2.3),

$$\rho \sum_{i=1}^N \underline{V}_i Y_i \int_{T^0}^T C_{p,i} dT = -\rho D \underline{\nabla} \int_{T^0}^T C_p dT + \rho D C_p \underline{\nabla} T \quad (2.27)$$

Substituting the above expression (Eq. 2.27) in Eq. 2.25 yields the general equation for the conservation of energy as

$$\frac{\partial}{\partial t} \left[\rho \int_{T^0}^T C_p dT \right] + \nabla \cdot \left[\rho \underline{v} \left(\int_{T^0}^T C_p dT \right) - \rho D \nabla \left(\int_{T^0}^T C_p dT \right) + (\rho D C_p - \lambda) \nabla T \right] = - \sum_{i=1}^N h_i^0 \dot{\omega}_i \quad (2.28)$$

which for liquid and gas phases can be written as

(i) **liquid phase**

$$\frac{\partial}{\partial t} \left[\hat{\rho} \int_{\hat{T}^0}^{\hat{T}} \hat{C}_p d\hat{T} \right] + \nabla \cdot \left[\hat{\rho} \hat{\underline{v}} \left(\int_{\hat{T}^0}^{\hat{T}} \hat{C}_p d\hat{T} \right) - \hat{\rho} \hat{D} \nabla \left(\int_{\hat{T}^0}^{\hat{T}} \hat{C}_p d\hat{T} \right) + (\hat{\rho} \hat{D} \hat{C}_p - \hat{\lambda}) \nabla \hat{T} \right] = - \sum_{i=1}^N h_i^0 \dot{\omega}_i \quad (2.29)$$

(ii) **gas phase**

$$\frac{\partial}{\partial t} \left[\rho \int_{T^0}^T C_p dT \right] + \nabla \cdot \left[\rho \underline{v} \left(\int_{T^0}^T C_p dT \right) - \rho D \nabla \left(\int_{T^0}^T C_p dT \right) + (\rho D C_p - \lambda) \nabla T \right] = - \sum_{i=1}^N h_i^0 \dot{\omega}_i \quad (2.30)$$

2.4 Modeling for Multicomponent Fuel Droplet Combustion

For the present problem, it is assumed that a single multicomponent fuel droplet is burning in a hot quiescent atmosphere. The only flow that is generated in the gas phase is due to the evaporation velocity in the radial direction that arises due to the evaporation of fuels from the droplet surface. Since, there is no transverse flow in the gas phase, the shear stress at droplet surface is zero. Therefore, momentum transport within the droplet is completely absent. So, for the present study of multicomponent droplet burning, only mass transfer and heat transfer aspects are considered.

2.4.1 Liquid Phase

(i) **Species conservation equations**

Substituting the expression for diffusion velocity (\underline{V}_i) from Fick's law of diffusion, Eq. 2.3 into Eq. 2.7 and since there is no generation or consumption of species inside the liquid

droplet i.e. $\omega_i=0$ and also the mass average velocity, $\hat{u} = 0$ within the droplet, the species conservation equations for the liquid phase can be expressed as,

$$\frac{\partial (\hat{\rho} \hat{Y}_i)}{\partial t} - \nabla \cdot (\hat{\rho} \hat{D} \nabla \hat{Y}_i) = 0 \quad (2.31)$$

where i stands for the two species of fuels f1(fuel1) and f2(fuel2).

The above equation for fuel 1 and fuel 2 for spherically symmetric case, will be read as

$$\frac{\partial (\hat{Y}_{f1})}{\partial t} - \frac{\hat{D}}{r^2} \frac{\partial}{\partial r} \left(r^2 \frac{\hat{Y}_{f1}}{\partial r} \right) = 0 \quad (2.32a)$$

$$\frac{\partial (\hat{Y}_{f2})}{\partial t} - \frac{\hat{D}}{r^2} \frac{\partial}{\partial r} \left(r^2 \frac{\hat{Y}_{f2}}{\partial r} \right) = 0 \quad (2.32b)$$

(ii) Energy conservation equation

The properties including C_p for the liquid phase are constant. Therefore, the liquid phase conservation Eq. 2.29 can be rewritten by, first evaluating the definite integrals and then by simplifying the algebra as

$$\frac{\partial (\hat{\rho} \hat{C}_p \hat{T})}{\partial t} - \nabla \cdot (\hat{\lambda} \nabla \hat{T}) = 0 \quad (2.33)$$

Dividing both sides by $\hat{\rho} \hat{C}_p$, and writing for the spherically symmetric case,

$$\frac{\partial \hat{T}}{\partial t} - \frac{\hat{\alpha}}{r^2} \frac{\partial}{\partial r} \left(r^2 \frac{\partial \hat{T}}{\partial r} \right) = 0 \quad (2.34)$$

2.4.2 Gas Phase

(i) Species conservation equations

The species conservation Eq. 2.9 for the gas phase can be simplified in a manner similar to that adopted for the liquid phase, and by using the constant property assumption, it can be written as

$$\frac{\partial (\rho Y_i)}{\partial t} + \nabla \cdot (\rho \underline{u} Y_i - \rho D \nabla Y_i) = \dot{\omega}_i \quad (2.35)$$

for spherically symmetric case,

$$\frac{\partial Y_i}{\partial t} + \frac{1}{r^2} \frac{\partial}{\partial r} \left(r^2 v_r Y_i - r^2 D \frac{\partial Y_i}{\partial r} \right) = \frac{\dot{\omega}_i}{\rho} \quad (2.36)$$

where, i stands for fuel1($f1$), fuel2($f2$) and the oxidiser(x) for the gas phase. Replacing i by $f1$, $f2$ and x in Eq. 2.36 yields

$$\frac{\partial Y_{f1}}{\partial t} + \frac{1}{r^2} \frac{\partial}{\partial r} \left(r^2 v_r Y_{f1} - r^2 D \frac{\partial Y_{f1}}{\partial r} \right) = \frac{\dot{\omega}_{f1}}{\rho} \quad (2.37a)$$

$$\frac{\partial Y_{f2}}{\partial t} + \frac{1}{r^2} \frac{\partial}{\partial r} \left(r^2 v_r Y_{f2} - r^2 D \frac{\partial Y_{f2}}{\partial r} \right) = \frac{\dot{\omega}_{f2}}{\rho} \quad (2.37b)$$

$$\frac{\partial Y_x}{\partial t} + \frac{1}{r^2} \frac{\partial}{\partial r} \left(r^2 v_r Y_x - r^2 D \frac{\partial Y_x}{\partial r} \right) = \frac{\dot{\omega}_x}{\rho} \quad (2.37c)$$

It is assumed here that all the species produced during combustion are represented by one single product, p such that

$$\sum_{i=1}^N Y_i = Y_{f1} + Y_{f2} + Y_x + Y_p = 1$$

or,

$$Y_p = 1 - Y_{f1} - Y_{f2} - Y_x \quad (2.38)$$

Once Y_{f1} , Y_{f2} and Y_x are solved by the three species Eqs. 2.37a,b,c, the average mass-fraction for the product can be obtained from the above relation.

(ii) **Energy conservation equation**

The gas phase energy Eq. 2.30 is

$$\frac{\partial}{\partial t} \left[\rho \int_{T^0}^T C_p dT \right] + \underline{\nabla} \cdot \left[\rho \underline{v} \left(\int_{T^0}^T C_p dT \right) - \rho D \underline{\nabla} \left(\int_{T^0}^T C_p dT \right) + (\rho D C_p - \lambda) \underline{\nabla} T \right] = - \sum_{i=1}^N h_i^0 \dot{\omega}_i$$

Using spherical symmetry,

$$\begin{aligned} \frac{\partial}{\partial t} \left[\int_{T^0}^T C_p dT \right] + \frac{1}{r^2} \frac{\partial}{\partial r} \left[r^2 v_r \left(\int_{T^0}^T C_p dT \right) - D r^2 \frac{\partial}{\partial r} \left(\int_{T^0}^T C_p dT \right) + r^2 \left(D C_p - \frac{\lambda}{\rho} \right) \frac{\partial T}{\partial r} \right] \\ = - \frac{1}{\rho} \left(\sum_{i=1}^N h_i^0 \dot{\omega}_i \right) \end{aligned} \quad (2.39)$$

2.4.3 Boundary Conditions

Two factors control or influence any physical system. They include the processes within the system, as well as the interaction of the system with it's surrounding. So, unless the boundary conditions are properly specified or implemented, the analysis of any physical system remains incomplete. The physical system chosen for the present problem includes both liquid and gas phases. The balance of species, mass and energy fluxes at the interface of the liquid and the gas phases lead to the coupling conditions between the two phases. The coupling parameters are, obviously, functions of time. The boundary condition at the droplet centre is obtained from the condition of symmetry. The condition of symmetry signifies that there is no transfer of species or energy across the droplet centre. The boundary conditions at the outer boundary of the gas phase solution domain come from free stream conditions.

(a) **Droplet centre** ($r = 0$) : Using the condition of symmetry at the droplet centre, boundary conditions can be written as

$$\frac{\partial \hat{Y}_{f1}}{\partial r} = 0 \quad (2.40a)$$

$$\frac{\partial \hat{Y}_{f2}}{\partial r} = 0 \quad (2.40b)$$

$$\frac{\partial \hat{T}}{\partial r} = 0 \quad (2.40c)$$

(b) **Interface of liquid and gas phases i.e. Droplet surface** ($r = 1$)

(i) *mass balance:*

In absence of any flow in θ or, ϕ direction, all the tangential velocity and shear stress components at the liquid- gas interface are zero. The radial flow, which is generated in the gas phase due to the surface regression of the liquid droplet, is the only component of velocity that prevails in the gas phase. Therefore, if we neglect the value of ρ in comparison to $\hat{\rho}$ because $\hat{\rho} \gg \rho$, the mass -balance at the interface, at a given time gives rise to the condition

$$\rho u_d = -\hat{\rho} \hat{u}_d = -\hat{\rho} \frac{dr_d}{dt} \quad (2.41)$$

where r_d is the droplet radius at the given instant, $\hat{u}_d \left(\frac{dr_d}{dt} \right)$ is the droplet regression rate, u_d the evaporation velocity of the evaporating fuel vapour at the droplet surface at that given instant. Through out the thesis, the positive value of \hat{u}_d is always used. Therefore whenever \hat{u}_d is used in equations, this information is kept in mind.

(ii) species balance

In both the phases, species are transported due to both convection as well as diffusion. Therefore, species flux, \underline{n}_i for the i^{th} species in the gas phase is given as

$$\underline{n}_i = \rho_i \underline{v} + \underline{j}_i \quad (2.42)$$

where, $\rho_i \underline{v}$ is the convective component and \underline{j}_i is the diffusive component of the species flux, \underline{v} is the bulk velocity and ρ_i is the density for the i^{th} species. For the present problem, since there is only radial component, the above expression becomes

$$n_{i,r} = \rho_i v_r + j_{i,r}$$

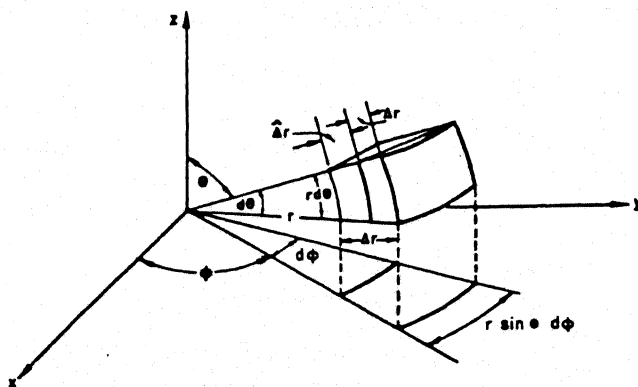
where, $j_{i,r} = \rho_i V_{i,r} = \rho Y_i V_{i,r} = -\rho D \frac{\partial Y_i}{\partial r}$ (using Fick's law)

or,

$$n_{i,r} = \rho Y_i v_r - \rho D \frac{\partial Y_i}{\partial r} \quad (2.43)$$

Similarly, for the liquid phase,

$$\hat{n}_{i,r} = \hat{\rho} \hat{Y}_i \hat{v}_r - \hat{\rho} \hat{D} \frac{\partial \hat{Y}_i}{\partial r} \quad (2.44)$$



Elemental volume in spherical coordinates

Consider a differential volume (as shown above) . $r^2 d\theta \sin\theta d\phi dr$ in the spherical

polar coordinates (see Fig. 2.2). The net efflux of the species i in r -direction is

$$\begin{aligned}
 &= \left[n_{i,r} \big|_{r+\Delta r} - \hat{n}_{i,r} \big|_{r-\Delta r} \right] r^2 \sin\theta \, d\theta d\phi \\
 &= \left[\left(\rho Y_i v_r - \rho D \frac{\partial Y_i}{\partial r} \right) - \left(\hat{\rho} \hat{Y}_i \hat{v}_r - \hat{\rho} \hat{D} \frac{\partial \hat{Y}_i}{\partial r} \right) \right] r^2 \sin\theta \, d\theta d\phi
 \end{aligned}$$

Now, efflux + storage = production. In the limiting case, as $\Delta r \rightarrow 0$ and $\Delta \hat{r} \rightarrow 0$, the control volume approaches a control surface. Assuming that the storage and production of species are zero at the interface, the expression for the net efflux of species i can be expressed as

$$\left[\left(\rho Y_i v_r - \rho D \frac{\partial Y_i}{\partial r} \right) \bigg|_{r=r_d} - \left(\hat{\rho} \hat{Y}_i \hat{v}_r - \hat{\rho} \hat{D} \frac{\partial \hat{Y}_i}{\partial r} \right) \bigg|_{r=r_d} \right] r^2 \sin\theta \, d\theta d\phi = 0$$

or,

$$r^2 \sin\theta \, d\theta d\phi \rho \left(Y_i v_r - D \frac{\partial Y_i}{\partial r} \right) \bigg|_{r=r_d} = \hat{\rho} \left(\hat{Y}_i \hat{v}_r - \hat{D} \frac{\partial \hat{Y}_i}{\partial r} \right) \bigg|_{r=r_d} r^2 \sin\theta \, d\theta d\phi \quad (2.45)$$

The L.H.S. of the above expression is the species flux, \dot{m}_i for the i^{th} component at the gas side interface and R.H.S. is the species flux, $\hat{\dot{m}}_i$ for the i^{th} component at the liquid side interface. Since, there is no production or storage at the interface,

$$\hat{\dot{m}}_i = \dot{m}_i \quad (2.46)$$

Thus, by physical analysis also, one can arrive at the same expression (see Eq. 2.45) for species conservation. Rewriting the species flux, \dot{m}_i for the gas phase,

$$r^2 \sin\theta \, d\theta d\phi \rho v_r \left[Y_i - \frac{D}{v_r} \frac{\partial Y_i}{\partial r} \right]_{r=r_d} = \dot{m}_i \quad (2.47)$$

Since, $v_r = u_d$ and $Y_i = Y_{is}$ at $r = r_d$,

$$r^2 \sin\theta \, d\theta d\phi \rho u_d \left[Y_{is} - \frac{D}{u_d} \frac{\partial Y_i}{\partial r} \right]_{r=r_d} = \dot{m}_i$$

Again, $\dot{m} = r^2 \sin\theta \, d\theta d\phi \rho u_d$ = total mass evaporation rate. So,

$$Y_{is} - \frac{D}{u_d} \frac{\partial Y_i}{\partial r} \bigg|_{r=r_d} = \frac{\dot{m}_i}{\dot{m}} = \epsilon_i (\text{say}) \quad (2.48)$$

Final expression for gas side species conservation equation can be written as

$$\left. \frac{\partial Y_i}{\partial r} \right|_{r=r_d} + \frac{u_d}{D} (\epsilon_i - Y_{is}) = 0 \quad (2.49)$$

where, i stands for fuel1 ($f1$), fuel2 ($f2$) and oxidiser (x) of the gas phase and ϵ_i is called the fractional mass-gasification rate for the i^{th} species. So, **gas side species boundary conditions** for different species can be written as

$$\left. \frac{\partial Y_{f1}}{\partial r} \right|_{r=r_d} + \frac{u_d}{D} (\epsilon_{f1} - Y_{f1s}) = 0 \quad (2.50a)$$

$$\left. \frac{\partial Y_{f2}}{\partial r} \right|_{r=r_d} + \frac{u_d}{D} (\epsilon_{f2} - Y_{f2s}) = 0 \quad (2.50b)$$

$$\left. \frac{\partial Y_x}{\partial r} \right|_{r=r_d} + \frac{u_d}{D} (-Y_{xs}) = 0 \quad (2.50c)$$

Similarly, the **liquid side species boundary conditions** for different species can be written as

$$\left. \frac{\partial \hat{Y}_{f1}}{\partial r} \right|_{r=r_d} + \frac{\hat{u}_d}{\hat{D}} (\epsilon_{f1} - \hat{Y}_{f1s}) = 0 \quad (2.51a)$$

$$\left. \frac{\partial \hat{Y}_{f2}}{\partial r} \right|_{r=r_d} + \frac{\hat{u}_d}{\hat{D}} (\epsilon_{f2} - \hat{Y}_{f2s}) = 0 \quad (2.51b)$$

Here ϵ_{f1} and ϵ_{f2} represents the fractional mass gasification rates for fuel 1 and fuel 2 respectively.

(iv) heat balance

In evaluating the overall heat balance at the liquid-gas interface, we find that in absence of any storage or production of energy at the interface, the total amount of heat available from the gas phase is used up for droplet heating as well as for fuel evaporation at the droplet surface. Therefore, the heat balance at the interface can be written as

$$\lambda \left. \frac{\partial T}{\partial r} \right|_{r=r_d} = \hat{\lambda} \left. \frac{\partial \hat{T}}{\partial r} \right|_{r=r_d} + \rho u_d \sum_{i=1}^N \epsilon_i L_i \quad (2.52)$$

where, ρ is the mixture density for the gas phase, u_d is the evaporation velocity, ϵ_i and L_i are respectively the fractional mass-gasification rate and the latent heat of vaporization for

the i^{th} species, λ and $\hat{\lambda}$ are the thermal conductivities for the gas phase and liquid phase respectively.

(v) phase equilibrium at interface

For the present problem, the component in the liquid phase are assumed to form a miscible mixture. For a miscible mixture, the vapour pressure (P_{is}) of species i depends on it's liquid phase mole fraction (\hat{X}_{is}) and on it's vapour pressure, p_{is}^0 when it is pure [Law, 1982]. It is assumed that the molecular structure for the liquid phase constituents are sufficiently similar. In such a case, the mixture can be assumed to be ideal so that the Raoult's Law remains valid. Therefore,

$$P_{is} = \hat{X}_{is} P_{is}^0$$

or,

$$X_{is} = \hat{X}_{is} X_{is}^0 \quad (2.53)$$

where, X_{is} is the mole fraction for the i^{th} species on the gas phase side and X_{is}^0 is the concentration for the i^{th} species on the gas phase side when that species is pure. Now, X_{is}^0 is given by Clausius-Clapeyron relation as

$$X_{is}^0(T_s) = \frac{P_n}{P} \exp \left\{ \frac{L_i W_i}{R_u} \left(\frac{1}{T_{bi}} - \frac{1}{T_s} \right) \right\} \quad (2.54)$$

where, T_s is the surface temperature, T_{bi} is the normal boiling point evaluated at the normal atmospheric pressure, P_n , P is the prevailing system pressure and W_i and L_i are the molecular weight and latent heat of vaporization respectively for the i^{th} species, and R_u is the universal gas constant. Three fundamental assumptions are involved in Eq. 2.54. Firstly, the gas near the liquid surface is ideal. Secondly, the vapour pressure of the fuel is not affected by the presence of any other species. Finally, finite mass-transfer rate at the droplet surface has negligible influence on the equilibrium condition. Now, by using the Raoult's Law and the Clausius-Clapeyron relation, the gas side surface mole fractions for the two fuels can be expressed as

$$X_{f1s} = \hat{X}_{f1s} \exp \left[\frac{W_{f1} L_{f1}}{R_u} \left(\frac{1}{T_{bf1}} - \frac{1}{T_s} \right) \right] \quad (2.55)$$

$$X_{f2s} = \hat{X}_{f2s} \exp \left[\frac{W_{f2} L_{f2}}{R_u} \left(\frac{1}{T_{bf2}} - \frac{1}{T_s} \right) \right] \quad (2.55b)$$

(c) Outer boundary of the gas phase domain ($r \rightarrow \infty$)

This outer boundary of the gas phase domain is far away from the reaction zone. Therefore, there is no influence of combustion at this boundary. So, it can be safely assumed that the free stream conditions prevail at the outer boundary. Therefore, the boundary conditions at $r \rightarrow \infty$ can be written as

$$T = T_\infty \quad (2.56a)$$

$$Y_{f1} = 0, \quad (2.56b)$$

$$Y_{f2} = 0, \quad (2.56c)$$

$$Y_x = Y_{x,\infty} \quad (2.56d)$$

where the subscript, ∞ refers to the free stream conditions.

2.4.4 Initial Conditions

When micron-size droplets are sprayed into the combustion chamber, combustion can start in two ways. When the initial temperature of the combustion chamber is high (e.g. 1000 K) and uniform, combustion will start near the droplet surface where the stoichiometric ratio of the fuel and the oxidiser is prevalent. Combustion may also start at a fixed point by supplying high temperature spark (>1500 K) at that point in an otherwise normal ambient (300 K) atmosphere. Initially, the gas phase is completely devoid of any of the fuels. Also, the initial mass-fraction profiles, as well as the temperature profile for the liquid phase are uniform. Therefore, the initial conditions for both the liquid and the gas phases can be expressed as

(a) Liquid phase

$$\hat{T}(r, 0) = \hat{T}_{in}, \quad (2.57a)$$

$$\hat{Y}_{f1}(r, 0) = \hat{Y}_{in,f1}, \quad (2.56b)$$

$$\hat{Y}_{f2}(r, 0) = \hat{Y}_{in,f2} \quad (2.57c)$$

(b) Gas phase

$$T(r, 0) = T_{in}, \quad (2.58a)$$

$$Y_{f1}(r, 0) = Y_{in,f1}, \quad (2.58b)$$

$$Y_{f2}(r, 0) = Y_{in,f2}, \quad (2.58c)$$

$$Y_x(r, 0) = Y_{in,x} \quad (2.58d)$$

Present study uses both of the above mentioned methods for starting ignition.

2.4.5 Non-dimensionalization

Non-dimensionalization of the governing differential equations clearly reveals the relative importance of the various aspects of the transport processes. This gives rise to some very important non-dimensional quantities, such as, Schmidt number, Prandtl number, Lewis number etc. Schmidt number indicates the relative importance of species diffusion over viscous diffusion, Prandtl number indicates the relative importance of heat diffusion over viscous diffusion and Lewis number indicates the effect of heat transfer over mass transfer. Non-dimensional quantities related to the present problem are indicated by the asterisk (*) mark as

$$\begin{aligned} D^* &= \frac{D}{D_\infty}, \quad L_i^* = \frac{L_i}{\Delta h}, \quad C_p^* = \frac{C_p}{C_{p,\infty}}, \\ \lambda^* &= \frac{\lambda}{\lambda_\infty}, \quad r^* = \frac{r}{r_d}, \quad \nabla^* = \frac{1}{r_d} \nabla, \quad t^* = \int_0^t \frac{D_\infty}{r_d^2(t)} dt', \\ u_d^* &= \frac{u_d}{\eta_\infty / (\rho_\infty r_d)}, \quad T^* = \frac{T}{\Delta h / C_{p,\infty}}, \quad Sc = \frac{\eta_\infty}{\rho_\infty D_\infty}, \\ Pr &= \frac{\eta_\infty C_{p,\infty}}{\lambda_\infty}, \quad Le = \frac{Sc}{Pr}, \quad \hat{D}^* = \frac{\hat{D}}{D_\infty}, \\ \hat{\lambda}^* &= \frac{\hat{\lambda}}{\lambda_\infty}, \quad \hat{C}_p^* = \frac{\hat{C}_p}{C_{p,\infty}}, \quad \hat{u}_d^* = \frac{\hat{u}_d}{\eta_\infty / (\rho_\infty r_d)}, \\ x^* &= \frac{x}{r_d}, \quad y^* = \frac{y}{r_d}, \quad z^* = \frac{z}{r_d} \end{aligned} \quad (2.59)$$

For the sake of convenience, from now onwards, the asterisk (*) mark will be omitted if otherwise not mentioned.

Using the above parameters, the governing differential eqs. 2.32, 2.34, 2.37 and 2.39, the boundary conditions given by Eqs. 2.40, 2.41, 2.50, 2.51, 2.52, 2.55 and 2.56, and

initial conditions given by Eqs. 2.57 and 2.58 can be nondimensionalized and the following equations are obtained.

A. Non-Dimensional Governing Differential Equations

(a) Liquid phase

$$\frac{\partial \hat{Y}_{f1}}{\partial t} + \frac{\rho}{\hat{\rho}} r Sc u_d \frac{\partial \hat{Y}_{f1}}{\partial r} - \frac{\hat{D}}{r^2} \frac{\partial}{\partial r} \left(r^2 \frac{\partial \hat{Y}_{f1}}{\partial r} \right) = 0 \quad (2.60a)$$

$$\frac{\partial \hat{Y}_{f2}}{\partial t} + \frac{\rho}{\hat{\rho}} r Sc u_d \frac{\partial \hat{Y}_{f2}}{\partial r} - \frac{\hat{D}}{r^2} \frac{\partial}{\partial r} \left(r^2 \frac{\partial \hat{Y}_{f2}}{\partial r} \right) = 0 \quad (2.60b)$$

$$\frac{\partial \hat{T}}{\partial t} + \frac{\rho}{\hat{\rho}} r Sc u_d \frac{\partial \hat{T}}{\partial r} - \frac{Le \hat{\alpha}}{r^2} \frac{\partial}{\partial r} \left(r^2 \frac{\partial \hat{T}}{\partial r} \right) = 0 \quad (2.60c)$$

(b) Gas phase

$$\frac{\partial Y_{f1}}{\partial t} + \frac{\rho}{\hat{\rho}} r Sc u_d \frac{\partial Y_{f1}}{\partial r} + \frac{Sc}{r^2} \frac{\partial}{\partial r} (r^2 v_r Y_{f1}) - \frac{D}{r^2} \frac{\partial}{\partial r} \left(r^2 \frac{\partial Y_{f1}}{\partial r} \right) = \frac{\dot{\omega}_{f1}}{\rho} \frac{r_d^2}{\rho_\infty D_\infty} \quad (2.61a)$$

$$\frac{\partial Y_{f2}}{\partial t} + \frac{\rho}{\hat{\rho}} r Sc u_d \frac{\partial Y_{f2}}{\partial r} + \frac{Sc}{r^2} \frac{\partial}{\partial r} (r^2 v_r Y_{f2}) - \frac{D}{r^2} \frac{\partial}{\partial r} \left(r^2 \frac{\partial Y_{f2}}{\partial r} \right) = \frac{\dot{\omega}_{f2}}{\rho} \frac{r_d^2}{\rho_\infty D_\infty} \quad (2.61b)$$

$$\frac{\partial Y_x}{\partial t} + \frac{\rho}{\hat{\rho}} r Sc u_d \frac{\partial Y_x}{\partial r} + \frac{Sc}{r^2} \frac{\partial}{\partial r} (r^2 v_r Y_x) - \frac{D}{r^2} \frac{\partial}{\partial r} \left(r^2 \frac{\partial Y_x}{\partial r} \right) = \frac{\dot{\omega}_x}{\rho} \frac{r_d^2}{\rho_\infty D_\infty} \quad (2.61c)$$

$$\begin{aligned} \frac{\partial (\rho Y_T)}{\partial t} + \frac{\rho}{\hat{\rho}} r Sc u_d \frac{\partial (\rho Y_T)}{\partial r} + \frac{Sc}{r^2} \frac{\partial}{\partial r} (r^2 v_r (\rho Y_T)) - \frac{D}{r^2} \frac{\partial}{\partial r} \left(r^2 \frac{\partial (\rho Y_T)}{\partial r} \right) \\ + \frac{1}{r^2} \frac{\partial}{\partial r} \left((\rho D C_p - \lambda Le) r^2 \frac{\partial T}{\partial r} \right) = - \frac{r_d^2}{\rho_\infty D_\infty} \frac{1}{\Delta h} \sum_{i=1}^N h_i^0 \dot{\omega}_i \end{aligned} \quad (2.61d)$$

where $Y_T = \int_{T_0}^T C_p dT$.

B. Non-Dimensional Boundary Conditions

(a) Droplet centre ($r = 0$)

$$\frac{\partial \hat{Y}_{f1}}{\partial r} = 0, \quad (2.62a)$$

$$\frac{\partial \hat{Y}_{f2}}{\partial r} = 0, \quad (2.62b)$$

$$\frac{\partial \hat{T}}{\partial r} = 0 \quad (2.62c)$$

(b) Droplet surface ($r = 1$)

(i) mass balance

$$\rho u_d = -\hat{\rho} \hat{u}_d = -\hat{\rho} \frac{dr_d}{dt} \quad (2.63)$$

(ii) *gas side species balance*

$$\left. \frac{\partial Y_{f1}}{\partial r} \right|_{r=1} + \frac{u_d S c}{D} (\epsilon_{f1} - Y_{f1s}) = 0 \quad (2.64a)$$

$$\left. \frac{\partial Y_{f2}}{\partial r} \right|_{r=1} + \frac{u_d S c}{D} (\epsilon_{f2} - Y_{f2s}) = 0 \quad (2.64b)$$

$$\left. \frac{\partial Y_x}{\partial r} \right|_{r=1} + \frac{u_d S c}{D} (-Y_{xs}) = 0 \quad (2.64c)$$

(iii) *liquid side species balance*

$$\left. \frac{\partial \hat{Y}_{f1}}{\partial r} \right|_{r=1} + \frac{\hat{u}_d S c}{\hat{D}} (\epsilon_{f1} - \hat{Y}_{f1s}) = 0 \quad (2.65a)$$

$$\left. \frac{\partial \hat{Y}_{f2}}{\partial r} \right|_{r=1} + \frac{\hat{u}_d S c}{\hat{D}} (\epsilon_{f2} - \hat{Y}_{f2s}) = 0 \quad (2.65b)$$

(iv) *heat balance*

$$\lambda \left. \frac{\partial T}{\partial r} \right|_{r=1} = Pr \rho u_d \sum_{i=1}^N \epsilon_i L_i + \hat{\lambda} \left. \frac{\partial \hat{T}}{\partial r} \right|_{r=1} \quad (2.66)$$

(v) *phase equilibrium at interface*

$$X_{f1s} = \hat{X}_{f1s} \exp \left[\beta_{f1} \left(\frac{1}{T_{bf1}} - \frac{1}{T_s} \right) \right] \quad (2.67a)$$

$$X_{f2s} = \hat{X}_{f2s} \exp \left[\beta_{f2} \left(\frac{1}{T_{bf2}} - \frac{1}{T_s} \right) \right] \quad (2.67b)$$

where,

$$\beta_{f1} = \frac{W_{f1} L_{f1} C_{p,\infty}}{R_u} \quad \text{and,} \quad \beta_{f2} = \frac{W_{f2} L_{f2} C_{p,\infty}}{R_u} \quad (2.67c)$$

(c) **At outer boundary ($r \rightarrow \infty$)**

$$T = T_{\infty}, \quad (2.68a)$$

$$Y_{f1} = 0 \quad (2.68b)$$

$$Y_{f2} = 0 \quad (2.68c)$$

$$Y_x = Y_{x,\infty} \quad (2.68d)$$

C. Non-Dimensional Initial Conditions

(a) Liquid phase

$$\hat{T}(r, 0) = \hat{T}_{in}, \quad (2.69a)$$

$$\hat{Y}_{f1}(r, 0) = \hat{Y}_{in,f1}, \quad (2.69b)$$

$$\hat{Y}_{f2}(r, 0) = \hat{Y}_{in,f2} \quad (2.69c)$$

(b) Gas phase

$$T(r, 0) = T_{in} \quad (2.70a)$$

$$Y_{f1}(r, 0) = Y_{in,f1} \quad (2.70b)$$

$$Y_{f2}(r, 0) = Y_{in,f2} \quad (2.70c)$$

$$Y_x(r, 0) = Y_{in,x} \quad (2.70d)$$

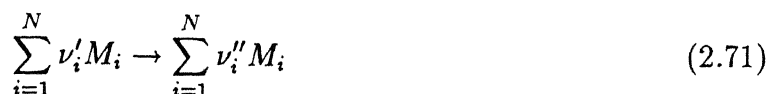
2.5 Thermo-chemistry

Chemistry involved in any combustion process is practically very very complicated. Though, the reactions here are represented by a single step global reaction, the factual chemical reactions are almost infinite in number before the final products are generated. Therefore, whatever simplified model one may select, the knowledge of **heat of reaction** and **rate of chemical reaction** are essential.

2.5.1 Heat of Reaction

The science of thermo-chemistry is concerned with the energy change associated with chemical reaction or in other words, it deals with the conversion of chemical energy into heat energy and vice-versa. A chemical reaction is merely a recombination of elements to form new products. This reaction may be endothermic or exothermic, depending on whether heat is being absorbed or released in the reaction. Obviously, a combustion process is necessarily exothermic. There are a number of ways in which heat of reaction can be defined or measured. In general, the heat of reaction is defined as the energy released by the system when the products are restored to the same temperature as that of the

reactants. This amount depends on reactant temperature and the variation of the system pressure. It is customary to measure the heat released at standard atmospheric pressure. For a general chemical reaction involving N species can be written as



The heat of reaction equals the change in enthalpy of the system under constant pressure.

It is calculated from heat of formation of the reactants and the products as

$$\Delta h = \sum_{i=1}^N \nu_i'' h_i^0 - \sum_{i=1}^N \nu_i' h_i^0 \quad (2.72)$$

at standard state at T_0 where h_i^0 = heat of formation of species, i , at temperature, T^0 , ν_i' and ν_i'' = stoichiometric coefficients of reactants and products respectively, M_i = arbitrary specification of chemical species. The heat of formation, h_i of a species i at any temperature T , is defined as the enthalpy of the substance relative to that of its constituents elements at the same temperature. It is to be noted here that the heat of reaction is used to find out the ADIABATIC FLAME TEMPERATURE. If a combustion process takes place adiabatically such that there is no work or change in kinetic or potential energy then for such a process, the temperature of the products is referred to as the adiabatic flame temperature. This is the maximum temperature that can be achieved ideally for given reactants. This is because any heat transfer from the reacting substances and any incomplete combustion would tend to lower the temperature of the products. This adiabatic temperature can be controlled with the amount of excess air used for combustion.

2.5.2 Chemical Kinetics

It is that part of chemical science that deals with the quantitative study of the rates of chemical reactions and the factors upon which they depend. It also deals with the interpretation of the empirical kinetic laws in terms of reaction mechanisms. All chemical reactions take place at a definite rate, depending on concentration, temperature, pressure catalyst etc. For a general combustion reaction involving N species such as given by Eq

2.71, the individual rate of reaction ($\dot{\omega}_i$) may be expressed as the rate of decrease of concentration (or, consumption) of a reactant i in moles/ m^3 /sec as

$$\dot{\omega}_i = -(\nu'_i - \nu''_i)\dot{\omega} \quad (2.73)$$

where, $\dot{\omega}$ is the overall reaction rate for the above reaction. From conservation of mass,

$$\sum_{i=1}^N \dot{\omega}_i = 0 \quad (2.74)$$

The law of mass action states that the rate of disappearance of a chemical species is proportional to the products of the concentrations of the reacting chemical species, each concentration being raised to a power equal to the corresponding stiochiometric coefficients. Thus the reaction rate for a combustion reaction is given as (Kuo, 1986)

$$\dot{\omega} = K \prod_{i=1}^M (C_{Mi})^{\nu'_i} \quad (2.75)$$

where, M is the number of reacting species and K is the proportionality constant known as the specific reaction rate constant with a strong temperature dependence. The above relation is valid only for simple reactions. But for complex reactions represented by a single step, the above relation can also be used to serve the practical purpose. In such a case ν'_i is known as the order of reaction. This order of reaction is understood to be the number of colliding particles which participate at the molecular level. For a simple gas phase reaction taking place at a normal pressure, the order of reaction is not expected to be more than 2. The specific rate constant, K , can be estimated from Arrhenius equation as (Kuo, 1986)

$$K = AT^\alpha \exp\left(-\frac{E}{R_u T}\right) \quad (2.76)$$

where, E is known as the activation energy, α and A are constants, α lies between 0 and 1, E/R indicates the temperature below which K is small. This law reveals the fact that only those molecules which have sufficient energy to overcome the opposing activation energy (E) and approach each other from preferred directions can participate in the combustion reaction. Here we see that this generation term ($\dot{\omega}$) is highly non-linear which makes the proper analysis of combustion process quite difficult.

ENTRAL LIBRARY
I. I. T., KANPUR

No. A 123594

2.5.3 Dissociation Reactions

At high temperature, dissociation of the products becomes very important, as it brings down the flame temperature in practical situations. The dissociation reactions are represented as



$$K_{p1} = \frac{P_{CO}P_{O_2}^{\frac{1}{2}}}{P_{CO_2}} \quad (2.79)$$

$$K_{p2} = \frac{P_{H_2}P_{O_2}^{\frac{1}{2}}}{P_{H_2O}} \quad (2.80)$$

Where, K_{p1} and K_{p2} are the two equilibrium constants for the above two reactions which are functions of temperature (Kuo, 1986). Considering the reaction for fuel, ν_{CO_2f1} , ν_{COf1} , ν_{O_2f1} , ν_{H_2Of1} , ν_{H_2f1} are the stoichiometric coefficients. They are dependent on the equilibrium constants and also on the type of fuel being burnt.

$$\nu_{Tf1} = \nu_{CO_2f1} + \nu_{COf1} + \nu_{O_2f1} + \nu_{H_2Of1} + \nu_{H_2f1} \quad (2.81)$$

Relations for K_{p1} and K_{p2} can be simplified to yield

$$K_{p1} = \left[\frac{\nu_{COf1}}{\nu_{CO_2f1}} \right] \left[\frac{\nu_{O_2f1}}{\nu_{Tf1}} \right]^{1/2} \quad (2.82)$$

$$K_{p2} = \left[\frac{\nu_{H_2f1}}{\nu_{H_2Of1}} \right] \left[\frac{\nu_{O_2f1}}{\nu_{Tf1}} \right]^{1/2} \quad (2.83)$$

$$7\nu_{f1} = \nu_{COf1} + \nu_{CO_2f1} \quad (2.84)$$

$$2\nu_{xf1} = 2\nu_{O_2f1} + \nu_{COf1} + \nu_{CO_2f1} + \nu_{H_2Of1} \quad (2.85)$$

$$16\nu_{f1} = 2\nu_{H_2Of1} + 2\nu_{H_2f1} \quad (2.86)$$

Solving Eqs. 2.81 through 2.86 by Newton-Raphson iterative scheme, the stoichiometric coefficients corresponding to different temperatures, can be determined.

2.6 Closure

This chapter deals with the modeling of spray combustion. The governing differential equations, the boundary conditions and the initial conditions in the nondimensional form for liquid and gas phases are given by Eqs. 2.60 through 2.70 which need to be solved for determining the mass fractions of the fuels f_1 and f_2 in the liquid and gas phases and that of oxidant in the gas phase. The temperature time history can also be determined.

Chapter 3

Semi Analytical Solution

3.1 Introduction

In practical situations, atomised fuel droplets are generally very small in size. In such a case, when they are sprayed into a combustion chamber, they move with velocities almost equal to that of the gas. Keeping such situations in mind, present study stresses upon the study of transient burning for a multicomponent single droplet fuel in an otherwise quiescent atmosphere. The initial radius of the droplet is of the order of 100 microns. The fuel is atomised and injected into the combustion chamber in a fairly hot (1000 K) atmosphere. There is no generation of species inside the droplet. Therefore, the net mass transfer inside the droplet is zero. The spray is assumed to be dilute in nature, so that the burning of one single droplet is not influenced by the presence of the neighbouring droplets. Stress is also put on the multicomponent aspect of droplet burning. Though the neglect of the external flow as well as the influence of neighbouring droplets is not physically realistic, it still gives enough physical insight into the fundamental aspects of multicomponent fuel burning. These two above mentioned major assumptions do not affect the fundamental aspects of fuel burning in general. A schematic diagram of such a droplet burning in a quiescent atmosphere is shown in fig. 2.1. Since, there is no external flow around the droplet and hence, the evaporation of fuel vapour at the droplet surface is only radial, the combustion process becomes symmetric in θ and ϕ directions. So, the process becomes a function of radial distance (r) and time (t) only. A coordinate system (r), fixed to the droplet centre, is considered here. In absence of any external flow, the droplet surface as well as the surrounding flame remain spherical. There is an inherent tendency of the droplet to remain spherical when the size of the droplet is very small. Due to continuous evaporation, the droplet surface regresses continually giving rise to a moving boundary. When the stationary coordinate is transformed into moving coordinate such that the droplet surface always remains at $r=1$, this moving boundary gives rise to a convective term in the liquid phase transport equations. For the present study, transient feature of liquid phase species and energy equations are retained, while the gas phase is

ned to be quasi-steady because, any change in the gas phase occurs in a much smaller time-scale compared to that for the liquid phase. Properties for both the phases are taken to be constants. The combustion takes place at normal atmospheric pressure and the liquid fuel has two species. The phenomenon of micro-explosion is not considered here. The assumptions of thin flame and unit Lewis number for the gas phase are retained. Dissociation of the products at high temperature near the flame is neglected. Schvab-Zeldovich variables (to be described later) were incorporated to eliminate the non-linear generation term ($\dot{\omega}$) in the gas phase. The quasi-steady gas phase is solved analytically. The free stream conditions are applied at the outer boundary of the gas phase domain. The liquid phase equations are solved in a semi-analytical manner. The general solution for the liquid phase equations is constructed in a series form for each discrete time step Δt , assuming that the gradients at the droplet surface remains constant over this time period Δt . Then the overall solution is obtained in a quasi-linearized form using superposition principle.

3.2 Mathematical Formulation

For the liquid phase ($r < 1$), Eqs.2.60a,b,c are :

$$\frac{\partial \hat{Y}_{f1}}{\partial t} + \frac{\rho}{\hat{\rho}} r Sc u_d \frac{\partial \hat{Y}_{f1}}{\partial r} - \frac{\hat{D}}{r^2} \frac{\partial}{\partial r} \left(r^2 \frac{\partial \hat{Y}_{f1}}{\partial r} \right) = 0 \quad (3.1a)$$

$$\frac{\partial \hat{Y}_{f2}}{\partial t} + \frac{\rho}{\hat{\rho}} r Sc u_d \frac{\partial \hat{Y}_{f2}}{\partial r} - \frac{\hat{D}}{r^2} \frac{\partial}{\partial r} \left(r^2 \frac{\partial \hat{Y}_{f2}}{\partial r} \right) = 0 \quad (3.1b)$$

$$\frac{\partial \hat{T}}{\partial t} + \frac{\rho}{\hat{\rho}} r Sc u_d \frac{\partial \hat{T}}{\partial r} - \frac{Le \hat{\alpha}}{r^2} \frac{\partial}{\partial r} \left(r^2 \frac{\partial \hat{T}}{\partial r} \right) = 0 \quad (3.1c)$$

Now, using $\hat{Y}_{f1}^* = \frac{\hat{Y}_{f1}}{-\nu_{f1}}$, and $\hat{Y}_{f2}^* = \frac{\hat{Y}_{f2}}{-\nu_{f2}}$, equations (3.1a-b) can be rewritten as

$$\frac{\partial \hat{Y}_{f1}^*}{\partial t} + \frac{\rho}{\hat{\rho}} r Sc u_d \frac{\partial \hat{Y}_{f1}^*}{\partial r} - \frac{\hat{D}}{r^2} \frac{\partial}{\partial r} \left(r^2 \frac{\partial \hat{Y}_{f1}^*}{\partial r} \right) = 0 \quad (3.2a)$$

$$\frac{\partial \hat{Y}_{f2}^*}{\partial t} + \frac{\rho}{\hat{\rho}} r Sc u_d \frac{\partial \hat{Y}_{f2}^*}{\partial r} - \frac{\hat{D}}{r^2} \frac{\partial}{\partial r} \left(r^2 \frac{\partial \hat{Y}_{f2}^*}{\partial r} \right) = 0 \quad (3.2b)$$

Since $\hat{\rho} \gg \rho$, the convective part arising out of droplet surface regression ($\frac{dr_d}{dt}$) is small for considerable part of the droplet burning. And also, for the sake of simplicity, this convective part of liquid phase equations are neglected. The gas phase Lewis number is assumed to be unity and, using $\hat{Y}_{f1}^* = \frac{\hat{Y}_{f1}}{-\nu_{f1}}$, and $\hat{Y}_{f2}^* = \frac{\hat{Y}_{f2}}{-\nu_{f2}}$, Therefore, eqs. 3.2a, 3.2b and 3.2c can be written as:

$$\frac{\partial \hat{Y}_{f1}^*}{\partial t} - \frac{\hat{D}}{r^2} \frac{\partial}{\partial r} \left(r^2 \frac{\partial \hat{Y}_{f1}^*}{\partial r} \right) = 0 \quad (3.3a)$$

$$\frac{\partial \hat{Y}_{f2}^*}{\partial t} - \frac{\hat{D}}{r^2} \frac{\partial}{\partial r} \left(r^2 \frac{\partial \hat{Y}_{f2}^*}{\partial r} \right) = 0 \quad (3.3b)$$

$$\frac{\partial \hat{T}}{\partial t} - \frac{\hat{\alpha}}{r^2} \frac{\partial}{\partial r} \left(r^2 \frac{\partial \hat{T}}{\partial r} \right) = 0 \quad (3.3c)$$

For the quasi-steady gas phase : $r > 1$

The gas phase Eqs. 2.61a through 2.61d for fuel1, fuel2, oxidiser, and temperature can also be simplified in a similar manner as that used for simplifying the liquid phase equations and by using $u_d = r^2 v_r$ (from mass conservation), they can be written as

$$\frac{\partial Y_{f1}}{\partial t} + \frac{\rho}{\hat{\rho}} S_c u_d r \frac{\partial Y_{f1}}{\partial r} + \frac{1}{r^2} \frac{\partial}{\partial r} \left[S_c u_d Y_{f1} - D r^2 \frac{\partial Y_{f1}}{\partial r} \right] = Q_{f1} \quad (3.4a)$$

$$\frac{\partial Y_{f2}}{\partial t} + \frac{\rho}{\hat{\rho}} S_c u_d r \frac{\partial Y_{f2}}{\partial r} + \frac{1}{r^2} \frac{\partial}{\partial r} \left[S_c u_d Y_{f2} - D r^2 \frac{\partial Y_{f2}}{\partial r} \right] = Q_{f2} \quad (3.4b)$$

$$\frac{\partial Y_x}{\partial t} + \frac{\rho}{\hat{\rho}} S_c u_d r \frac{\partial Y_x}{\partial r} + \frac{1}{r^2} \frac{\partial}{\partial r} \left[S_c u_d Y_x - D r^2 \frac{\partial Y_x}{\partial r} \right] = Q_x \quad (3.4c)$$

and using constant gas phase C_p ,

$$\frac{\partial (c_p T)}{\partial t} + \frac{\rho}{\hat{\rho}} S_c u_d r \frac{\partial (C_p T)}{\partial r} + \frac{1}{r^2} \frac{\partial}{\partial r} \left[S_c u_d (C_p T) - \alpha Le r^2 \frac{\partial (C_p T)}{\partial r} \right] = Q_T \quad (3.4d)$$

where,

$$Q_{f1} = \frac{r_d^2}{\rho_\infty D_\infty \rho} \dot{\omega}_{f1} ; \quad Q_{f2} = \frac{r_d^2}{\rho_\infty D_\infty \rho} \dot{\omega}_{f2} ; \quad Q_x = \frac{r_d^2}{\rho_\infty D_\infty \rho} \dot{\omega}_x$$

$$Q_T = \frac{r_d^2}{\rho_\infty D_\infty \rho} \frac{(-\sum_{i=1}^N h_i^0 \dot{\omega}_i)}{\Delta h} ;$$

$\dot{\omega}_{f1}$, $\dot{\omega}_{f2}$, and $\dot{\omega}_x$ = rate of consumptions of species fuel1, fuel2 and oxidiser respectively in moles/ m^3 /sec.

Now, using

$$Y_{f1}^* = \frac{Y_{f1}}{-\nu_{f1}}, \quad Y_{f2}^* = \frac{Y_{f2}}{-\nu_{f2}}, \quad Y_x^* = \frac{Y_x}{-\nu_x} \quad (3.5a)$$

and from Eq. 2.73,

$$\dot{\omega} = -\frac{\dot{\omega}_{f1}}{\nu_{f1}} = -\frac{\dot{\omega}_{f2}}{\nu_{f2}} = -\frac{\dot{\omega}_x}{\nu_x} \quad (3.5b)$$

where, ν_{f1} , ν_{f2} , and ν_x are the stoichiometric coefficients for fuel1, fuel2, and oxidiser, the species equations for fuel1, fuel2 and the oxidiser can be written as

$$\frac{\partial Y_{f1}^*}{\partial t} + \frac{\rho}{\hat{\rho}} S_c u_d r \frac{\partial Y_{f1}^*}{\partial r} + \frac{1}{r^2} \frac{\partial}{\partial r} \left[S_c u_d Y_{f1}^* - D r^2 \frac{\partial Y_{f1}^*}{\partial r} \right] = \dot{\omega}^* \quad (3.6a)$$

$$\frac{\partial Y_{f2}^*}{\partial t} + \frac{\rho}{\hat{\rho}} S_c u_d r \frac{\partial Y_{f2}^*}{\partial r} + \frac{1}{r^2} \frac{\partial}{\partial r} \left[S_c u_d Y_{f2}^* - D r^2 \frac{\partial Y_{f2}^*}{\partial r} \right] = \dot{\omega}^* \quad (3.6b)$$

and

$$\frac{\partial Y_x^*}{\partial t} + \frac{\rho}{\hat{\rho}} S_c u_d r \frac{\partial Y_x^*}{\partial r} + \frac{1}{r^2} \frac{\partial}{\partial r} \left[S_c u_d Y_x^* - D r^2 \frac{\partial Y_x^*}{\partial r} \right] = \dot{\omega}^* \quad (3.6c)$$

For the gas phase energy equation,

$$\sum_{i=1}^N h_i^0 \dot{\omega}_i = h_{f1}^0 \dot{\omega}_{f1} + h_{f2}^0 \dot{\omega}_{f2} + h_x^0 \dot{\omega}_x + h_p^0 \dot{\omega}_p$$

and since from Eq. 2.73,

$$\dot{\omega} = -\frac{\dot{\omega}_{f1}}{\nu_{f1}} = -\frac{\dot{\omega}_{f2}}{\nu_{f2}} = -\frac{\dot{\omega}_x}{\nu_x} = +\frac{\dot{\omega}_p}{\nu_p}$$

Therefore,

$$-\sum_{i=1}^N h_i^0 \dot{\omega}_i = -\dot{\omega} [\nu_p h_p^0 - \nu_{f1} h_{f1}^0 - \nu_{f2} h_{f2}^0 - \nu_x h_x^0] = \dot{\omega} \Delta h$$

Where,

$$\Delta h = -\nu_p h_p^0 + \nu_{f1} h_{f1}^0 + \nu_{f2} h_{f2}^0 + \nu_x h_x^0$$

and $\nu_p, \nu_{f1}, \nu_{f2}, \nu_x$ are the stoichiometric coefficients for products, p and the reactants, f1, f2 and x. Therefore, the above Eqs. 3.6a-d becomes

$$\frac{\partial (C_p T)}{\partial t} + \frac{\rho}{\hat{\rho}} S_c u_d r \frac{\partial (C_p T)}{\partial r} + \frac{1}{r^2} \frac{\partial}{\partial r} \left[S_c u_d (C_p T) - \alpha L e r^2 \frac{\partial (C_p T)}{\partial r} \right] = \dot{\omega}^* \quad (3.6d)$$

where, $\dot{\omega}^* = \dot{\omega} \frac{r_d^2}{\rho_\infty D_\infty \rho}$ and $\dot{\omega}$ = overall reaction rate for the above reaction in moles/ m^3 /sec. For reasons given earlier, the convective part containing $u_d \frac{\rho}{\rho}$ is neglected in Eqs. 3.6a-d, and incorporating the gas phase quasi-steadiness, and using $\alpha = D$ because gas phase Lewis number is unity, the species and energy equation for the gas phase become

$$\frac{1}{r^2} \frac{d}{dr} \left(Sc u_d Y_{f1}^* - r^2 D \frac{dY_{f1}^*}{dr} \right) = \dot{\omega}^* \quad (3.7a)$$

$$\frac{1}{r^2} \frac{d}{dr} \left(Sc u_d Y_{f2}^* - r^2 D \frac{dY_{f2}^*}{dr} \right) = \dot{\omega}^* \quad (3.7b)$$

$$\frac{1}{r^2} \frac{d}{dr} \left(Sc u_d Y_x^* - r^2 D \frac{dY_x^*}{dr} \right) = \dot{\omega}^* \quad (3.7c)$$

$$\frac{1}{r^2} \frac{d}{dr} \left(Sc u_d (C_p T) - r^2 D \frac{d(C_p T)}{dr} \right) = \dot{\omega}^* \quad (3.7d)$$

The non-dimensional boundary and initial conditions given by Eqs. 2.62 through 2.70 can be rewritten in terms of variables defined by Eq. 3.5 as:

a. At the droplet centre ($r = 0$),

$$\frac{\partial \hat{Y}_{f1}^*}{\partial r} = 0 \quad (3.8a)$$

$$\frac{\partial \hat{Y}_{f2}^*}{\partial r} = 0 \quad (3.8b)$$

$$\frac{\partial \hat{T}}{\partial r} = 0 \quad (3.8c)$$

b. At droplet surface ($r = 1$),

(i) Mass conservation

$$\rho u_d = -\hat{\rho} \hat{u}_d = -\hat{\rho} \frac{dr_d}{dt} \quad (3.9)$$

where, u_d is the evaporation velocity and \hat{u}_d is the radius regression rate.

(ii) Gas-side flux balance for each of the species (two fuels and an oxidiser),

$$\left. \frac{\partial Y_{f1}^*}{\partial r} \right|_{r=1} + \frac{u_d Sc}{D} (\Omega_{f1} \epsilon_{f1} - Y_{f1s}^*) = 0 \quad (3.10a)$$

$$\left. \frac{\partial Y_{f2}^*}{\partial r} \right|_{r=1} + \frac{u_d Sc}{D} (\Omega_{f2} \epsilon_{f2} - Y_{f2s}^*) = 0 \quad (3.10b)$$

$$\left. \frac{\partial Y_x^*}{\partial r} \right|_{r=1} + \frac{u_d Sc}{D} (-Y_{xs}^*) = 0 \quad (3.10c)$$

where, $\Omega_{f1} = -\frac{1}{\nu_{f1}}$, $\Omega_{f2} = -\frac{1}{\nu_{f2}}$, ϵ_{f1} and ϵ_{f2} are the fractional mass gasification rate for fuel1 and fuel2 respectively.

(iii) Liquid-side flux balance for the fuels,

$$\left. \frac{\partial \hat{Y}_{f1}^*}{\partial r} \right|_{r=1} + \frac{aa Sc}{\hat{D}} (\Omega_{f1} \epsilon_{f1} - \hat{Y}_{f1s}^*) = 0 \quad (3.11a)$$

$$\left. \frac{\partial \hat{Y}_{f2}^*}{\partial r} \right|_{r=1} + \frac{aa Sc}{\hat{D}} (\Omega_{f2} \epsilon_{f2} - \hat{Y}_{f2s}^*) = 0 \quad (3.11b)$$

where, $aa = \rho u_d / \hat{\rho}$

(iv) From heat balance at the interface,

$$\lambda \frac{\partial T}{\partial r} \Big|_{r=1} = \text{Pr} \rho u_d (\epsilon_{f1} L_{f1} + \epsilon_{f2} L_{f2}) + \hat{\lambda} \frac{\partial \hat{T}}{\partial r} \Big|_{r=1} \quad (3.12)$$

where, L_{f1} and L_{f2} are the latent of evaporation for fuel 1 and 2 respectively.

(v) phase equilibrium at interface :

Assuming that the liquid fuel behaves as an ideal mixture and the fuel vapour is saturated corresponding to the surface temperature, the Raoult's law and the Clasius-Clapeyron relation can be considered valid. Accordingly, the liquid -phase and the gas-phase mole-fractions are related through the expressions:

at $r = 1.0$,

$$X_{f1s} = \hat{X}_{f1s} \exp(\beta_{f1} (1/T_{bf1} - 1/T_s)) \quad (3.13a)$$

$$X_{f2s} = \hat{X}_{f2s} \exp(\beta_{f2} (1/T_{bf2} - 1/T_s)) \quad (3.13b)$$

where,

$$\beta_{f1} = \frac{W_{f1} L_{f1} C_{p,\infty}}{R_u} \quad \text{and} \quad \beta_{f2} = \frac{W_{f2} L_{f2} C_{p,\infty}}{R_u}, \quad (3.13c)$$

R_u is the universal gas constant, W_{f1} and W_{f2} are molecular weights for fuel 1 and 2 respectively, and T_s is the droplet surface temperature.

(c) In the ambience ($r \rightarrow \infty$):

$$T = T_\infty \quad (3.14a)$$

$$Y_{f1}^* = 0.0 \quad (3.14b)$$

$$Y_{f2}^* = 0.0 \quad (3.14c)$$

$$Y_x^* = Y_{x,\infty}^* \quad (3.14d)$$

(d) The initial conditions are:

$$\hat{T}(r, 0) = \hat{T}_{\text{in}} \quad (3.15a)$$

$$\hat{Y}_{f1}^*(r, 0) = \hat{Y}_{\text{in},f1}^* \quad (3.15b)$$

$$\hat{Y}_{f2}^*(r, 0) = \hat{Y}_{\text{in},f2}^* \quad (3.15c)$$

3.3 Analytical Solutions

3.3.1 Gas-Phase

It is seen that due to the presence of the generation term ($\dot{\omega}^*$), the gas phase Eqs. 3.7 are highly non-linear. Analytical solutions are not possible as long as $\dot{\omega}^*$ is present in the equations. This generation term is eliminated by using thin flame approximation and consequently, applying the Schvab-Zeldovich variables (Kuo, 1986). In thin flame approximation, the fuels and the oxidiser are assumed to be fully consumed at the flame surface so that the oxidiser mass-fraction is always zero inside the flame and the fuel mass-fractions are always zero outside the flame. The Schvab-Zeldovich variables are defined as

$$G_1 = Y_{f1}^* - Y_x^* \quad (3.16a)$$

$$G_2 = Y_{f2}^* - Y_x^* \quad (3.16b)$$

$$H = C_p T - Y_x^* \quad (3.16c)$$

Now, subtracting eq. 3.7c from eqs. 3.7a, 3.7b and 3.7d and then applying the Schvab-Zeldovich variables, we have

$$\frac{1}{r^2} \frac{d}{dr} \left(Sc u_d G_1 - r^2 D \frac{dG_1}{dr} \right) = 0 \quad (3.17a)$$

$$\frac{1}{r^2} \frac{d}{dr} \left(Sc u_d G_2 - r^2 D \frac{dG_2}{dr} \right) = 0 \quad (3.17b)$$

$$\frac{1}{r^2} \frac{d}{dr} \left(Sc u_d H - r^2 D \frac{dH}{dr} \right) = 0 \quad (3.17c)$$

By virtue of thin flame approximation, for $1 < r < r_f$, $Y_x^* = 0$. Therefore, in this range,

$$G_1 = Y_{f1}^* \quad (3.18a)$$

$$G_2 = Y_{f2}^* \quad (3.18b)$$

$$H = C_p T \quad (3.18c)$$

Again, for $r_f < r < \infty$, $Y_{f1}^* = 0$ and $Y_{f2}^* = 0$. Therefore, in this range,

$$G_1 = G_2 = -Y_x^* \quad (3.19a)$$

and

$$H = C_p T - Y_x^* \quad (3.19b)$$

The **boundary** conditions for the gas phase in terms of Schvab-Zeldovich variables can be written as

at $r=1$

$$\left. \frac{dG_1}{dr} \right|_{r=1} + \frac{u_d Sc}{D} [\Omega_{f1} \epsilon_{f1} - G_1|_{r=1}] \quad (3.20a)$$

$$\left. \frac{dG_2}{dr} \right|_{r=1} + \frac{u_d Sc}{D} [\Omega_{f1} \epsilon_{f1} - G_2|_{r=1}] \quad (3.20b)$$

and

$$\left. \frac{\partial H}{\partial r} \right|_{r=1} = \frac{\rho C_p u_d Pr}{\lambda} \sum_{i=1}^N \epsilon_i L_i + \frac{C_p}{\lambda} \hat{\lambda} \left. \frac{\partial \hat{T}}{\partial r} \right|_{r=1} \quad (3.21)$$

At $r \rightarrow \infty$,

$$G_1 = G_2 = Y_{x,\infty} \quad (3.22a)$$

and

$$H = C_p T_\infty - Y_{x,\infty} \quad (3.22b)$$

Equations 3.17a through 3.17c along with the boundary conditions represented by Eqs. 3.20a through 3.22b can be solved analytically in terms of the Schvab-Zeldovich variables,

G_1 , G_2 and H . Then, by using the relations 3.16a,b,c, the final analytical expressions for species and temperature of the gas phase can be given as

for $1 < r < r_f$,

$$Y_{f1}^* = \Omega_{f1} \left[\epsilon_{f1} - \left(\frac{Y_{x,\infty}^*}{\Omega_{f1}} + \epsilon_{f1} \right) \exp \left(-\frac{u_d S c}{D r} \right) \right] \quad (3.23a)$$

$$Y_{f2}^* = \Omega_{f2} \left[\epsilon_{f2} - \left(\frac{Y_{x,\infty}^*}{\Omega_{f2}} + \epsilon_{f2} \right) \exp \left(-\frac{u_d S c}{D r} \right) \right] \quad (3.23b)$$

$$\begin{aligned} T &= T_\infty - Y_{x,\infty}^* \\ &+ \left[\epsilon_{f1} L_{f1} + \epsilon_{f2} L_{f2} + \frac{\hat{\lambda} \frac{\partial \hat{T}}{\partial r} \big|_{r=1}}{u_d S c} \right] \exp \left(\frac{u_d S c}{D} \right) \left[\exp \left(-\frac{u_d S c}{D r} \right) \right] \end{aligned} \quad (3.23c)$$

for $r_\infty > r > r_f$,

$$Y_x^* = -\Omega_{f1} \left[\epsilon_{f1} - \left(\frac{Y_{x,\infty}^*}{\Omega_{f1}} + \epsilon_{f1} \right) \exp \left(-\frac{u_d S c}{D r} \right) \right] \quad (3.24a)$$

$$\begin{aligned} T &= T_\infty + (Y_x^* - Y_{x,\infty}^*) \\ &+ \left[\epsilon_{f1} L_{f1} + \epsilon_{f2} L_{f2} + \frac{\hat{\lambda} \frac{\partial \hat{T}}{\partial r} \big|_{r=1}}{u_d S c} \right] \exp \left(\frac{u_d S c}{D} \right) \left[\exp \left(-\frac{u_d S c}{D r} \right) \right] \end{aligned} \quad (3.24b)$$

3.3.2 Liquid-Phase

Equations 3.3a,b,c along with boundary and initial conditions given by Eqs. 3.8, 3.11, 3.12 and 3.15, can be transformed defining new variables of the form :

$$\hat{u}_i = r \hat{Y}_i^* \text{ and } \hat{w} = r \hat{T} \quad (3.25)$$

Where, i corresponds to the two components of the liquid phase. The resulting governing equations are :

$$\frac{\partial \hat{u}_i}{\partial t} = \hat{D} \frac{\partial^2 \hat{u}_i}{\partial r^2} \quad (3.26a)$$

$$\frac{\partial \hat{w}}{\partial t} = \hat{\alpha} \frac{\partial^2 \hat{w}}{\partial r^2} \quad (3.26b)$$

The transformed boundary conditions from Eqs. 3.11 and 3.12 are given by

at $r = 1$:

$$\frac{\partial \hat{u}_i}{\partial r} = C_i(t) \quad (3.27a)$$

$$\frac{\partial \hat{w}}{\partial r} = C_T(t) \quad (3.27b)$$

where,

$$C_i(t) = \left(1 + \frac{\hat{u}_d Sc}{\hat{D}}\right) \hat{u}_{i,s} - \frac{\hat{u}_d Sc}{\hat{D}} \Omega_i \epsilon_i \quad (3.28a)$$

and

$$C_T(t) = \frac{1}{\hat{\lambda}} \left(\hat{\lambda} \frac{\partial \hat{T}}{\partial r} \Big|_{r=1} - \text{Pr} \rho u_d \sum \epsilon_i L_i \right) + \hat{T}_s \quad (3.28b)$$

and at $r = 0$:

$$\hat{u} = 0; \hat{w} = 0. \quad (3.29)$$

The initial conditions from Eq. 3.15 are:

$$\hat{u}_i(r, 0) = r \hat{Y}_{\text{in},i}^*(r) \quad (3.30a)$$

$$\hat{w}(r, 0) = r \hat{T}_{\text{in}}(r) \quad (3.30b)$$

The general solutions for the above system can be constructed in a series form for each discrete time step Δt , using the solutions for the constant gradient case. The fundamental solutions, corresponding to constant interfacial gradients, can be obtained in the following way. In solving eq. 3.26a, let us assume that the solution, \hat{u}_i consists of two parts namely steady state and transient parts as given by

$$\hat{u}_i = \bar{u}(r) + v(r, t) \quad (3.31)$$

Then, $\bar{u}_{rr} = 0$ and $v_t = \hat{D} v_{rr}$

Let us assume the steady state boundary conditions as

at $r=1$,

$$\frac{\partial \bar{u}}{\partial r} \Big|_{r=1} = C_i \quad (3.32a)$$

and, at $r=0$,

$$\bar{u}(r) = 0 \quad (3.32b)$$

Therefore, applying the above steady state boundary conditions, we get the steady state solution as

$$\bar{u}(r) = C_i r \quad (3.33)$$

The corresponding transient boundary conditions for $v_t = \hat{D}v_{rr}$ yields

$$v_r(r=1, t) = C_i - C_i = 0 \quad (3.34a)$$

$$v(r=0, t) = 0 \quad (3.34b)$$

and the initial condition becomes

$$v(r, t=0) = -r(C_i - \hat{Y}_{in}) \quad (3.35)$$

Analytical solution for the above transient Eq. 3.26 can be obtained by the method of separation of variables by using the above boundary conditions and can be written in a series form as (Myers, 1971)

$$v(r, t) = \sum_{n=0}^{\infty} A_n \sin(p\pi r) \exp(p^2 \pi^2 \hat{D}t) \quad (3.36)$$

Now, satisfying the initial condition, we get

$$A_n = \frac{-2C_i(-1)^n}{p^2 \pi^2} + 2 \int_0^1 \hat{Y}_{in}^*(r) r \sin(p\pi r) dr \quad (3.37)$$

where, $p = \frac{2n+1}{2}$, $i = f1$ (for fuel1) and $f2$ (for fuel2). Therefore, the complete solutions for $\hat{u}_i(r, t)$ can be expressed as

$$\hat{u}_i(r, t) = C_i r + \sum_{n=0}^{\infty} A_n \sin p\pi r \exp(p^2 \pi^2 \hat{D}t) \quad (3.38)$$

since, $\hat{u}_i = r\hat{Y}_i^*$,

$$\hat{Y}_i^*(r, t) = C_i + \frac{1}{r} \sum_{n=0}^{\infty} A_n \sin(p\pi r) \exp(-p^2 \pi^2 \hat{D}t) \quad (3.39a)$$

where,

$$A_{ni} = \frac{-2C_i}{p^2\pi^2}(-1)^n + 2 \int_0^1 \hat{Y}_{i,ni}^* r \sin(p\pi r) dr \quad (3.39b)$$

and, $p = \frac{2n+1}{2}$, $i = f1$ (for fuel 1) and $f2$ (for fuel 2), The analytical solution to Eq. 3.26b for the liquid side temperature can also be obtained in a similar manner and is expressed as

$$\hat{T}(r, t) = C_T + \frac{1}{r} \sum_{n=0}^{\infty} A_{nT} \sin(p\pi r) \exp(-p^2\pi^2 \hat{\alpha} t) \quad (3.40a)$$

where,

$$A_{nT} = \frac{-2C_T}{p^2\pi^2}(-1)^n + 2 \int_0^1 \hat{T}_{in} r \sin(p\pi r) dr \quad (3.40b)$$

Assuming that the surface gradients remain constant over the period t to $(t + \Delta t)$, the quasi-linearized solutions at $t = m\Delta t$ are obtained using the superposition principle as follows :

At $t=0$, $\hat{Y}_i^{*0} = \hat{Y}_{i,in}^* = C_i^0$ and $A_{ni}^0 = 0$

Now, at $t = \Delta t$

$$\begin{aligned} \hat{Y}_i^{*1}(r, t = \Delta t) &= C_i^1 + \frac{1}{r} \sum_{n=0}^{\infty} A_{ni}^1 \sin(p\pi r) \exp(-p^2\pi^2 \hat{D} \Delta t) \\ &= \hat{Y}_i^{*0} + (\hat{Y}_i^{*1} - \hat{Y}_i^{*0}) \\ &= \hat{Y}_i^{*0} + (C_i^1 - C_i^0) + \frac{1}{r} \sum_{n=0}^{\infty} (A_{ni}^1 - A_{ni}^0) \sin(p\pi r) \exp(-xx) \end{aligned}$$

where,

$$\begin{aligned} A_{ni}^1 &= \frac{2(-1)^n}{p^2\pi^2} (\hat{Y}_{i,in}^* - C_i^1) \\ &= \frac{2(-1)^n}{p^2\pi^2} \sum_{k=0}^0 (C_i^0 - C_i^1) \exp(-k xx) \end{aligned}$$

where, $xx = p^2\pi^2 \hat{D} \Delta t$.

Similarly, at $t = 2\Delta t$

$$\begin{aligned} \hat{Y}_i^{*2}(r, t = 2\Delta t) &= C_i^2 + \frac{1}{r} \sum_{n=0}^{\infty} A_{ni}^2 \sin(p\pi r) \exp(-xx) \\ &= \hat{Y}_i^{*1} + (\hat{Y}_i^{*2} - \hat{Y}_i^{*1}) \end{aligned}$$

$$\begin{aligned}
&= \hat{Y}_i^{*1} + (C_i^2 - C_i^1) + \frac{1}{r} \sum_{n=0}^{\infty} (A_{ni}^2 - A_{ni}^1) \sin(p\pi r) \exp(-xx) \\
&= \hat{Y}_i^{*0} + (C_i^1 - C_i^0) + \frac{1}{r} \sum_{n=0}^{\infty} (A_{ni}^1 - A_{ni}^0) \sin(p\pi r) \exp(-xx) \\
&+ (C_i^2 - C_i^1) + \frac{1}{r} \sum_{n=0}^{\infty} (A_{ni}^2 - A_{ni}^1) \sin(p\pi r) \exp(-xx)
\end{aligned}$$

where,

$$\begin{aligned}
A_{ni}^2 &= \frac{2(-1)^n}{p^2\pi^2} [(C_i^1 - C_i^2) \exp(-0.xx) + (C_i^0 - C_i^1) \exp(-xx)] \\
&= \frac{2(-1)^n}{p^2\pi^2} \sum_{k=0}^1 (C_i^{2-k-1} - C_i^{2-k}) \exp(-k xx)
\end{aligned}$$

And, at $t = 3\Delta t$

$$\begin{aligned}
\hat{Y}_i^{*3}(r, t = 3\Delta t) &= C_i^3 + \frac{1}{r} \sum_{n=0}^{\infty} A_{ni}^3 \sin(p\pi r) \exp(-xx) \\
&= \hat{Y}_i^{*2} + (\hat{Y}_i^{*3} - \hat{Y}_i^{*2}) \\
&= \hat{Y}_i^{*2} + (C_i^3 - C_i^2) + \frac{1}{r} \sum_{n=0}^{\infty} (A_{ni}^3 - A_{ni}^2) \sin(p\pi r) \exp(-xx) \\
&= \hat{Y}_i^{*0} + (C_i^1 - C_i^0) + \frac{1}{r} \sum_{n=0}^{\infty} (A_{ni}^1 - A_{ni}^0) \sin(p\pi r) \exp(-xx) \\
&+ (C_i^2 - C_i^1) + \frac{1}{r} \sum_{n=0}^{\infty} (A_{ni}^2 - A_{ni}^1) \sin(p\pi r) \exp(-xx) \\
&+ (C_i^3 - C_i^2) + \frac{1}{r} \sum_{n=0}^{\infty} (A_{ni}^3 - A_{ni}^2) \sin(p\pi r) \exp(-xx)
\end{aligned}$$

where,

$$\begin{aligned}
A_{ni}^3 &= \frac{2(-1)^n}{p^2\pi^2} [(C_i^2 - C_i^3) \exp(-0.xx) + (C_i^1 - C_i^2) \exp(-xx) + (C_i^0 - C_i^1) \exp(-2xx)] \\
&= \frac{2(-1)^n}{p^2\pi^2} \sum_{k=0}^2 (C_i^{3-k-1} - C_i^{3-k}) \exp(-k xx)
\end{aligned}$$

Thus, at $t = m\Delta t$, the solution can be written in series form as

$$\begin{aligned}
\hat{Y}_i^{*m} &= \hat{Y}_i^{*0} + \sum_{j=1}^m \Delta \hat{Y}_i^{*j} \\
\hat{Y}_i^{*m} &= \hat{Y}_i^{*0} + \frac{1}{r} \sum_{j=1}^m \left((C_i^j - C_i^{j-1}) r + \sum_{n=0}^{\infty} (A_{ni}^j - A_{ni}^{j-1}) \exp(-xx) \sin(p\pi r) \right) \quad (3.41a)
\end{aligned}$$

where, $xx = p^2 \pi^2 \hat{D} \Delta t$

$$\text{and, } A_{ni}^j = \frac{2(-1)^n}{p^2 \pi^2} \sum_{k=0}^{j-1} (C_i^{j-k-1} - C_i^{j-k}) \exp(-k \, xx) \quad (3.41b)$$

Similarly, solution for the liquid side temperature can be expressed as

$$\begin{aligned} \hat{T}^m &= \hat{T}^0 + \sum_{j=1}^m \Delta \hat{T}^j \\ \hat{T}^m &= \hat{T}^0 + \frac{1}{r} \sum_{j=1}^m \left((C_T^j - C_T^{j-1}) r + \sum_{n=0}^{\infty} (A_{nT}^j - A_{nT}^{j-1}) \exp(-yy) \sin(p\pi r) \right) \end{aligned} \quad (3.42a)$$

where, $yy = p^2 \pi^2 \hat{\alpha} \Delta t$

$$\text{and, } A_{nT}^j = \frac{2(-1)^n}{p^2 \pi^2} \sum_{k=0}^{j-1} (C_T^{j-k-1} - C_T^{j-k}) \exp(-k \, yy) \quad (3.42b)$$

3.4 Numerical Evaluation

The liquid phase temperature and mass fraction profiles were evaluated using Eqs. 3.41 and 3.42 by truncating the infinite series to 100 terms. The semi-analytical solution was also compared with the finite difference solution of the same governing differential equations and excellent agreement (up to 4 places of decimals) was observed between them. It was found that the semi-analytical solution was about ten times faster than the numerical solution. For the finite difference procedure it was necessary to use at least a mesh size of 1/1000 within the droplet, for achieving a good match with the analytical results. Another advantageous feature of the semi-analytical procedure is that it could be applied to calculate only the surface quantities for each time step, if so desired. The process time required for evaluating the solution for 100 time steps by these three methods are given as:

- i) 250 seconds for numerical approach.
- ii) 30 seconds for full semi-analytical approach.
- iii) 4 seconds for evaluating only the surface parameters through semi-analytical procedure.

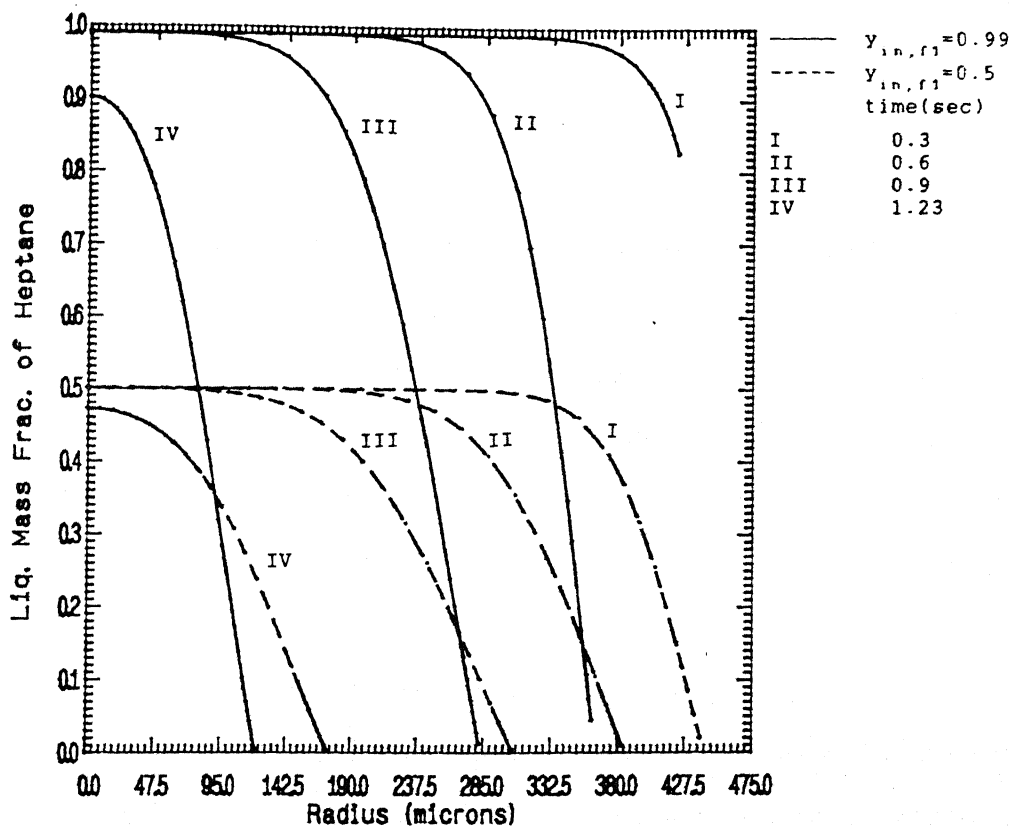
3.5 RESULTS AND DISCUSSION

Results have been predicted for the liquid phase temperature and concentration profiles and the fractional as well as the total gasification rates. The fuel combinations of *n*-heptane, *n*-octane, *n*-decane, undecane and dodecane have been considered, over the initial mass fraction range (0.1-0.99) of the more volatile component. In order to highlight the salient features of multicomponent fuel burning, results are presented for a binary mixture of heptane and decane with an initial proportion of (0.99 hep.- 0.01 dod), in the following sections.

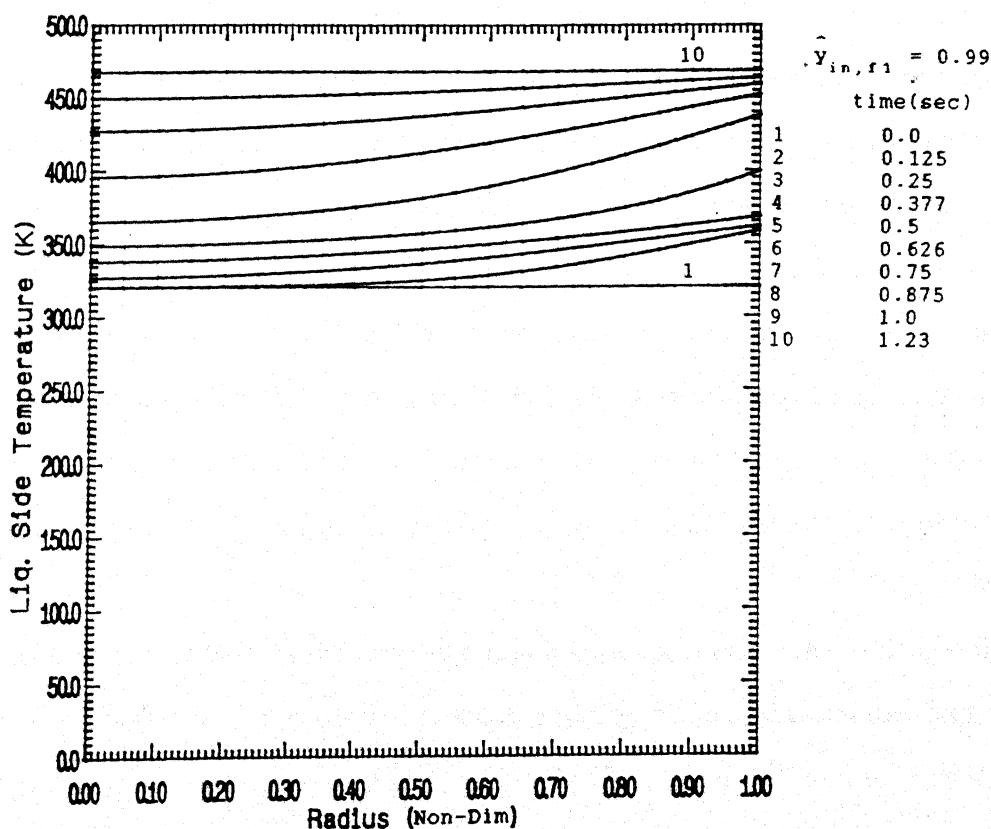
3.5.1 Transient Features of Multicomponent Combustion

The time history of mass-fraction and temperature profiles of a heptane-dodecane droplet is depicted in Figs. 3.1(a, b). Shortly after the introduction of the droplet, a concentration boundary layer is established near the surface due to rapid evaporation of the more volatile component. The concentration gradient near the surface is maintained almost throughout the droplet lifetime by the high liquid side diffusional resistance. This trend also implies a high surface regression rate compared to the liquid side mass diffusion rate. The boundary layer penetrates more into the core as time progresses.

In contrast to the mass-fraction profiles, the temperature profiles do not show the existence of a steep thermal boundary layer. This can be attributed to the relatively higher liquid side thermal diffusivity, because of which heat is conducted very fast to the core of the droplet. Fig.3.1b also indicates the presence of two distinct d^2 -law periods. In the first d^2 -law period, the droplet surface temperature remains nearly constant around the boiling point of the more volatile component. At the end of the first d^2 -law period (when the more volatile component is nearly depleted), rapid droplet heating occurs once again to raise it's temperature closer to the boiling point of the less volatile fuel. This is followed by the second d^2 -law period for the less volatile fuel. If the degree of superheat for the more volatile component is high, microexplosion is likely to occur, which in the



a



b

Fig. 3.1 Time history of liquid side mass fraction and temperature profiles.

present work has been ignored.

Figs. 3.2(a, b) shows four distinct periods namely initial transient, first $d^2 - law$ period, transition and second $d^2 - law$ period. In the initial transient period, the rate of evaporation is low and the droplet surface temperature rises very sharply due to high heat input for droplet heating. As a consequence of increasing surface temperature, evaporation of the more volatile fuel (heptane) and the rate of surface regression increase rapidly. Since initial mass-fraction of heptane is very high and the initial surface temperature is much below the boiling point of dodecane, the fractional mass gasification rate of heptane (ϵ_{f1}) is very high during this period.

After the initial transients, the first d^2 -law period starts. During this period, the droplet surface temperature remains close to the boiling point of heptane. The total evaporation rate and hence the surface regression rate exhibit quasi-steady behaviour. For heptane, surface mass-fraction and fractional mass gasification rate are high, indicating complete domination of the combustion of more volatile fuel. Very gradual decline in the surface mass-fraction of heptane is observed due to the high liquid side mass diffusional resistance.

The transition period starts at a time when the surface temperature crosses the boiling point of heptane. During this time, most of the heat is consumed in heating up the droplet. Enough heat is not available to maintain high rates of evaporation and surface regression, and hence these quantities decrease with time. This is also indicated by flame contraction (table 3.1). The surface mass-fraction and fractional mass gasification rate of heptane fall steeply because of high diffusional resistance as well as a decrease in the surface regression rate.

During the 2nd d^2 -law period, as the droplet temperature approaches the boiling point of dodecane, droplet heating becomes negligibly small and the surface temperature increases asymptotically. As the entire heat is used up for evaporation only, surface regression rate increases again and the droplet radius decreases exponentially. However, the total evaporation rate increases initially, and decreases later because of smaller droplet volume.

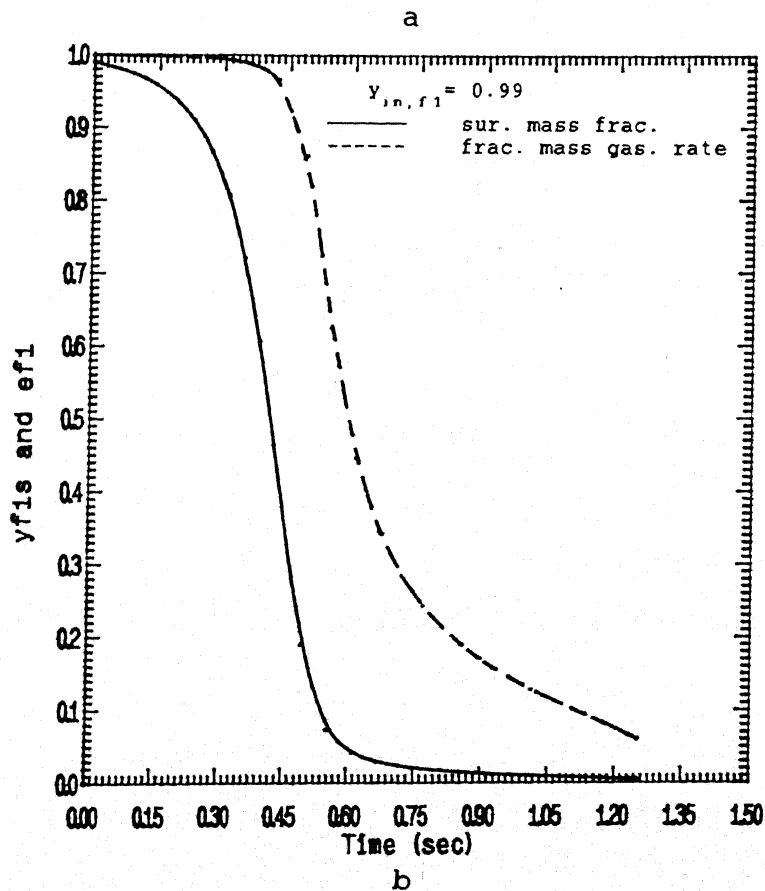
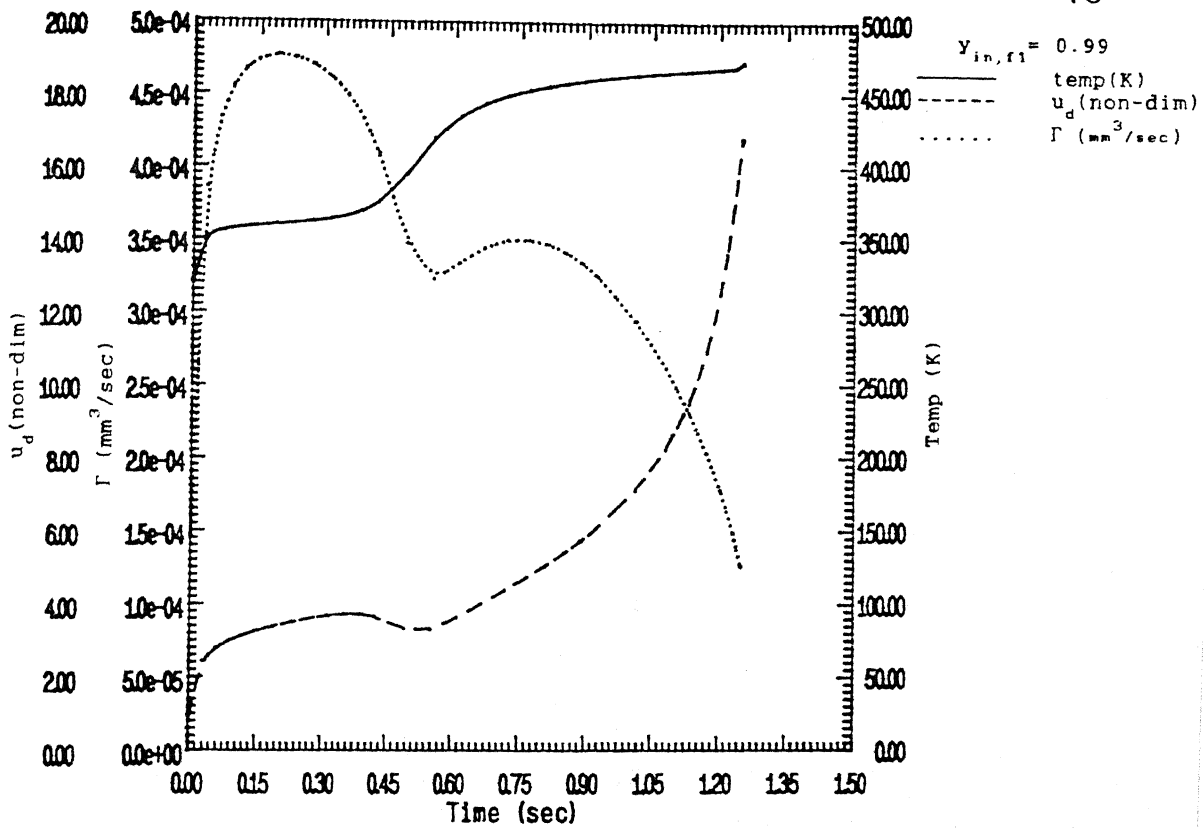


Fig. 3.2 Transient variation of surface temperature, evaporation velocity, volumetric mass gasification rate, surface mass fraction and fractional mass gasification rate.

time (sec)	Flame Stand Off Ratio (Non-Dim)
0.11	33.62
0.23	35.91
0.31	36.27
0.35	36.02
0.39	35.34
0.42	34.04
0.49	29.62
0.55	28.10
0.61	30.08
0.66	32.20
0.76	35.33
0.89	38.07
1.13	40.85
1.254	41.26

Table 3.1 Variation of Flame Stand Off Ratio With Time.

It can be seen that during the initial transient and the intermediate transient periods, liquid droplet heating is very important and can not be neglected.

3.5.2 Effects of Volatility Differential

Figures 3.3(a – e) show the two d^2 -law periods very prominently when the volatility differential is maximum (for the heptane- dodecane combination). The intermediate transition period also become narrower. Distinction of the two d^2 -law regions gradually decreases for smaller volatility differential and the transition period broadens. This is an indication of approaching the single component fuel burning behaviour in the limit. Fig. 3.3b shows that vigorous droplet heating is completed in the initial transient stage itself for smaller volatility differential. Fig 3.3d shows that the evaporation rate has a longer quasi-steady period with a decrease in volatility differential. So, on the whole, the transient as well as the multicomponent nature of combustion are reduced if the volatility differential is less.

3.5.3 Effects of Initial Mass Fraction

The effects of initial mass fraction on the burning characteristics are shown in Figs. 3.4(a – e) for the fuel combination of heptane and dodecane. It is evident from the figures that the first d^2 -law period is almost absent when the initial mass-fraction of the more volatile fuel is very low and except for the initial transient period, the second d^2 -law period is present all through. This is because the droplet does not possess enough more volatile component (especially close to the surface) to control the evaporation rate at any time. As the initial mass-fraction of heptane is increased, more heptane is available at the surface for evaporation in the initial stage. So, the first d^2 -law period increases and the second d^2 -law period decreases gradually. It is evident that the transition from heptane to dodecane burning is merged with the initial transient for small initial liquid side mass fraction of

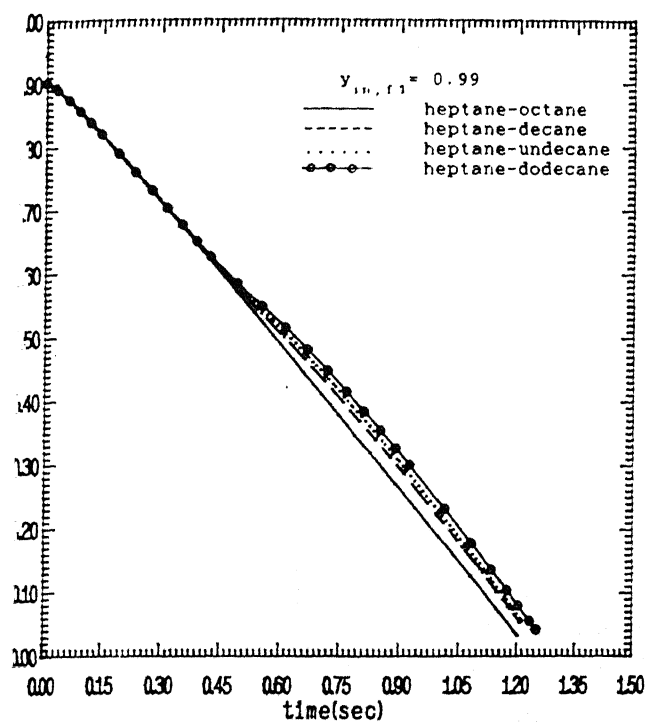


Fig. 3.3a

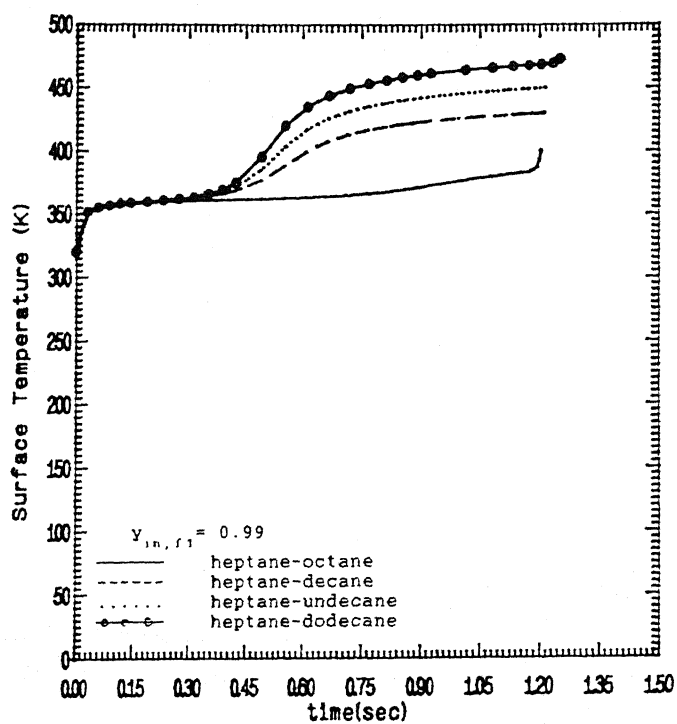


Fig. 3.3b

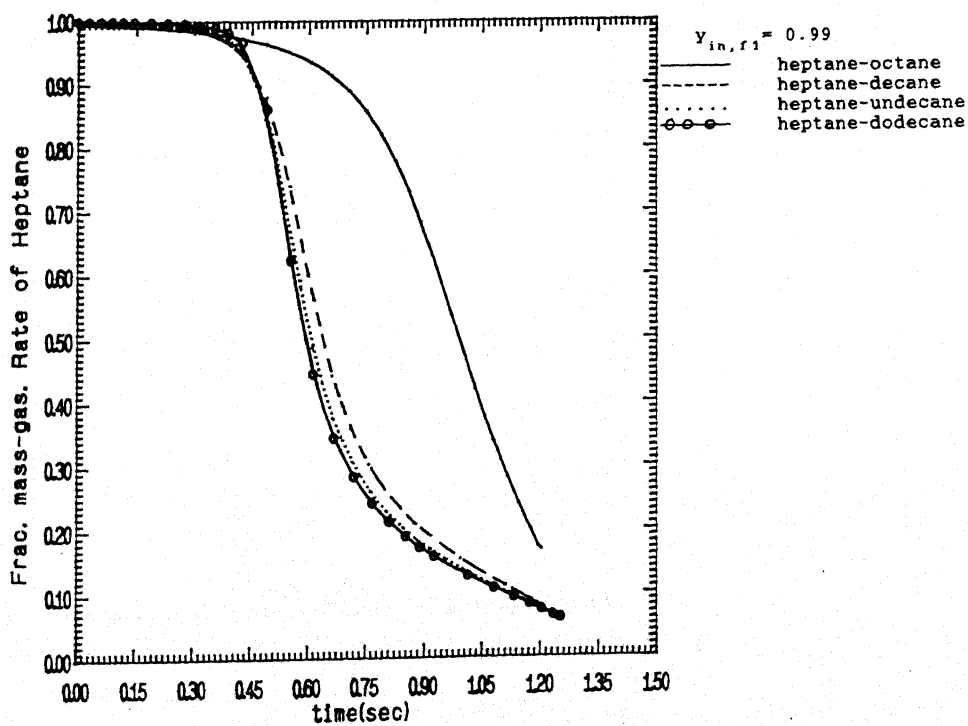


Fig. 3.3c

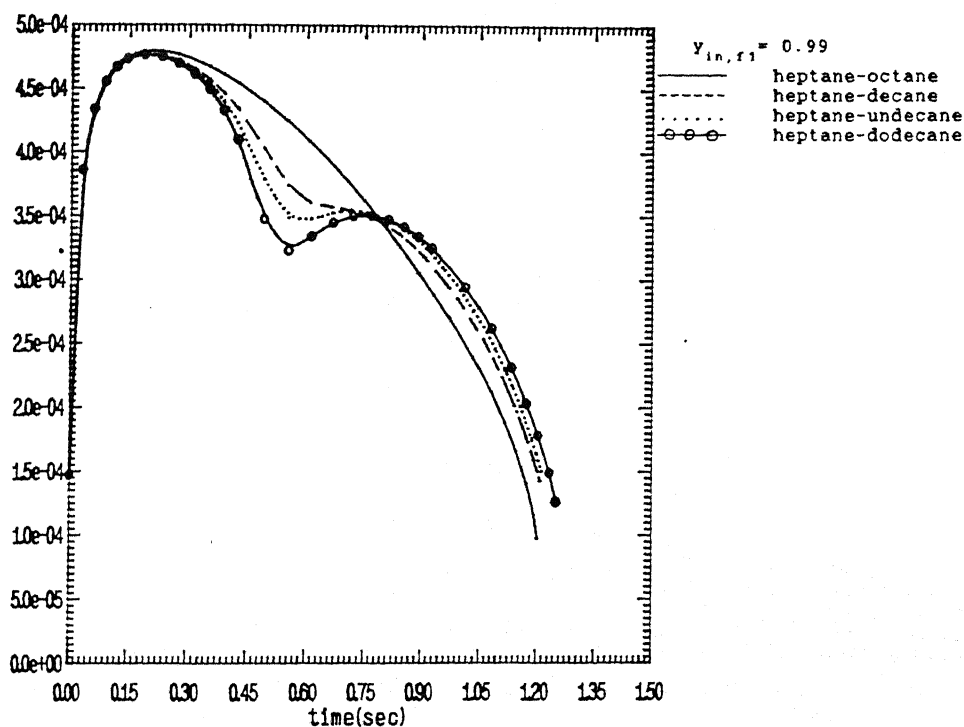


Fig. 3.3d

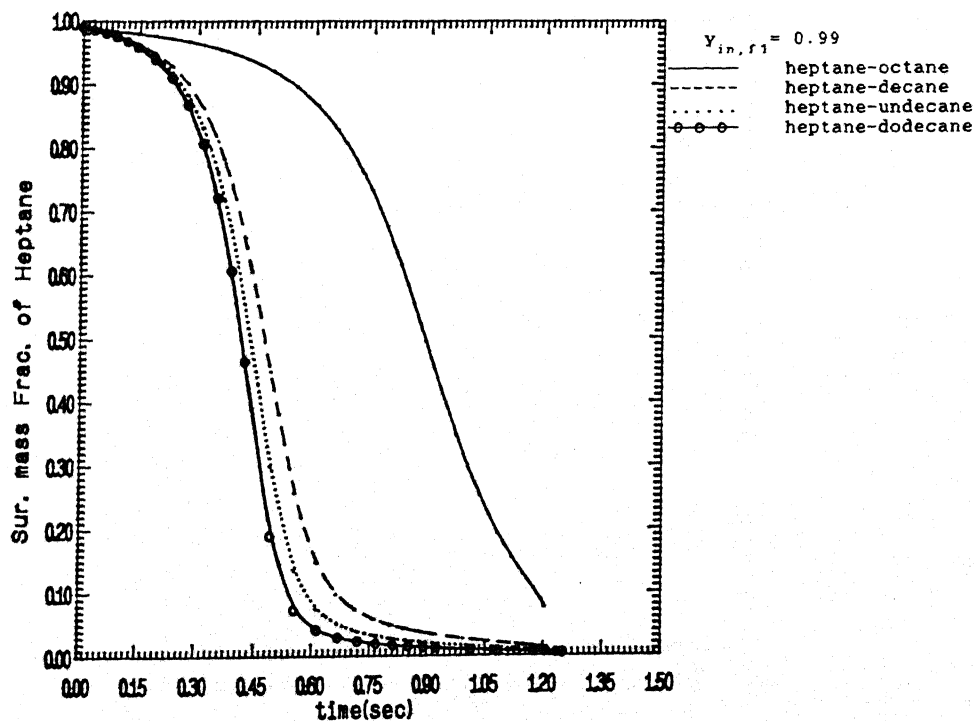


Fig. 3.3e

Fig. 3.3 Effect of volatility differential on the transient variations of square of the diameter, surface temperature, fractional mass gasification rate, volumetric mass gasification rate

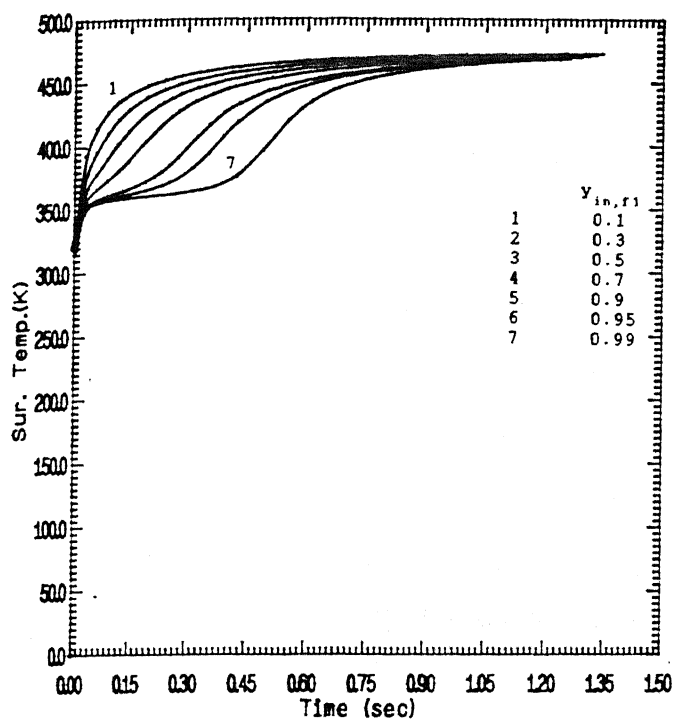


Fig. 3.4a

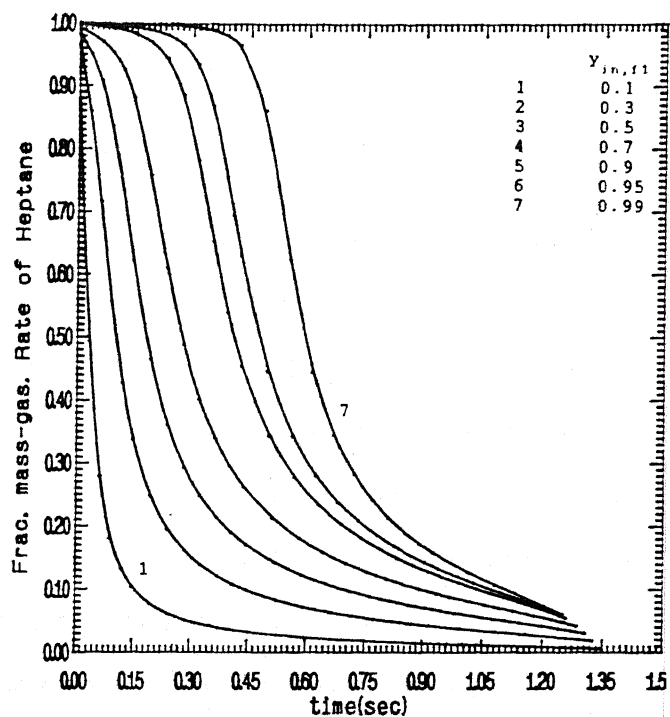


Fig. 3.4b

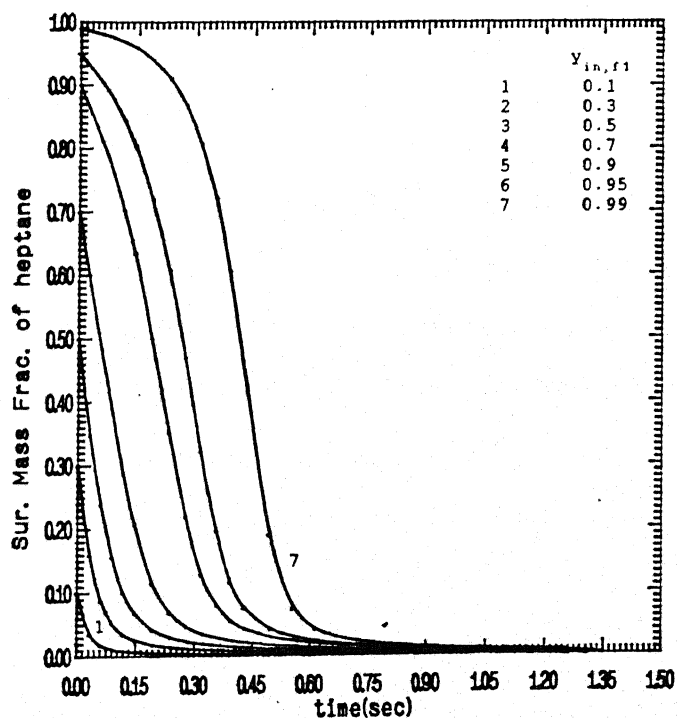


Fig. 3.4c

heptane. For higher values of initial liquid side mass fraction of heptane, the first d^2 -law period occurs distinctly and the transition is also clearly observed.

3.5.4 Comparison with Earlier Work

Fig. 3.5a presents a comparison for the liquid phase mass fraction profiles between the predictions of the present study and those of Shaw (1990). Mixtures of heptane-dodecane with different initial mass fractions have been considered. The comparison is made at a time when the surface mass fraction of heptane is same for both the cases. A good match is observed between the two studies. In Fig. 3.5b, the normalised burning rate prediction, $[\bar{k} = (k - k_{\text{octanol}})/(k_{\text{undecane}} - k_{\text{octanol}})]$ of octanol-undecane mixture has been compared with the experimental measurements of Law & Law (1982). Here also good agreement is seen, with minor deviations which may be attributed to the approximations invoked in the theoretical model.

3.6 Conclusions

A semi-analytical model has been developed here which is computationally much faster compared to the numerical model. This study shows very clearly the two d^2 -law periods in multicomponent fuel burning, as observed in experiments. It is also found that the multicomponent nature is predominant for large volatility differential and a high initial mass fraction of the more volatile component.

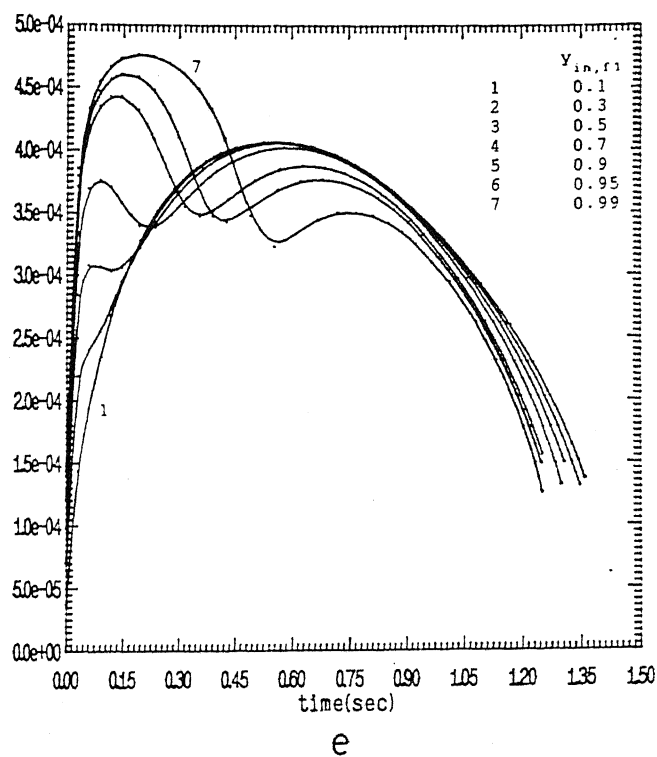
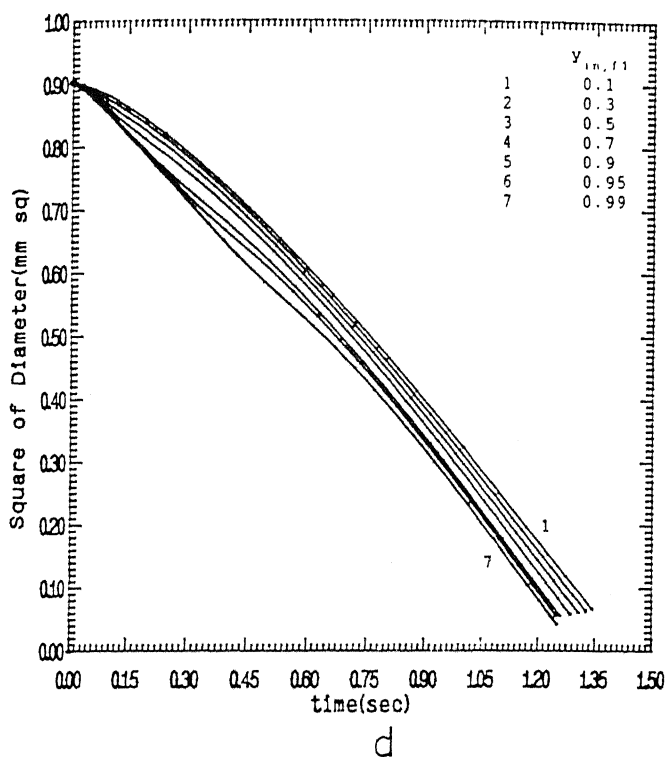


Fig. 3.4 Effect of initial mass fraction on the transient variations of square of the diameter, surface temperature, fractional mass gasification rate, volumetric mass gasification rate and surface mass fraction.

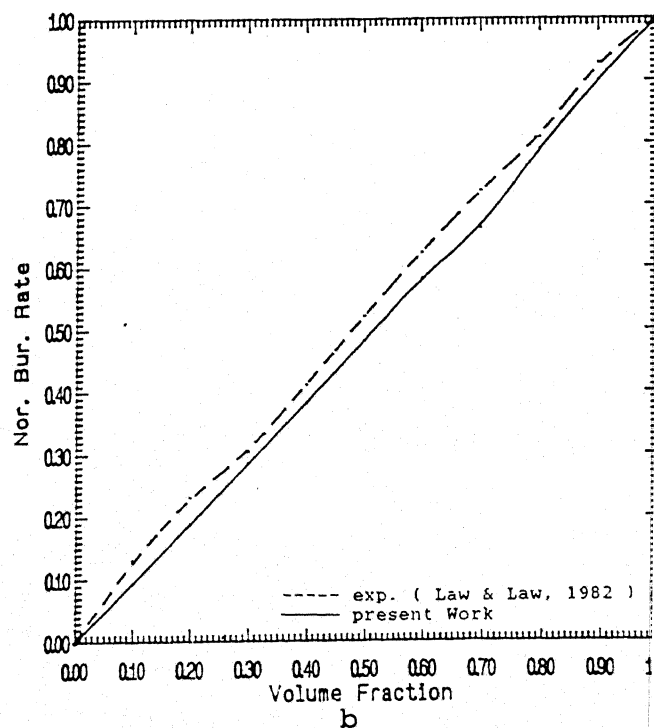
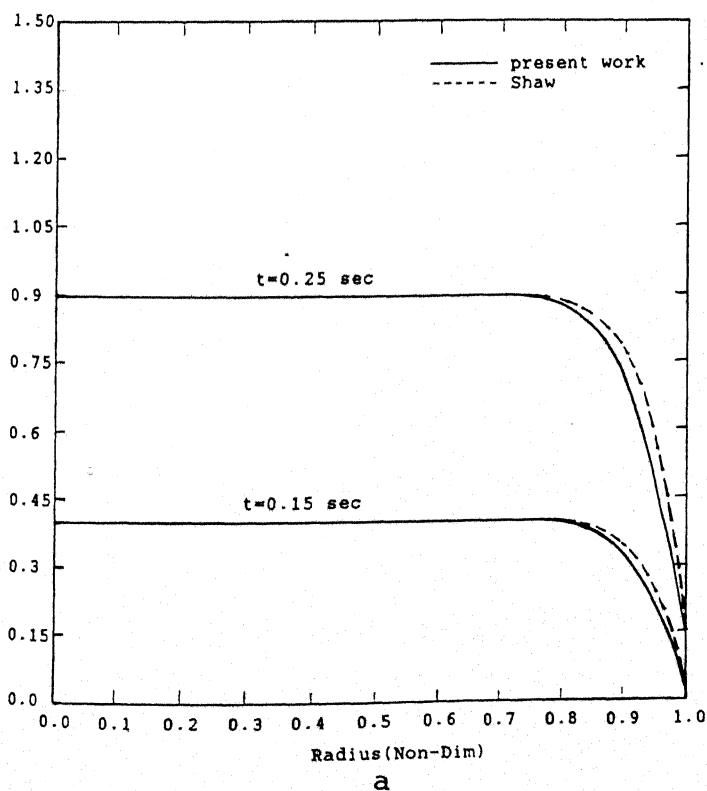


Fig. 3.5a Comparison of predicted surface mass fraction of Shaw, 1990.

Fig. 3.5b Comparison of normalised burning rate with earlier work of Law and Law, 1982.

Chapter 4

Numerical Solution Using Adaptive Grid Generation

4.1 Introduction

In the previous chapter, stress was given to obtain semi-analytical solution to see the fundamental aspect of multicomponent single droplet burning in quiescent atmosphere. In the present chapter, some of the important assumptions of the previous chapter are relaxed, and a more thorough and detailed study of spherically symmetric multicomponent single droplet burning is undertaken through elaborate numerical analysis. Thin flame approximation is relaxed, and the non-linear generation term ($\dot{\omega}$) is evaluated directly. Unity Lewis number condition for the gas phase has been relaxed. Adaptive grid generation technique has been used to track the flame movement throughout the history of droplet burning. The flame chemistry for droplet combustion is very complicated because, in reality, a very large number of chemical reactions take place before final products are reached. For all practical purposes, it is reasonable to assume a single step global reaction for each of the fuel. The contribution of each of the fuel has been considered separately. In reality, above a certain flame temperature (Kuo, 1986), the CO_2 and H_2O dissociate to form CO , O_2 and H_2 . Since they involve endothermic reactions, the flame temperature is not allowed to increase beyond a certain limit. This dissociation aspect of combustion has also been included in the present analysis. This study includes two extremely transient processes, namely, ignition and extinction. Because of the adaptive grid generation technique, it is possible to make a detailed study of flame movement, ignition, and extinction processes. Constant properties for both liquid and gas phases are retained in general. However, for one case, variable gas phase specific heat (as a function of temperature) was also considered. The present model can be extended to include the effect of flow, as well.

For the liquid and gas phases, governing differential equations along with boundary conditions and initial conditions were discussed in section 2.4.5 and 3.2. Before discussing the full numerical solutions, these equations along with the boundary and initial conditions are first summarized for the sake of completeness.

4.2 Liquid Phase Transport Equations

For the problem attempted here, since there is no generation inside the droplet, the net mass transfer inside the droplet is zero. But, since the moving boundary (the droplet surface) is always fixed at $r=1$, this gives rise to a convective term in the liquid phase transport equations. In absence of any flow field, the liquid phase equations (2.60a-c) for the species and energy transport equations for spherically symmetric burning, can be rewritten as

(a) Species transport equation

$$\frac{\partial \hat{Y}_{f1}}{\partial t} + \left(\frac{\rho Sc u_d r}{\hat{\rho}} - \frac{2\hat{D}}{r} \right) \frac{\partial \hat{Y}_{f1}}{\partial r} - \hat{D} \frac{\partial^2 \hat{Y}_{f1}}{\partial r^2} = 0 \quad (4.1a)$$

$$\frac{\partial \hat{Y}_{f2}}{\partial t} + \left(\frac{\rho Sc u_d r}{\hat{\rho}} - \frac{2\hat{D}}{r} \right) \frac{\partial \hat{Y}_{f2}}{\partial r} - \hat{D} \frac{\partial^2 \hat{Y}_{f2}}{\partial r^2} = 0 \quad (4.1b)$$

(b) Energy transport equation

$$\frac{\partial \hat{T}}{\partial t} + \left(\frac{\rho Sc u_d r}{\hat{\rho}} - \frac{2\hat{\alpha}Le}{r} \right) \frac{\partial \hat{T}}{\partial r} - \hat{\alpha}Le \frac{\partial^2 \hat{T}}{\partial r^2} = 0 \quad (4.1c)$$

4.3 Gas Phase Transport Equations

Similarly, and using $u_d = r^2 v_r$ (mass conservation), the gas phase species and energy equations (2.61a-d) are

(a) Species conservation equation

$$\frac{\partial Y_{f1}}{\partial t} + Sc u_d \left(\frac{1}{r^2} + \frac{\rho r}{\hat{\rho}} \right) \frac{\partial Y_{f1}}{\partial r} - \frac{D}{r^2} \frac{\partial}{\partial r} \left(r^2 \frac{\partial Y_{f1}}{\partial r} \right) = Q_{f1} \quad (4.2a)$$

$$\frac{\partial Y_{f2}}{\partial t} + Sc u_d \left(\frac{1}{r^2} + \frac{\rho r}{\hat{\rho}} \right) \frac{\partial Y_{f2}}{\partial r} - \frac{D}{r^2} \frac{\partial}{\partial r} \left(r^2 \frac{\partial Y_{f2}}{\partial r} \right) = Q_{f2} \quad (4.2b)$$

$$\frac{\partial Y_x}{\partial t} + Sc u_d \left(\frac{1}{r^2} + \frac{\rho r}{\hat{\rho}} \right) \frac{\partial Y_x}{\partial r} - \frac{D}{r^2} \frac{\partial}{\partial r} \left(r^2 \frac{\partial Y_x}{\partial r} \right) = Q_x \quad (4.2c)$$

(b) Energy conservation equation

$$\frac{\partial Y_T}{\partial t} + Sc u_d \left(\frac{1}{r^2} + \frac{\rho r}{\hat{\rho}} \right) \frac{\partial Y_T}{\partial r} - \frac{D}{r^2} \frac{\partial}{\partial r} \left(r^2 \frac{\partial Y_T}{\partial r} \right) + \frac{1}{r^2} \frac{\partial}{\partial r} \left(\left(\frac{\rho D C_p - \lambda Le}{\rho} \right) r^2 \frac{\partial T}{\partial r} \right) = Q_T \quad (4.2d)$$

where,

$$\begin{aligned}
 Q_{f1} &= \frac{r_d^2}{\rho_\infty D_\infty \rho} \dot{\omega}_{f1}, & Q_{f2} &= \frac{r_d^2}{\rho_\infty D_\infty \rho} \dot{\omega}_{f2}, \\
 Q_x &= \frac{r_d^2}{\rho_\infty D_\infty \rho} \dot{\omega}_x, & Q_T &= -\frac{r_d^2}{\rho_\infty D_\infty \rho} \left(\sum_{i=1}^N h_i^0 \dot{\omega}_i \right) / \Delta h \\
 Y_T &= \int_{T^0}^T C_p dT
 \end{aligned} \tag{4.2e}$$

and $\dot{\omega}_{f1}$, $\dot{\omega}_{f2}$ and $\dot{\omega}_x$ are the rates of consumption for fuel 1, fuel 2 and oxidiser respectively in $\text{mole}/\text{m}^3/\text{s}$. The process of calculating these rates and also the term, $\sum_{i=1}^N h_i^0 \dot{\omega}_i$, are described in the next section. Here, $f1$, $f2$ and x stand for fuel1, fuel2 and oxidiser respectively.

4.4 Boundary and Initial Conditions

Boundary Conditions

(a) Droplet centre ($r = 0$)

$$\frac{\partial \hat{Y}_{f1}}{\partial r} = 0, \tag{4.3a}$$

$$\frac{\partial \hat{Y}_{f2}}{\partial r} = 0, \tag{4.3b}$$

$$\frac{\partial \hat{T}}{\partial r} = 0 \tag{4.3c}$$

(b) Droplet surface ($r = 1$)

(i) mass balance

$$\rho u_d = -\hat{\rho} \hat{u}_d = -\hat{\rho} \frac{dr_d}{dt} \tag{4.4}$$

(ii) gas side species balance

$$\left. \frac{\partial Y_{f1}}{\partial r} \right|_{r=1} + \frac{u_d S_c}{D} (\epsilon_{f1} - Y_{f1s}) = 0 \tag{4.5a}$$

$$\left. \frac{\partial Y_{f2}}{\partial r} \right|_{r=1} + \frac{u_d S_c}{D} (\epsilon_{f2} - Y_{f2s}) = 0 \tag{4.5b}$$

$$\left. \frac{\partial Y_x}{\partial r} \right|_{r=1} + \frac{u_d S_c}{D} (-Y_{xs}) = 0 \tag{4.5c}$$

(iii) liquid side species balance

$$\left. \frac{\partial \hat{Y}_{f1}}{\partial r} \right|_{r=1} + \frac{aa}{\hat{D}} Sc (\epsilon_{f1} - \hat{Y}_{f1s}) = 0 \quad (4.6a)$$

$$\left. \frac{\partial \hat{Y}_{f2}}{\partial r} \right|_{r=1} + \frac{aa}{\hat{D}} Sc (\epsilon_{f2} - \hat{Y}_{f2s}) = 0 \quad (4.6b)$$

where, $aa = u_d \rho / \hat{\rho}$.

(iv) heat balance

$$H_g = \lambda \left. \frac{\partial T}{\partial r} \right|_{r=1} = Pr \rho u_d \sum_{i=1}^N \epsilon_i L_i + \hat{\lambda} \left. \frac{\partial \hat{T}}{\partial r} \right|_{r=1} \quad (4.7)$$

(v) phase equilibrium at interface

$$X_{f1s} = \hat{X}_{f1s} \exp \left[\beta_{f1} \left(\frac{1}{T_{bf1}} - \frac{1}{T_s} \right) \right] \quad (4.8a)$$

$$X_{f2s} = \hat{X}_{f2s} \exp \left[\beta_{f2} \left(\frac{1}{T_{bf2}} - \frac{1}{T_s} \right) \right] \quad (4.8b)$$

where,

$$\beta_{f1} = \frac{W_{f1} L_{f1} C_{p,\infty}}{R_u} \text{ and, } \beta_{f2} = \frac{W_{f2} L_{f2} C_{p,\infty}}{R_u} \quad (4.8c)$$

(c) At outer boundary ($r \rightarrow \infty$)

$$T = T_\infty, \quad (4.9a)$$

$$Y_{f1} = 0 \quad (4.9b)$$

$$Y_{f2} = 0 \quad (4.9c)$$

$$Y_x = Y_{x,\infty} \quad (4.9d)$$

Initial Conditions

(a) Liquid phase

$$\hat{T}(r, 0) = \hat{T}_{in}, \quad (4.10a)$$

$$\hat{Y}_{f1}(r, 0) = \hat{Y}_{in,f1}, \quad (4.10b)$$

$$\hat{Y}_{f2}(r, 0) = \hat{Y}_{in,f2} \quad (4.10c)$$

(b) Gas phase

$$T(r, 0) = T_{in} \quad (4.11a)$$

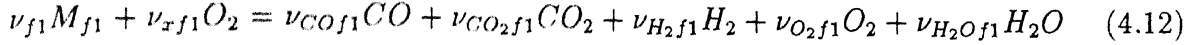
$$Y_{f1}(r, 0) = Y_{in,f1} \quad (4.11b)$$

$$Y_{f2}(r, 0) = Y_{in,f2} \quad (4.11c)$$

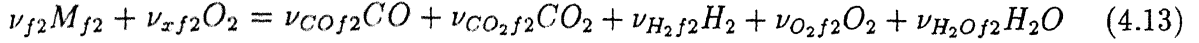
$$Y_x(r, 0) = Y_{in,x} \quad (4.11d)$$

4.5 Calculation of Heat of Reaction

The combustion reaction of the two fuels $f1$ and $f2$ can be represented separately as



and,



where, ν are the stoichiometric coefficients corresponding to different reactants (M_{f1} , M_{f2} , O_2) and products (CO , CO_2 , H_2 , O_2 , H_2O) and are indicated by the subscripts. Now, the reaction rate for the reactants as well as for the products ($\dot{\omega}_i$) can be evaluated from the overall reaction rates ($\dot{\omega}_1$ and $\dot{\omega}_2$ for the present case) as

$$\begin{aligned} \dot{\omega}_{f1} &= -\nu_{f1}\dot{\omega}_1 & \dot{\omega}_{xf1} &= -\nu_{xf1}\dot{\omega}_1 \\ \dot{\omega}_{COf1} &= -\nu_{COf1}\dot{\omega}_1 & \dot{\omega}_{CO_2f1} &= -\nu_{CO_2f1}\dot{\omega}_1 \\ \dot{\omega}_{H_2f1} &= -\nu_{H_2f1}\dot{\omega}_1 & \dot{\omega}_{H_2Of1} &= -\nu_{H_2Of1}\dot{\omega}_1 \end{aligned} \quad (4.14a)$$

and

$$\begin{aligned} \dot{\omega}_{f2} &= -\nu_{f2}\dot{\omega}_2 & \dot{\omega}_{xf2} &= -\nu_{xf2}\dot{\omega}_2 \\ \dot{\omega}_{COf2} &= -\nu_{COf2}\dot{\omega}_2 & \dot{\omega}_{CO_2f2} &= -\nu_{CO_2f2}\dot{\omega}_2 \\ \dot{\omega}_{H_2f2} &= -\nu_{H_2f2}\dot{\omega}_2 & \dot{\omega}_{H_2Of2} &= -\nu_{H_2Of2}\dot{\omega}_2 \end{aligned} \quad (4.14b)$$

$\dot{\omega}_{f1}$ and $\dot{\omega}_{f2}$ can be calculated from Eqs. 4.14a and 4.14b, and $\dot{\omega}_x$ can be calculated as

$$\dot{\omega}_x = \frac{\nu_{xf1}}{\nu_{f1}}\dot{\omega}_{f1} + \frac{\nu_{xf2}}{\nu_{f2}}\dot{\omega}_{f2} \quad (4.14c)$$

where, $\dot{\omega}_1$ is the overall reaction rate for the reaction given by Eq. 4.12 and $\dot{\omega}_2$ is the overall reaction rate for the reaction given by Eq. 4.13. These reaction rates for the two Eqs. 4.12 and 4.13 can be calculated from the relations

$$\dot{\omega}_1(\text{mole}/\text{m}^3/\text{sec}) = A_1 T^{\alpha_1} [C_{f1}]^{a_1} [C_{x1}]^{b_1} \exp\left[-\frac{E_1}{R_u T}\right] \quad (4.15a)$$

and,

$$\dot{\omega}_2(\text{mole}/\text{m}^3/\text{sec}) = A_2 T^{\alpha_2} [C_{f2}]^{\alpha_2} [C_{x2}]^{\beta_2} \exp\left[-\frac{E_2}{R_u T}\right] \quad (4.15b)$$

Heat of reaction for fuels 1 and 2 can be calculated as

$$\Delta h_{r,f1} = \nu_{f1} h_{f1}^0 + \nu_{xf1} h_x^0 - \nu_{CO f1} h_{CO}^0 - \nu_{CO_2 f1} h_{CO_2}^0 - \nu_{H_2 f1} h_{H_2}^0 - \nu_{O_2 f1} h_{O_2}^0 - \nu_{H_2O f1} h_{H_2O}^0 \quad (4.16a)$$

and,

$$\Delta h_{r,f2} = \nu_{f2} h_{f2}^0 + \nu_{xf2} h_x^0 - \nu_{CO f2} h_{CO}^0 - \nu_{CO_2 f2} h_{CO_2}^0 - \nu_{H_2 f2} h_{H_2}^0 - \nu_{O_2 f2} h_{O_2}^0 - \nu_{H_2O f2} h_{H_2O}^0 \quad (4.16b)$$

Now,

$$\begin{aligned} -\sum_{i=1}^N h_i^0 \dot{\omega}_i &= -\left[h_{f1}^0 \dot{\omega}_{f1} + h_{f2}^0 \dot{\omega}_{f2} + h_x^0 \dot{\omega}_{xf1} + h_x^0 \dot{\omega}_{xf2} \right. \\ &\quad \left. + h_{H_2O}^0 \dot{\omega}_{H_2O f1} + h_{H_2O}^0 \dot{\omega}_{H_2O f2} + h_{CO_2}^0 \dot{\omega}_{CO_2 f1} + h_{CO_2}^0 \dot{\omega}_{CO_2 f2} \right] \\ &= -\left[h_{f1}^0 \dot{\omega}_{f1} + h_{f2}^0 \dot{\omega}_{f2} + h_x^0 (\dot{\omega}_{xf1} + \dot{\omega}_{xf2}) \right. \\ &\quad \left. + h_{H_2O}^0 (\dot{\omega}_{H_2O f1} + \dot{\omega}_{H_2O f2}) + h_{CO_2}^0 (\dot{\omega}_{CO_2 f1} + \dot{\omega}_{CO_2 f2}) \right] \\ &= -\left[-h_{f1}^0 \nu_{f1} \dot{\omega}_1 - h_{f2}^0 \nu_{f2} \dot{\omega}_2 - h_x^0 (\nu_{xf1} \dot{\omega}_1 + \nu_{xf2} \dot{\omega}_2) \right. \\ &\quad \left. + h_{H_2O}^0 (\nu_{H_2O f1} \dot{\omega}_1 + \nu_{H_2O f2} \dot{\omega}_2) + h_{CO_2}^0 (\nu_{CO_2 f1} \dot{\omega}_1 + \nu_{CO_2 f2} \dot{\omega}_2) \right] \\ &= \dot{\omega}_1 \left[\nu_{f1} h_{f1}^0 + \nu_{xf1} h_x^0 - \nu_{H_2O f1} h_{H_2O}^0 - \nu_{CO_2 f1} h_{CO_2}^0 \right] \\ &\quad + \dot{\omega}_2 \left[\nu_{f2} h_{f2}^0 + \nu_{xf2} h_x^0 - \nu_{H_2O f2} h_{H_2O}^0 - \nu_{CO_2 f2} h_{CO_2}^0 \right] \\ &= \dot{\omega}_1 \Delta h_{r,f1} + \dot{\omega}_2 \Delta h_{r,f2} \end{aligned}$$

So, $-\sum_{i=1}^N h_i^0 \dot{\omega}_i$, in $J/\text{m}^3/\text{s}$, can be calculated by the expression

$$-\sum_{i=1}^N h_i^0 \dot{\omega}_i = \dot{\omega}_1 \Delta h_{r,f1} + \dot{\omega}_2 \Delta h_{r,f2} \quad (4.17)$$

where, $\dot{\omega}_1$ and $\dot{\omega}_2$ are calculated in $\text{mole}/\text{m}^3/\text{s}$, and $\Delta h_{r,f1}$ and $\Delta h_{r,f2}$ are calculated in J/mole .

4.6 Finite Difference Method of Solution for Liquid phase

In the present problem of droplet combustion, once the droplets are sprayed into the combustion chamber, the droplet surface immediately starts regressing, giving rise to moving boundary at the liquid-gas interface. For the sake of computational analysis, when this moving surface is converted into a stationary surface by a suitable transformation, a convective term appears in the transport equations of the liquid phase, although there is no motion inside the droplet. For a finite difference solution this convective term creates problem if the whole differential equation is discretized using central difference scheme. To eliminate this difficulty, upwind scheme is applied for discretizing the convective part and central differencing scheme is used for discretizing the the diffusive part. Thus, by discretization of the liquid phase equations, a set of algebraic equations is obtained. This set of algebraic equations are put into a tri-diagonal-matrix form to obtain the solution. The program, developed for solving the liquid phase, is quite general in nature. It can handle implicit, explicit and, Crank- Nicholson schemes separately. For the present case, implicit scheme has been used considering the freedom for choosing the time step, Δt .

4.6.1 Domain Discretization

It is seen that the equations are very steep near the droplet surface. Therefore, a non-uniform exponential grid was applied to discretize the domain inside the liquid droplet. This exponential distribution of the grid points was obtained by applying the relation (Sanyal, 1991),

$$r = B \exp(A\delta) + C \quad (4.18a)$$

where,

$$A = \frac{n_r \ln(e_r)}{n_r - 1} \quad B = \frac{r_1 - r_2}{\exp(A - 1)} \quad C = 1 - B \quad (4.18b)$$

n_r = number of radial elements,

$e_r = \frac{\text{maximum grid length}}{\text{minimum grid length}},$

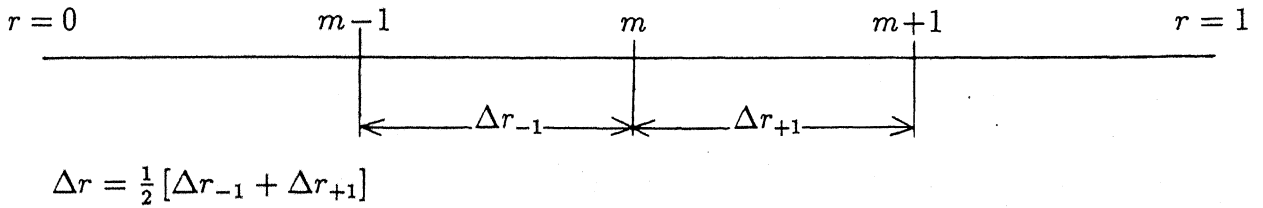
r_1 = starting of the domain for liquid phase,

r_2 = end of the domain for liquid phase,

and δ varies from 0 to 1 in uniform step size ($1/n_r$). For the present problem, $n_r = 30$ and $e_r = 500$ were chosen.

4.6.2 Algebraic Equations

The set of governing differential Eqs. 4.1 for the liquid phase and the corresponding boundary conditions given by Eqs. 4.3 through 4.9 are discretized as follows.



$$\Delta r = \frac{1}{2} [\Delta r_{-1} + \Delta r_{+1}]$$

Applying the central difference scheme, the derivatives can be expressed as

$$\left. \frac{d\hat{Y}}{dr} \right|_m = \frac{\hat{Y}_{m+1} - \hat{Y}_{m-1}}{2\Delta r} \quad (4.19a)$$

$$\frac{d^2\hat{Y}}{dr^2} = \left[\frac{\hat{Y}_{m+1}}{\Delta r_{+1}} - \left(\frac{1}{\Delta r_{+1}} + \frac{1}{\Delta r_{-1}} \right) \hat{Y}_m + \frac{\hat{Y}_{m-1}}{\Delta r_{-1}} \right] \frac{1}{\Delta r} \quad (4.19b)$$

and, applying the upwind scheme, we have

$$\left. \frac{d\hat{Y}}{dr} \right|_m = \frac{\hat{Y}_m - \hat{Y}_{m-1}}{\Delta r_{-1}} \quad (4.19c)$$

Equation (4.1a) can be discretized by applying the central difference for the diffusive term, and upwind scheme for the convective term as follows.

$$\begin{aligned} \frac{\hat{Y}_{f1}^{p+1} - \hat{Y}_{f1}^p}{\Delta t} &= \theta \left. \frac{\partial \hat{Y}_{f1}}{\partial t} \right|_m^{p+1} + (1 - \theta) \left. \frac{\partial \hat{Y}_{f1}}{\partial t} \right|_m^p \\ &= \theta \left[\left(\frac{2}{r} \frac{\partial \hat{Y}_{f1}}{\partial r} + \frac{\partial^2 \hat{Y}_{f1}}{\partial r^2} \right) \hat{D} - \left(\frac{Sc u_d \rho r}{\hat{\rho}} \right) \frac{\partial \hat{Y}_{f1}}{\partial r} \right]_m^{p+1} \\ &+ (1 - \theta) \left[\left(\frac{2}{r} \frac{\partial \hat{Y}_{f1}}{\partial r} + \frac{\partial^2 \hat{Y}_{f1}}{\partial r^2} \right) \hat{D} - \left(\frac{Sc u_d \rho r}{\hat{\rho}} \right) \frac{\partial \hat{Y}_{f1}}{\partial r} \right]_m^p \end{aligned}$$

$$\begin{aligned}
&= \theta \left[\left\{ \frac{2}{r} \left(\frac{\hat{Y}_{f1,m+1} - \hat{Y}_{f1,m-1}}{2\Delta r} \right) + \left(\frac{\hat{Y}_{f1,m+1}}{\Delta r_{+1}} - \left(\frac{1}{\Delta r_{+1}} + \frac{1}{\Delta r_{-1}} \right) \hat{Y}_{f1,m} \right. \right. \right. \\
&\quad \left. \left. + \frac{\hat{Y}_{f1,m-1}}{\Delta r_{-1}} \right) \frac{1}{\Delta r} \right\} \hat{D} - \left(\frac{Sc u_d \rho r}{\hat{\rho}} \right) \frac{(\hat{Y}_{f1,m} - \hat{Y}_{f1,m-1})}{\Delta r_{-1}} \right]^{p+1} \\
&+ (1 - \theta) \left[\left\{ \frac{2}{r} \left(\frac{\hat{Y}_{f1,m+1} - \hat{Y}_{f1,m-1}}{2\Delta r} \right) + \left(\frac{\hat{Y}_{f1,m+1}}{\Delta r_{+1}} - \left(\frac{1}{\Delta r_{+1}} + \frac{1}{\Delta r_{-1}} \right) \hat{Y}_{f1,m} \right. \right. \right. \\
&\quad \left. \left. + \frac{\hat{Y}_{f1,m-1}}{\Delta r_{-1}} \right) \frac{1}{\Delta r} \right\} \hat{D} - \left(\frac{Sc u_d \rho r}{\hat{\rho}} \right) \frac{(\hat{Y}_{f1,m} - \hat{Y}_{f1,m-1})}{\Delta r_{-1}} \right]^{p+1}
\end{aligned}$$

Finally, rearranging the above expression, we arrive at the following form of discretized equation for the liquid phase species, $f1$, as

$$A_{f1} \hat{Y}_{f1,m-1}^{p+1} + B_{f1} \hat{Y}_{f1,m}^{p+1} + C_{f1} \hat{Y}_{f1,m+1}^{p+1} = A1_{f1} \hat{Y}_{f1,m-1}^p + B1_{f1} \hat{Y}_{f1,m}^p + C1_{f1} \hat{Y}_{f1,m+1}^p \quad (4.20a)$$

where, the coefficients can be expressed as

$$A_{f1} = -\theta \Delta t \left[\frac{-\hat{D}}{r \Delta r} + \frac{\hat{D}}{\Delta r \Delta r_{-1}} + \frac{Sc u_d \rho r}{\hat{\rho} \Delta r_{-1}} \right] \quad (4.20b)$$

$$B_{f1} = 1 + \frac{\theta \Delta t \hat{D}}{\Delta r} \left(\frac{1}{\Delta r_{+1}} + \frac{1}{\Delta r_{-1}} \right) + \frac{\theta \Delta t Sc u_d \rho r}{\hat{\rho} \Delta r_{-1}} \quad (4.20c)$$

$$C_{f1} = \frac{-\theta \Delta t \hat{D}}{\Delta r} \left[\frac{1}{r} + \frac{1}{\Delta r_{+1}} \right] \quad (4.20d)$$

$$A1_{f1} = (1 - \theta) \Delta t \left[\frac{-\hat{D}}{r \Delta r} + \frac{\hat{D}}{\Delta r \Delta r_{-1}} + \frac{Sc u_d \rho r}{\hat{\rho} \Delta r_{-1}} \right] \quad (4.20e)$$

$$B1_{f1} = 1 - \frac{(1 - \theta) \Delta t \hat{D}}{\Delta r} \left(\frac{1}{\Delta r_{+1}} + \frac{1}{\Delta r_{-1}} \right) - \frac{(1 - \theta) \Delta t Sc u_d \rho r}{\hat{\rho} \Delta r_{-1}} \quad (4.20f)$$

$$C1_{f1} = \frac{(1 - \theta) \Delta t \hat{D}}{\Delta r} \left[\frac{1}{r} + \frac{1}{\Delta r_{+1}} \right] \quad (4.20g)$$

Similarly, the energy transport equation for the liquid phase can discretized and expressed in the form

$$A_T \hat{T}_{m-1}^{p+1} + B_T \hat{T}_m^{p+1} + C_T \hat{T}_{m+1}^{p+1} = A1_T \hat{T}_{m-1}^p + B1_T \hat{T}_m^p + C1_T \hat{T}_{m+1}^p \quad (4.21a)$$

Where, the coefficients are expressed as

$$A_T = -\theta \Delta t \left[\frac{-\hat{\alpha} Le}{r \Delta r} + \frac{\hat{\alpha} Le}{\Delta r \Delta r_{-1}} + \frac{Sc u_d \rho r}{\hat{\rho} \Delta r_{-1}} \right] \quad (4.21b)$$

$$B_T = 1 + \frac{\theta \Delta t \hat{\alpha} Le}{\Delta r} \left(\frac{1}{\Delta r_{+1}} + \frac{1}{\Delta r_{-1}} \right) + \frac{\theta \Delta t Sc u_d \rho r}{\hat{\rho} \Delta r_{-1}} \quad (4.21c)$$

$$C_T = \frac{-\theta \Delta t \hat{\alpha} Le}{\Delta r} \left[\frac{1}{r} + \frac{1}{\Delta r_{+1}} \right] \quad (4.21d)$$

$$Al_T = (1 - \theta) \Delta t \left[\frac{-\hat{\alpha} Le}{r \Delta r} + \frac{\hat{\alpha} Le}{\Delta r \Delta r_{-1}} + \frac{Sc u_d \rho r}{\hat{\rho} \Delta r_{-1}} \right] \quad (4.21e)$$

$$B1_T = 1 - \frac{(1 - \theta) \Delta t \hat{\alpha} Le}{\Delta r} \left(\frac{1}{\Delta r_{+1}} + \frac{1}{\Delta r_{-1}} \right) - \frac{(1 - \theta) \Delta t Sc u_d \rho r}{\hat{\rho} \Delta r_{-1}} \quad (4.21f)$$

$$C1_T = \frac{(1 - \theta) \Delta t \hat{\alpha} Le}{\Delta r} \left[\frac{1}{r} + \frac{1}{\Delta r_{+1}} \right] \quad (4.21g)$$

The above discretized Eqs. 4.20a and 4.21a are very general, and can be used for either of the three schemes, explicit, Crank-Nicholson or implicit. Here,

$\theta = 0$ for explicit scheme,

$\theta = \frac{1}{2}$ for Crank-Nicholson scheme,

$\theta = 1$ for implicit scheme.

4.6.3 Discretization of Boundary Conditions

(i) for droplet center ($r = 0$)

The spherical coordinate system can not be applied at $r=0$. So, at $r=0$, the differential equations are discretized in rectangular coordinate system as follows.

Equations 2.32a and 2.34 for species (\hat{Y}_{f1}) and temperature (\hat{T}) can be expressed in 3-dimensional rectangular coordinates as

$$\frac{\partial \hat{Y}_{f1}}{\partial t} + Sc aa \left[x \frac{\partial \hat{Y}_{f1}}{\partial x} + y \frac{\partial \hat{Y}_{f1}}{\partial y} + z \frac{\partial \hat{Y}_{f1}}{\partial z} \right] - \hat{D} \left[\frac{\partial^2 \hat{Y}_{f1}}{\partial x^2} + \frac{\partial^2 \hat{Y}_{f1}}{\partial y^2} + \frac{\partial^2 \hat{Y}_{f1}}{\partial z^2} \right] = 0 \quad (4.22a)$$

and

$$\frac{\partial \hat{T}}{\partial t} + Sc aa \left[x \frac{\partial \hat{T}}{\partial x} + y \frac{\partial \hat{T}}{\partial y} + z \frac{\partial \hat{T}}{\partial z} \right] - \hat{D} \left[\frac{\partial^2 \hat{T}}{\partial x^2} + \frac{\partial^2 \hat{T}}{\partial y^2} + \frac{\partial^2 \hat{T}}{\partial z^2} \right] = 0 \quad (4.22b)$$

where, $aa = \rho u_d / \hat{\rho}$. Equations 4.22a and 4.22b can be discretized in a manner similar to that done on Eq. 4.1a in the previous section, and the simplified form can be written as

$$\frac{\hat{Y}_{f1}^{p+1} - \hat{Y}_{f1}^p}{\Delta t} \Big|_{m,n,l} = \theta \frac{\partial \hat{Y}_{f1}}{\partial t} \Big|_{m,n,l}^{p+1} + (1 - \theta) \frac{\partial \hat{Y}_{f1}}{\partial t} \Big|_{m,n,l}^p$$

The right hand side (R.H.S.) of the above equation is expressed as

R.H.S.

$$\begin{aligned}
 &= -\theta Sc aa \left[x \frac{\partial \hat{Y}_{f1}}{\partial x} + y \frac{\partial \hat{Y}_{f1}}{\partial y} + z \frac{\partial \hat{Y}_{f1}}{\partial z} \right]_{m,n,l}^{p+1} - (1-\theta) Sc aa \left[x \frac{\partial \hat{Y}_{f1}}{\partial x} + y \frac{\partial \hat{Y}_{f1}}{\partial y} + z \frac{\partial \hat{Y}_{f1}}{\partial z} \right]_{m,n,l}^p \\
 &+ \theta \hat{D} \left[\frac{\partial^2 \hat{Y}_{f1}}{\partial x^2} + \frac{\partial^2 \hat{Y}_{f1}}{\partial y^2} + \frac{\partial^2 \hat{Y}_{f1}}{\partial z^2} \right]_{m,n,l}^{p+1} + (1-\theta) \hat{D} \left[\frac{\partial^2 \hat{Y}_{f1}}{\partial x^2} + \frac{\partial^2 \hat{Y}_{f1}}{\partial y^2} + \frac{\partial^2 \hat{Y}_{f1}}{\partial z^2} \right]_{m,n,l}^p \\
 &= -\theta Sc aa \left[x \frac{\hat{Y}_{f1,m,n,l} - \hat{Y}_{f1,m-1,n,l}}{\Delta x} + y \frac{\hat{Y}_{f1,m,n,l} - \hat{Y}_{f1,m,n-1,l}}{\Delta y} + z \frac{\hat{Y}_{f1,m,n,l} - \hat{Y}_{f1,m,n,l-1}}{\Delta z} \right]^{p+1} \\
 &- (1-\theta) Sc aa \left[x \frac{\hat{Y}_{f1,m,n,l} - \hat{Y}_{f1,m-1,n,l}}{\Delta x} + y \frac{\hat{Y}_{f1,m,n,l} - \hat{Y}_{f1,m,n-1,l}}{\Delta y} + z \frac{\hat{Y}_{f1,m,n,l} - \hat{Y}_{f1,m,n,l-1}}{\Delta z} \right]^p \\
 &+ \theta \hat{D} \left[\frac{(\hat{Y}_{f1,m+1,n,l} - 2\hat{Y}_{f1,m,n,l} + \hat{Y}_{f1,m-1,n,l})}{(\Delta x)^2} + \frac{(\hat{Y}_{f1,m,n+1,l} - 2\hat{Y}_{f1,m,n,l} + \hat{Y}_{f1,m,n-1,l})}{(\Delta y)^2} \right. \\
 &+ \left. \frac{(\hat{Y}_{f1,m,n,l+1} - 2\hat{Y}_{f1,m,n,l} + \hat{Y}_{f1,m,n,l-1})}{(\Delta z)^2} \right]^{p+1} + (1-\theta) \hat{D} \left[\frac{(\hat{Y}_{f1,m+1,n,l} - 2\hat{Y}_{f1,m,n,l} + \hat{Y}_{f1,m-1,n,l})}{(\Delta x)^2} \right. \\
 &+ \left. \frac{(\hat{Y}_{f1,m,n+1,l} - 2\hat{Y}_{f1,m,n,l} + \hat{Y}_{f1,m,n-1,l})}{(\Delta y)^2} + \frac{(\hat{Y}_{f1,m,n,l+1} - 2\hat{Y}_{f1,m,n,l} + \hat{Y}_{f1,m,n,l-1})}{(\Delta z)^2} \right]^p
 \end{aligned}$$

Now, assuming equal grid spacing in all the three directions, we have $\Delta x = \Delta y = \Delta z$.

Due to symmetric condition at $r=0$,

$$\hat{Y}_{f1,m-1,n,l} = \hat{Y}_{f1,m,n,l}, \quad \hat{Y}_{f1,m,n-1,l} = \hat{Y}_{f1,m,n,l}, \quad \hat{Y}_{f1,m,n,l-1} = \hat{Y}_{f1,m,n,l} \quad (4.23)$$

Therefore, the above discretized equation for species $f1$ at $r=0$ becomes

$$\frac{\hat{Y}_{f1}^{p+1} - \hat{Y}_{f1}^p}{\Delta t} \Big|_{l,m,n} = \theta \hat{D} \left[\frac{6\hat{Y}_{f1,m+1,n,l} - 6\hat{Y}_{f1,m,n,l}}{(\Delta x)^2} \right]^{p+1} + (1-\theta) \hat{D} \left[\frac{6\hat{Y}_{f1,m+1,n,l} - 6\hat{Y}_{f1,m,n,l}}{(\Delta x)^2} \right]^p$$

or,

$$[(1 + 6q\theta) \hat{Y}_{f1,m} - 6q\theta \hat{Y}_{f1,m+1}]^{p+1} = [(1 + 6q\theta) \hat{Y}_{f1,m} - 6q\theta \hat{Y}_{f1,m+1}]^p \quad (4.24a)$$

where,

$$q = \frac{\hat{D} \Delta t}{(\Delta x)^2} \quad (4.24b)$$

Therefore, the co-efficients for Eqs. 4.20a at $r=0$, are

$$A_{f1} = 0 \quad B_{f1} = 1 + \frac{6\theta \hat{D} \Delta t}{(\Delta r)^2} \quad C_{f1} = \frac{-6\theta \hat{D} \Delta t}{(\Delta r)^2} \quad (4.25a)$$

$$Al_{f1} = 0 \quad Bl_{f1} = 1 - \frac{6(1-\theta)\hat{D}\Delta t}{(\Delta r)^2} \quad Cl_{f1} = \frac{6(1-\theta)\hat{D}\Delta t}{(\Delta r)^2} \quad (4.25b)$$

and, those for Eq. 4.21a at $r=0$, are

$$A_T = 0 \quad B_T = 1 + \frac{6\theta\hat{\alpha}Le\Delta t}{(\Delta r)^2} \quad C_T = \frac{-6\theta\hat{\alpha}Le\Delta t}{(\Delta r)^2} \quad (4.26a)$$

$$Al_T = 0 \quad Bl_T = 1 - \frac{6(1-\theta)\hat{\alpha}Le\Delta t}{(\Delta r)^2} \quad Cl_T = \frac{6(1-\theta)\hat{\alpha}Le\Delta t}{(\Delta r)^2} \quad (4.26b)$$

(iii) for droplet surface ($r = 1$)

Discretizing the boundary conditions (Eq 4.6a) at $r=1$, we get the following discretized equation

$$\frac{\hat{Y}_{f1,m+1} - \hat{Y}_{f1,m-1}}{2\Delta r} + \frac{aa Sc}{\hat{D}} (\epsilon_{f1} - \hat{Y}_{f1,m}) = 0$$

or,

$$\hat{Y}_{f1,m+1} = \hat{Y}_{f1,m-1} - 2\frac{\Delta r aa Sc}{\hat{D}} (\epsilon_{f1} - \hat{Y}_{f1,m}) \quad (4.27a)$$

Similarly, discretizing the boundary condition (Eq. 4.7) at $r=1$, we get

$$\hat{T}_{m+1} = \frac{2\Delta r H_l}{\hat{\lambda}} + \hat{T}_{m-1} \quad (4.27b)$$

Now, substituting the expressions for $\hat{Y}_{f1,m+1}$ and \hat{T}_{m+1} from Eqs. 4.27a and 4.27b into Eqs. 4.20a and 4.21a, we get

$$\begin{aligned} & (A_{f1} + C_{f1}) \hat{Y}_{f1,m-1}^{p+1} + \left(B_{f1} + \frac{2\Delta r aa Sc}{\hat{D}} \right) \hat{Y}_m^{p+1} \\ &= (Al_{f1} + Cl_{f1}) \hat{Y}_{f1,m-1}^p + \left(Bl_{f1} + \frac{2\Delta r aa Sc}{\hat{D}} \right) \hat{Y}_m^p + \frac{2\Delta r aa Sc \epsilon_{f1}}{\hat{D}} C_{f1} \Big|^{p+1} - \frac{2\Delta r aa Sc \epsilon_{f1}}{\hat{D}} \end{aligned} \quad (4.28a)$$

$$\begin{aligned} & (A_T + C_T) T_{m-1}^{p+1} + B_T T_m^{p+1} \\ &= (Al_T + Cl_T) T_{m-1}^p + B_{lT} T_m^p - \frac{2\Delta r H_l}{\hat{\lambda}} C_T \Big|^{p+1} + \frac{2\Delta r H_l}{\hat{\lambda}} C_{lT} \Big|^p \end{aligned} \quad (4.28b)$$

The whole set of algebraic equations can be represented in the form of tri-diagonal matrices and solved through standard algorithm.

4.7 Finite Element Method of Solution for Gas Phase

Finite Element Method is basically an integral approach to solve governing differential equations representing a given process in a given domain. For the present study, Galerkin's Weighted Residual Method is used to discretize the gas phase equations. In this method, the entire domain is discretized into a number of neighbouring elements. By substituting the approximate numerical solution back into the differential equation, one gets a residue. In order to minimise the residue in an integral sense, the residue is integrated with respect to a suitable weighting function, known as the interpolation function, over each elemental domain and then it is put to zero. As an outcome of the integration performed by applying a suitable quadrature rule, a set of algebraic equations is obtained for each element. All these equations are then assembled into a global matrix. Then the boundary conditions are added. Later this global matrix is solved by a suitable algorithm.

For the present analysis, the global matrix takes the shape of a tri-diagonal matrix (TDM) due to one dimensional spherical geometry. This TDM was solved by a standard TDM solver.

4.7.1 Domain Discretization

The domain discretization for the gas phase solution is very important for the present problem. This is because finite rate chemistry has been taken into account while the problem is modeled. Here, an adaptive grid generation technique is applied for tracking the flame movement. For this, adaptive grid generation technique is developed as a separate module. As the solution scheme marches in time direction, after each time step, the adaptive grid generation module is called separately to check the necessity of changing grid point distribution. This is based on an error calculation method which is done statistically. This process is separately discussed later.

4.7.2 Finite Element Formulation for the Gas Phase

$$\begin{array}{ccc} r_1 & \xrightarrow{\hspace{10em}} & r_2 \\ 1 & & 2 \\ \xi=-1 & & \xi=+1 \end{array}$$

In finite element formulation, the interpolation functions, also known as the shape functions, are generally selected from polynomial functions like Lagrangian, Hermitian etc. For iso-parametric elements, the shape function for the variable and the mapping function for coordinate transformation are taken to be identical. Here, the iso-parametric feature of the elements are retained and the shape functions (N_i) are chosen to be linear, for the sake of simplicity, as

$$N_i = \frac{1}{2}(1 + \xi\xi_i), \quad i = 1, 2 \quad (4.29)$$

where, ξ is the local coordinate, varying from -1 to +1 within each element.

The global coordinate, r , can be transformed into the local coordinate, ξ , by the relation

$$\xi = \frac{r - \left(\frac{r_1+r_2}{2}\right)}{\frac{r_2-r_1}{2}} \quad (4.30)$$

where, r_1, r_2 = global coordinates for points 1 and 2 respectively as shown in the sketch above. Following the above iso-parametric formulation, the variables and the coordinates vary linearly within the elements and can be expressed as

$$r = \sum_{i=1}^N r_i N_i, \quad Y_{f1} = \sum_{i=1}^N Y_{f1,i} N_i, \quad Y_{f2} = \sum_{i=1}^N Y_{f2,i} N_i, \quad Y_x = \sum_{i=1}^N Y_{x,i} N_i \text{ and } Y_T = \sum_{i=1}^N Y_{T,i} N_i \quad (4.31)$$

where $Y_T = \int_{T^0}^T C_p dT$ and $i=1,2$. By applying Galerkin weighted residual technique, the gas phase equations are weighted by the linear shape functions, N_i . Applying this technique, the Eqs. 4.2a through 4.2d can be written as

$$R_{Y_{f1}}^e = \int_e N_i \left[\frac{\partial Y_{f1}}{\partial t} + Sc u_d \left(\frac{1}{r^2} + \frac{\rho r}{\hat{\rho}} \right) \frac{\partial Y_{f1}}{\partial r} - \frac{D}{r^2} \frac{\partial}{\partial r} \left(r^2 \frac{\partial Y_{f1}}{\partial r} \right) - Q_{f1} \right] 4\pi r^2 dr = 0 \quad (4.32a)$$

$$R_{Y_{f2}}^e = \int_e N_i \left[\frac{\partial Y_{f2}}{\partial t} + Sc u_d \left(\frac{1}{r^2} + \frac{\rho r}{\hat{\rho}} \right) \frac{\partial Y_{f2}}{\partial r} - \frac{D}{r^2} \frac{\partial}{\partial r} \left(r^2 \frac{\partial Y_{f2}}{\partial r} \right) - Q_{f2} \right] 4\pi r^2 dr = 0 \quad (4.32b)$$

$$R_{Y_x}^e = \int_e N_i \left[\frac{\partial Y_x}{\partial t} + Sc u_d \left(\frac{1}{r^2} + \frac{\rho r}{\hat{\rho}} \right) \frac{\partial Y_x}{\partial r} - \frac{D}{r^2} \frac{\partial}{\partial r} \left(r^2 \frac{\partial Y_x}{\partial r} \right) - Q_x \right] 4\pi r^2 dr = 0 \quad (4.32c)$$

$$R_{Y_T}^e = \int_e N_i \left[\frac{\partial Y_T}{\partial t} + Sc u_d \left(\frac{1}{r^2} + \frac{\rho r}{\hat{\rho}} \right) \frac{\partial Y_T}{\partial r} - \frac{D}{r^2} \frac{\partial}{\partial r} \left(r^2 \frac{\partial Y_T}{\partial r} \right) + \frac{1}{r^2} \frac{\partial}{\partial r} \left(\left(\frac{\rho D C_p - \lambda Le}{\rho} \right) r^2 \frac{\partial \bar{T}}{\partial r} \right) - Q_T \right] 4\pi r^2 dr = 0 \quad (4.32d)$$

where, $\bar{}$ indicates the previously iterated value. In Eq. 4.32a, the integrals containing the double derivative term can be further simplified by applying integration by parts to those highest order derivatives and consequently the double derivatives can be reduced to single derivatives as follows.

R.H.S. of equation(4.32a)

$$\begin{aligned} &= \int_e N_i \dot{Y}_{f1} r^2 dr + Sc u_d \int_e N_i \left(1 + \frac{\rho r^3}{\hat{\rho}} \right) \frac{\partial Y_{f1}}{\partial r} dr - D \int_e N_i r^2 \frac{\partial^2 Y_{f1}}{\partial r^2} dr \\ &- 2D \int_e N_i r \frac{\partial Y_{f1}}{\partial r} dr - \int_e N_i Q_{f1} r^2 dr \end{aligned}$$

Since,

$$-D \int_e N_i r^2 \frac{\partial^2 Y_{f1}}{\partial r^2} dr = -N_i r^2 D \frac{\partial Y_{f1}}{\partial r} \Big|_{r_1}^{r_2} + \int_e \left(2r N_i D + D r^2 \frac{\partial N_i}{\partial r} \right) \frac{\partial Y_{f1}}{\partial r} dr$$

R.H.S. of equation(4.32a)

$$\begin{aligned} &= \int_e N_i \dot{Y}_{f1} r^2 dr + Sc u_d \int_e N_i \left(1 + \frac{\rho r^3}{\hat{\rho}} \right) \frac{\partial Y_{f1}}{\partial r} dr + D \int_e r^2 \frac{\partial N_i}{\partial r} \frac{\partial Y_{f1}}{\partial r} dr - \int_e N_i Q_{f1} r^2 dr \\ &- N_i r^2 D \frac{\partial Y_{f1}}{\partial r} \Big|_{r=r_2} + N_i r^2 D \frac{\partial Y_{f1}}{\partial r} \Big|_{r=r_1} = 0 \end{aligned}$$

Therefore,

$$R_{Y_{f1}}^e = \int_e N_i \dot{Y}_{f1} r^2 dr + Sc u_d \int_e N_i \left(1 + \frac{\rho r^3}{\hat{\rho}}\right) \frac{\partial Y_{f1}}{\partial r} dr + D \int_e r^2 \frac{\partial N_i}{\partial r} \frac{\partial Y_{f1}}{\partial r} dr \\ - \int_e N_i Q_{f1} r^2 dr - N_i r_2^2 D \frac{\partial Y_{f1}}{\partial r} \Big|_{r=r_2} + N_i r_1^2 D \frac{\partial Y_{f1}}{\partial r} \Big|_{r=r_1} = 0$$

Boundary conditions appear as a part of the finite element expression given by Eq. 4.33a.

Similarly, Eqs. 4.32b,c,d can also be simplified to get the following relations.

$$R_{Y_{f2}}^e = \int_e N_i \dot{Y}_{f2} r^2 dr + Sc u_d \int_e N_i \left(1 + \frac{\rho r^3}{\hat{\rho}}\right) \frac{\partial Y_{f2}}{\partial r} dr + D \int_e r^2 \frac{\partial N_i}{\partial r} \frac{\partial Y_{f2}}{\partial r} dr \\ - \int_e N_i Q_{f2} r^2 dr - N_i r_2^2 D \frac{\partial Y_{f2}}{\partial r} \Big|_{r=r_2} + N_i r_1^2 D \frac{\partial Y_{f2}}{\partial r} \Big|_{r=r_1} = 0$$

$$R_{Y_x}^e = \int_e N_i \dot{Y}_x r^2 dr + Sc u_d \int_e N_i \left(1 + \frac{\rho r^3}{\hat{\rho}}\right) \frac{\partial Y_x}{\partial r} dr + D \int_e r^2 \frac{\partial N_i}{\partial r} \frac{\partial Y_x}{\partial r} dr \\ - \int_e N_i Q_x r^2 dr - N_i r_2^2 D \frac{\partial Y_x}{\partial r} \Big|_{r=r_2} + N_i r_1^2 D \frac{\partial Y_x}{\partial r} \Big|_{r=r_1} = 0$$

and,

$$R_{Y_T}^e = \int_e N_i \dot{Y}_T r^2 dr + Sc u_d \int_e N_i \left(1 + \frac{\rho r^3}{\hat{\rho}}\right) \frac{\partial Y_T}{\partial r} dr + D \int_e r^2 \frac{\partial N_i}{\partial r} \frac{\partial Y_T}{\partial r} dr \\ - \int_e r^2 \left(\frac{\rho D C_p - \lambda Le}{\rho} \right) \frac{\partial N_i}{\partial r} \frac{\partial \bar{T}}{\partial r} dr - \int_e N_i Q_T r^2 dr \\ + \left(\frac{\rho D C_p - \lambda Le}{\rho} \right) N_i r_2^2 \frac{\partial \bar{T}}{\partial r} \Big|_{r=r_2} - \left(\frac{\rho D C_p - \lambda Le}{\rho} \right) N_i r_1^2 \frac{\partial \bar{T}}{\partial r} \Big|_{r=r_1} \\ - N_i r_2^2 D \frac{\partial Y_T}{\partial r} \Big|_{r=r_2} + N_i r_1^2 D \frac{\partial Y_T}{\partial r} \Big|_{r=r_1} = 0$$

Reduction of highest order derivative is achieved through weak formulation for the case of multiple integrals. The advantage of such a reduction is that the order of the shape functions can be reduced upto which this need be complete. By assembling all the elemental matrices and vectors into one global assembly, we arrive at the following relations for the expressions 4.33a,b,c,d.

$$\begin{aligned}
R_{Y_{f1}} &= \sum_{e=1}^N R_{Y_{f1}}^e = \sum_{e=1}^N \left[\int_e N_i N_j r^2 dr \right] \{ \dot{Y}_{f1,j} \} \\
&+ \sum_{e=1}^N \left[S_c u_d \int_e N_i \left(1 + \frac{\rho r^3}{\hat{\rho}} \right) \frac{\partial N_j}{\partial r} dr + D \int_e r^2 \frac{\partial N_i}{\partial r} \frac{\partial N_j}{\partial r} dr \right] \{ Y_{f1,j} \} \\
&- \sum_{e=1}^N Q_{f1} \int_e N_i r^2 dr - N_i r_\infty^2 D \frac{\partial Y_{f1}}{\partial r} \Big|_{r=r_\infty} + N_i D \frac{\partial Y_{f1}}{\partial r} \Big|_{r=1}
\end{aligned}$$

$$\begin{aligned}
R_{Y_{f2}} &= \sum_{e=1}^N R_{Y_{f2}}^e = \sum_{e=1}^N \left[\int_e N_i N_j r^2 dr \right] \{ \dot{Y}_{f2,j} \} \\
&+ \sum_{e=1}^N \left[S_c u_d \int_e N_i \left(1 + \frac{\rho r^3}{\hat{\rho}} \right) \frac{\partial N_j}{\partial r} dr + D \int_e r^2 \frac{\partial N_i}{\partial r} \frac{\partial N_j}{\partial r} dr \right] \{ Y_{f2,j} \} \\
&- \sum_{e=1}^N Q_{f2} \int_e N_i r^2 dr - N_i r_\infty^2 D \frac{\partial Y_{f2}}{\partial r} \Big|_{r=r_\infty} + N_i D \frac{\partial Y_{f2}}{\partial r} \Big|_{r=1}
\end{aligned}$$

$$\begin{aligned}
R_{Y_x} &= \sum_{e=1}^N R_{Y_x}^e = \sum_{e=1}^N \left[\int_e N_i N_j r^2 dr \right] \{ \dot{Y}_{x,j} \} \\
&+ \sum_{e=1}^N \left[S_c u_d \int_e N_i \left(1 + \frac{\rho r^3}{\hat{\rho}} \right) \frac{\partial N_j}{\partial r} dr + D \int_e r^2 \frac{\partial N_i}{\partial r} \frac{\partial N_j}{\partial r} dr \right] \{ Y_{x,j} \} \\
&- \sum_{e=1}^N Q_x \int_e N_i r^2 dr - N_i r_\infty^2 D \frac{\partial Y_x}{\partial r} \Big|_{r=r_\infty} + N_i D \frac{\partial Y_x}{\partial r} \Big|_{r=1}
\end{aligned}$$

$$\begin{aligned}
R_{Y_T} &= \sum_{e=1}^N R_{Y_T}^e = \sum_{e=1}^N \left[\int_e N_i N_j r^2 dr \right] \{ \dot{Y}_{Tj} \} \\
&+ \sum_{e=1}^N \left[S_c u_d \int_e N_i \left(1 + \frac{\rho r^3}{\hat{\rho}} \right) \frac{\partial N_j}{\partial r} dr + D \int_e r^2 \frac{\partial N_i}{\partial r} \frac{\partial N_j}{\partial r} dr \right] \{ Y_{Tj} \} \\
&- \sum_{e=1}^N \left[\int_e r^2 \left(\frac{\rho D C_p - \lambda Le}{\rho} \right) \frac{\partial N_i}{\partial r} \frac{\partial N_j}{\partial r} dr \right] \{ \bar{T}_j \} - \sum_{e=1}^N Q_T \int_e N_i r^2 dr \\
&+ \left(\frac{\rho D C_p - \lambda Le}{\rho} \right) N_i r_\infty^2 \frac{\partial \bar{T}}{\partial r} \Big|_{r=r_\infty} - \left(\frac{\rho D C_p - \lambda Le}{\rho} \right) N_i r_1^2 \frac{\partial \bar{T}}{\partial r} \Big|_{r=r_1} \\
&- N_i r_\infty^2 D \frac{\partial Y_T}{\partial r} \Big|_{r=r_\infty} + N_i D \frac{\partial Y_T}{\partial r} \Big|_{r=1}
\end{aligned}$$

where, N = number of elements, r_1 and r_2 refers to the two boundaries on either side of each element as shown in the sketch at the beginning of this section.

It is to be noted here that when all the elements are assembled globally, the derivatives at $r = 1$ and at $r = r_2$ cancel out for all the internal elements. Only the the derivative at $r = 1$ and $r = r_\infty$ remain for all the expressions, 4.34a through 4.34d. At $r = 1$, Y_{f1} , Y_{f2} and Y_T have specified boundary condition, and at $r = r_\infty$, all Y_{f1} , Y_{f2} , Y_x and Y_T have specified boundary conditions. Therefore, for Y_{f1} , Y_{f2} and Y_T , the derivative boundary conditions at $r=1$ and at $r = r_\infty$ and that for Y_x at $r = r_\infty$ that arise in the finite element expressions 4.34a,b,d are ignored, because they do not contribute to the assembled matrix. For Y_x , the derivative boundary condition at $r = 1$, can be written by applying $Y_x = \sum_{i=1}^2 Y_{xi} N_i$ as

$$N_i D \frac{\partial Y_x}{\partial r} \bigg|_{r=1} = N_i u_d S c Y_{xs} |_{r=1} = [N_i N_j u_d S c] \{Y_{xj}\} |_{r=1} \quad (4.35)$$

Using the above conditions and Eq. 4.35 the finite element expressions, 4.34a through 4.34d can be written in discretized form as

$$[gmass] \{\dot{Y}_{f1,j}\} + [gcon] \{Y_{f1,j}\} = \{ggen\} \quad (4.36a)$$

$$[gmass] \{\dot{Y}_{f2,j}\} + [gcon] \{Y_{f2,j}\} = \{ggen\} \quad (4.36b)$$

$$[gmass] \{\dot{Y}_{x,j}\} + [gcon] \{Y_{x,j}\} = \{ggen\} \quad (4.36c)$$

$$[gmass] \{\dot{Y}_{Tj}\} + [gcon] \{Y_{Tj}\} = \{ggen\} \quad (4.36d)$$

$$\text{where, } gmass = \sum_{e=1}^N emass; \quad gcon = \sum_{e=1}^N econ; \quad ggen = \sum_{e=1}^N egen .$$

For Y_{f1} :

$$\begin{aligned} emass &= \int_e N_i N_j r^2 dr ; & egen &= \int_e Q_{f1} r^2 N_i dr \\ econ &= S c u_d \int_e N_i \left(1 + \frac{\rho r^3}{\hat{\rho}} \right) \frac{\partial N_j}{\partial r} dr + D \int_e r^2 \frac{\partial N_i}{\partial r} \frac{\partial N_j}{\partial r} dr \end{aligned} \quad (4.37a)$$

For Y_{f2} :

$$\begin{aligned} emass &= \int_e N_i N_j r^2 dr ; & egen &= \int_e Q_{f2} r^2 N_i dr \\ econ &= Sc u_d \int_e N_i \left(1 + \frac{\rho r^3}{\hat{\rho}}\right) \frac{\partial N_j}{\partial r} dr + D \int_e r^2 \frac{\partial N_i}{\partial r} \frac{\partial N_j}{\partial r} dr \end{aligned} \quad (4.37b)$$

For Y_x :

$$\begin{aligned} emass &= \int_e N_i N_j r^2 dr ; & egen &= \int_e Q_x r^2 N_i dr \\ econ &= Sc u_d \int_e N_i \left(1 + \frac{\rho r^3}{\hat{\rho}}\right) \frac{\partial N_j}{\partial r} dr + D \int_e r^2 \frac{\partial N_i}{\partial r} \frac{\partial N_j}{\partial r} dr + u_d Sc N_i N_j|_{r=1} \end{aligned} \quad (4.37c)$$

For Y_T :

$$\begin{aligned} emass &= \int_e N_i N_j r^2 dr ; \\ egen &= \int_e Q_T r^2 N_i dr + \left[\int_e r^2 \left(\frac{\rho D C_p - \lambda Le}{\rho} \right) \frac{\partial N_i}{\partial r} \frac{\partial N_j}{\partial r} dr \right] \{ \bar{T}_j \} \\ econ &= Sc u_d \int_e N_i \left(1 + \frac{\rho r^3}{\hat{\rho}}\right) \frac{\partial N_j}{\partial r} dr + D \int_e r^2 \frac{\partial N_i}{\partial r} \frac{\partial N_j}{\partial r} dr \end{aligned} \quad (4.37d)$$

The above integrations were performed numerically after transforming the global coordinate to the local coordinate. The local coordinate, ξ , varies from -1 to +1. For such numerical integration, Gauss-Legendre method was applied. Now,

$$\dot{Y}_{f1,j} = \frac{Y_{f1,j}^{k+1} - Y_{f1,j}^k}{\Delta t}$$

Therefore, Eq. 4.36a can be discretized in terms of explicit, implicit or Crank-Nicholson scheme as

$$[gmass] \left\{ \frac{Y_{f1,j}^{k+1} - Y_{f1,j}^k}{\Delta t} \right\} + \theta [gcon] \{Y_{f1,j}\}^{k+1} + (1 - \theta) [gcon] \{Y_{f1,j}\}^k = \{ggen\} \quad (4.38)$$

where, $\theta = 0$ for explicit scheme

$= \frac{1}{2}$ for Crank Nicholson scheme

$= 1$ for implicit scheme.

Rearranging Eq. 4.38,

$$[[gmass] + \theta \Delta t [gcon]] \{Y_{f1,j}\}^{k+1} = [[gmass] - (1 - \theta) \Delta t [gcon]] \{Y_{f1,j}\}^k + \{ggen\} \Delta t \quad (4.39a)$$

Similarly, the discretized equations for Y_{f2} , Y_x and Y_T can be expressed as

$$[[gmass] + \theta \Delta t [gcon]] \{Y_{f2,j}\}^{K+1} = [[gmass] - (1 - \theta) \Delta t [gcon]] \{Y_{f2,j}\}^K + \{ggen\} \Delta t \quad (4.39b)$$

$$[[gmass] + \theta \Delta t [gcon]] \{Y_{x,j}\}^{K+1} = [[gmass] - (1 - \theta) \Delta t [gcon]] \{Y_{x,j}\}^K + \{ggen\} \Delta t \quad (4.39c)$$

$$[[gmass] + \theta \Delta t [gcon]] \{Y_{Tj}\}^{K+1} = [[gmass] - (1 - \theta) \Delta t [gcon]] \{Y_{Tj}\}^K + \{ggen\} \Delta t \quad (4.39d)$$

4.8 Iterative Scheme for the entire Solution Procedure

The transport equations for the gas phase and the liquid phase are highly non-linear. The liquid phase and the gas phase equations are coupled together by clausius-Clapeyron equations. The coupling parameters at the interface are the evaporation velocity at the surface, u_d , heat transfer rate from the gas phase to the liquid droplet, H_l and the fractional mass gasification rate, ϵ_i . These parameters appear in both the liquid phase and the gas phase equations, and they are functions of time. For the iterative scheme, these three coupling parameters are adopted to converge upon. Due to the highly non-linear reaction term, underrelaxation has to be used in the later part of the combustion period. This iterative scheme is based on a two-step sequential process as depicted in Fig. 4.1. Both of these sequential processes come under the outer time-step loop (indicated by the loop 100 in Fig. 4.1) i.e. for each time step, these two processes are carried out one after another.

In the beginning, the required input data are fed to the program and the initial grid distribution is chosen from experience. With this arbitrary initial grid, it goes to the first module or, step. In the first step, first starting with an initial guess of u_d , H_l and ϵ_{f1} , the liquid phase solutions are obtained by solving Eqs. 4.28a and 4.28b in subroutine 'funda'. Once the liquid phase solutions are obtained, the droplet parameters, Y_{f1s} , Y_{f2s} and T_s at the liquid side become known. Now, using Clausius-Clapeyron relation (Eqs. 4.18a,b,c

), the gas side surface parameters, Y_{f1sg} , Y_{f2sg} , T_s are calculated. Now, using the values at the surface as the given boundary conditions, the gas phase solutions are obtained by solving the Eqs. 4.39a-d. Then from Eqs. 4.5a,b and 4.7, the coupling surface parameters (ϵ_{f1} , ϵ_{f2} , H_L , u_d) are calculated from Eqs. 4.42a-d and they are compared to previous guess values for convergence. If it fails to converge then the coupling parameters are updated by choosing a suitable underrelaxation factor. This process of solution is repeated in the next iteration loop 10 (see Fig. 4.1) till convergence. When these values converge within the tolerance limit, it moves on to the second module (subroutine 'adgrid'). In the second module, first error in each element is calculated statistically by substituting the converged solutions for each node into the energy conservation equation of the gas phase. Then overall global error is calculated by taking root mean square of all the elemental errors. If this global error exceeds the global tolerance limit, then refinement and derefinement of grid takes place according to the relative errors of the different elements. After adaption it goes back to the starting of iteration loop 10 and starts the first module once again. In this way, the sequential, operation of step1 and step2 is repeated within a certain time-loop till the global error satisfies the global tolerance limit. When this criterion is fulfilled, it moves on to the next time step loop. In this way the whole solution marches in time-direction. The second module which covers the entire adaption process is given separately in details in Fig. 4.2.

4.9 Processing of Parameters after each Time-step

(i) Calculation of droplet radius (r_d)

The droplet radius (r_d), after each time step, is calculated explicitly.

mass of droplet at a given time (t) is

$xmass$ = mass of droplet at the previous time step (t-1)

- amount of mass evaporated at the previous step (t-1).

This mass of the droplet at a given time is known explicitly. Therefore, from this relation

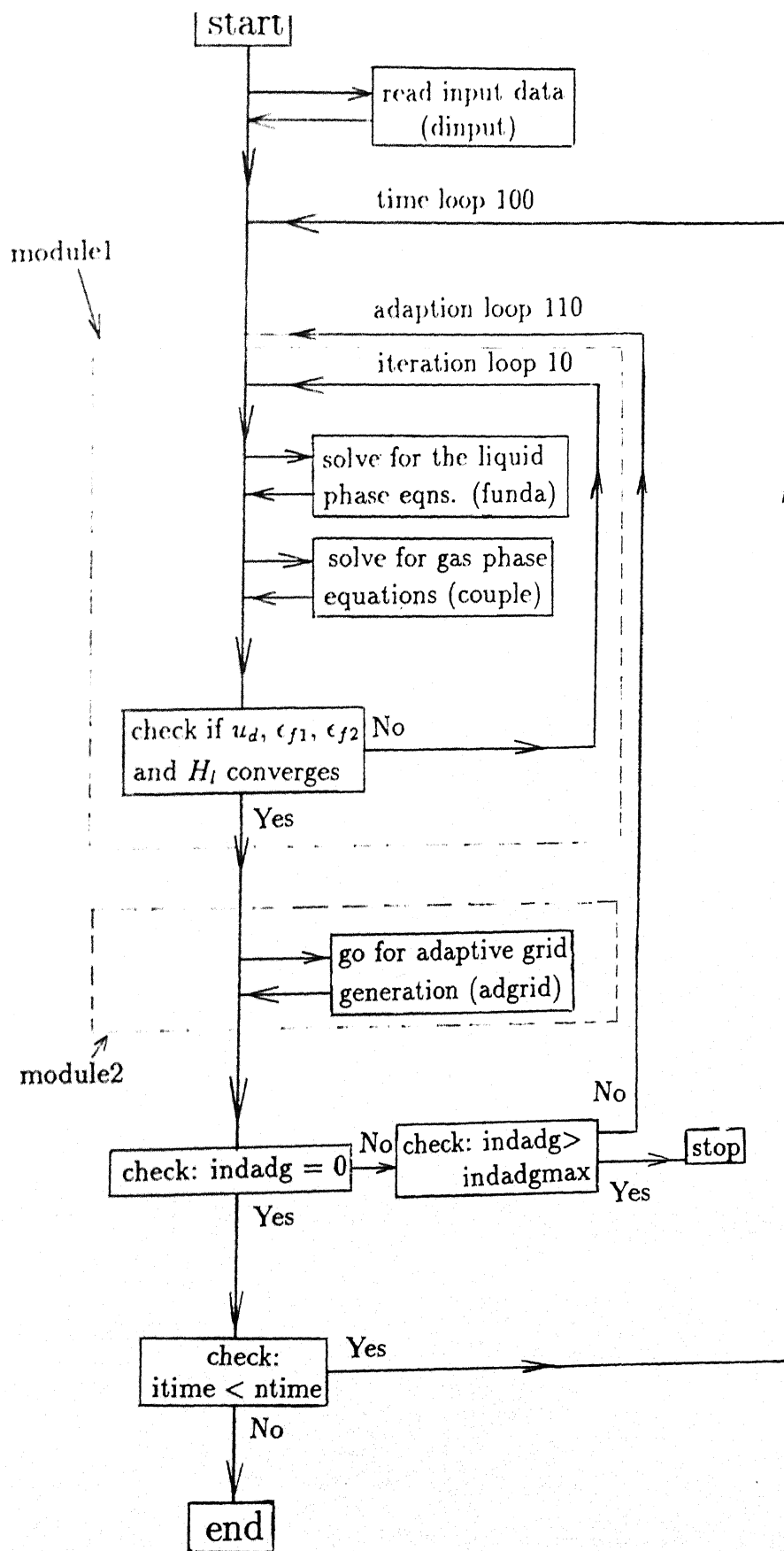


Fig. 4.1 Flow Chart for the Overall Numerical Scheme

the droplet radius, r_d can be calculated as

$$r_d = \left(\frac{3}{4\pi} \frac{x_{mass}}{\rho} \right)^{\frac{1}{3}}. \quad (4.40)$$

Thus, droplet radius, r_d , can be calculated at each time step explicitly.

(ii) Calculation of u_d , H_l , ϵ_{f1} , ϵ_{f2}

The gas phase boundary conditions for fuel1, fuel2 and temperature are given by Eqs.

$$\left. \frac{\partial Y_{f1}}{\partial r} \right|_{r=1} + \frac{u_d Sc}{D} (\epsilon_{f1} - Y_{f1s}) = 0 \quad (4.41a)$$

$$\left. \frac{\partial Y_{f2}}{\partial r} \right|_{r=1} + \frac{u_d Sc}{D} (\epsilon_{f2} - Y_{f2s}) = 0 \quad (4.41b)$$

$$H_l = \hat{\lambda} \left. \frac{\partial \hat{T}}{\partial r} \right|_{r=1} = \lambda \left. \frac{\partial T}{\partial r} \right|_{r=1} - Pr \rho u_d \sum_{i=1}^N \epsilon_i L_i \quad (4.41c)$$

solving these three boundary conditions (Eqs. 4.41a,b,c),

$$u_d = \frac{D}{Sc} \frac{\left(\left. \frac{\partial Y_{f1}}{\partial r} \right|_{r=1} + \left. \frac{\partial Y_{f2}}{\partial r} \right|_{r=1} \right)}{(Y_{f1s} + Y_{f2s} - 1)} \quad (4.42a)$$

$$\epsilon_{f1} = - \frac{D}{u_d Sc} \left. \frac{\partial Y_{f1}}{\partial r} \right|_{r=1} + Y_{f1s} \quad (4.42b)$$

$$\epsilon_{f2} = 1 - \epsilon_{f1} \quad (4.42c)$$

and,

$$H_l = \lambda \left. \frac{\partial T}{\partial r} \right|_{r=1} - Pr \rho u_d \sum_{i=1}^N \epsilon_i L_i \quad (4.42d)$$

Assuming a linear distribution of Y_{f1} , Y_{f2} and T at the gas phase boundary,

$$\left. \frac{\partial Y_{f1}}{\partial r} \right|_{r=1} = \frac{Y_{f1,2} - Y_{f1,1}}{\Delta r}$$

$$\left. \frac{\partial Y_{f2}}{\partial r} \right|_{r=1} = \frac{Y_{f2,2} - Y_{f2,1}}{\Delta r}$$

and,

$$\left. \frac{\partial T}{\partial r} \right|_{r=1} = \frac{T_2 - T_1}{\Delta r}$$

So, after solving the gas phase equations the three surface coupling parameters (u_d , ϵ_{f1} and H_l) can be retrieved from the three Eqs. 4.42a,b,c,d given above.

4.10 Adaptive Grid Generation

4.10.1 Introduction

The solutions for the governing differential equations of certain physical processes like combustion etc., contains regions in which the variables exhibit high spatial activity like steep fronts and sharp peaks. In such problems, these high activity regions need to be resolved adaptively in order to ensure an efficient solution to the problem. This feature of sharp peaks is predominant in the present problem of droplet combustion. This adaption of grid points in the region of high spatial activity zone is based on an attempt to equidistribute positive weight functions. In implementing the one dimensional adaptive grid strategy, first the problem is solved for an initial coarse grid. Substituting this coarse grid solutions back into the equations, local discretization errors (E_e) are calculated statistically (Smooke et al., 1989; Rao, 1992). These discretization errors form the basis for the positive weight functions. Then it is checked whether the total error satisfies the global tolerance limit (gtol), if not, grid points are added to the high error zones and removed from low error zones. Then, once again the equations are solved by using the newly adapted grids, and again the global tolerance limit is checked. This process goes on till this tolerance limit is satisfied. After each adaption, the coarse grid solution is then interpolated linearly onto the new grid. The interpolated results serve as an initial solution estimate for the iteration procedure on the new mesh. For the present problem, this whole process of mesh adaption is repeated at each time step as the solution proceeds in time. Here the low activity zone and the high activity zone keep on changing from time to time. So, refinement and derefinement both take place according to the need depending on situations and circumstances.

4.10.2 Formulation for Adaptive Grid Generation

For the present problem, temperature profile has been used as an indicator for locating the high activity zone and the low activity zone. So, here, the gas phase energy Eq. 4.2d has

been used for calculating the elemental errors, mean, standard deviation etc. as a part of mesh adaption.

After substituting the approximate numerical solution, \bar{T} , into the energy Eq. 4.2d, the elemental error, E_e can be calculated by integrating the square of the residue $[r_e^2]$ over the entire element as

$$E_e = \eta_e^2 = \frac{h_e^2}{\pi^2} \int_{r_1}^{r_2} r_e^2 dr \quad (4.43)$$

where, the residue, r_e is given as (see Eq. 4.32d)

$$r_e = \frac{\partial \bar{Y}_T}{\partial t} + Sc u_d \left(\frac{1}{r^2} + \frac{\rho r}{\hat{\rho}} \right) \frac{\partial \bar{Y}_T}{\partial r} - \frac{\alpha Le}{r^2} \frac{\partial}{\partial r} \left(r^2 \frac{\partial \bar{Y}_T}{\partial r} \right) - Q_T \quad (4.44)$$

, h_e = length of the element, e and $\bar{\cdot}$ indicates approximate numerical solution and In the present problem, linear shape functions as indicated in the previous sections, are used. For such a case, $\frac{\partial^2 \bar{Y}_T}{\partial r^2} = 0$. So the residue, r_e is calculated as

$$r_e = \frac{\partial \bar{Y}_T}{\partial t} + \left(Sc u_d \left(\frac{1}{r^2} + \frac{\rho r}{\hat{\rho}} \right) - \frac{2 \alpha Le}{r} \right) \frac{\partial \bar{Y}_T}{\partial r} - Q_T \quad (4.45)$$

where, both the spatial and time derivatives are calculated as (using Eq. 4.31)

$$\begin{aligned} \left. \frac{\partial \bar{Y}_T}{\partial r} \right|^{K+1} &= \frac{\partial}{\partial r} \sum_{i=1}^2 N_i \bar{Y}_{Ti} = \frac{\partial}{\partial r} (N_1 \bar{Y}_{T1} + N_2 \bar{Y}_{T2}) \\ &= \bar{Y}_{T1} \frac{\partial N_1}{\partial r} + \bar{Y}_{T2} \frac{\partial N_2}{\partial r} \\ &= [\theta_g \bar{Y}_{T1}^{K+1} + (1 - \theta_g) \bar{Y}_{T1}^K] \frac{\partial N_1}{\partial r} + [\theta_g \bar{Y}_{T2}^{K+1} + (1 - \theta_g) \bar{Y}_{T2}^K] \frac{\partial N_2}{\partial r} \end{aligned}$$

and,

$$\begin{aligned} \frac{\partial \bar{Y}_T}{\partial t} &= \frac{\partial}{\partial t} (N_1 \bar{Y}_{T1} + N_2 \bar{Y}_{T2}) \\ &= N_1 \left(\frac{\bar{Y}_{T1}^{K+1} - \bar{Y}_{T1}^K}{\Delta t} \right) + N_2 \left(\frac{\bar{Y}_{T2}^{K+1} - \bar{Y}_{T2}^K}{\Delta t} \right) \end{aligned}$$

where, $\theta_g = 0$ for explicit scheme

=1/2 for Crank-Nicholson scheme

=1 for implicit scheme

The total global error (η) is calculated by adding all the elemental errors and then taking square root of the summation as

$$\eta = \left[\sum_{e=1}^N \eta_e^2 \right]^{1/2} \quad (4.47a)$$

where, $N = \text{number of elements}$.

The mean(μ), standard deviation (σ) and J_{max} are calculated as

$$\mu = \sum_{e=1}^N \frac{\eta_e^2}{N} \quad (4.47b)$$

$$\sigma = \frac{\left[\sum_{e=1}^N (E_e - \mu)^2 \right]^{1/2}}{N - 1} \quad (4.47c)$$

$$J_{max} = \frac{E_{max} - E_{min}}{\sigma} + 1 \quad (4.47d)$$

where, E_{max} = maximum elemental error and,

E_{min} = minimum elemental error.

Here, J_{max} is an indicator such that $(E_{max} - E_{min}) < \sigma J_{max}$. It indicates that the elemental error, E_e cannot exceed $(\mu + J_{max} \sigma)$. The algorithm for the adaption process is represented in the form of the flow chart given in Fig. 4.2.

4.10.3 Testing of Adaptive Grid Algorithm

Adaption of grid points are based on the energy equation for the gas phase (see Eq. 4.2d). In order to test the adaptive grid generation algorithm, an analytical solution is chosen of the form

$$\bar{Y}_T(r, \bar{t}) = c_1 + \tanh[c_2(r - 1) - a t] \quad (4.48)$$

where, \bar{Y}_T is a function of r and t and c_1 , c_2 and a are constants. Depending on the values of c_2 , the steepness of the analytical solution varies. So, this analytical solution containing tangent hyperbolic function, can be used for testing the adaption over a wide range of spatial steepness. In this method of assuming the analytical solution for the gas phase energy equation, the source term is calculated by replacing the analytical solution back

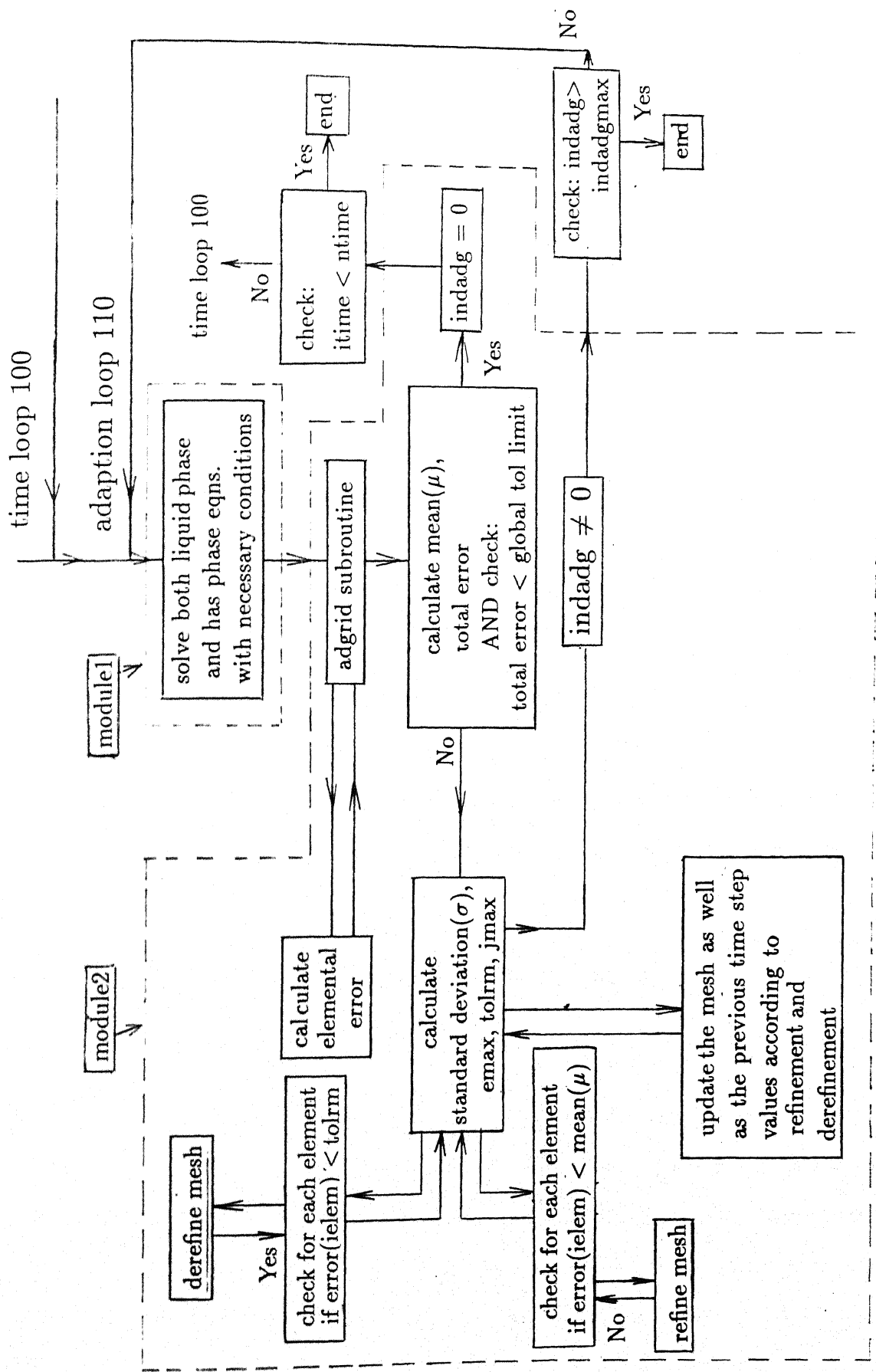


Fig. 4.2 Flow Chart for Adaptive Grid Generation

into the original governing equation as

$$Q = \frac{\partial \bar{Y}_T}{\partial t} - \left(\frac{2 \alpha Le}{r} - Sc u_d \left(\frac{1}{r^2} + \frac{\rho r}{\hat{\rho}} \right) \right) \frac{\partial \bar{Y}_T}{\partial r} - \alpha Le \frac{\partial^2 \bar{Y}_T}{\partial r^2} \quad (4.49)$$

By using the expression for the assumed analytical solution, we get

$$\frac{\partial \bar{Y}_T}{\partial r} = c_2 \sec^2 h [c_2 (r - 1) - a t] \quad (4.50a)$$

$$\frac{\partial^2 \bar{Y}_T}{\partial r^2} = 2c_2^2 \sec^2 h [c_2 (r - 1) - a t] \tanh [c_2 (r - 1) - a t] \quad (4.50b)$$

and,

$$\frac{\partial \bar{Y}_T}{\partial t} = -a \sec^2 h [c_2 (r - 1) - a t] \quad (4.50c)$$

Therefore, the corresponding source term for the assumed analytical solution is calculated, by using the above relations, as

$$Q = \left[2 \alpha Le c_2^2 \tanh (xx) - \left(\frac{2 \alpha Le}{r} - Sc u_d \left(\frac{1}{r^2} + \frac{\rho r}{\hat{\rho}} \right) \right) c_2 - a \right] \sec^2 h (xx) \quad (4.51)$$

where, $xx = c_2 (r - 1) - a t$

So, if one substitutes the source term given by Eq. 4.51 into the governing Eq. 4.49, then the assumed analytical solution for the gas phase energy equation remains valid and the effective governing equation becomes

$$\begin{aligned} \frac{\partial \bar{Y}_T}{\partial t} - \left(\frac{2 \alpha Le}{r} - Sc u_d \left(\frac{1}{r^2} + \frac{\rho r}{\hat{\rho}} \right) \right) \frac{\partial \bar{Y}_T}{\partial r} - \alpha Le \frac{\partial^2 \bar{Y}_T}{\partial r^2} \\ = \left[2 \alpha Le c_2^2 \tanh (xx) - \left(\frac{2 \alpha Le}{r} - Sc u_d \left(\frac{1}{r^2} + \frac{\rho r}{\hat{\rho}} \right) \right) c_2 - a \right] \sec^2 h (xx) \end{aligned}$$

The authenticity of the grid generation can be checked by comparing the solution of the gas phase energy equation obtained through mesh adaption, using Eq. 4.39d, with the solution obtained from the analytical expression given by Eq. 4.48. Using this process, only the discretization error can be checked. so, this process gives a fairly good verification for the adaption of grids. Neither the boundary conditions, nor the original source term can be checked by this method.

4.10.4 Results of the Test Problem

Based on the analytical solution (see Eq. 4.48), choosing suitable values of c_1 , c_2 and a , various checks are carried out. Basically the goals of verification are to check

- (i) the efficiency of refinement and derefinement, and
- (ii) whether or not the solution is marching properly in time direction or not.

Case I : Efficiency of refinement and derefinement are cheked in two ways. Figs. 4.3a-d shows the first process. Firstly, the adaption process is started with only 2 elements. Then through refinement and derefinement, the adaption process proceeds forward in a number of steps to the final grid configuration depending on the tolerance limit. Figs. 4.3a-d show that this adaption process is very smooth in reaching the desired condition. For this case, it is observed that after the 7th adaption, the numerical solution and analytical solutions are very close to each other.

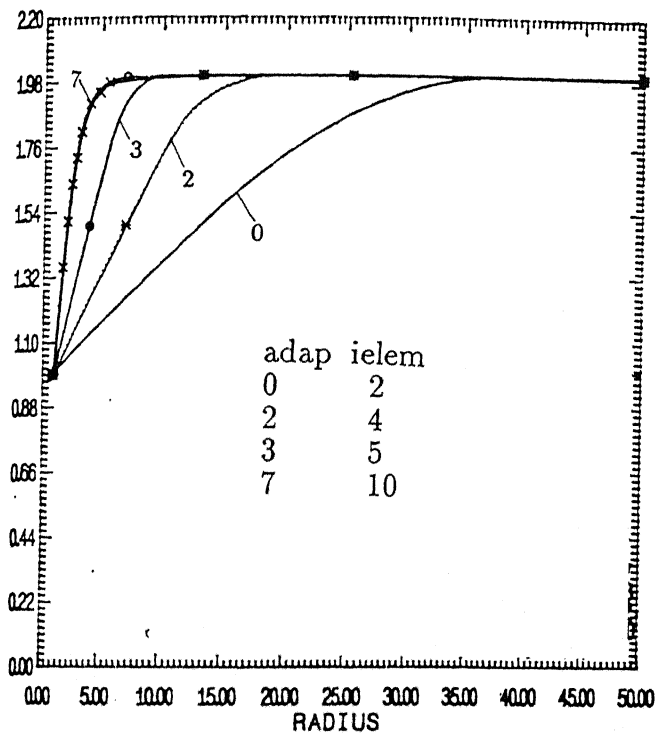
Secondly, the adaption process is started with a large number of uniformly distributed elements (30 elements) (see Figs. 4.4a-d). Here also, it is observed that during adaption, grids are removed from the low activity (spatially less steep) zone and, are added to the high activity (spatially very steep) zone. This removal and addition takes place very smoothly as seen in the figure .

In both of the above situations, it is observed that the numerical solution perfectly matches with the analytical solution. This indicates that spatial discretization of the governing differential equations is fairly accurate. So, this case demonstrates the efficiency and smoothness with which the present algorithm works in spatial coordinates.

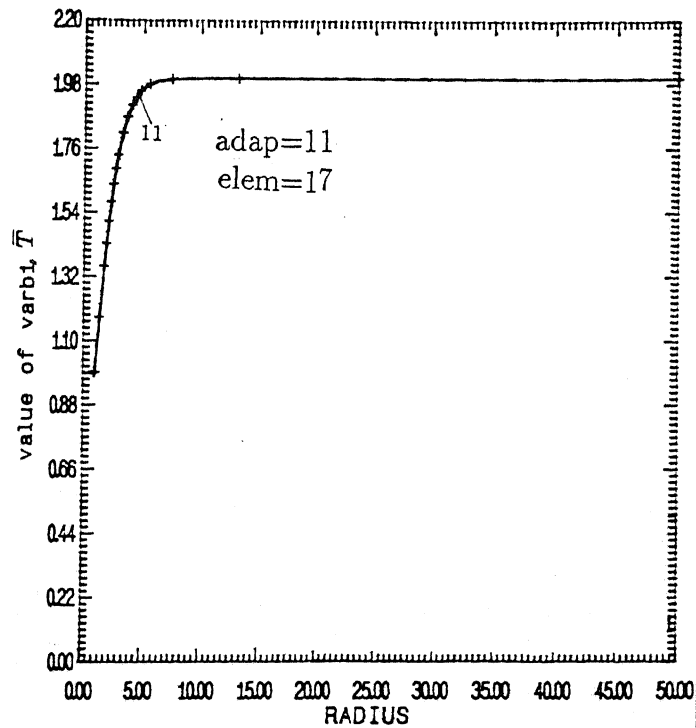
Case II : This case (Fig. 4.5) demonstrates the efficiency of the algorithm regarding how it moves in time direction. These results indicate that the transient part of the discretization is also fairly accurate. We can see from Fig. 4.5 that the numerical results and the analytical results match nicely with each other at all time steps.

In verifying the above conditions, the values of the constants were taken to be $c_1 = 1.0$, $c_2 = 0.5$ and $a = 1.0$. The above conditions were also checked for different steep-

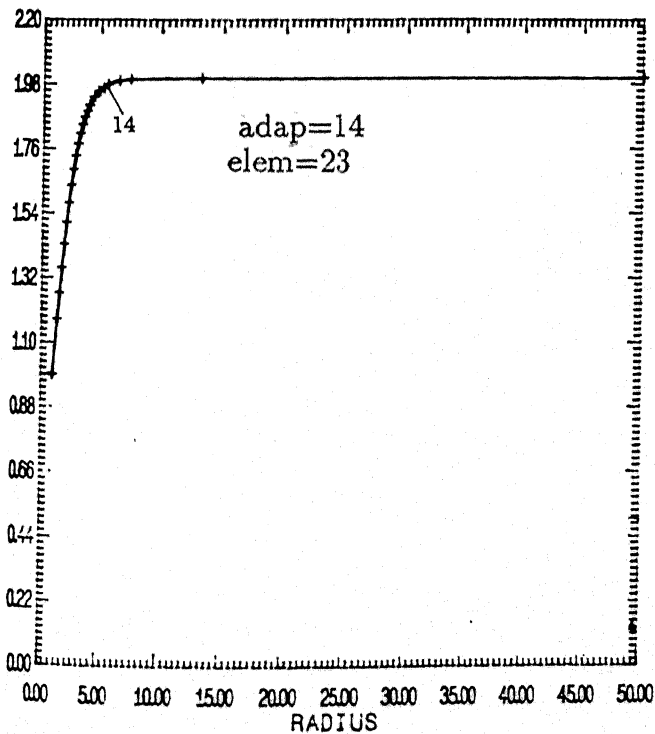
———— Numerical Solution
 - - - - - Analytical Solution



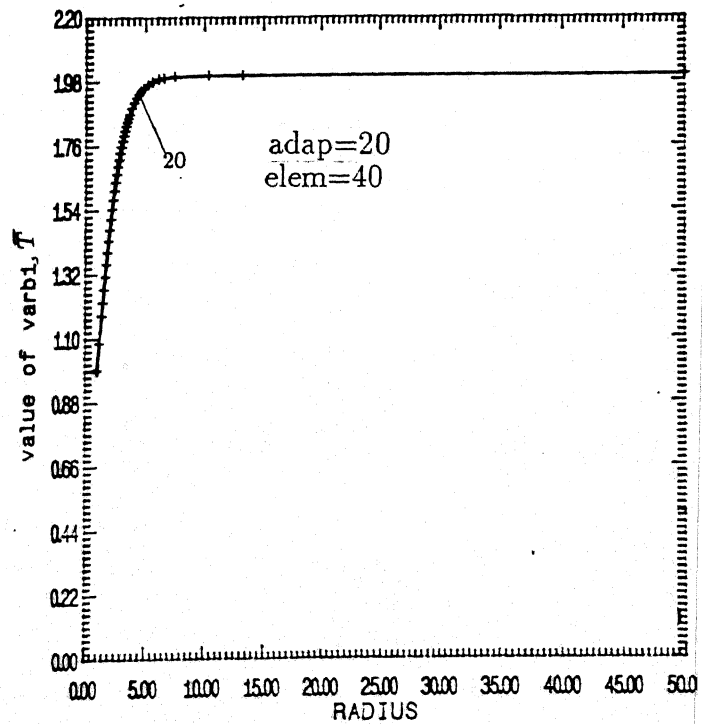
a



b



c

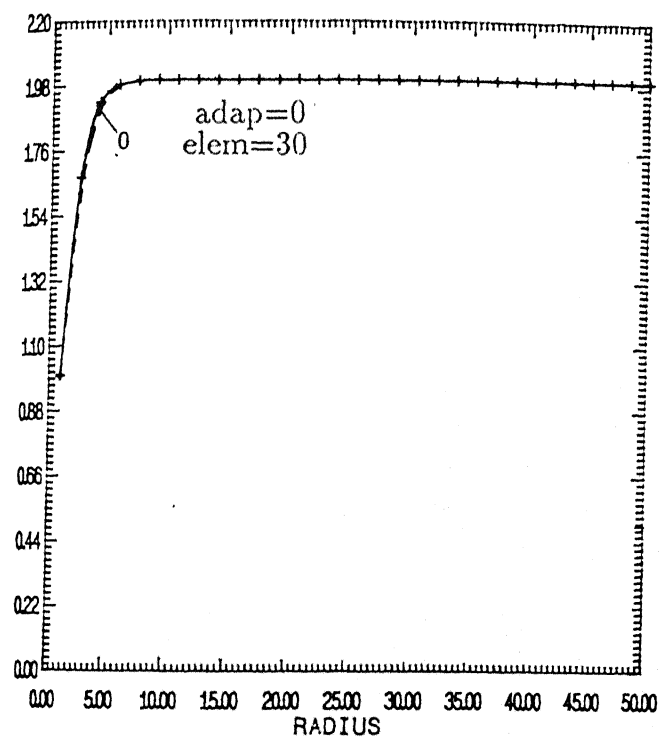


d

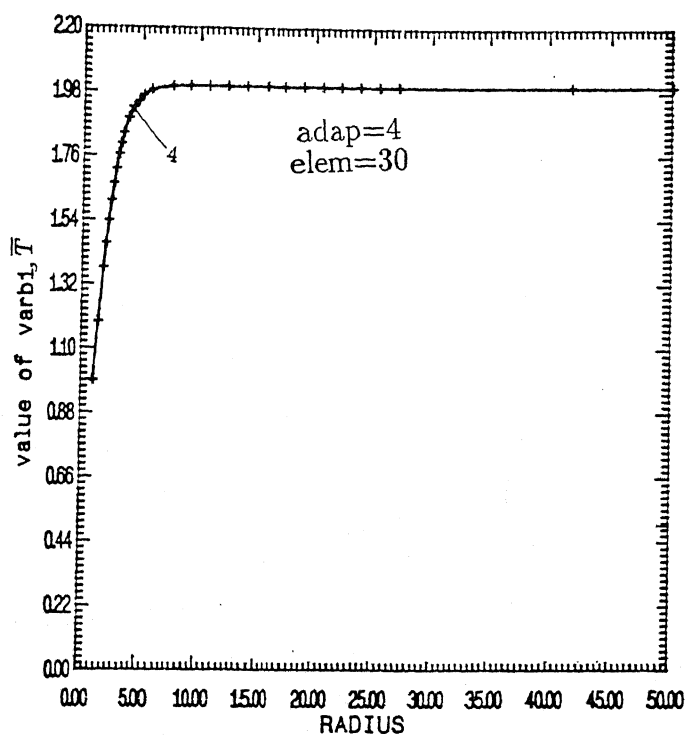
Fig. 4.3 Evolution of grids at a given time starting with only two elements.

———— Numerical Solution

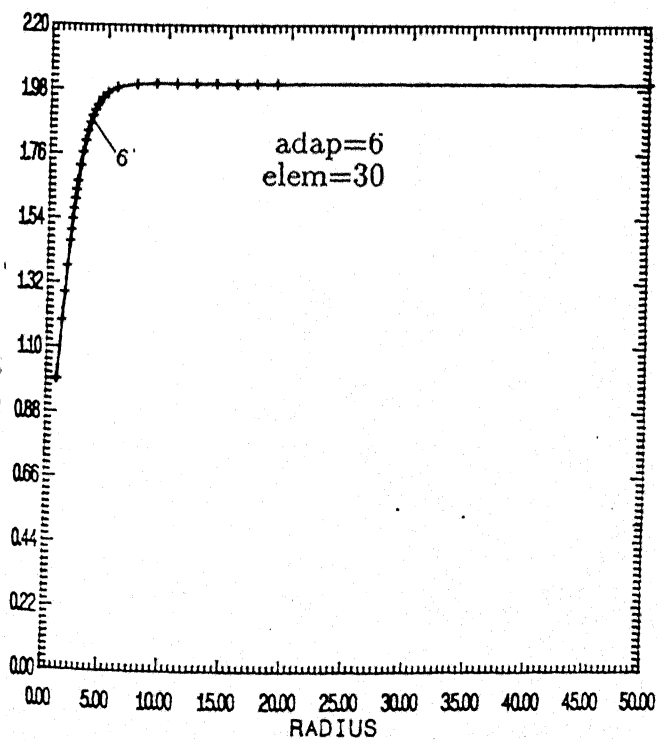
----- Analytical Solution



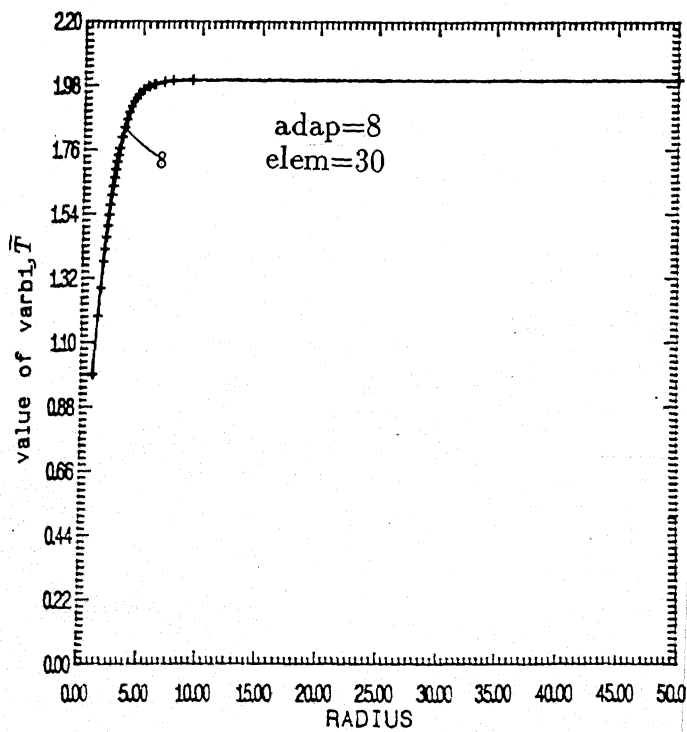
a



b



c



d

Fig. 4.4 Evolution of grids at a given time starting with only thirty elements.

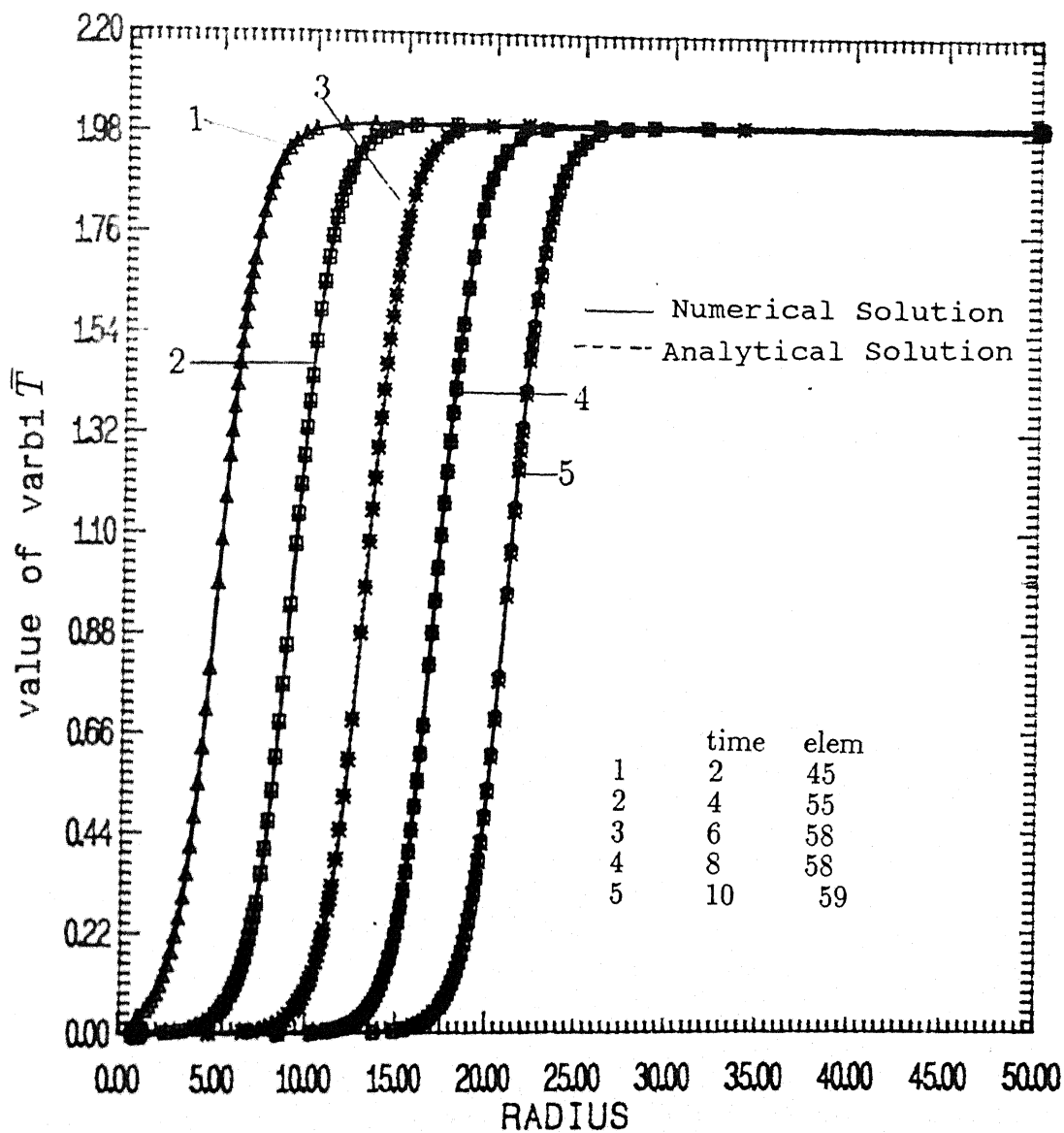


Fig. 4.5 Evolution of grids at different times.

ness of the analytical tangent hyperbolic solution. This was done by choosing $c_2 = 0.9, 0.7, 0.3, 0.1, 0.01$. Similar matching was observed for all the cases.

4.11 Closure

In this chapter, both liquid gas phase transient equations are discretized for numerical solution for the case of spherico-symmetric burning of multicomponent fuel droplet. Liquid phase equations are discretized by Finite Difference Method (FDM) and the gas phase equations are discretized by using Galerkin Finite Element Method (FEM). Adaptive grid generation based on local elemental error calculation was used to determine the position of grid points. Gas phase energy equation was used as the basis for error calculation. The adaptive grid generation technique is tested with a known analytical solution which is tan hyperbolic in nature. Discussions of the results for these discretized equations are presented in the next chapter in details.

Chapter 5

Results and Discussions

5.1 Introduction

This chapter, throws light on various important features of multicomponent single droplet fuel combustion. The elaborations include both liquid phase and gas phase profiles for the temperature and mass-fractions at different times throughout the history of droplet burning. They show how these profiles evolve initially during the highly transient ignition period, how they develop into the intermediate period (first $d^2 - law$ period, transition and second $d^2 - law$ period) comprising the major portion of the burning history, and finally how they move towards extinction. The structure of the flame is closely looked into taking the help of grid generation technique to track down the flame movement. In multicomponent fuel burning, the difference in volatility of the two fuels plays an important role. The effect of volatility differential on different burning characteristics has been looked into. How does any change in the initial mass-fraction affect the nature of burning, is also included in the present discussion. Several other important features, such as effect of dissociation, ambient temperature, variable and constant gas phase specific heats, gas phase and liquid phase diffusion coefficients etc. are also included in the discussion. Finally the comparison with the semi-analytical model as well as with existing experimental results are also made. The property values are used from different sources such as Reid et al. (1988), penner (1957) etc.

5.2 Surface Parameters

This section discusses the transient variation of the surface parameters namely surface temperature, T_s , total volumetric gasification rate, V , flame stand-off ratio, r_f , flame position from droplet center, r'_f , flame position from droplet surface, r''_f , heat coming from the gas phase, H_g , heat input to the liquid droplet, H_l , heat of evaporation, H_{ev} , fractional mass gasification rate, ϵ_{f1} , liquid side and gas side mass fractions, Y_{f1ls} , Y_{f1sg} , and Y_{f2sg} , droplet radius, r_d and square of droplet diameter, d^2 with time. Here, heptane and hexadecane fuel mixture with an initial liquid side mass-fraction combination of 0.9-0.1 is chosen for

discussing these parameters. It is seen from the figures that there are six distinct periods that cover the entire burning history namely (i) ignition delay period, (ii) ignition period (iii) $1^{st} d^2 - law$ period, (iv) transition (from first $d^2 - law$ period to the $2^{nd} d^2 - law$ period) period, (v) $2^{nd} d^2 - law$ period and finally, (vi) the extinction period. The extinction period is basically a volatility limited period during which the more volatile component is rapidly depleted from the entire droplet composition. After the droplet is introduced into the combustion chamber, there is a time lag before ignition takes place. This is the ignition delay period of droplet burning. Starting from the beginning, this period exists approximately up to 0.0015s, which is about 2.28 % of the total burning time for the present case and is 0.0013 s for the burning of heptane-dodecane fuel with an initial mass fraction combination of 0.9-0.1. During this period, the peak temperature starts rising very slowly at around $r_f=4.2721$, due to very slow reaction rate. Here, curves are not steep. Since the flame is almost absent, this period falls under the category of pure evaporation.

At the end of this period, at $r_f=4.2721$ the reaction starts gathering momentum and the initial transient marked by ignition, expansion of the flame towards the droplet surface and vigorous droplet heating sets in. As this initial transient sets in, the reaction at the flame region becomes vigorous and the flame temperature rises almost instantly to 3223 K at $t = 0.00166957s$. At $t=0.002s$, heat coming from the gas phase (H_g), heat going into the liquid droplet (H_l) and the heat available for evaporation (H_{ev}) all reach their peak values. At this point, 65 % of the total heat available from the gas phase goes for droplet heating and the rest (H_{ev}) is available for fuel evaporation. Then the percentage of the heat available for the evaporation gradually increases and that available for droplet heating gradually decreases. As the flame temperature rises, the flame gradually moves and expands towards the droplet surface from $r_f = 4.2721$ to $r_f = 3.31$ because during this initial period, fuel is available only at the droplet surface. Therefore, the temperature gradient at the gas side of the droplet surface becomes very high. So, the droplet heating becomes very vigorous due to this high temperature gradient at the droplet surface. This results in a sharp rise

in surface temperature (T_s). As heat of evaporation, H_{ev} becomes high and the surface temperature rises sharply and approaches the boiling point of heptane (371K), the evaporation of heptane also increases vigorously. Thus, the total volumetric gasification rate increases sharply. The liquid side surface mass-fraction, Y_{f1ls} , of the more volatile fuel is very high due to its high initial value, but it falls steeply due to high diffusional resistance and low surface regression rate. Due to the high value of liquid side surface mass-fraction of the more volatile fuel (heptane), its mass-fraction on the gas-side, Y_{f1sg} also increases very sharply. But, since the surface mass-fraction of the less volatile fuel on the liquid side is very small, its gas-side value (Y_{f2sg}) remains very small. In this period, mainly the more volatile fuel (heptane) contributes to the total gasification rate, V as the surface is enriched with heptane and the temperature is much below the boiling point of the less volatile fuel (hexadecane). So, the fractional mass gasification rate, ϵ_{f1} , for the more volatile fuel is also very high. Though, initially the flame is situated very near the droplet surface ($r_f = 3.31$), but immediately after the flame is established, sharp increase in the gasification rate, V , causes fuel vapour accumulation between the flame and the droplet surface, and as a result, the flame starts moving away from the surface as indicated in Fig. 5.1c by r'_f . The initial transient period spans for about 0.0015 s, starting at 0.0015s and ending at 0.003s approximately. It covers 2.285 % of the total burning time.

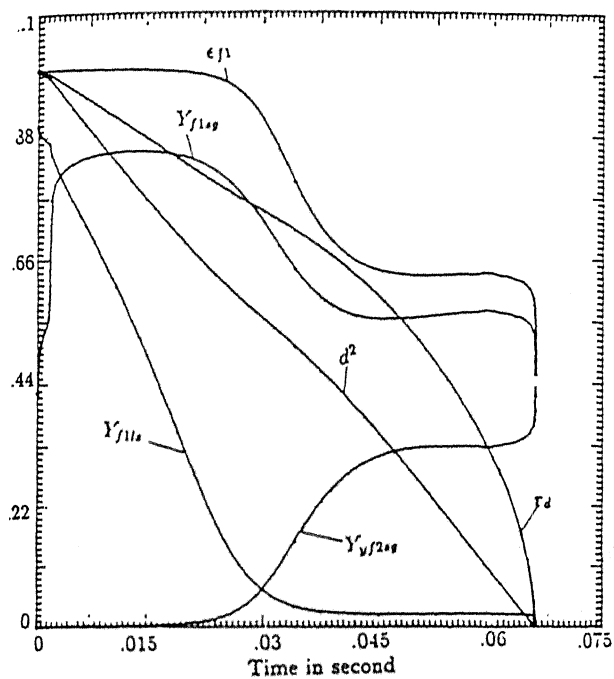
After the initial transient is over, $1^{st} d^2 - law$ period starts around 0.003s. This period covers nearly 35.63 % of the total burning time and is maintained till 0.2625s approximately. During this period, as the flame moves away from the droplet surface, the gas side temperature gradient at the droplet surface gradually decreases and becomes almost steady. Therefore, the heat available from the gas phase also decreases, initially very fast, then gradually and finally becomes almost steady. The liquid side surface mass-fraction of the more volatile fuel, Y_{f1ls} , decreases at a constant rate. This decrease is due to high liquid-side diffusional resistance for which enough heptane cannot reach the surface for maintaining its surface mass-fraction. And, also, since the droplet radius regression rate

during the $1^{st} d^2 - law$ period is neither too high nor too low, the slope of the Y_{f1ls} curve is maintained at an intermediate value. During this period, the gas side surface mass-fraction of heptane remains high due to its high liquid side initial value and consequently, the surface temperature remains in the vicinity of the boiling point of the more volatile fuel. In the initial part, H_l falls very fast and then decreases gradually and finally becomes almost steady. At about $t = 0.015s$, heat going into the droplet reaches a minimum and about 69 % of the total heat available from the gas phase goes for droplet evaporation. The amount of heat available for evaporation, H_{ev} , remains nearly constant. And since, the droplet surface area gradually decreases, the total gasification rate decreases quite steadily as shown in Fig. 5.1b. Due to the relatively large amount of the more volatile fuel present at the droplet surface, the fractional mass gasification rate of the more volatile component, ϵ_{f1} , remains quite high and is maintained almost at a constant value during this period. The gas-side mass-fraction of the less volatile fuel remains low due to its low initial value. As the overall gasification rate decreases steadily, the fuel vapour accumulation becomes progressively lesser towards the end of this period. So, the flame movement slows down steadily. Because of the fast flame movement in the initial part of this period, the flame stand-off ratio remains quite steep. But, towards the end of this period, the flame stand-off ratio increases at a much slower rate more due to the slow rate of droplet radius regression.

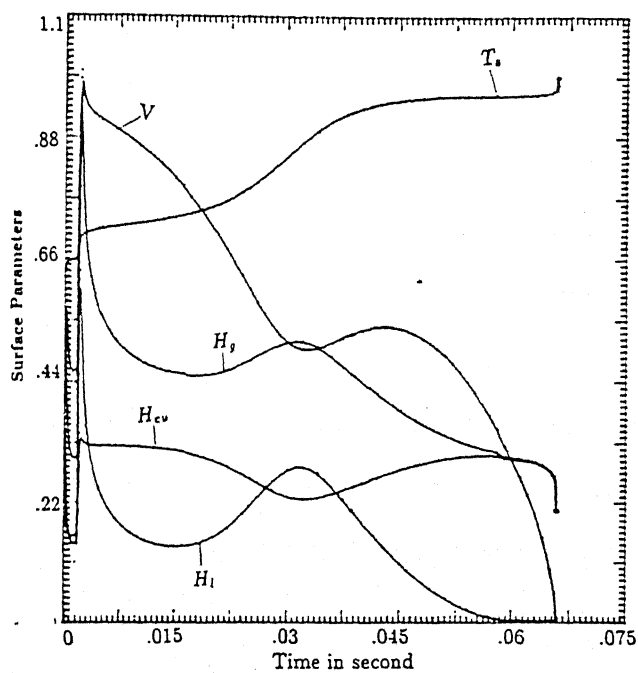
Due to the liquid side mass-diffusional resistance and low regression rate, the liquid side surface mass-fraction of heptane falls continuously and when it falls below 0.10325, its gas side surface mass fraction could not be maintained any more around 0.84 and eventually, it starts falling and the gas side surface mass fraction of hexadecane starts rising. Therefore, as a result of the above surface change, the transition from one $d^2 - law$ period to the next starts which causes the surface temperature to cross the boiling point (371K) of the more volatile fuel. The time of such occurrence depends upon the liquid side mass-fractions of the fuels at the surface as mentioned above. For the present case, the transition starts approximately around 0.02575 s when Y_{f1sg} , Y_{f1ls} and T_s are around

0.79, 0.10325 and 374 K respectively, and it ends around 0.039 s approximately when the values of the above parameters become 0.57, 0.02 and 465 K. This transition period covers about 19.5 % of the total burning time. In this period, the gas side temperature gradient at the surface again increases resulting in an increase of total heat flow (H_t) from gas side. And also, the droplet heating is again increased as the droplet surface temperature makes a move towards the boiling point of hexadecane as indicated by the curve for H_t and T_s . At about $t=0.0315$ s (about half way through the transition), the total heat coming from the gas phase (H_g) as well as the heat going into the liquid droplet (H_l) reaches their maximum values and consequently, heat going for evaporation (H_{ev}) reaches it's minimum value; 56.2 % of the available heat goes for droplet heating. It is seen from Fig. 5.1b that in the first half (from 0.02625 s to 0.0315 s) of the transition period, the heat available for evaporation gradually falls. Therefore, during this period, the gradient of the gasification rate curve, V , increases relatively, indicating a decrease in the gasification rate (Fig. 5.1b) and consequently, surface regression rate also falls as indicated by the decrease in gradient for the d^2 curve of Fig. 5.1a. But, in the second half (0.0315 s to 0.039 s) of the transition period, the heat of evaporation again increases and also, the surface temperature approaches more towards the boiling point of hexadecane, thereby increasing the gasification rate for hexadecane as indicated by the curve for Y_{f2sg} in Fig. 5.1a. Therefore, the total gasification rate is increased during the later part of transition. So, the surface regression again picks up momentum as shown by the $d^2 - law$ curve in Fig. 5.1a. During transition, fuel vapour accumulation becomes very near to zero. At this stage, the rate of fuel consumption at the flame is nearly equal to the rate at which it is being evaporated at the droplet surface. This transition from 1st $d^2 - law$ period to the 2nd $d^2 - law$ period is gradual and is caused by the high droplet radius regression rate. The latter (i.e. high droplet radius regression rate) maintains the surface mass-fraction of the fuels by exposing the inner core to the surface, depending on their initial values. This also nullifies the effect of high diffusional resistance.

After the transition from $1^{st} d^2 - law$ period to the $2^{nd} d^2 - law$ period is over, the second d-square law period starts at around $t=0.039$ s and it continues till the end of droplet burning. For the present case, the second $d^2 - law$ period covers approximately 40 % of the total droplet lifetime. As the droplet surface temperature rises above the boiling point of heptane (during transition) and eventually reaches an asymptotic value, the droplet heating gradually decreases and becomes negligibly small. This asymptotic value of surface temperature depends upon the liquid side surface mass-fraction combination of the fuels. Most of the heat available from the gas phase is used up for evaporation only. At $t=0.039$ s (i.e. at the start of the second $d^2 - law$ period), 58 % of the available heat goes for evaporation and it increases upto 100 % near the end of burning. So, the surface regression rate is maintained till the end. The gasification rate initially increases due to the inertial effect of the later half of the transition. After 0.04275 s, it falls initially less steeply, but later on, the steepness increases owing to the small droplet volume, though the heat for evaporation goes on till the end. The droplet radius also decreases very fast due to the insufficient volume of the droplet. Results show that only 18.5 % of the initial droplet volume and 43 % of the initial surface area remains at the start of the second $d^2 - law$ period. They become 5.7 % and 14.8 % respectively at $t=0.057$ s when both the gasification rate and the radius start to fall very steeply. During this period, the flame remains steady, maintaining almost a fixed distance from the droplet center. The flame stand-off ratio increases with lesser steepness during the initial part of the period indicating that the droplet radius falls less steeply. But later on, the flame stand-off ratio becomes very steep owing to the very high rate of fall of the droplet radius. During second $d^2 - law$ period, the species are transported to and exposed at the regressing surface approximately at a constant rate. In this period, the droplet radius decreases so fast that both liquid side and gas side mass-fractions of heptane are not only maintained but, actually they increase very gradually (Fig. 5.1a) as a result of the droplet core being exposed to the surface. However, the liquid side and the gas side mass fractions of hexadecane fall very gradually



a



b

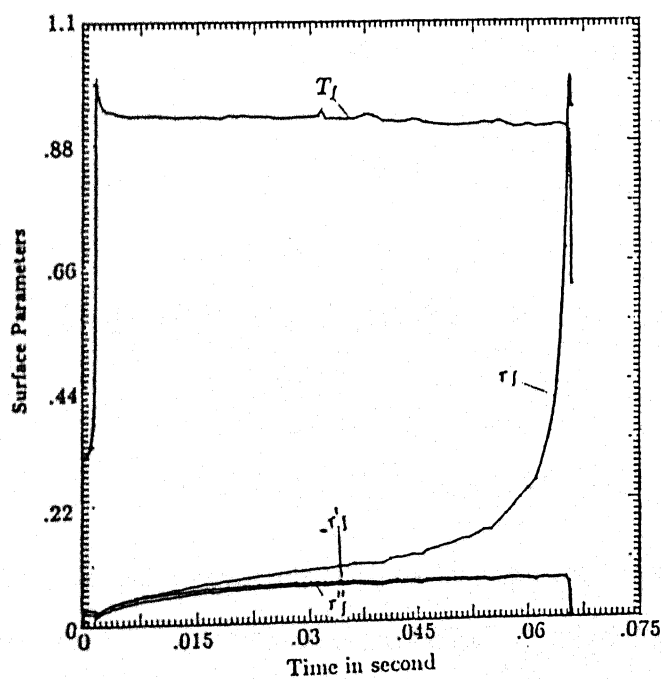


Fig. 5.1 Transient variation of different surface parameters for heptane-hexadecane fuel burning with $\hat{Y}_{in,f1} = 0.9$.

due to its lower initial liquid side value (0.1). The distance between the curves r'_f and r''_f indicates the instantaneous droplet radius.

At the end of the $2^{nd} d^2 - law$ period, the highly transient phenomenon of extinction begins. This extinction starts at about 0.06548881 s, when the volume, surface area and diameter of the droplet becomes approximately 0.0257 %, 0.4044 % and 6.36 % respectively of their initial values. This is marked by a sharp decrease in flame temperature and is finished in approximately 260 μs s. Therefore, the time gradient for the flame temperature like all other parameters e.g. droplet radius, overall gasification rate, both liquid-side and gas-side mass-fractions etc. become, practically, infinite during the extinction period. The flame also starts moving towards the droplet in search of fuel at an almost infinite rate. The droplet radius becomes very small at this stage. During this final period (which may also be called volatility limited period), the more volatile component (heptane) is rapidly depleted from the entire droplet composition. This happens because at this stage, the droplet size (less than 2-3 microns) becomes comparable to the characteristic mass diffusion length. Therefore, the liquid side mass diffusional transport becomes effectively very high causing perpetual uniformization of concentration. Thus, the volatility differential becomes the rate controlling factor for evaporation at the droplet surface. So, the surface temperature rises sharply, approaching the equilibrium gasification temperature of the less volatile component (hexadecane). This phenomenon was referred by Law (1982).

5.3 Liquid-Side Mass-Fraction and Temperature Profiles

This section describes the time history of mass-fraction and temperature distribution within the liquid droplet for heptane-dodecane combination with 0.9 initial mass-fraction of heptane (see Figs. 5.2a and 5.3a). Due to the non-dimensionalization of r-coordinate with respect to the instantaneous droplet radius, the droplet surface always remains at $r=1$. Thus, the r-coordinate shrinks as the droplet surface regresses.

Figure 5.2a shows that as soon as the droplet is introduced into the hot environment, a concentration boundary layer is established near the droplet surface on the liquid side. This happens because the more volatile component evaporates very rapidly from the droplet surface, and because of liquid side diffusional resistance, it cannot be supplied fast enough from the inner core to the droplet surface. Due to this, the liquid side surface mass-fraction of the more volatile fuel falls continuously and the concentration gradient at the liquid-side surface becomes progressively steeper. This happens up to 0.04 s (indicated by curve 10) which is just before the beginning of $2^{nd}d^2 - law$ period. During the $2^{nd}d^2 - law$ period, the concentration gradient at the liquid-side boundary increases very very slowly and remains almost constant as indicated by the curves 10, 11, 13, 14 and 15 of Fig. 5.2a. This happens because the liquid side mass-fractions of the fuels are almost maintained at constant values due to high radius regression rate.

It is observed from figure 5.2a that after 0.065 s i.e. towards the end of combustion, the concentration boundary layer falls apart and the concentration gradient at the droplet surface becomes lesser and lesser and, the liquid side concentration becomes perpetually uniform. As discussed in the previous section, this uniformization of concentration happens because mass diffusional transport inside the droplet becomes highly enhanced owing to the small droplet size towards the end of combustion. This is corroborated by Fig. 5.2b which shows that the mass fraction of heptane at the droplet centre is maintained around its initial value (0.9) till 0.065 s which is very near to the end of burning. Then the value (mass fraction of heptane at the droplet centre) starts falling very fast, almost with an infinite gradient.

It is seen that the temperature profiles (see Fig. 5.3a) do not approve the existence of any steep thermal boundary layer. This happens because of relatively high thermal diffusivity which causes the heat to be conducted very fast to the core. This is in contrast to the nature of the mass-fraction profiles, where the steep concentration boundary layer is present almost from the beginning.

Two distinct zones, corresponding to the two $d^2 - law$ periods, are observed from Fig 5.3a. In the initial transient, which exists approximately upto 0.005 s (curve 3), the surface temperature makes a move towards the boiling point(371 K) of the more volatile fuel(heptane) and it remains near this temperature till the end of the 1st $d^2 - law$ period i.e. almost upto 0.02 s (curve 6) and more heat is used up for fuel evaporation. During the 1st $d^2 - law$ period, the heat from the surface region gets enough time to be conducted to the droplet core. So, the temperature profiles become flatter compared to those prevailing during the initial transient. The second transient starts at the end of of the 1st $d^2 - law$ period (between curves 6 and 7) and exists almost upto 0.04 s(curve 10) . During this period, the surface temperature rises above the boiling point (371K) of the more volatile fuel (heptane) and the surface is heated up more, leaving behind the droplet core. The period of the second transient is longer and less steep compared to the initial transient. This happens due to high radius regression rate for which surface mass-fraction of heptane at the surface is maintained resulting in a gradual shifting of surface temperature from the boiling point (371 K) of the more volatile component (i.e. heptane) to a higher value beyond 371 K depending upon the liquid side surface mass-fraction combination of the fuels. This does not happen during the initial transient, as then the radius regresses very slowly. After the second transient, the 2nd $d^2 - law$ period starts at around 0.04 s (curve 10) and it continues till the end of burning. During this period, again heat goes from the surface to the core for heating it up, whereas the surface temperature hardly changes because of almost constant values of gas and liquid side surface mass-fractions of the fuels (see also Fig. 5.1a).

It is seen from Fig. 5.3a that after 0.065 s i.e. almost at the end of combustion, the entire droplet surface temperature starts rising. During this rise of droplet surface temperature, no gradient is observed near the droplet surface. This means that the droplet core is also heated up instantaneously along with the droplet surface. This instantaneous uniformization of droplet temperature happens due the very small droplet size (less than

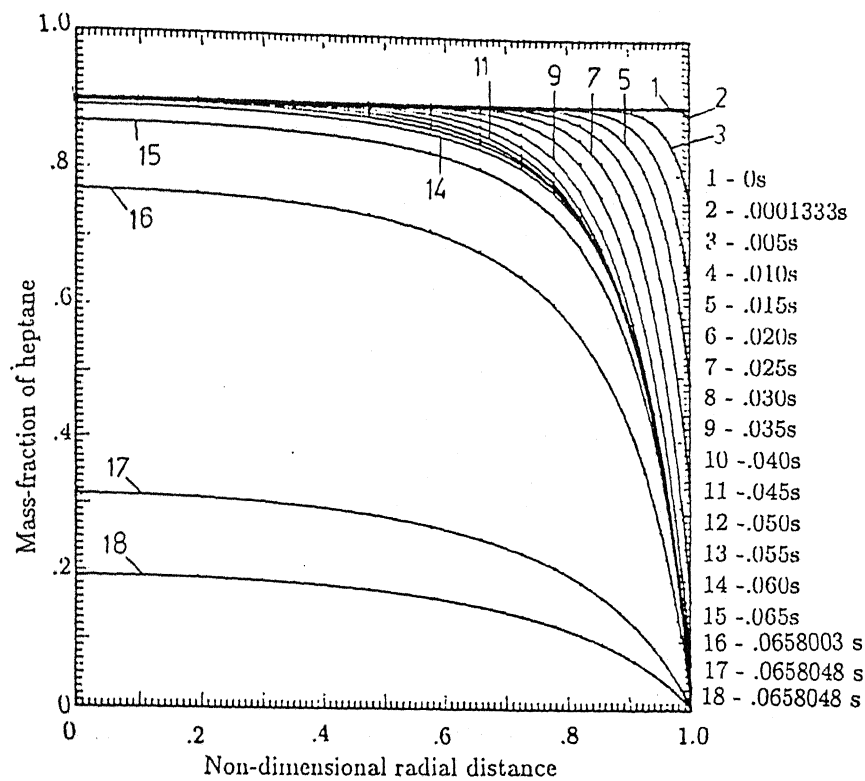


Fig. 5.2a Time history of mass-fraction profiles for heptane inside the fuel droplet for heptane-hexadecane burning with $\dot{Y}_{in,f1} = 0.9$.

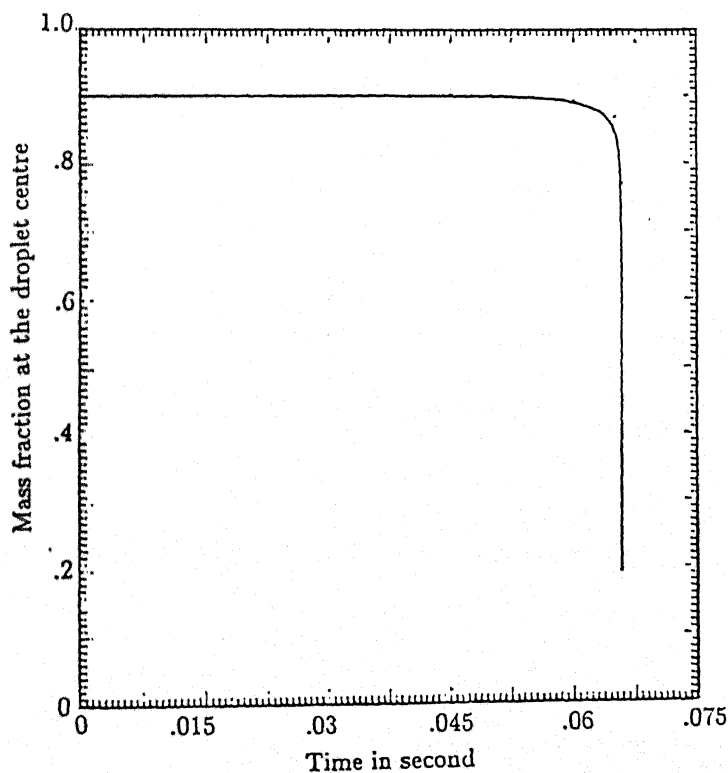


Fig. 5.2b Transient variation of heptane mass fraction at the liquid droplet centre for heptane-hexadecane fuel burning with $\dot{Y}_{in,f1} = 0.9$

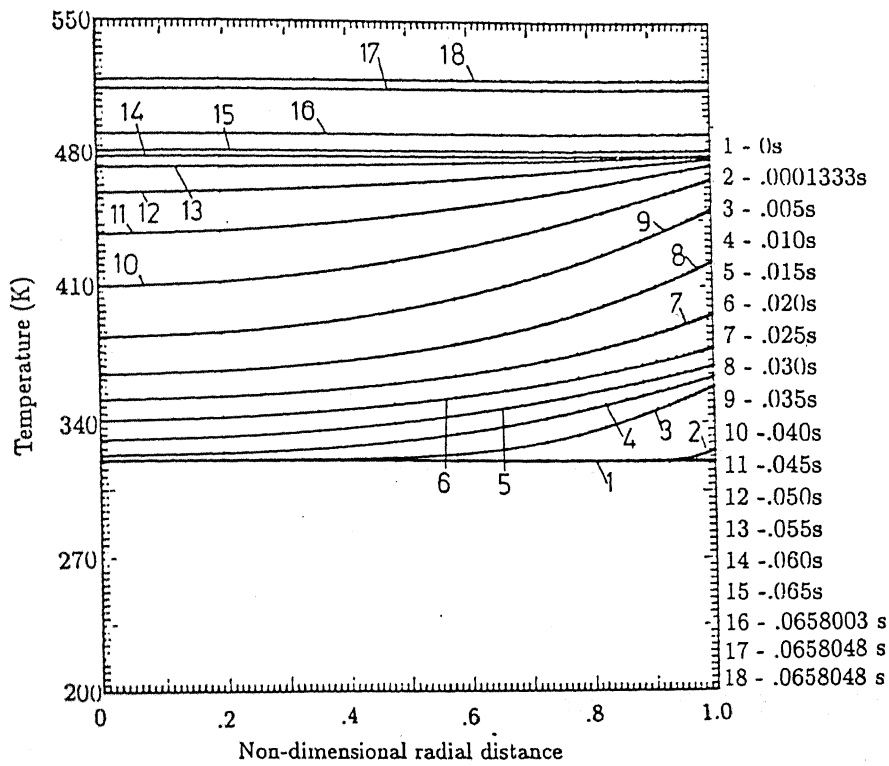


Fig. 5.3a Time history of liquid side temperature profiles for heptane inside the fuel droplet for heptane-hexadecane burning with $\dot{Y}_{in,f1} = 0.9$.

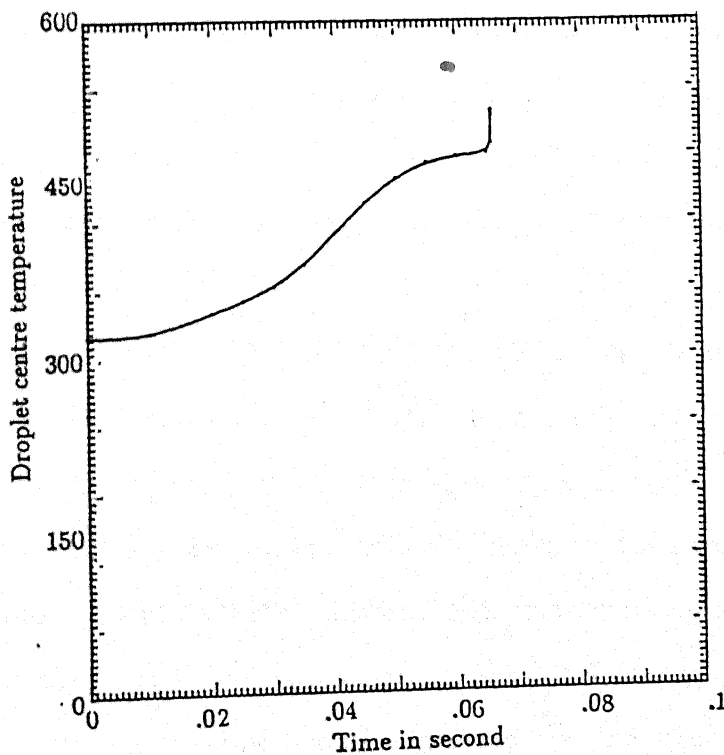


Fig. 5.3b Transient variation of liquid droplet centre temperature for heptane-hexadecane fuel burning with $\dot{Y}_{in,f1} = 0.9$

2-3 microns) towards the end of burning. Owing to the small droplet size, heat transfer rate becomes highly effective and causes instantaneous uniformization of temperature. This effect is also seen from Fig. 5.3b where towards the end of droplet burning, the temperature of the droplet centre is seen to increase almost instantaneously. Figures 5.2b and 5.3b indicate that the effect of multicomponent nature of droplet burning is strong enough to influence the temperature but not the concentration at the droplet centre for most of the droplet lifetime. The present work has ignored the possibility of micro-explosion. It is expected that if the degree of superheat for the more volatile fuel is high then micro-explosion may take place.

5.4 Gas-Side Mass-Fraction and Temperature Profiles

Figures 5.4a-d, 5.5a-c and 5.6a-c depict the time history of mass-fraction profiles for the gas-phase species and also the temperature profiles for the same phase. For all these figures, non-dimensional radial distance has been used as the abscissa. So, the movement and the position of the flame region indicated in all these figures are always in comparison to the movement of the droplet surface. However, Fig. 5.4d indicates both the actual position and movement of the flame region in relation to the droplet center and the flame stand-off ratio.

Figure 5.4a explains how the temperature profile evolves during the initial transient period. In this initial period of burning, since the droplet surface hardly regresses, non-dimensional and normalised radial distances (i.e. dimensional radial distance divided by the initial droplet radius) are almost identical. Therefore, the flame movement as shown in Fig. 5.4a is almost identical with the actual flame movement. It shows that the ignition takes place very near the droplet surface at about $r=4$. Initially, the entire gas phase is maintained at 1000 K. The flame region is indicated by the steep temperature gradient region. After the ignition starts, the chemical reaction at the flame becomes vigorous

and as a result of the enormous amount of heat released during the chemical reaction, the temperature of the reaction zone becomes progressively higher. But, after some time, flame temperature reaches more or less a steady value. This is because, the heat evolved in the reaction is balanced by the amount of heat being conducted away on either side of the flame region as well as by the heat consumed by the dissociation reactions. When the flame temperature becomes high, the products like carbon dioxide and water dissociate into carbon monoxide, hydrogen and oxygen and form an equilibrium mixture depending on the temperature. These dissociation reactions, being endothermic in nature, do not allow the flame temperature to exceed a certain limit. The present model does not consider the effect of radiation and convection. It (the present model) uses both constant and variable specific heat in the gas phase. Figures 5.4a, b, c & d are for constant specific heat which also results in a slight overprediction of the flame temperature. The present results show the flame temperature to be as high as 3000 K. Whereas, for variable specific heat case, the flame temperature is predicted to be around 2950 K.

During the initial transient, the amount of fuel vapour present, relative to the oxidiser, is quite small due to low evaporation rate. So, while the flame is being fully established, the flame region moves and expands towards the droplet surface in search of more fuel to sustain combustion. Thus, the gas-side temperature gradient at the droplet surface becomes progressively higher. This enables vigorous droplet heating. So, during this period, the droplet surface temperature increases very rapidly, and as a result mass-gasification rate increases very fast. This results in fuel vapour accumulation between the flame and the droplet surface as a result of which the flame gradually moves away from the surface (Fig. 5.4a and 5.4d). After the initial transient is over, the flame movement slows down and almost stops with respect to the droplet center after the transition period and remains in that region almost till extinction (see Fig. 5.4d).

Figure 5.4c sheds light into the extinction phenomenon. It is a highly transient process. The figure shows that the flame gradually moves towards the outer boundary of the solution

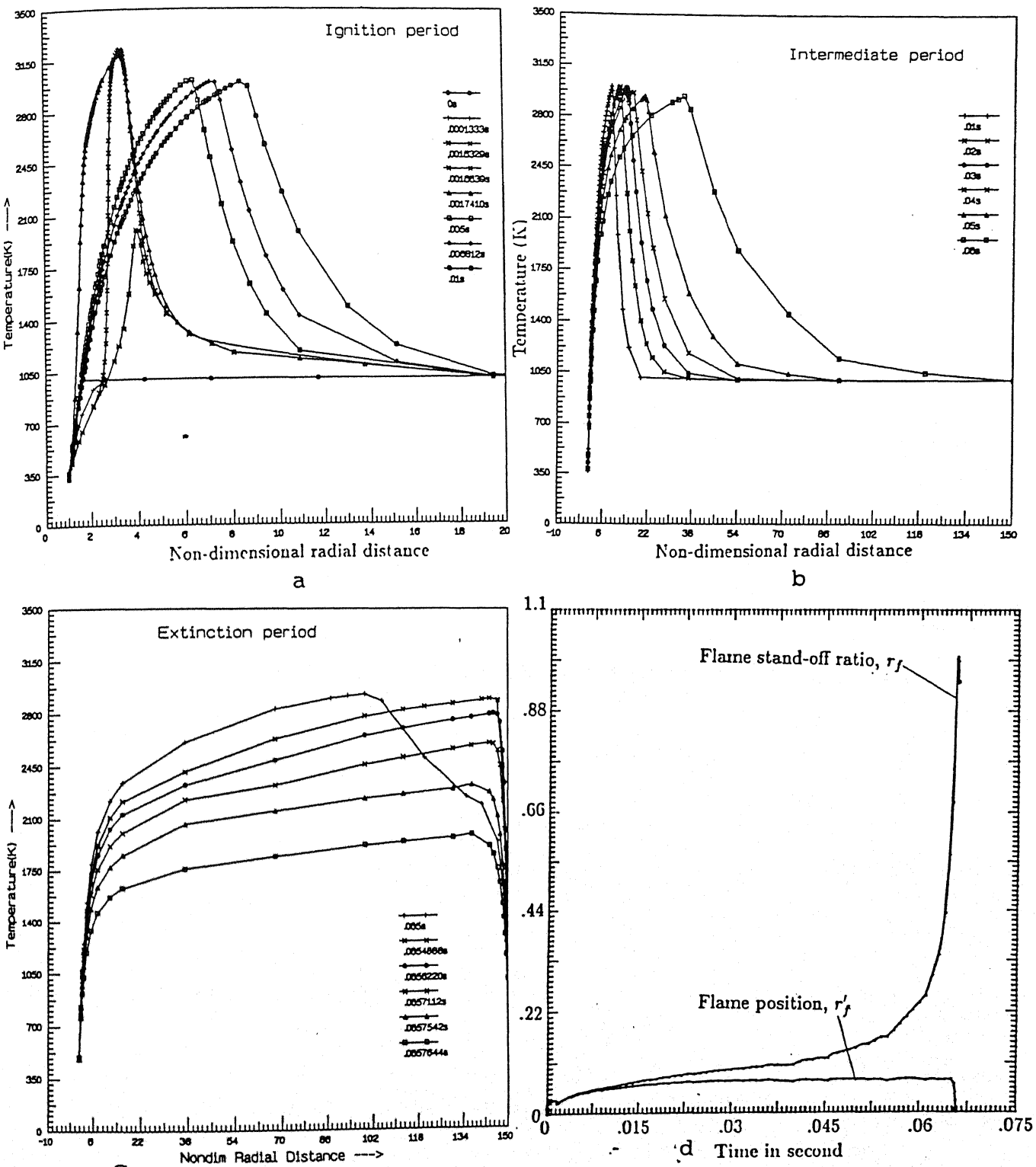
domain where the free stream conditions are forced though the flame actually remainsⁱⁿ the same region w.r.t. the droplet center. This happens because the r-coordinate shrinks along with the droplet surface, although the flame remains almost at the same position. As the extinction starts, the sharpness of the flame progressively reduces and gradually the peak temperature comes down.

Figures 5.4a,b,c also reveal the efficient adaptive nature of the grid generation technique. They show that the grids are removed from the low temperature gradient zone and are added to the high temperature gradient zone as the flame front moves one position to another. In this way, the tracking of the flame movement is done quite efficiently for the present study.

Figures 5.5a-c show the mass-fraction profiles for heptane and oxygen. It is seen from Fig. 5.5a that the mass-fraction profiles for heptane are initially very steep near the droplet surface. The steepness at the flame becomes initially flatter (curves 1, 2, 3) but then as the flame expands towards the droplet surface, this steepness at the flame increases (curves 3, 4, 5) and then, finally, as the flame moves away from the droplet surface due to fuel vapour accumulation, the steepness at the flame falls gradually (curves 5, 6). The mass fraction profiles of heptane at the droplet surface are initially quite steep (curves 1, 2), then becomes a little bit flatter for a small time (curves 3, 4, around 0.001647 s), then again steeper (curve 5, around 0.00174 s) and then, finally, becomes flatter (curve 6, around 0.005 s). This is also evident from the curve of liquid side surface mass fraction for heptane in Fig. 5.1a. In case of oxidiser mass-fraction profiles, it is seen that initially (when the flame is not fully established), the profiles are flatter (curves 1, 2), but, as the flame is fully established (curve 3 and 4, around $t = 0.0016329$ s), steepness of oxidiser mass-fraction profiles at the flame region also increases till the flame starts moving outward. From Fig. 5.5b, one can see that as the flame moves away from the droplet surface, the mass-fraction profiles for heptane become progressively flatter in the flame region. The same thing happens for the oxidiser mass-fraction profiles also. It is clearly

understood from Fig. 5.5a-c that the fuels and the oxidiser are almost fully consumed at the flame zone. The figures certify that the flame is not thick. Figure 5.5b depicts mainly the intermediate period including first $d^2 - law$ period, transition and second $d^2 - law$ period, which is extended upto extinction (refer Fig. 5.4c). In the extinction period, it is observed that as the flame moves towards the end of the solution domain (as a result of reduced droplet diameter), the oxidiser mass fraction profiles at the outer boundary becomes steeper due to the enforcement of the boundary conditions. This happens up to 0.0655396 s. Then again the oxidiser mass fraction profile becomes more and more flat at the flame zone and the flame moves inward towards the droplet surface at a rate faster than that of the surface regression rate. Therefore, the flame again moves inward relative to the outer boundary of the solution domain. The heptane concentration gradient at the droplet surface falls steadily because of the volatility limited mode of evaporation. From figure 5.5c, it is quite evident that the consumption at the flame surface becomes progressively lesser and the oxidiser mass fraction profile gradually tends towards it's initial uniform distribution which was prevailing before ignition. This feature is more clearly shown in Figure 5.6c.

Figures 5.6a-c show the mass-fraction profile for the less volatile fuel (hexadecane). The trend of the profile histories for both fuels is of similar nature. The only difference is that the surface mass-fraction for the more volatile fuel grows much faster and is maintained at a higher value (0.84) due to it's higher initial liquid side value (0.9) and this growth is over in the initial period only, whereas for the less volatile fuel, this change takes place more slowly over a long period and is maintained at a much lower value (0.16) owing to it's lower initial liquid side mass-fraction (0.1). Figure 5.6c shows that towards the end of burning, the mass fraction of hexadecane rises very sharply both at the droplet surface and also away from the droplet surface. Increase at the droplet surface is due to the volatility limited mode of evaporation and this increase is also penetrated away from the droplet surface because the consumption at the flame becomes negligibly small.



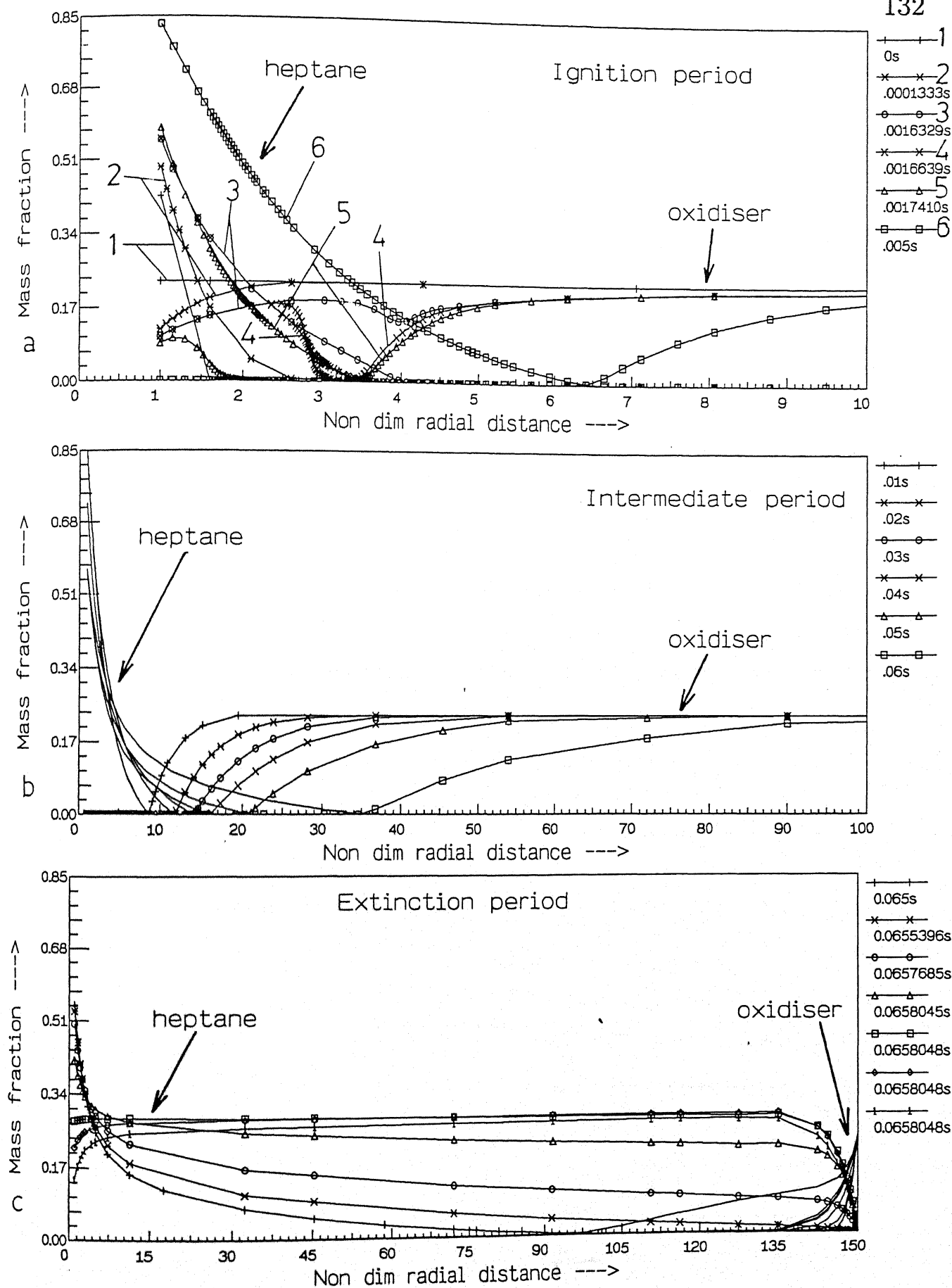


Fig. 5.5 Evolution of gas-phase mass-fraction profiles for heptane and oxidiser for heptane-hexadecane burning with $\dot{Y}_{in,1} = 0.9$.

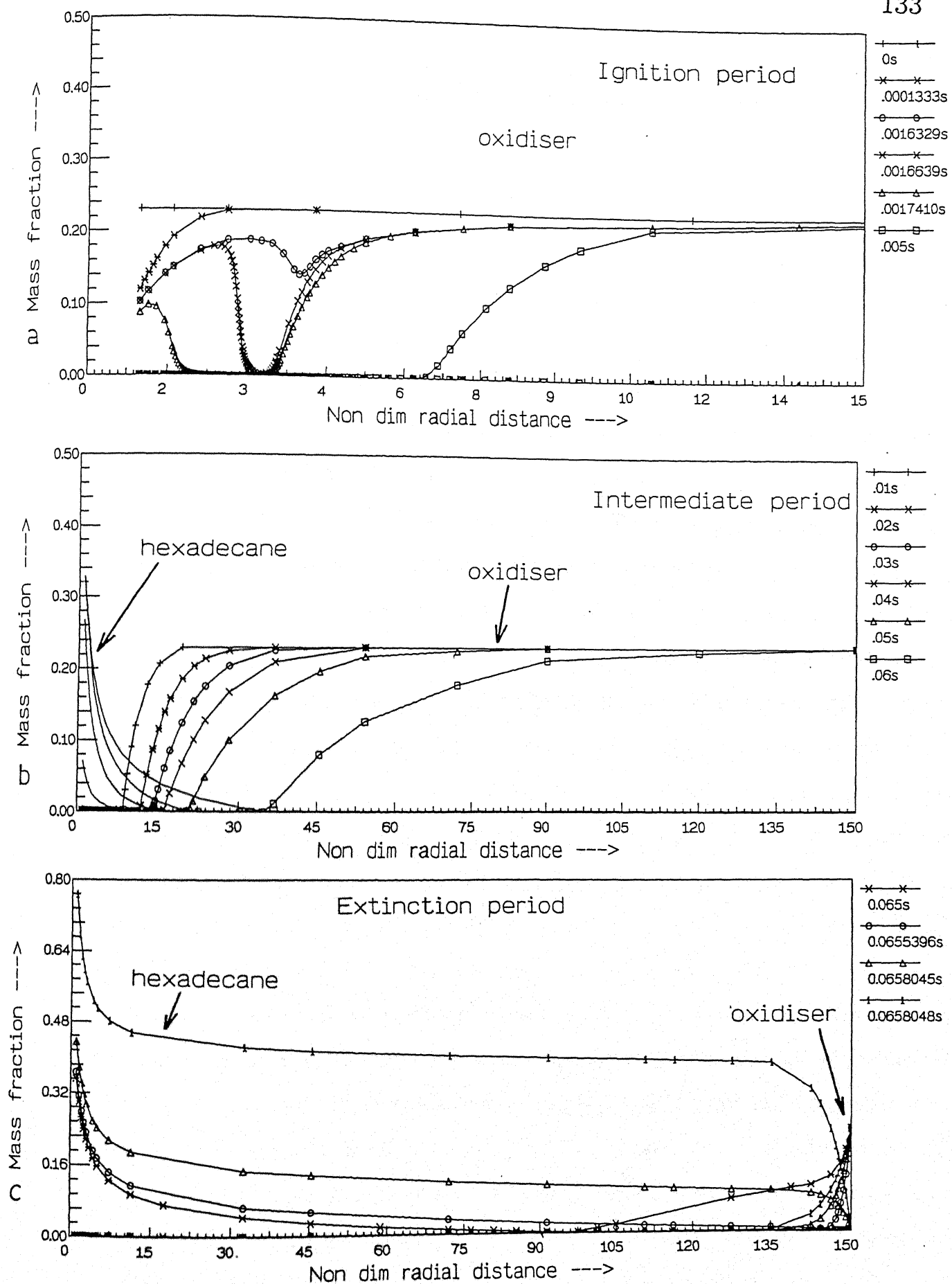


Fig. 5.6 Evolution of gas-phase mass-fraction profiles for hexadecane and oxidiser for heptane-hexadecane burning with $\dot{Y}_{in,fl} = 0.9$.

5.5 Effect of Initial Mass-fraction Variation on Surface Parameters

Surface parameters namely T_s , V , H_l , H_{ev} , H_g , ϵ_{f1} , Y_{f1ls} , Y_{f1sg} , Y_{f2sg} , r_d , d^2 , r_f , r'_f , T_f and r''_f were discussed in section 5.2. This section highlights the effect of varying the initial mass-fraction combination on these parameters plus a few other related parameters. Figures 5.7 through 5.9 show the variation with time of T_s , V , H_l , Y_{f1ls} , Y_{yf1sg} , ϵ_{f1} , Y_{f2sg} , d^2 , r_f , and r'_f for various values of initial mass-fraction combination.

For 0.9 initial liquid side mass fraction of heptane, the entire burning period is divided into six zones (see Fig. 5.7a) as discussed in Section 5.2 (refer Fig 5.1a-c). The two $d^2 - law$ periods are clearly visible from Fig. 5.9a. The relative length and positions of the two $d^2 - law$ periods and the transition zone in between depend on the initial mass-fraction of the fuels. It is seen from Fig. 5.9a that when the initial mass-fraction of the more volatile fuel (heptane) is very high (0.99), the 2nd $d^2 - law$ period is almost absent and only the 1st $d^2 - law$ period is present all through before the extinction occurs. This happens because, for these cases, the droplet is always lacking in less volatile fuel (i.e. dodecane), specially at the surface (Fig. 5.8a). The transition zone in this case is shifted to the final stage of burning. But as the initial liquid side mass fraction of heptane is gradually decreased, influence of dodecane over the evaporation rate becomes progressively more significant. This is seen from Fig. 5.8c (ϵ_{f1} vs. t). It indicates that as the initial mass-fraction of heptane is gradually decreased, domination of heptane evaporation is also gradually decreased and the transition becomes faster and is over in the early stage of burning. Thus, length of first $d^2 - law$ period gradually decreases and length of the second $d^2 - law$ period gradually increases. When the initial mass-fraction of heptane becomes very small (e.g. 0.1), the first $d^2 - law$ period almost vanishes and the 2nd $d^2 - law$ period covers almost the entire time length except for the initial transient period because, we can see from Fig. 5.8d that for this case, the surface is almost totally dominated by dodecane.

The transition from the more volatile fuel burning to the less volatile fuel burning

becomes most distinct when the initial mass-fraction of heptane is 0.9 (see Figs. 5.7a, 5.8 b-d and 5.9a). As the mass-fraction of heptane is lowered, the transition zone becomes steeper and it shifts more towards the early part of droplet burning and vice versa. Figures 5.7a ,5.8a-d and 5.9a clearly show this change of burning characteristics as the initial mass-fraction combination of the two fuels gradually changes from one extreme to the other.

Figs. 5.7a and 5.7c indicate that droplet heating is more rigorous and it takes place in the early stage of droplet burning when initial mass-fraction of heptane is small (0.1). Since, the amount of heptane present inside the droplet is small, the surface is dominated by dodecane almost from the very beginning. Therefore, the surface temperature is also controlled by the boiling point of dodecane (472 K) from the very beginning. So, for this case, only one long initial transient exists. But, as the initial mass-fraction of heptane is increased gradually, the droplet surface becomes dominated with heptane for longer periods. So, the second transient gradually shifts to the later part of the droplet burning and essentially, the initial droplet heating as well as the rise of surface temperature take place in two stages depending on the initial value of liquid side heptane mass-fraction. This effect of initial liquid side mass-fraction on droplet heating and surface temperature is revealed in the Figs. 5.7a and 5.7c.

Another interesting feature of the Figs. 5.7a through 5.9a is, that as the initial mass-fraction of heptane is gradually increased, the total burning time is gradually decreased and is least for pure heptane fuel burning. This happens because the droplet heating associated with the second transition becomes lesser due to the larger domination of heptane fuel (see the area under the curves of Fig. 5.7c) and also, more heat is available for fuel evaporation during the same duration. This is corroborated by Fig. 5.7d. The area under each volumetric mass gasification rate, V curve represents the relative amount of total heat available for evaporation and one can see from Figs. 5.7b,d that more heat becomes available for evaporation when the initial mass-fraction of heptane is higher within the same time limit.

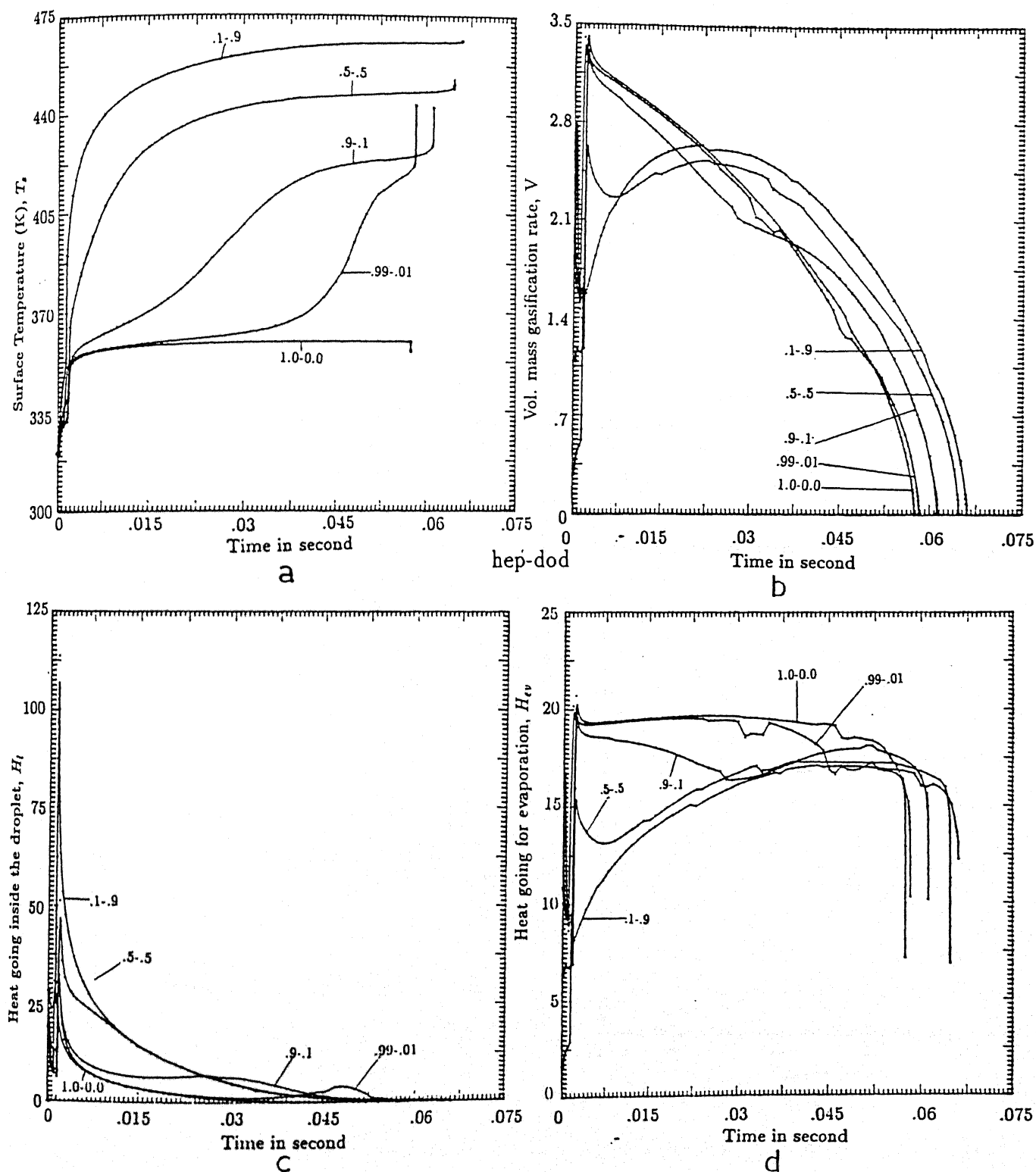


Fig. 5.7 Effect of initial mass-fraction on the transient variation of surface temperature, vol. mass gasification rate, droplet heating and heat available for evaporation.

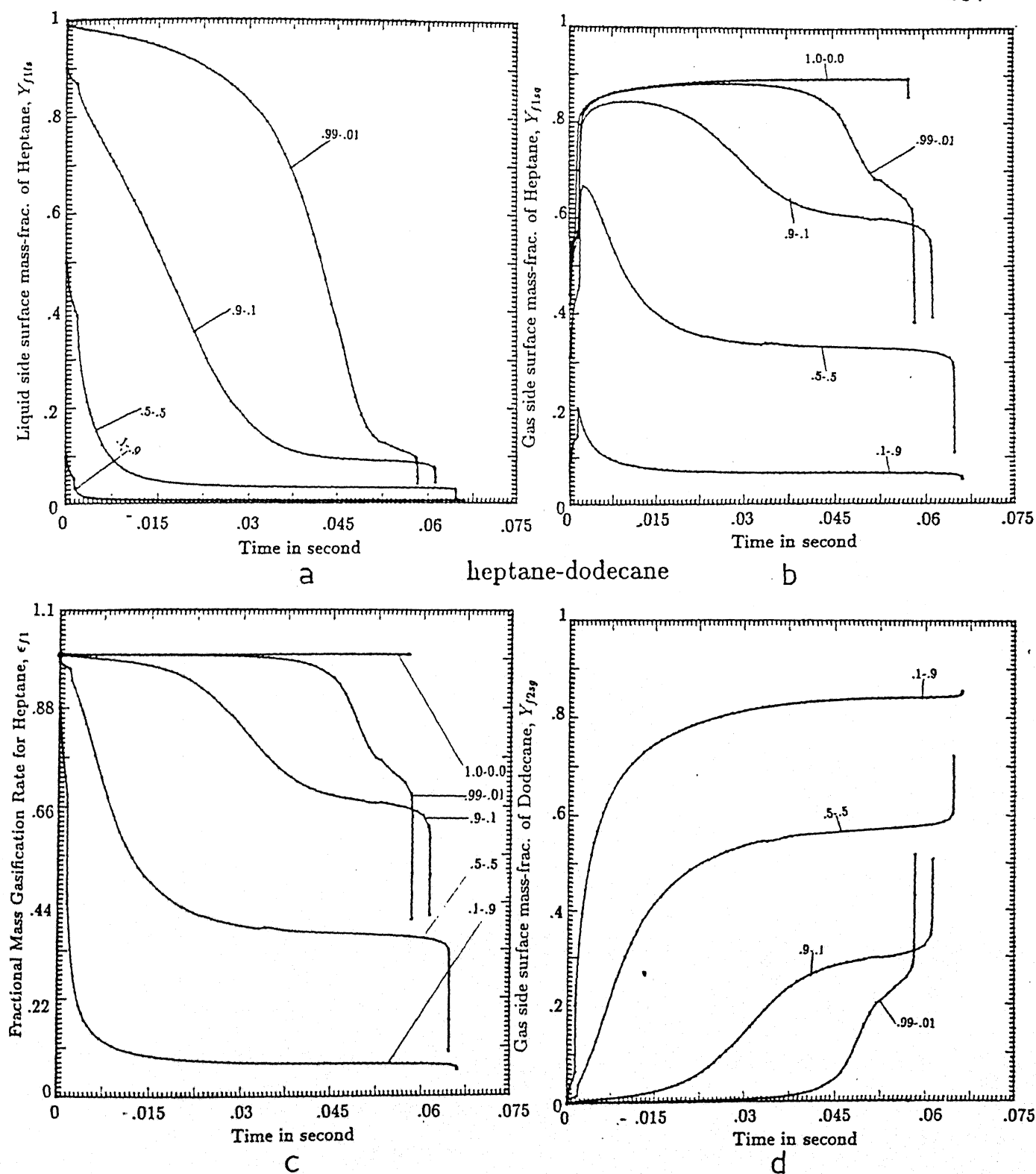


Fig. 5.8 Effect of initial mass-fraction on the transient variation of liquid and gas phase surface mass-fractions of heptane, gas phase surface mass-fraction of dodecane and fractional mass gasification rate of heptane.

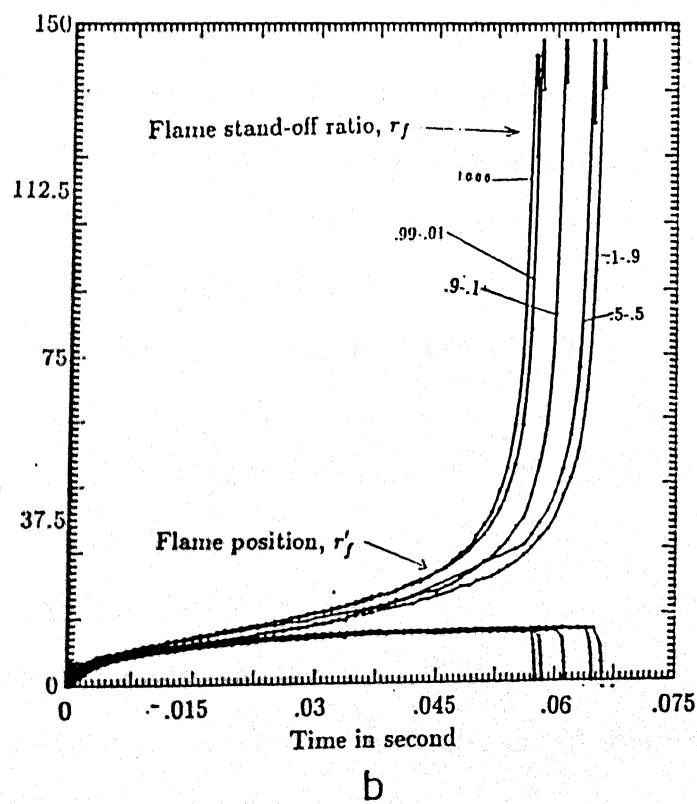
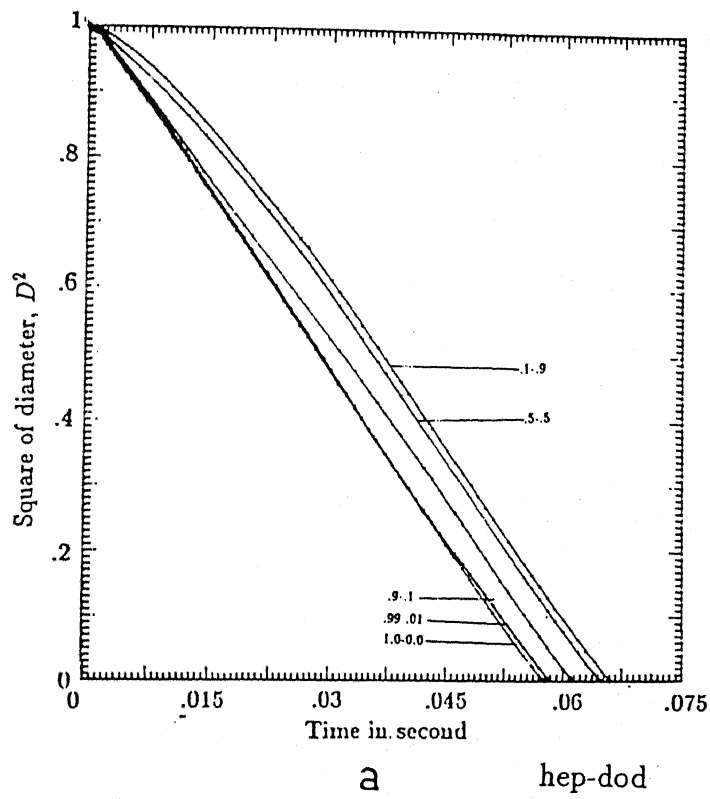


Fig. 5.9 Effect of initial mass-fraction on the transient variation of flame position, flame stand-off-ratio and square of the diameter.

Figures 5.8a-c show that as the initial mass-fraction of heptane is gradually increased, the curves become flatter and they are maintained at progressively higher values because, more amount of heptane becomes available at the droplet surface. Figure 5.8d shows that gas side surface mass-fraction profiles for dodecane are complementary to those of heptane mass fraction profiles. Fig. 5.9b indicates that the flame moves almost upto the the same distance for all the cases.

5.6 Effect of Volatility-Differential on Burning Characteristics

The nature of multicomponent combustion is highly dependent on the volatility-differential of the two individual fuels as can be seen from Figs. 5.10 through 5.12. Figure 5.12c shows that when the volatility-differential is very low (e.g. for heptane-octane combination), the two $d^2 - law$ periods merge with each other and become one single $d^2 - law$ period. As the volatility-differential between the two fuels gradually increases from heptane-octane combination to heptane-dodecane , the two $d^2 - law$ periods become more distinct and the transition from the 1st $d^2 - law$ period to the 2nd $d^2 - law$ period becomes more developed. The intermediate transition and thereby the multicomponent feature of fuel burning becomes more prominent when the volatility-differential is increased (see Figs. 5.10a,c; 5.11a-d; 5.12c).

One can see from Figs. 5.10a, 5.10c and 5.12c that When the volatility-differential is low, most of the droplet heating is over during the initial transient and then it is followed by a long quasi-steady period covering most of the droplet lifetime. As the volatility differential between the two fuels decreases, it approaches single component fuel burning in the limiting case. When the volatility-differential becomes large, it is seen that the droplet heating takes place twice. Firstly, just after ignition takes place and secondly, when the surface temperature makes a move beyond the boiling point of the more volatile fuel. This second transient, basically, corresponds to the transition zone where the combustion

process moves from $1^{st}d^2 - law$ period to the $2^{nd}d^2 - law$ period.

Figure 5.10b indicates that the overall evaporation rate has a longer quasi-steady period (similar to what is seen for a single component fuel) when the volatility-differential is small. As the volatility-differential is gradually increased, two quasi-steady periods separate out corresponding to the two $d^2 - law$ periods.

Figures 5.11a-d show how the liquid side and gas side surface mass-fractions of the two fuels as well as their relative strength of evaporation depend upon their volatility differential. Figure 5.11a shows that the liquid side surface mass-fraction of the more volatile fuel (heptane) falls more steeply as the volatility differential between them increases. Figure 5.11c indicates that the relative strength of evaporation for the two fuels remains almost constant for low volatility differential, whereas, for high volatility differential, two distinct regions separate out corresponding to the two $d^2 - law$ periods. Similar trend is also observed for Y_{f1sg} and Y_{f2sg} curves in Figs. 5.11b and 5.11d. The gas-side mass-fractions for heptane (Fig. 5.11b) initially increase and then decrease continuously, whereas, for the less volatile fuel (Fig 5.11d), they increase continuously. This happens because, when the volatility differential is very low (e.g. heptane-octane), both the fuels evaporate with equal preference. Therefore, almost constant values are maintained for all the curves for the low volatility differential case. Whereas, when the volatility differential is progressively higher, more volatile fuel is evaporated from the surface with higher preference. Therefore, the liquid side surface mass-fraction of the more volatile fuel falls more steeply. As a result of which relative evaporation strength, ϵ_{f1} , as well as its gas side surface mass-fraction also fall. Consequently, as the surface temperature makes a move towards the boiling point of dodecane, the gas side surface mass-fraction for dodecane increases. During the $2^{nd}d^2law$ period, Fractional mass-gasification rate and, liquid and gas-side mass-fractions of both fuels are maintained almost at constant values. As the volatility-differential is decreased, the distinction between the two periods vanishes into almost one long period.

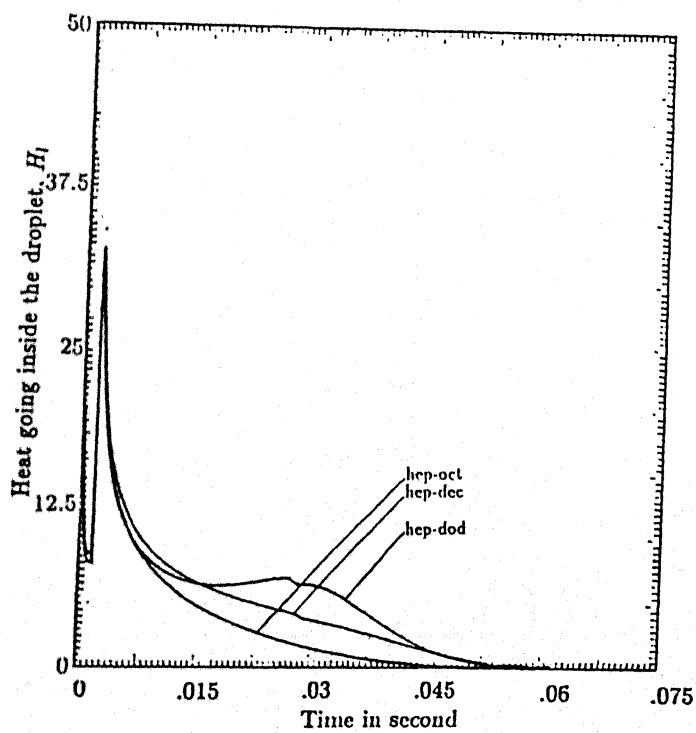
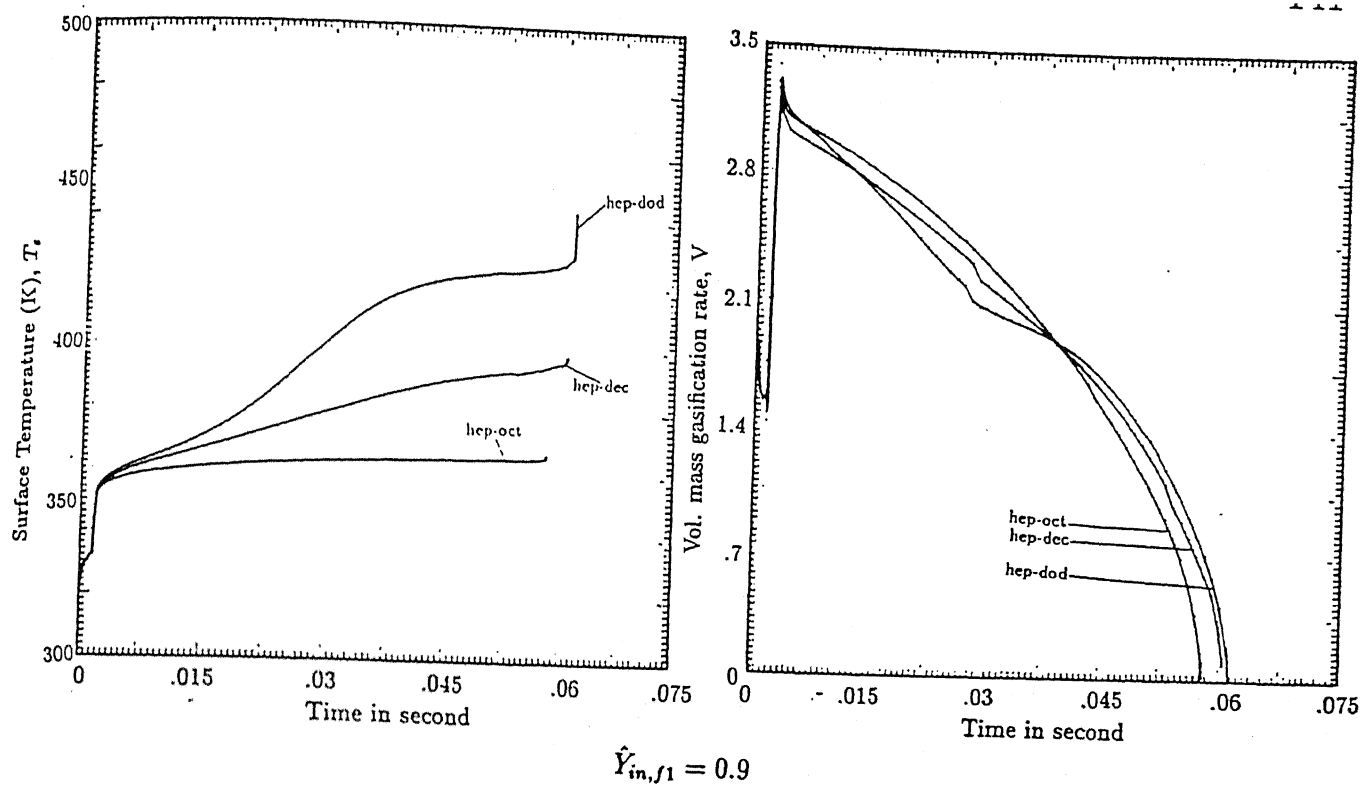


Fig. 5.10 Effect of volatility-differential on the transient variation of surface temperature, vol. mass gasification rate and droplet heating

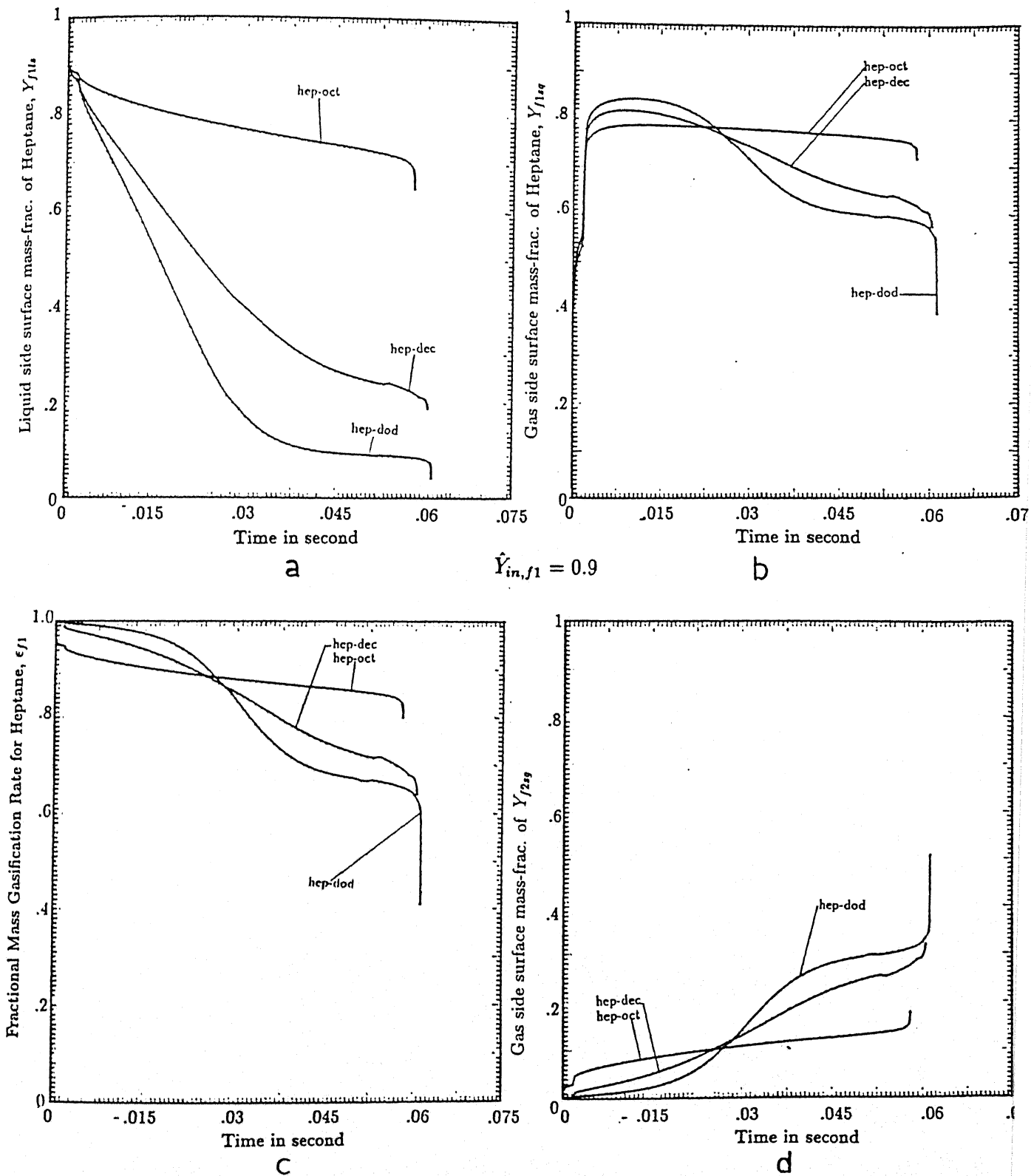


Fig. 5.11 Effect of volatility-differential on the transient variation of liquid and gas phase surface mass-fractions of heptane, gas phase surface mass-fraction of dodecane and fractional mass gasification rate of heptane.

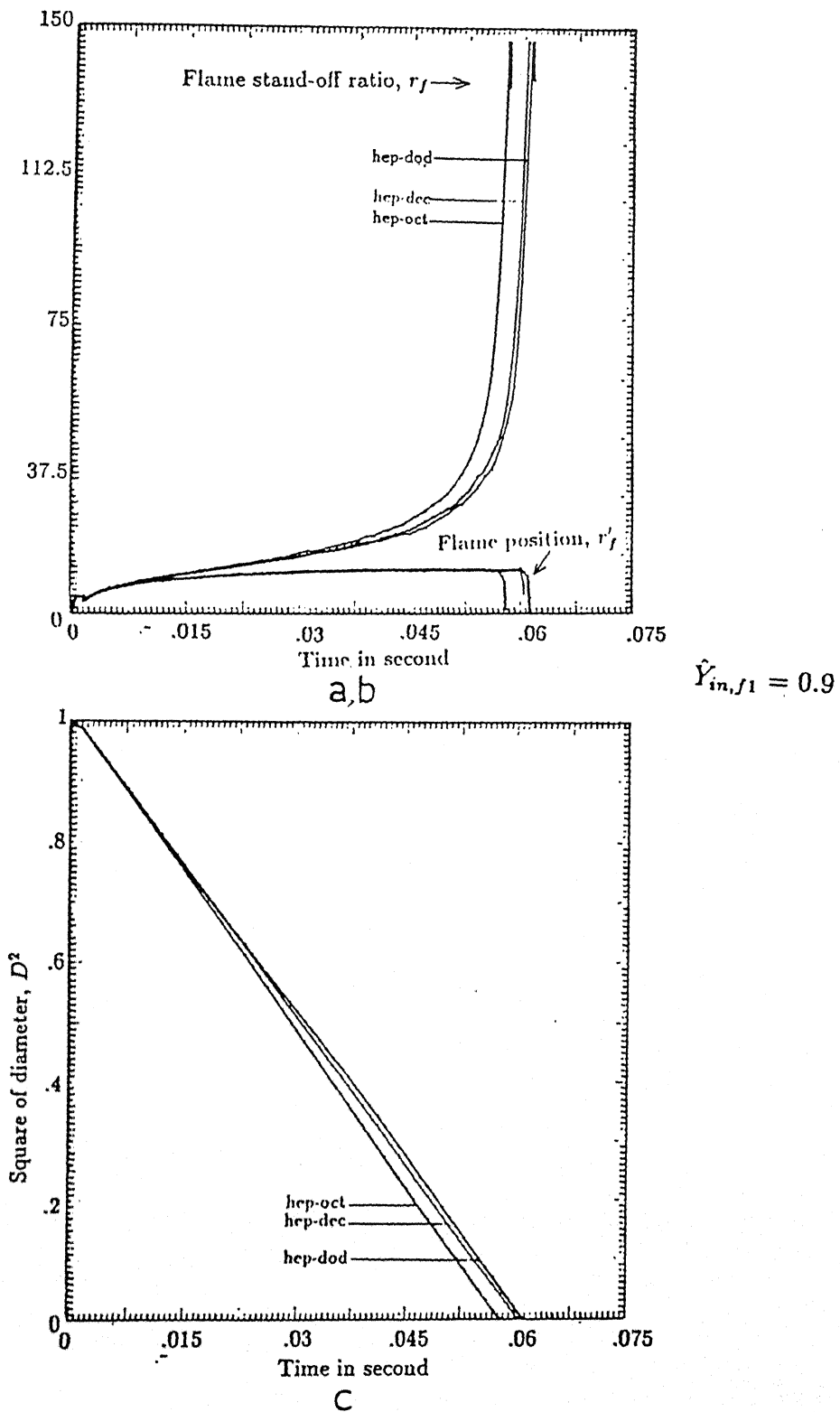


Fig. 5.12 Effect of volatility-differential on the transient variation of flame position, flame stand-off-ratio and square of the diameter.

5.7 Comparison of Analytical Models

This section describes the characteristics of the following three models:

- (i) Quasi-steady model
- (ii) Model neglecting the effect of surface regression
- (iii) Present model.

Figures 5.13 through 5.15 show the variation with time of Y_{f1ls} , Y_{f1sg} , ϵ_{f1} , Y_{f2sg} , H_l , T_s , r_f , r'_f and V for two values of initial mass-fraction combination for each of the above mentioned models. In the full quasi-steady model, the surface mass-fractions of both fuels are assumed to be maintained at the initial mass-fraction values throughout the entire burning history. For the present study, the full quasi-steady model (i) is valid as a special case when surface regression is assumed to be very high from the very beginning. Effect of mass diffusion is very small for this model. The continuous surface regression gives rise to a moving boundary problem. When the surface is fixed at $r=1$, the transformed coordinate becomes moving in nature. This transformation gives rise to a convection term in the transport equations for the liquid and phases as discussed earlier. In the second model, this convection term is neglected, considering that the regression rate of the droplet radius is very small. This case may be applicable in case of pure vaporization where the rate of evaporation is very low. But, in practical combustion, situations one can neither neglect the liquid side mass-diffusion (specially towards the end of burning) nor surface regression rate, because both are significant. Therefore, the present model (i.e. the third model), includes both mass-diffusion and surface regression. From the results also, one can see that the practical situations are combinations of these two extreme limits.

For elaborating upon the comparison, two cases of 0.9-0.1 and 0.5-0.5 initial mass-fraction combinations of heptane-dodecane mixture are chosen. From Fig. 5.13a, one can see that for the second model in which the effect of surface regression is neglected, the mass-fraction of the more volatile fuel at the surface falls very steeply. This happens due to the high liquid side diffusional resistance. One can see that the present model resembles

the second model only in the initial stage of droplet burning when the surface regression rate is very low due to the low evaporation rate. As evident from the figure, the degree of this tendency depends on the initial mass-fraction of the fuels. They closely approach each other if the initial mass-fraction of heptane is low. As the initial mass-fraction of heptane is increased, the present model increasingly deviates from the second model. As the burning proceeds beyond this initial period, surface regression rate gathers momentum due to more evaporation at the droplet surface. Therefore, the inner core is exposed to the surface very rapidly, supplying the necessary amount of fuels for maintaining the surface mass-fraction. So, for this later part of the burning, the present model behaves like the quasi-steady model in which the surface mass-fraction of the fuels remains almost constant. This behaviour continues till the end of the burning. The similarity of the first and third models in the later part of droplet burning is only qualitative. As evident from the Figs. 5.13 through 5.14, the quasi-steady model (1) basically behaves like a single component fuel burning model in the sense that it has only one $d^2 - law$ period (see Fig. 5.14d). But actually, the burning is controlled by the surface mass-fractions of the two fuels which, in turn, depend on both liquid phase mass-diffusion and surface regression rates. Therefore, when surface regression is not neglected, the role of initial mass-fraction, as evident from Fig. 5.13a, on burning characteristics becomes more important. For the quasi-steady model, the total droplet heating is much less which is represented by the area under the curves of Fig. 5.14b. Consequently, for this case, more heat becomes available (as a percentage of total heat available) for evaporation. It is seen from Fig. 5.14d that when the surface regression is neglected (model 2), the transition from one $d^2 - law$ period to the next becomes very sharp and the duration of the 1st $d^2 - law$ period as well as the total burning time are underpredicted. Compared to quasi-steady model, for models 2 and 3, a progressively larger amount of heat goes into the droplet and consequently, lesser amount of heat is available for evaporation. Hence, for all practical purposes, the regression rate cannot be neglected. Figures 5.15a,b show flame movement for these three models. It is seen that

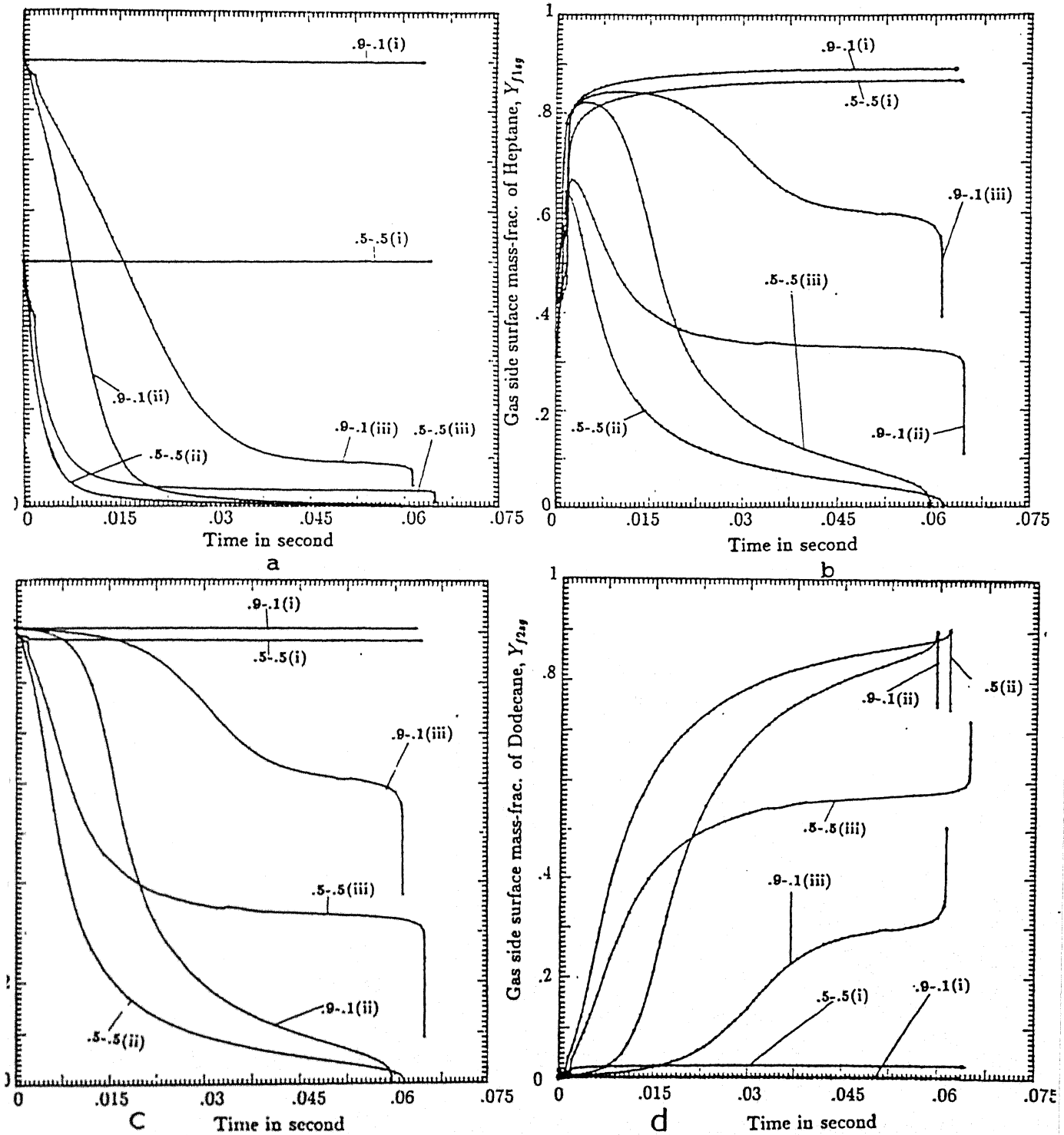


Fig. 5.13 Comparison among the quasi steady model (i), the model which neglects the effect of surface regression (ii) and the present numerical model (iii) for liquid and gas phase surface mass-fractions of heptane, fractional mass gasification rate of heptane and gas phase surface mass-fraction of dodecane.

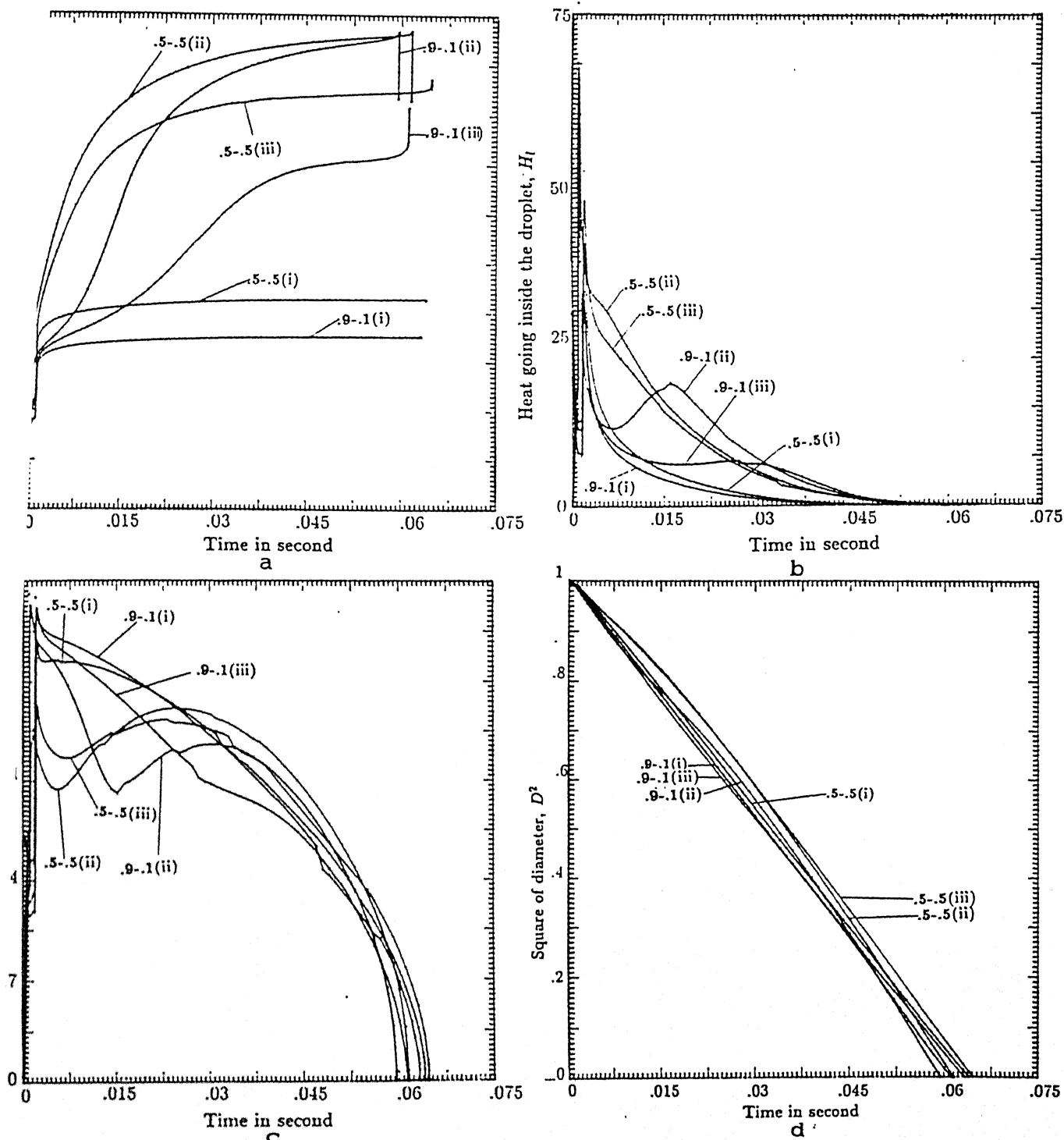
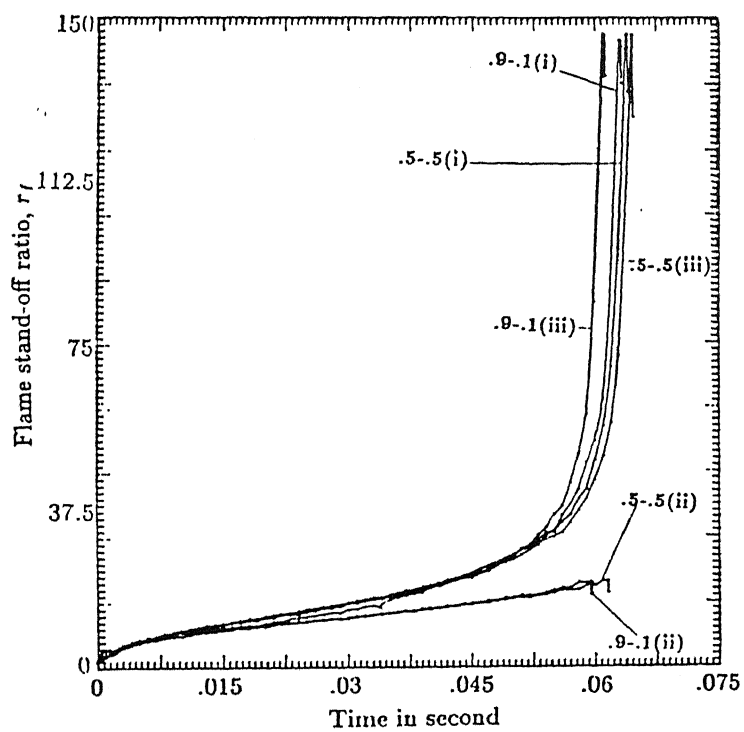
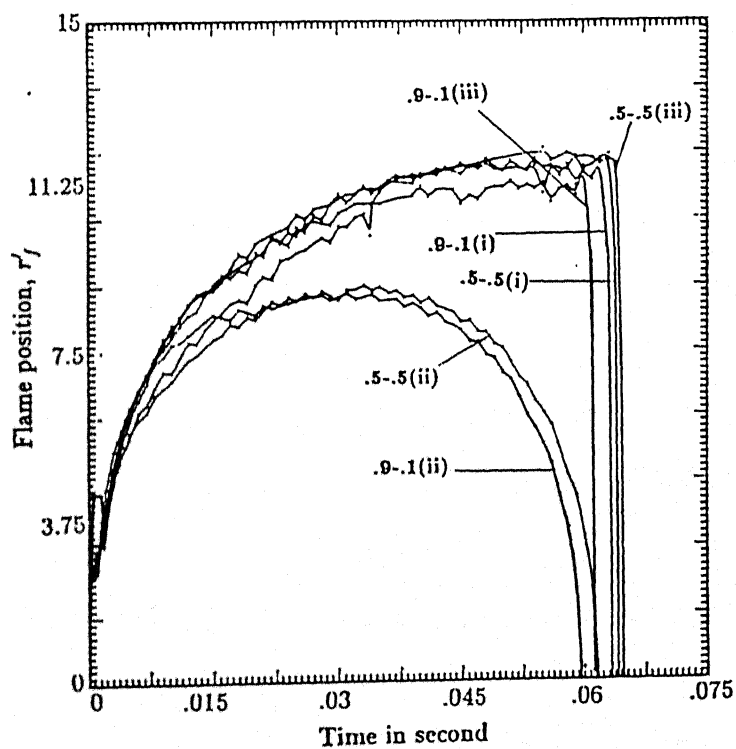


Fig. 5.14 Comparison among the quasi steady model (i), the model which neglects the effect of surface regression (ii) and the present numerical model (iii) for droplet heating, surface temperature, dsquare of the diameter and vol. mass gasification rate.



a



b

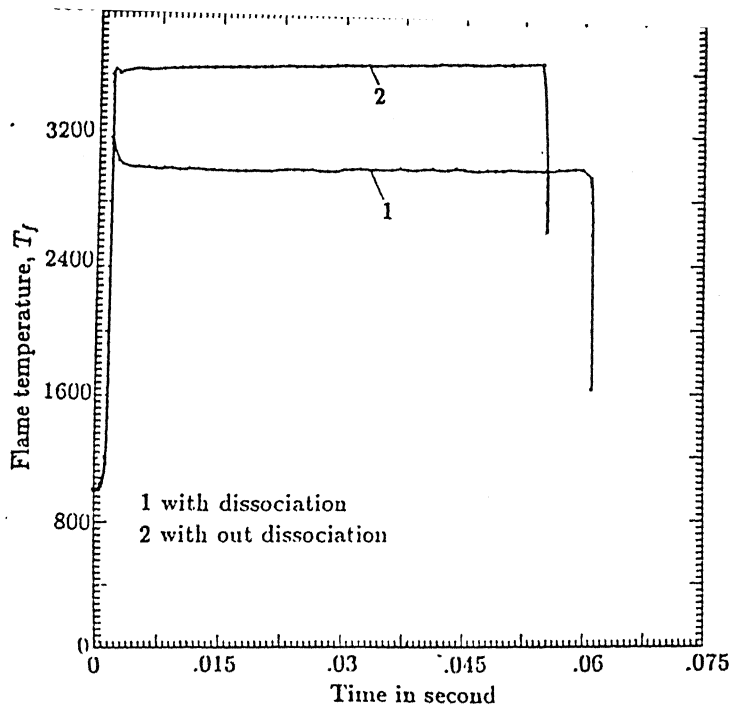
Fig. 5.15 Comparison among the quasi steady model (i), the model which neglects the effect of surface regression (ii) and the present numerical model (iii) for flame position and flame stand-off-ratio.

when the convective terms for the liquid and gas phase equations (arising out of surface regression) are neglected (in model 2), the flame comes back towards the droplet surface very gradually as against the movement of the flame for other two cases where the flame remains steady during the later half of the burning. And it comes back towards the droplet surface very steeply at the end period of the burning. This difference of flame movement occurs due to the neglecting of the convective term for the gas phase equations for model 2 because, the gas phase does not receive any information regarding the surface regression.

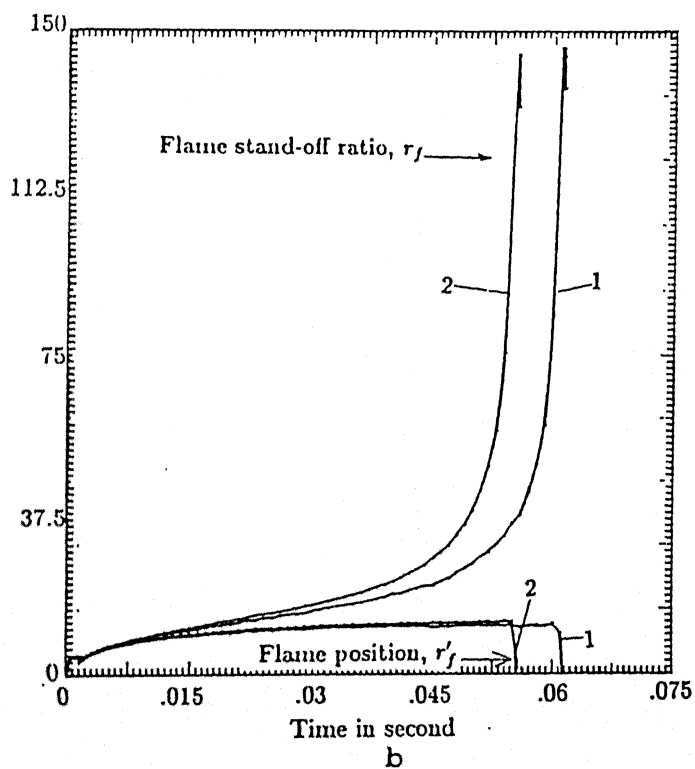
5.8 Gas Phase Dissociation

Various combustion parameters are strongly affected by gas phase dissociation. Figures 5.16 through 5.18 show the variation with time of Y_{f1ls} , Y_{f1sg} , ϵ_{f1} , Y_{f2sg} , H_l , r_f , $r_{f'}$, H_{ev} , T_s , d^2 , T_f and V with and without gas phase dissociation for heptane-dodecane burning with 0.9-0.1 initial mass-fraction.

Figures 5.16a and 5.16b show the effect of dissociation reaction on flame temperature, flame position and fuel vapour accumulation. When gas phase dissociation is included, flame temperature is considerably reduced due to the endothermic nature of dissociation reactions. The flame, however, moves in similar manner for both the cases (i.e. with and without dissociation as seen from Fig. 5.16b), the only difference being that the flame without dissociation, because of higher flame temperature which leads to slightly higher rate of fuel vapour accumulation, moves faster and also farther away from the droplet surface, and finally, comes back faster and vanishes into the droplet. Higher value of heat generation at the flame causes larger rate of heat flow from gas to liquid phase (Fig. 5.17a). This results in a higher rate of surface temperature rise (Fig. 5.17b). Larger rate of heat is also available for evaporation at the droplet surface (Fig. 5.17a). Consequently, gasification rate is also increased (Fig. 5.17c) which results in faster rate of fuel vapour accumulation and flame movement (Fig. 5.16a) and also faster regression of the droplet surface (Fig. 5.17d). Liquid side surface mass-fraction of heptane falls more steeply (



a



b

Fig. 5.16 Effect of gas phase dissociation on the transient variation of flame temperature, flame position and flame stand-off-ratio .

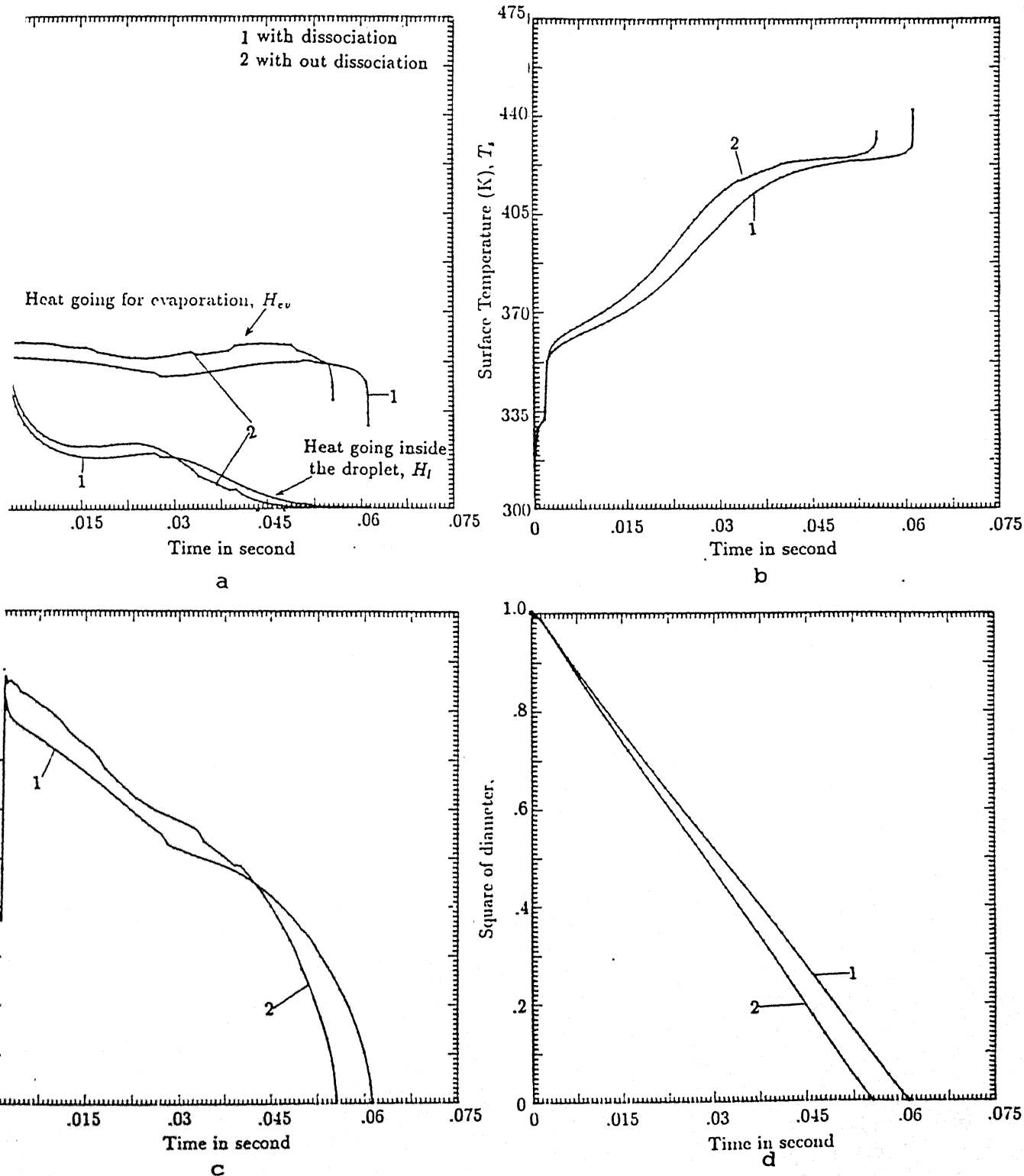


Fig. 5.17 Effect of gas phase dissociation on the transient variation of droplet heating, heat available for evaporation, surface temperature, vol. mass gasification rate and square of the diameter.

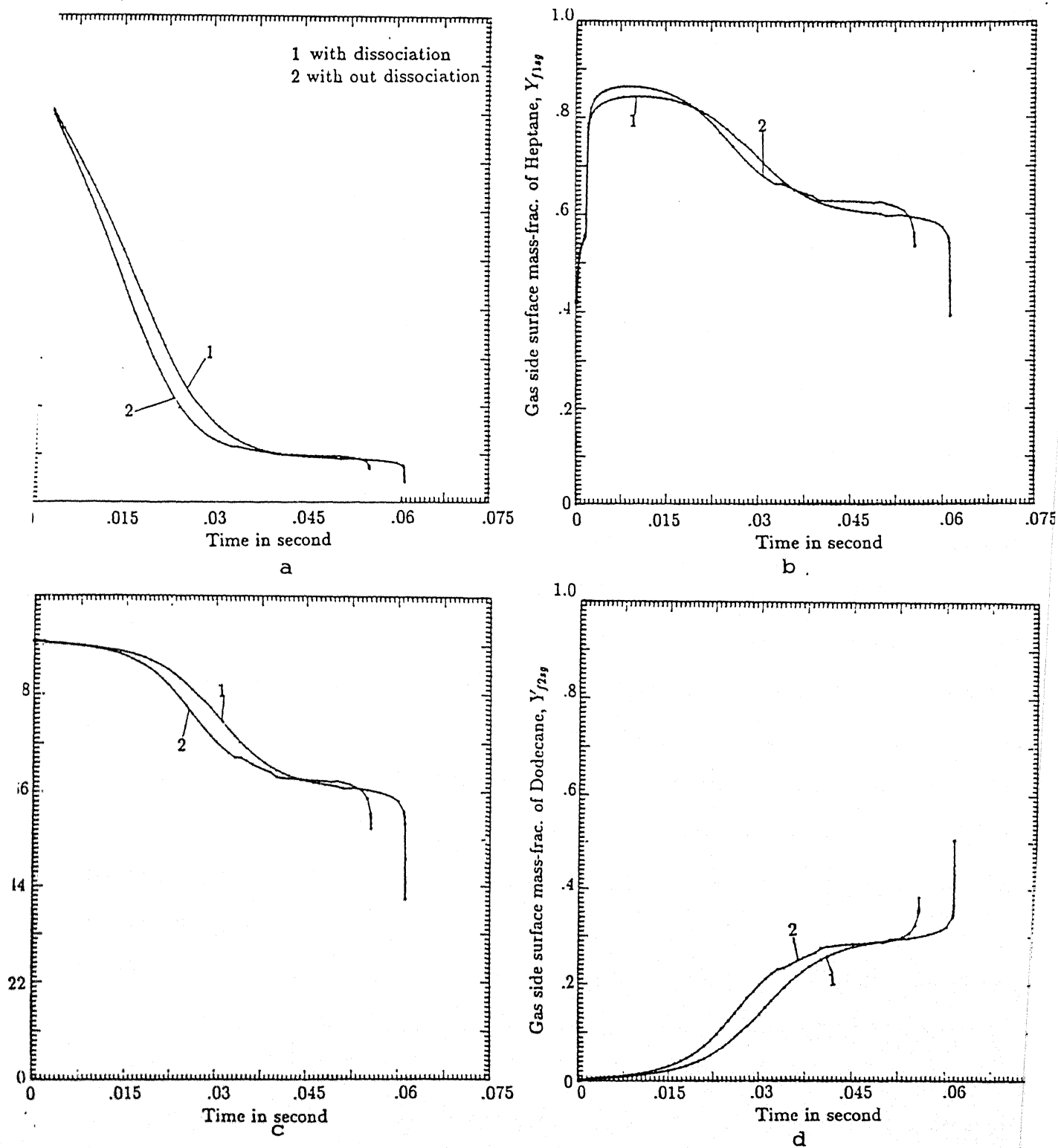


Fig. 5.18 Effect of gas phase dissociation on the transient variation of liquid and gas phase surface mass-fractions of heptane, fractional mass gasification rate of heptane and gas phase surface mass-fraction of dodecane.

Fig. 5.18a) due to higher initial gasification rate and reaches quasi-steady state faster due to relatively high regression rate in the earlier part. The temporal variation of gas-side mass-fraction of heptane and dodecane, and also that of fractional mass-gasification rate of heptane (Figs. 5.18b,c,d) behave in a similar manner. Liquid side temperature profiles do not indicate any significant change. Any change in the gas-phase is scaled down considerably in the liquid phase due to higher inertia of the liquid phase.

5.9 Effect of Ambient Temperature

In this section, Figs. 5.19 through 5.20 show the variation of different surface parameters such as T_f , H_l , T_s , V , d^2 , Y_{f1ls} , Y_{f1sg} , ϵ_{f1} and Y_{f2sg} have been plotted against time for three different ambient temperatures namely 300 K, 500 K and 1000 K for heptane-dodecane burning with 0.9-0.1 initial mass-fraction. When the ambient temperature is 1000 K, the flame temperature is maintained around 3000 K and for 500 K and 300 K, the flame temperatures are maintained around 2760 K and 2665 K respectively (see Fig.5.19a). This happens because the reaction is more vigorous for higher ambient temperature. Therefore, more heat becomes available for both droplet heating (see Fig. 5.19b) and for fuel evaporation. Consequently, the surface temperature, T_s , increases at a faster rate and it reaches a higher value (Fig. 5.19c). The volumetric mass gasification rate, V , also becomes faster (Fig. 5.19d) due to the easy availability of heat for fuel evaporation, H_{ev} and therefore, the burning is completed earlier (Fig. 5.19e).

Figures 5.19a-e and 5.20a-d reveal that the transition from $1^{st}d^2 - law$ period to the $2^{nd}d^2 - law$ period takes place earlier and the curves are shifted slightly to the left for the higher ambient temperature. Figures 5.20a and 5.20b indicate that for the higher ambient temperature, the liquid side mass-fraction for heptane falls more steeply before it reaches a constant value and it's gas-side mass-fraction reaches higher value faster and this higher value is maintained till the end of burning. As explained already, the volumetric mass gasification rate is higher for higher ambient temperature. Therefore, for this case,

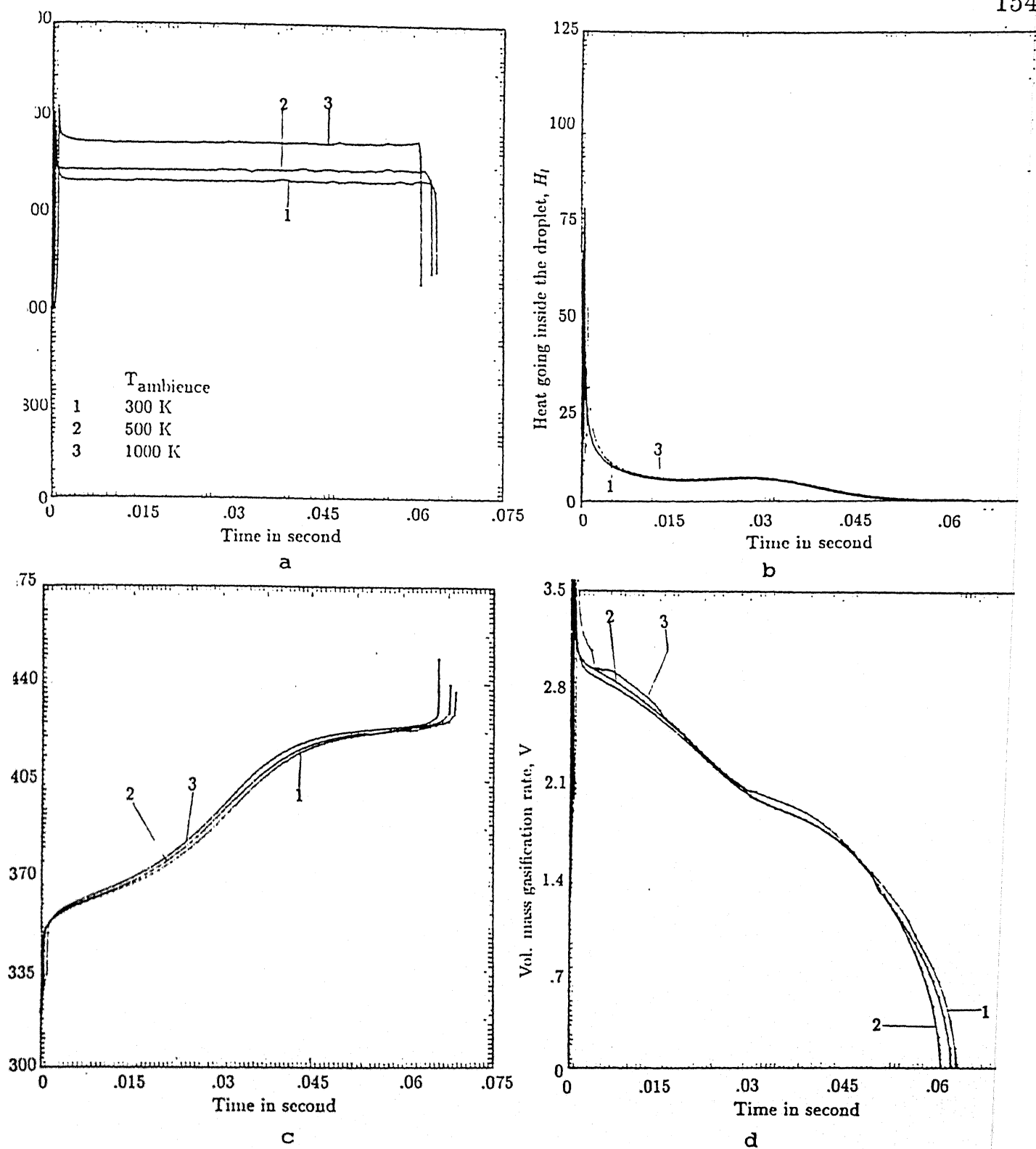
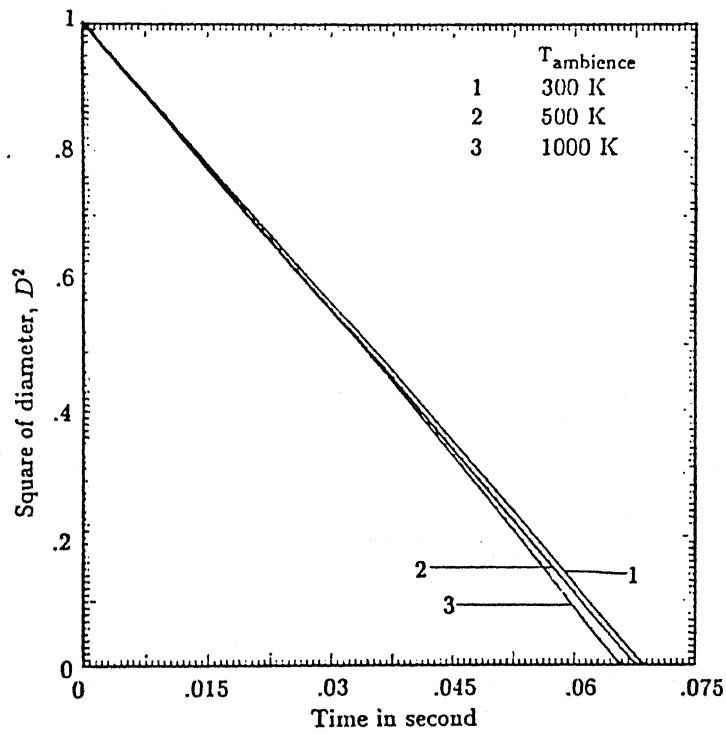


Fig. 5.19



e

Fig. 5.19 Effect of ambient temperature on the transient variation of flame temperature, droplet heating, surface temperature, vol. mass gasification rate and square of the diameter.

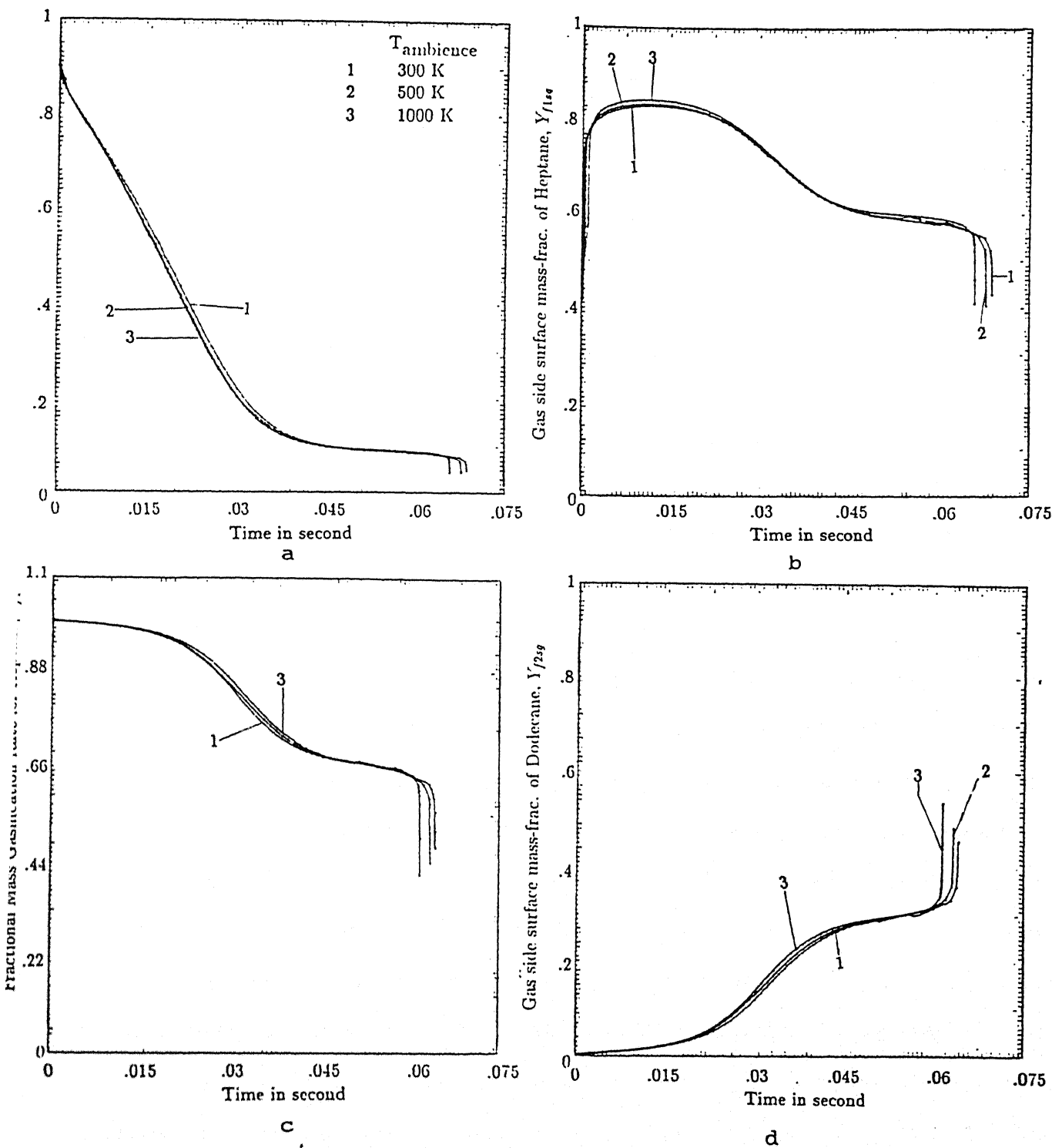


Fig. 5.20 Effect of ambient temperature on the transient variation of liquid and gas phase surface mass-fractions of heptane, fractional mass gasification rate of heptane and gas phase surface mass-fraction of dodecane.

heptane evaporates at a faster rate and as a result, its gas side surface mass-fraction increases at a faster rate and is maintained at a higher value. Figures 5.20c and 5.20d show that the variation in ambient temperature does not influence the fractional mass gasification rate for heptane and the gas side surface mass-fraction for dodecane during the initial and final part of burning. The influence is mainly in the transition region.

5.10 Variable Specific Heat for the Gas Phase

In the present section, the surface parameters, viz. T_f , H_g , H_l , H_{ev} , T_s , V , r_f , $r_{f'}$, Y_{f1s} and d^2 are chosen to highlight the effect of variable specific gas phase heat as against three constant values of specific heat for heptane-dodecane burning with 0.9-0.1 initial liquid side mass-fraction. The values chosen for the three constant specific heat cases are 1.0×10^3 , 1.25×10^3 and 1.5×10^3 J/kg-K.

It is observed that when variable specific heat is used, the flame temperature comes down to around 2950 K as compared to the constant specific heat (with value 1.0×10^3 J/kg-K) case when the flame temperature remains around 3000 K (see Fig. 5.21a). But, for all other surface parameters, the variation for the two cases (curves 1 and 2) are very small. The high specific heat at the flame region (for variable C_p case) does not allow the flame temperature to exceed a certain limit and that's why the flame temperature remains lower for this case. But, the temperature near the droplet surface and other places except for the flame region are not very high. Therefore, near the droplet surface and other places excepting the flame region, the value of specific heat for the above two cases are very close to each other. Therefore, the temperature gradient at the surface and consequently, the available heat from the gas phase for the two cases remains close to each other (5.21b). Therefore, almost the same amount of heat are available for the two cases for droplet heating (Fig. 5.21c) as well as for fuel evaporation (Fig. 5.21d). So, all other parameters such as surface temperature (Fig. 5.22a), volumetric mass gasification rate (Fig. 5.22b), flame movement and flame stand-off ratio (Fig. 5.22c), liquid side surface mass fraction (

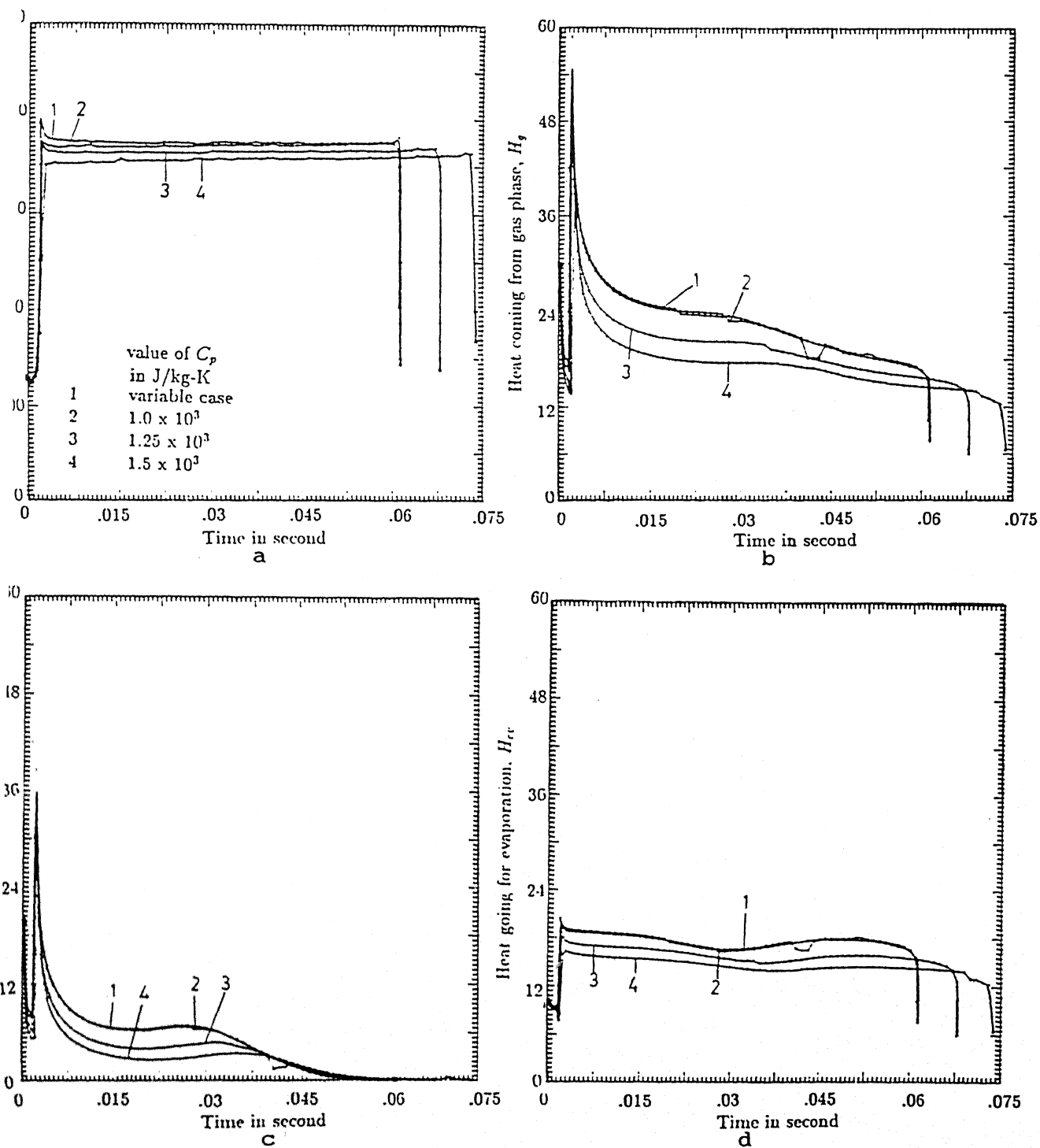


Fig. 5.21 Effect of variable specific heat as well as different values of constant specific heat on the transient variation of flame temperature, heat coming from the gas phase, droplet heating and heat available for evaporation.

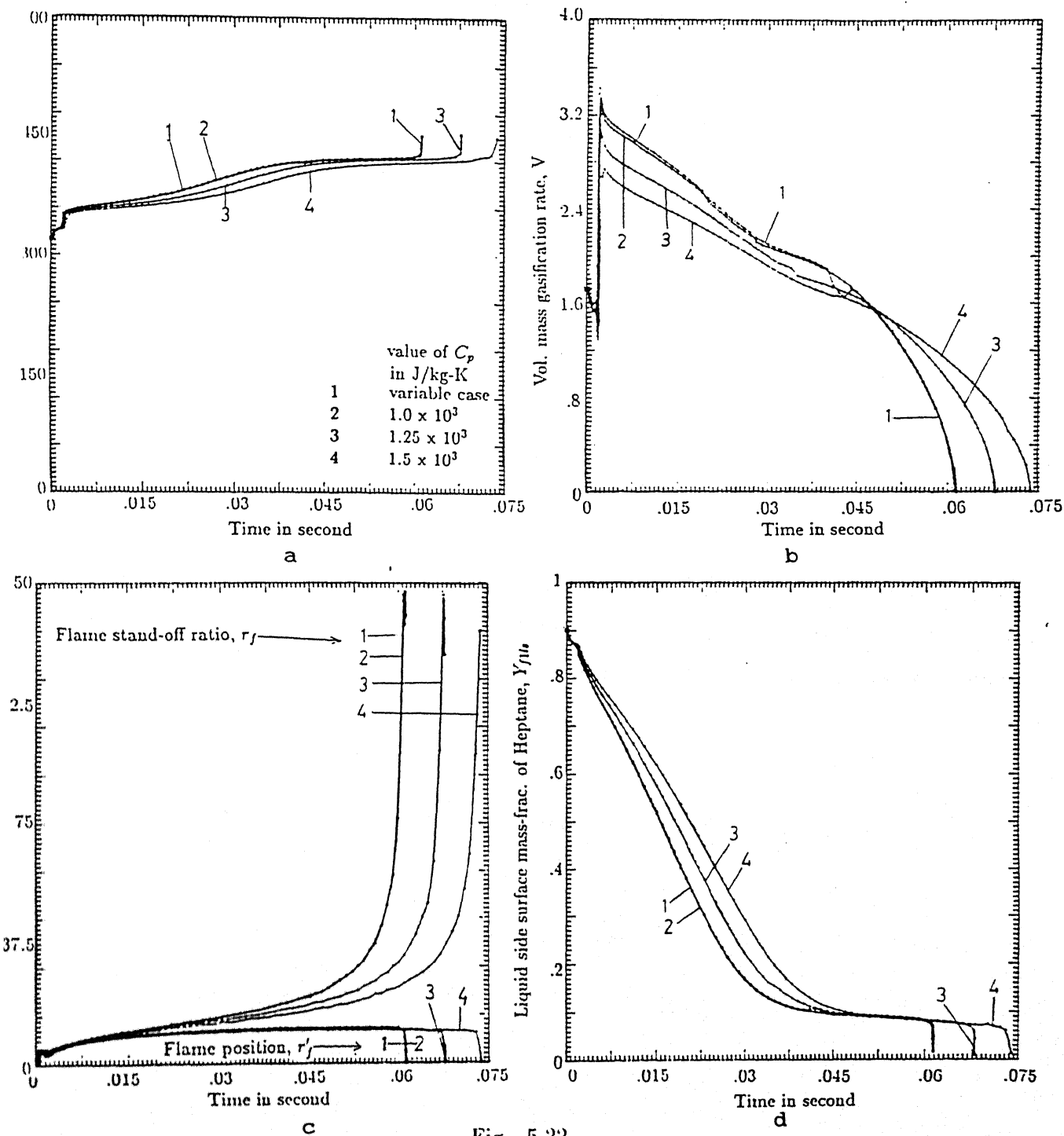


Fig. 5.22

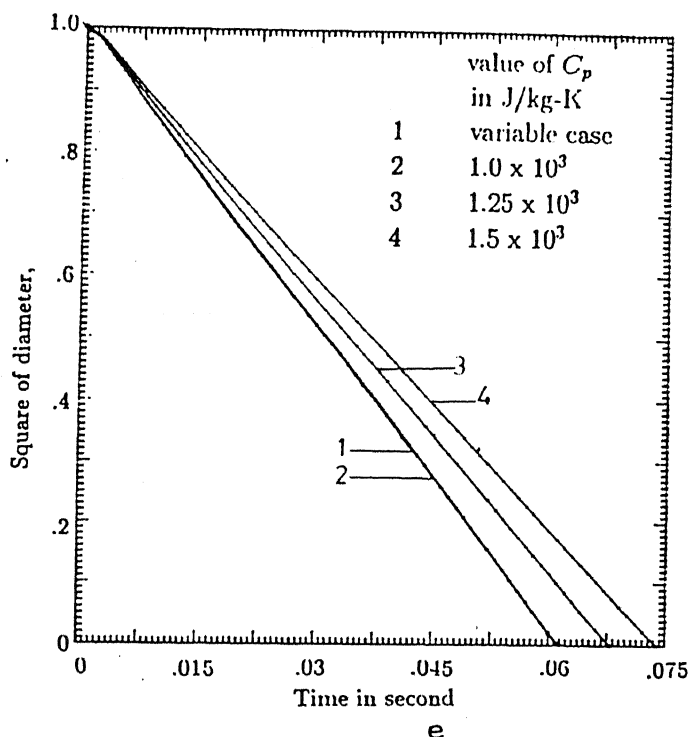


Fig. 5.22 Effect of variable specific heat as well as different values of constant specific heat on the transient variation of surface temperature, vol. mass gasification rate, flame position, flame stand-off-ratio, liquid phase surface mass-fractions of heptane, and square of the diameter.

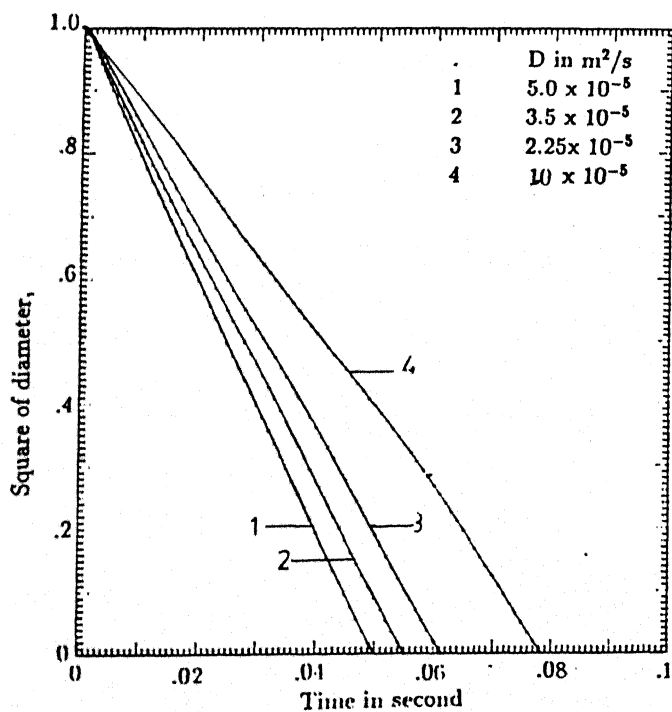


Fig. 5.23a

Fig. 5.22d) vary negligibly for these two cases. For the constant specific heat cases, we find that as the gas side specific heat is gradually increased, the flame temperature gradually decreases (Fig. 5.21a) and since specific heat is increased all over the domain uniformly, the temperature decreases over the entire domain. Therefore, the heat available from the gas phase becomes gradually less (Fig. 5.21b) due to the lower temperature gradient at the gas side of the droplet surface. Consequently, heat available for increasing the surface temperature (Fig. 5.21c) and fuel evaporation (Fig. 5.21d) also becomes less. Therefore, overall volumetric mass gasification rate falls (Fig. 5.22b) and consequently, evaporation rate constants become gradually lower (Fig. 5.22e) and the liquid side mass fraction of heptane falls with lower steepness (Fig. 5.22d). The nature of the flame movement remains similar (Fig. 5.22c). As a result of lower rate of fall of liquid side heptane mass-fraction at the droplet surface, surface temperature (Fig. 5.26a) increases more gradually over a larger time span. Therefore, the total burning time increases (Fig. 5.22e).

5.11 Gas Side Diffusion Coefficient

Figures 5.23 shows the the effect of varying the gas phase diffusion coefficient on the overall burning characteristics for heptane-dodecane burning with 0.9-0.1 initial mass-fraction combination. Diffusion coefficient of value $2.248 \times 10^{-5} \text{ m}^2/\text{s}$ corresponds to unity gas phase Lewis number. Values of gas phase diffusion coefficients used for the four curves in these figures are 1.0×10^{-5} , 2.248×10^{-5} , 3.5×10^{-5} and $5.0 \times 10^{-5} \text{ m}^2/\text{s}$. It is observed that as the diffusion coefficient is gradually decreased, the total burning time gradually increases and the intermediate transition becomes more gradual (Fig. 5.23a-e). As the diffusion coefficient of the species in the gas phase becomes progressively lower, the diffusion of the evaporated fuel vapour away from the droplet surface becomes progressively lesser. Therefore, effectively, the vaporization of the more volatile component (heptane) gets relatively suppressed. So, the liquid side surface mass-fraction of heptane (Fig. 5.23b) falls less steeply and since the surface temperature depends mainly on the surface mass-

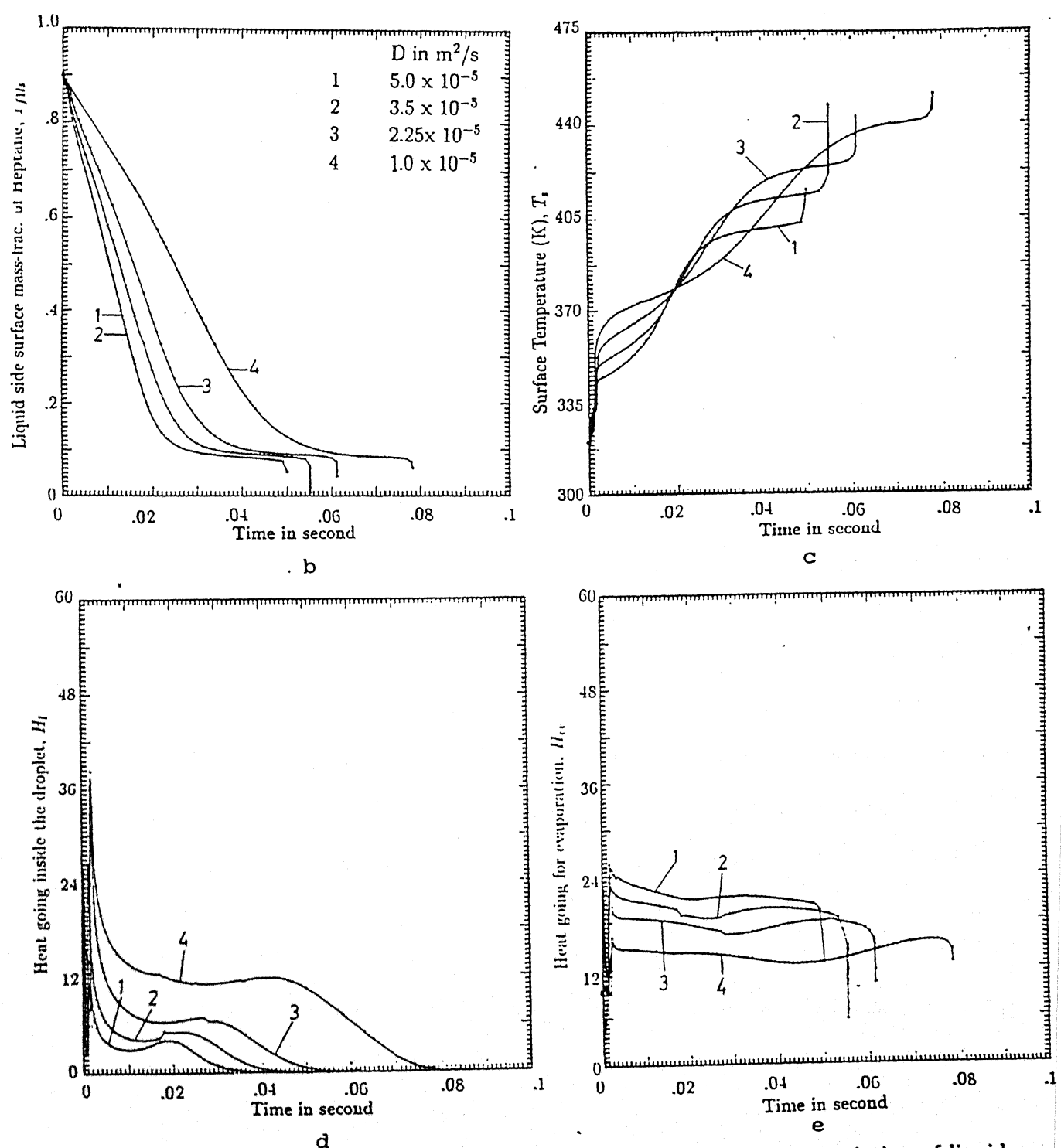


Fig. 5.23 Effect of gas phase mass diffusion coefficient on the transient variation of liquid phase surface mass-fractions of heptane, surface temperature, droplet heating, heat available for evaporation and square of the diameter.

fraction of the two fuels, the surface temperature (Fig. 5.23c) rises with lesser steepness. For the lower value of the gas phase diffusion coefficient, more heat is available for droplet heating (Fig. 5.23d), and therefore less heat is available for the fuel evaporation (Fig. 5.23e). Consequently, it takes longer time for combustion due to lower evaporation rate constant (5.23a).

5.12 Liquid Side Diffusion Coefficient

Figures 5.24 through 5.26 show the effect of liquid side diffusional resistance on the overall gasification behaviour for heptane-hexadecane fuel with 0.7-0.3 initial mass-fraction combination. Here the curves are plotted for different liquid side diffusion coefficients having values 5.0×10^{-10} , 5.0×10^{-09} , 5.0×10^{-08} and $5.0 \times 10^{-06} \text{ m}^2/\text{s}$. When the diffusional resistance is low, the first $d^2 - law$ period (controlled by the burning of the more volatile fuel) exists for a longer period due to it's supply from the interior of the droplet (Fig. 5.24a). But as the diffusional resistance becomes higher, the length of the first $d^2 - law$ period decreases because the mass-fraction of the more volatile fuel decreases at the surface due to it's insufficient supply from the droplet core. Therefore, for this case, the second $d^2 - law$ period exists for major part of the burning. Here, one interesting point to be noted is that for the case when the liquid side diffusion coefficient is very high (greater than $5.0 \times 10^{-6} \text{ m}^2/\text{s}$), as shown for curve 4 of the Figs. 5.24 through 5.25, there exists two distinct batch-distillation mode of burning regimes corresponding to the two different fuels. These two regimes are separated by one extremely narrow zone when very high rate of droplet heating takes place (Fig. 5.24d and 5.25a). This is also very distinctly observed in all the Figs. 5.24 through 5.25 for curve 4. Due to the very high value of liquid side diffusion coefficient the more volatile fuel (heptane) is constantly supplied to the surface as evident from Fig. 5.24b. So long as it is available inside the droplet interior (Fig. 5.26). Therefore, batch-distillation mode of burning for heptane occurs during this first $d^2 - law$ period. This is also very clearly shown in Fig. 5.24c where the fractional mass

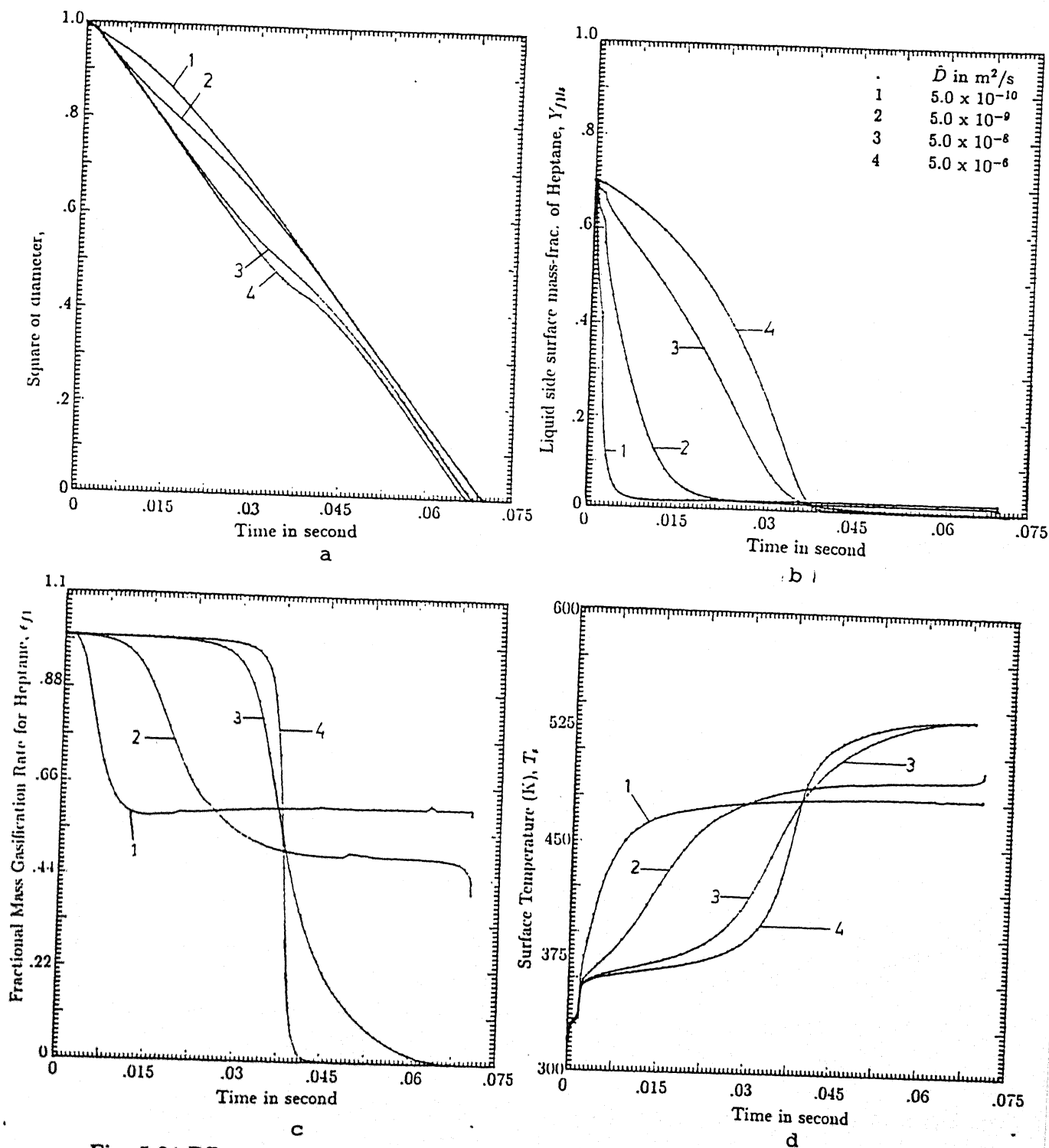


Fig. 5.24 Effect of liquid side mass diffusion coefficient on the transient variation of square of the diameter, liquid phase surface mass-fractions of heptane, fractional mass gasification rate of heptane, surface temperature.

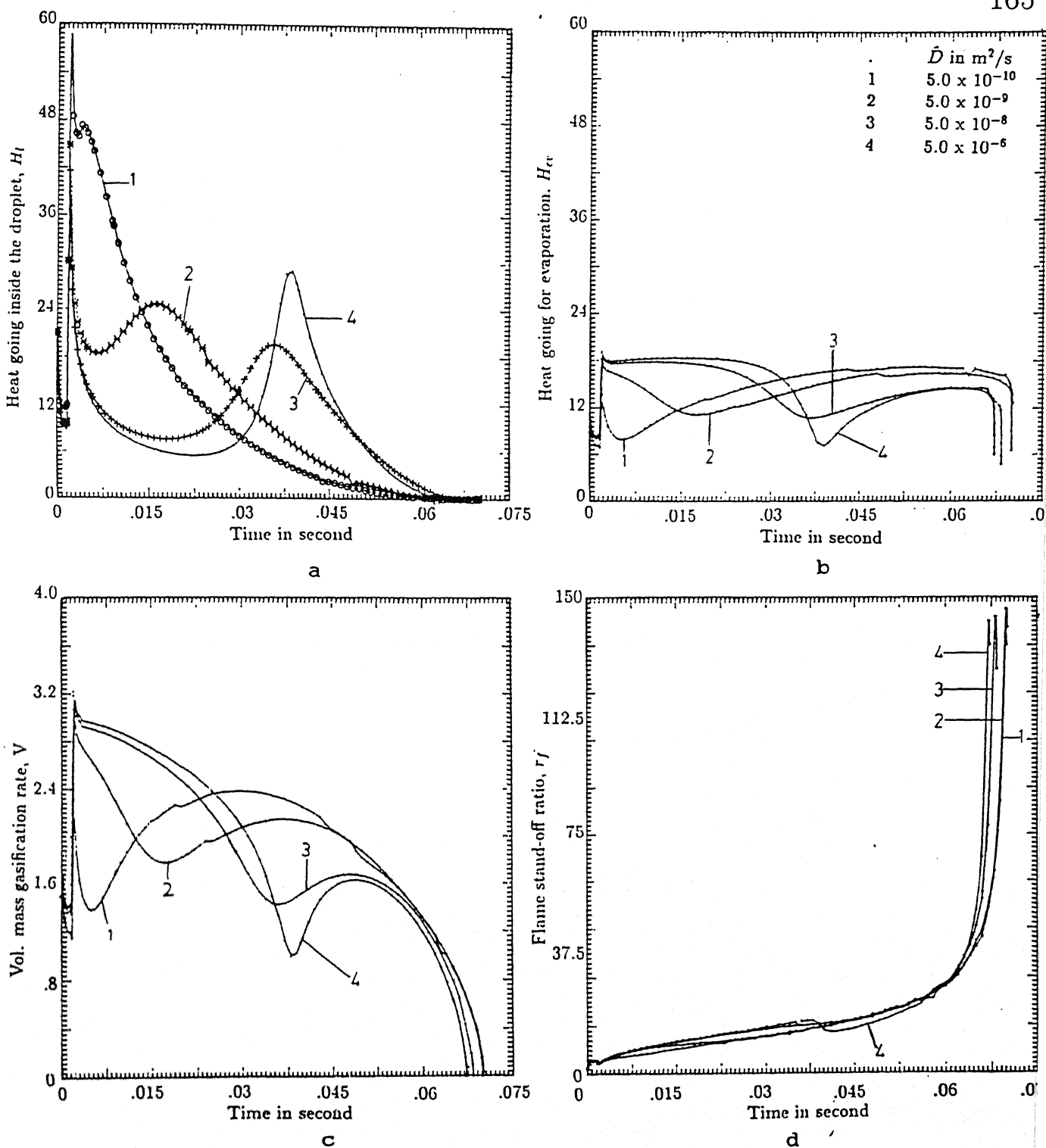


Fig. 5.25 Effect of liquid side mass diffusion coefficient on the transient variation of droplet heating, heat available for evaporation, vol. mass gasification rate, flame position, and flame stand-off-ratio.

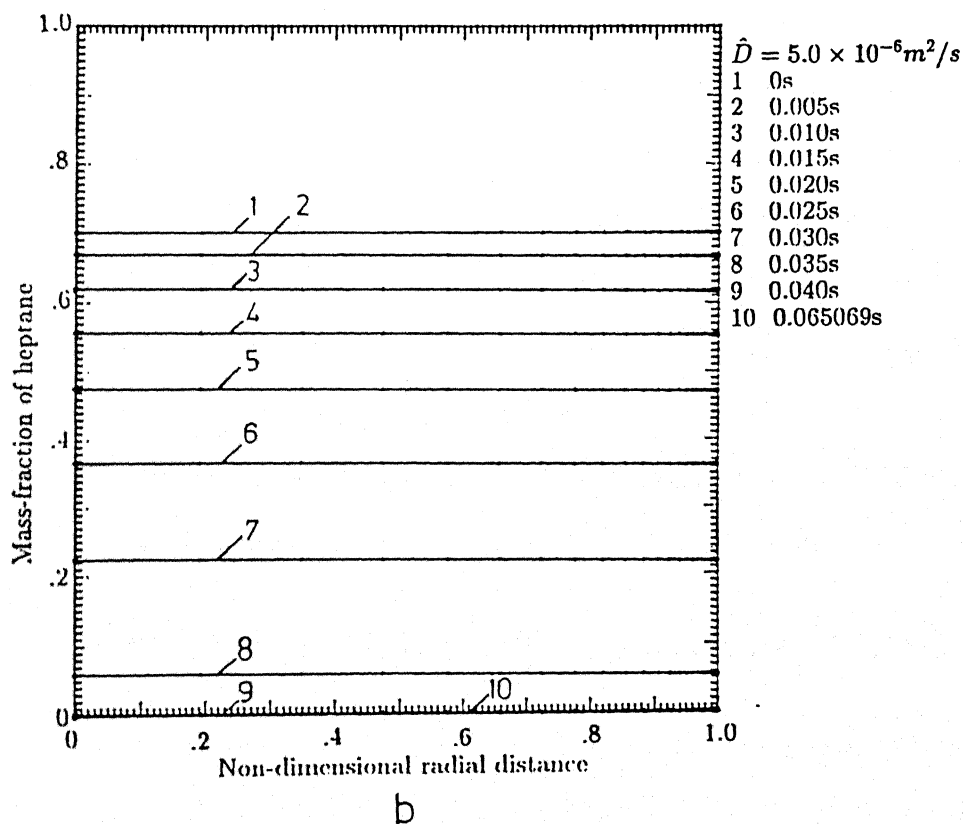
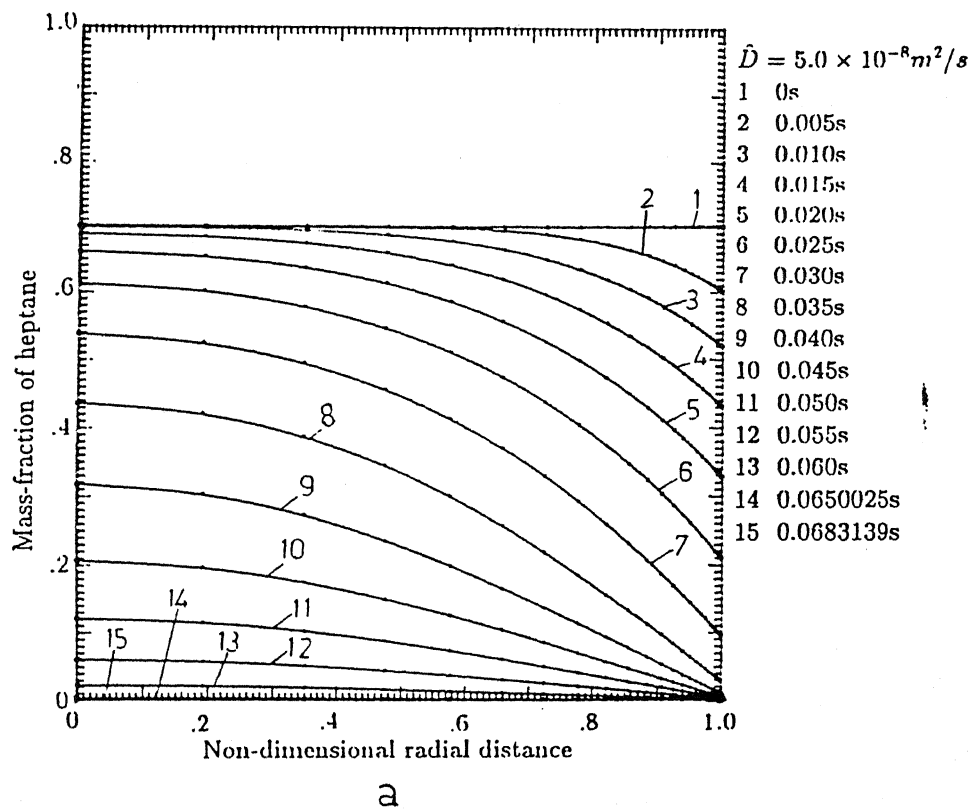


Fig. 5.26 Time history of liquid side mass-fraction profiles for heptane

gassification rate of heptane is almost 1. During this period, surface temperature remains near the boiling point of heptane. Then when the droplet interior is almost completely devoid of heptane fuel (This takes place at around $t=0.06$ s for $\hat{D} = 5.0 \times 10^{-8} m^2/s$ (curve 3 for Figs. 5.24 and 5.25) and at around $t=0.035$ s for $\hat{D} = 5.0 \times 10^{-6} m^2/s$ (curve 4 for Figs. 5.24 and 5.25)), the liquid side surface mass-fraction of heptane falls very sharply (see also Fig. 5.26) and becomes almost zero. Therefore, the surface temperature, being controlled by the surface fuel mass fraction combination, rises very steeply and reaches very near to the boiling point of hexadecane (560 K) in a very short time (Fig. 5.24d). This results in vigorous droplet heating (Fig. 5.25a) and consequently, heat available for evaporation falls steeply (Fig. 5.25b) during this short time span. Therefore, volumetric mass gasification rate also falls very steeply (Fig. 5.25c) for which sudden shrinkage of flame takes (prominent for $\hat{D} = 5.0 \times 10^{-6} m^2/s$, curve 4) place as indicated in Fig. 5.25d. This is indicated by the sudden lowering in slope of curve 4 in Fig. 5.24a. It is to noted that if thermal expansion of the liquid fuel were taken into account, then this change in slope for those two curves of Fig. 5.24a would be even sharper. After this transition, second $d^2 - law$ period corresponding to the second batch-distillation mode of hexadecane burning takes place (Fig. 5.24a) and it continues till the end of burning. The domination of hexadecane is clearly visible in Fig. 5.24c where the fractional mass-gasification rate of heptane is shown to be practically zero during this period. From this parametric study, one can see that for a very high value of liquid side mass-diffusion co-efficient, two batch distillation modes of burning can exist for a multicomponent fuel.

5.13 Comparison with the Semi Analytical Model

Figure 5.27 shows a comparison of the present numerical model with the semi-analytical model of chapter 3. The results are shown for heptane-undecane with 0.5-0.5 initial mass-fraction combination. Curve 1 represents the full numerical model where transient feature of the gas phase as well as the effect of surface regression are retained. Curve 2 represents

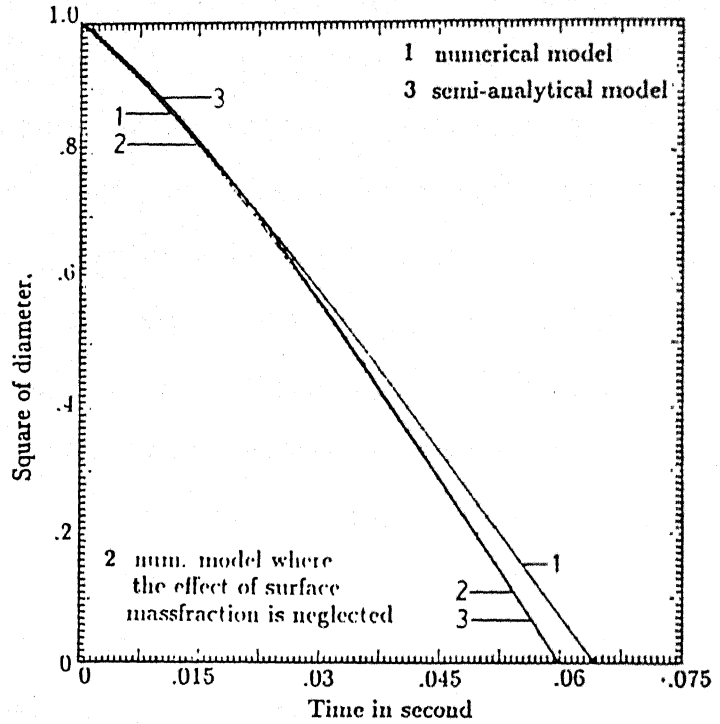


Fig. 5.27 Comparison of the semi-analytical model with two cases of the numerical model where for one case, the effect of surface regression is neglected and for the other case, the effect of surface regression is considered.

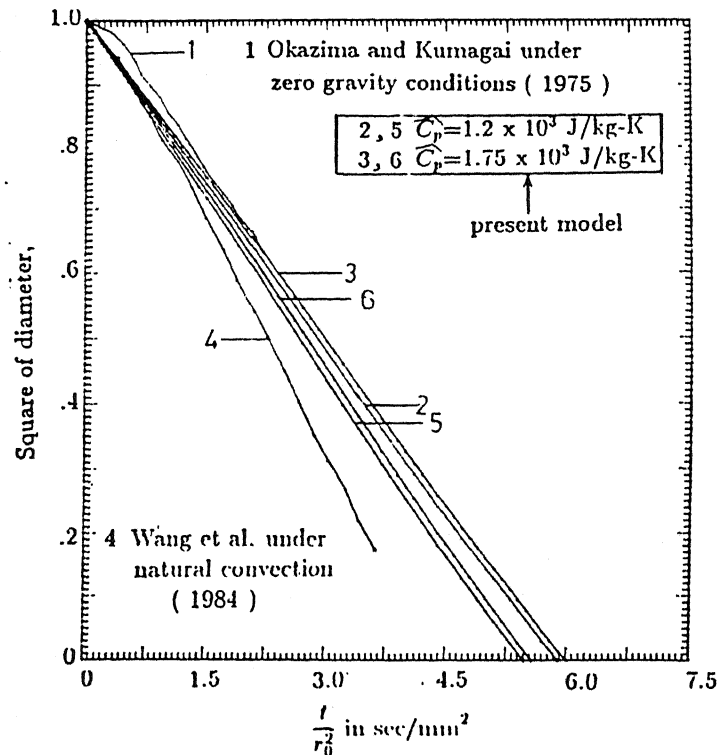


Fig. 5.28 Comparison of the present model with the experimental results of Okazima

the numerical model where the effect of surface regression is neglected. Curve 3 represents the semi-analytical model where the effect of surface regression is neglected and also, the gas phase is assumed to be quasi-steady. Curves 1 and 2 match perfectly in the initial stage of burning, but deviate during the later part. This happens because, initially, the effect of regression of droplet diameter is small and can be neglected. But, later on, the droplet diameter regression rate becomes quite high and therefore, it can not be neglected. The curve 3 deviates from curves 1 and 2 in the initial stage because, the semi-analytical model doesnot include the transient feature of the gas phase. Later on, it deviates more from curve 1 but, matches with curve 2 because the latter (i.e. curve 2) neglects the effect of surface regression rate. Therefore, the transient feature of the gas phase is prominent in the initial stage of droplet burning and consequently, the assumption of gas phase quasi-steadiness can well be applied for the later part of the burning.

5.14 Comparison with Earlier Work

Different values of evaporation rate constants for heptane burning at room temperature are available in literature (Aldred and Williams, 1966; Graves, 1952; Smith and Graves, 1957; Monaghan et al.,1968; Goldsmith, 1956). They are reported to vary from $0.8428 \text{ mm}^2/\text{s}$ to $1.0 \text{ mm}^2/\text{s}$ according to Fig. 10 of Williams (1973). Kumagai and Isoda (1957), in their experimental results, reported the value of the evaporation rate constant to be $0.49 \text{ mm}^2/\text{s}$ for zero gravity case for suspended droplet burning. Theoretical value of this constant calculated by Goldsmith and Penner (1954) was reported to be $0.86 \text{ mm}^2/\text{s}$ for steady state combustion. Kumagai and coworkers (1956, 1971) found the evaporation rate constants (for a 1 mm initial diameter) as $0.75 \text{ mm}^2/\text{s}$ for a suspended droplet and $0.79 \text{ mm}^2/\text{s}$ for a free droplet of heptane. Figure 5.28 shows comparison of the present numerical model with the experimental results of Okazima and Kumagai (1975) and Wang et al. (1984) under two different conditions for heptane burning. Okazima and Kumagai (1975) presented results (curve 1 of Fig. 5.28) for spherical combustion under zero gravity

condition in normal ambient conditions. According to Okazima and Kumagai (1975), evaporation rate constant is $0.78 \text{ mm}^2/\text{s}$. The present model predicts the evaporation rate constant to be $0.70175 \text{ mm}^2/\text{s}$ (see curve 2) and $0.6837 \text{ mm}^2/\text{s}$ (see curve 3) when liquid side specific heats are 1.2×10^3 and $1.75 \times 10^3 \text{ J/kg-K}$ respectively. It is seen that the liquid side specific heat generally varies from 1.2 to 2.0 J/gm-K (Reid et al., 1988) The variations are 9.1 % and 12.3 % respectively. The initial droplet diameter for Okazima and Kumagai was 1.327 mm whereas, for the present problem, the initial diameter is 0.2 mm.

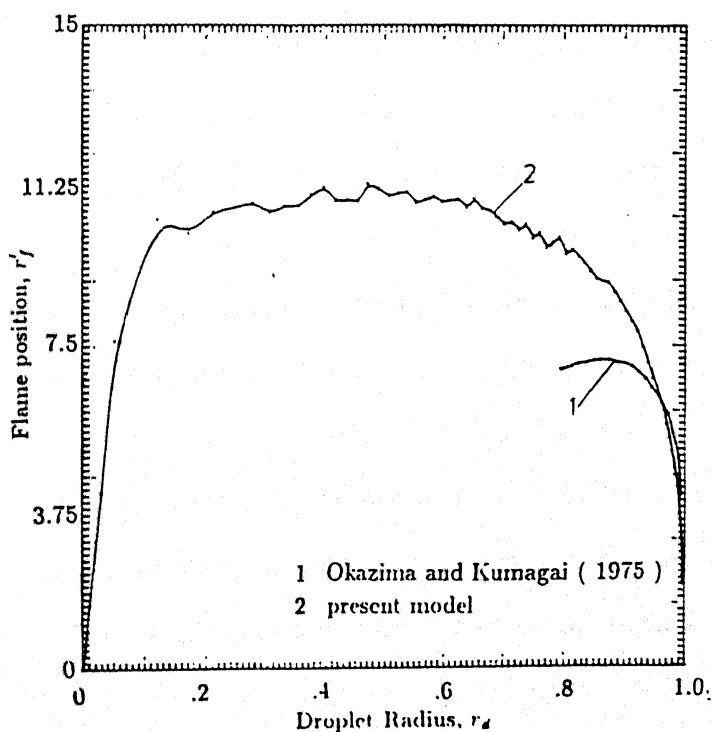
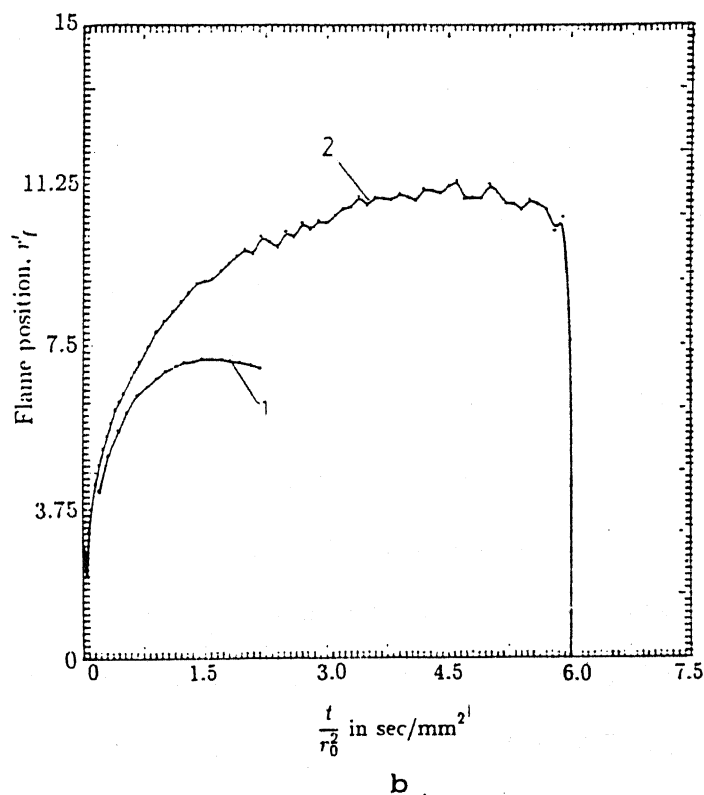
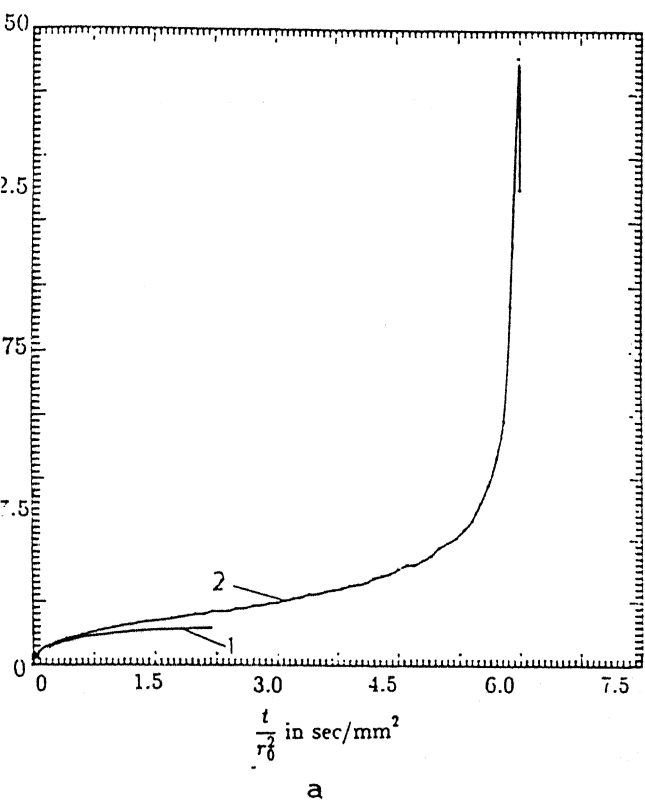
Experimental results of Wang et al. (1984) are shown as curve 4 for heptane droplet moving at a low Reynolds number (< 1) where the ambient temperature is as high as 1200 K. Curves 5 and 6 show the result obtained from the present model for 1200 K ambient temperature. The experimental curve 4 predicts the evaporation rate constant to be $0.9836 \text{ mm}^2/\text{s}$, whereas the present model estimates it to be $0.7565 \text{ mm}^2/\text{s}$ (curve 5) and $0.73059 \text{ mm}^2/\text{s}$ (curve 6) for 1.2×10^3 and $1.75 \times 10^3 \text{ J/kg/K}$ liquid side specific heat respectively. The variations are 23 % and 25.7 % respectively. It is seen that the curves 4, 5 and 6 show good agreement in the initial stage of the burning, but deviate later. Experiments of Wang et al. (1984) show that the droplet velocity was small in the initial stage and gradually increased towards the the end of the experiment under natural convection condition. Therefore, curves 3 and 4 show better agreement in the initial stage of burning. Okajima and Kumagai (1975) reported that the evaporation rate constant increases as the external flow (due to forced convection) was increased and this increase was 10 % at $U_\infty = 2 \text{ cm/s}$ when the ambient temperature was around 300 K and then remained almost constant. Their initial droplet diameter was $1.4 \pm 0.2 \text{ mm}$. Kumagai and Isoda (1957) in their suspended drop experiment reported that the evaporation rate constant varied from $0.49 \text{ mm}^2/\text{s}$ to $1.02 \text{ mm}^2/\text{s}$ for zero gravity and full gravity conditions respectively. Thus, they indicated the effect of natural convection to be quite significant for the evaporation rate constant. The droplet velocity reported in the experiment of Wang et al. (1984) under natural convection condition, was 90 cm/s on an average and they used droplet

diameter in the range 25 to 35 μm . Therefore, the deviation of curves 5 and 6 from curve 4 in the later part of the burning could be attributed to the external flow as well as greater initial droplet diameter.

Apart from the above mentioned reasons, other property variations specially in the gas phase (where the temperature varies over a wide range) and neglecting radiative heat-transfer can also be attributed to the cause for the overall deviation of curves 2 and 3 from curve 1, and also of curves 5 and 6 from curve 4. In addition, the reaction kinetics involved at the flame region is extremely complex. While modelling, these different complex situations are simplified to a great extent. Also, it is extremely difficult to estimate the accurate property values. As shown earlier, the dependence of burning characteristics on property values is sensitive. Keeping all these assumptions in account, curves 2 and 3 show a reasonably good agreement with the experimental curve 1.

Fig. 5.29a shows the comparison of the flame stand-off ratio (ratio of flame radius to the droplet radius) vs. t/r_0^2 curve for two cases. Curve 1 shows the experimental results of Okazima and Kumagai (1975) and curve 2 represents the present model. They agree very well upto 0.75 s/mm² and then deviate from each other. Similar agreement is also observed for Figs. 5.29b,c,d. For the above two cases, Fig. 5.29b shows the comparison for the variation of normalised flame radius (flame radius divided by the initial droplet radius) vs. t/r_0^2 and Fig. 5.29c shows the comparison for the normalised flame radius versus normalised droplet radius. Fig. 5.29a show the flame movement in relation to the movement of the droplet radius and Fig. 5.29b show the flame movement with respect to the droplet center. In Fig. 5.29c, curve 1 shows the experimental results of Okazima and Kumagai (1975) and curve 2 is plotted for the present model. This figure shows that the flame radius is proportional to droplet radius, only towards the end of droplet burning when extinction occurs. Therefore, the steady state burning reported by Goldsmith and Penner (1954) is not supported here.

Figure 5.30a shows a comparison of the present model with the experimental results

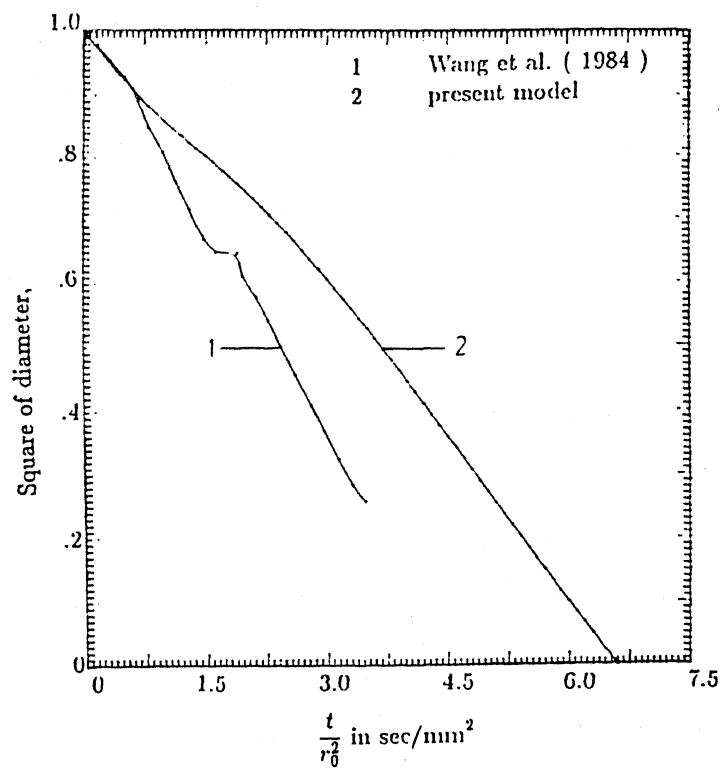


c

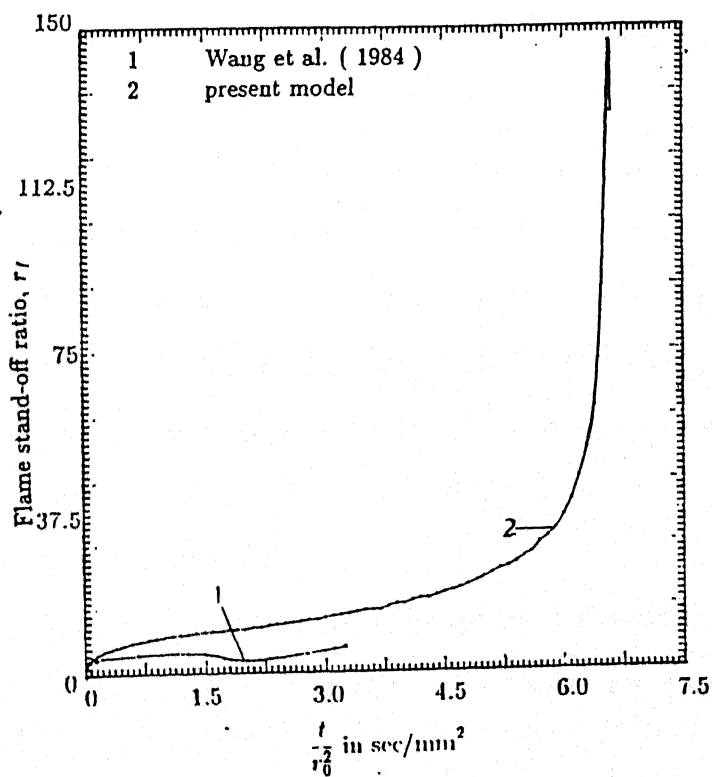
Fig. 5.29 Comparison with the experimental work of Okazima and Kumagai (1975) for heptane burning under zero gravity conditions.

of by Wang et al. (1984) for the burning of multicomponent (mixture of heptane and hexadecane with an initial mass-fraction combination of 0.7-0.3) fuel droplet. The result shows an excellent agreement in the initial part of the droplet burning. But the two results deviate as burning proceeds in time. The present numerical model predicts the evaporation constant to be $0.65 \text{ mm}^2/\text{s}$ for the first $d^2 - \text{law}$ period and $0.7 \text{ mm}^2/\text{s}$ for the second $d^2 - \text{law}$ period (curve 2). Whereas the experimental results (curve 1) predict the evaporation rate constant to be $1.022 \text{ mm}^2/\text{s}$ for the first $d^2 - \text{law}$ period, and $0.971 \text{ mm}^2/\text{s}$ for the second $d^2 - \text{law}$ period. For the curve 2, $C_p = 1.75 \times 10^3 \text{ J/kg-K}$, $\hat{\lambda} = 0.1 \text{ W/m-K}$ and $\hat{D} = 5.0 \times 10^{-9} \text{ m}^2/\text{s}$ were used. Curve 2 shifts towards curve 1 when the liquid side specific heat is decreased. One of the causes attributed to the variation in the total burning time can be the natural convection (average droplet velocity = 90 cm/s) present in case of Wang et al. (1984) and this effect of natural convection is not considered in the present model. As already discussed, according to Kumagai and Isoda (1957), this effect of natural convection on evaporation rate constant is very strong. For the experimental results, the droplet burns out much faster owing to larger value of the evaporation rate constants. The experimental result shows that the droplet diameter does not change in between 0.053714s and 0.059428s and remains at 0.29179mm . Wang et al. (1984) have claimed that this sharp change when burning shifts from the first $d^2 - \text{law}$ period to the second is caused mainly due to lowering of fuel evaporation rate as well as the thermal expansion of the liquid droplet which becomes prominent due to the intermediate stage of vigorous droplet heating during transition. Thus, their experiment showed three periods, the two periods correspond to the preferential gasification of the two fuels and the third period corresponds to the short intermediate transition in between as mentioned above. The present model also exhibits three dominant zones, two $d^2 - \text{law}$ periods separated by one transition zone. But, this transition from one $d^2 - \text{law}$ period to the next is gradual and takes place over a longer period of time for the present model.

After the initial transient is over, the temperature at the droplet surface will tend



a



b

Fig. 5.30 Comparison with the experimental results of Wang et al. (1984) for heptane-hexadecane fuel burning with 0.7-0.3 initial mass-fraction combination.

to approach closely the equilibrium boiling temperature of the mixture at the droplet surface. The boiling point of the mixture, in turn, depends upon the relative strength of the constituents at the surface. Now, since the liquid side mass diffusional resistance is high and initially, the surface regression is low, the liquid side mass fraction of the more volatile fuel falls sharply. Consequently, the gas side surface mass-fraction of the more volatile fuel also starts falling quite early in the droplet lifetime. But because of the continuity of the burning process and also due to the fact that as the burning proceeds, more amount of the more volatile fuel is supplied to the surface as a result of droplet radius regression, the change in the relative strength of the constituent fuels at the droplet surface takes place gradually. Therefore, the boiling point at the droplet surface, being dependent on the relative strength of the constituent fuels, also starts rising gradually. So, the droplet heating becomes gradual during this transition. It may be possible that the thermal expansion of the liquid droplet is quite high during the transition period and since the present model does not take into account the effect of thermal expansion, this may be responsible for the deviation in the predictions of the present model from the experimental observations of Wang et al. (1984).

However, it is worth mentioning here that this sudden droplet heating is very prominent for the case where, two distinct batch-distillation mode of burning take place. This is possible when the internal transport within the droplet is very high. This may be possible for the case when the external velocity is quite high (i.e. for high Reynold's number flow) which may give rise to a very high value of internal circulation (Law, 1976). Prakash and Sirignano (1978) have shown that spatial uniformity is not achievable even with an infinite circulation rate inside the droplet.

It is seen from Fig. 5.7a that when the volatility differential is sufficiently large (e.g. for heptane-dodecane mixture), sudden droplet heating during transition is observed for two cases:

(i) when the initial mass fraction of the low volatility fuel is very low (e.g. 0.01 as shown in Fig. 5.7a), the sudden droplet heating during transition occurs near the end of the burning, and it's intensity being less, the rise in surface temperature is much below the boiling point of the less volatile fuel and it's liquid side mass fraction remains much below 1.0 (Fig. 5.8a) and

(ii) when it's initial mass fraction is very high (e.g. 0.9), the sudden droplet heating during transition takes place at the very beginning of burning and subsequently, it's intensity being quite high, the surface temperature rises up pretty close to the boiling point of the low volatile fuel. For such a case, it's liquid side surface mass fraction reaches a value very close to 1.0 (Fig. 5.8a).

But for an intermediate value e.g. for the case of 0.1 initial mass fraction of the low volatile fuel which reveals multicomponent burning feature more distinctly, the droplet heating takes place over a longer period of time and the temperature rise lies in between the above mentioned two cases. Shaw and Williams (1990) also reported the sudden droplet heating to be present in their analysis for an n-decane droplet undergoing combustion with an initial low volatile impurity mass fraction of 0.1 or 0.02, but, the variation in temperature rise for different initial mass fraction combinations is not exhibited by the model of Shaw and Williams (1990). They showed that for both cases, the liquid side surface mass fraction of the low volatility fuel reaches almost unity after certain time. This means that their model does not take into account the effect of fuel supply from droplet interior to the surface. Fig. 5.8a shows that the highest liquid side mass fraction reached by the low volatility fuel varies depending on it's initial mass fraction and it remains around 0.82 and never reaches unity for the 0.1 initial mass fraction case. This happens because of the high droplet radius regression in the later part of droplet burning for which the more volatile fuel is constantly supplied to the droplet surface. Fig. 5.13a and 5.13b supports the above reasoning because Fig. 5.13a shows that when the effect of surface regression is

neglected, the liquid side surface mass fraction of the low volatile fuel reaches almost unity and correspondingly, the surface temperature (Fig. 5.14a) reaches the boiling point of the low volatile fuel earlier or later, depending on its initial mass fraction.

5.15 Conclusions

In the second part of the thesis, a full numerical model has been developed for the case of a transient multicomponent single droplet burning in an otherwise quiescent atmosphere. An adaptive grid generation technique has been used based on the equidistribution of a positive weight function such that the local discretization error is minimised. This adaptive grid generation technique helps to record accurately the flame structure as well as the position and movement of the flame. This study gives a critical analysis of how a diffusion flame around the liquid droplet evolves during the ignition period and then how it moves away from the droplet, and finally, how it is extinguished. The study reveals that the flame zone is initially established very near the droplet surface and then as the chemical reaction gathers momentum, the flame temperature rises very fast and almost instantly reaches its peak temperature. Almost simultaneously, the flame expands towards the droplet surface in search of fuel vapour for sustaining the enhanced chemical reaction at the flame. As the flame moves and expands towards the droplet surface, the temperature gradient at the surface becomes very high as a result of which the droplet surface is heated up very fast and the surface temperature approaches the boiling point of the more volatile fuel. So, the fuel starts evaporating vigorously. For this high evaporation rate, the flame starts moving away from the droplet surface due to fuel vapour accumulation. But as the burning proceeds, the droplet volume becomes progressively lesser for which the overall mass-gasification rate falls gradually. Therefore, fuel vapour accumulation between the droplet surface and the flame becomes progressively lesser. At about mid way of burning, the fuel evaporation rate at the surface almost equals the consumption rate at the flame and the flame becomes almost steady at one place. It is observed that the flame remains steady, maintaining a

fixed distance from the droplet center till the end of droplet burning. The flame exists till the droplet becomes very small. The total burning time for a heptane-hexadecane droplet for 0.9-0.1 initial mass fraction combination is about 65.625 milli seconds. Ignition becomes complete within 3 milli seconds and extinction takes about 31.9 μs . Present model identifies six distinct periods for the entire burning process. They are pre-ignition, ignition, first $d^2 - law$ period, transition, second $d^2 - law$ period and extinction. Results show that the pre-ignition period, ignition period, first $d^2 - law$ period, 2nd transient (transition), second $d^2 - law$ period and extinction covers approximately 2.28 %, 2.28 %, 35.6 %, 19.5 %, 40 % and 0.36 % respectively of the total burning time. These six zones or periods depend on three aspects: volatility differential of the species, their initial mass fraction combination and the prevailing ambient conditions. Liquid side surface mass fractions of the species are observed to be the direct causes that control the two $d^2 - law$ periods and their transition in between. From the results, it is seen that it is very difficult to point out one single parameter or the root cause which controls the distinct features of the 2 $d^2 - law$ periods during multicomponent fuel droplet combustion. Though apparantly, the liquid side mass fraction combination of the fuels seems to be the controlling factor. It is seen from the present study that during extinction, the droplet radius regresses very fast. As a result of this, the transformed non-dimentional coordinate system also shrinks very sharply. On the other hand, the flame position remains quite steady. Due to the shrinking coordinate system, the far stream boundary conditions comes very close to the flame, which does not happen in practical situations. Thus, error can creep in while studying the extinction phenomenon.

The study reveals that the multicomponent feature of burning is predominant when the volatility differential of the two components is high, and also, when the initial liquid side mass fraction of the more volatile fuel is high (around 0.9). Therefore, volatility differential and initial mass fraction combination are the two key parameters for studying multicomponent fuel droplet combustion. For the present study, liquid side Peclet number

is found to be around 150 which is very high. Therefore, the assumption of diffusion limit model is justified. This study brings out the two $d^2 - law$ periods quite explicitly. The second $d^2 - law$ period is identified with the 'quasi-steady' mode of burning during which the droplet composition and temperature remain almost constant. It is also seen that this period covers almost 95 % of the total burning time for heptane-dodecane burning with 0.1-0.9 initial mass fraction combination. This value decreases to about 27 % for the 0.9-0.1 combination case. This value increases when the boiling point difference of the two species is more and vice-versa. Results show that the flame is not thick. Comparison of the three analytical models (see Figs. 5.13 through 5.15) show that the surface regression rate is neither too high nor too low. Therefore, one can neither neglect the effect of surface regression, nor can we assume the quasi steady mode of burning to be valid from the very beginning. Droplet radius regression can be neglected only in the initial part of the droplet burning. But, later on, as the radius regression rate gathers momentum, the quasi steady mode of burning becomes more and more established. Gas phase dissociation, variable gas phase specific heat consideration and fuel vapour accumulation are important considerations and they should not be neglected. Through parametric study of important parameters such as \hat{D} , D , \hat{C}_p , C_p and ambient temperature, it is found that the total burning time as well as other burning characteristics are very much sensitive to the property values being used. Comparing with the quasi-steady model of chapter 3, it is observed that the quasi-steady assumption of the gas phase is quite reasonable barring the initial transient and the final extinction. But the effect of surface regression can not be neglected. The present result shows very good agreement with the experimental results of Okazima and Kumagai (1975) for hepane fuel burning under zero gravity condition with normal ambient conditions. When the present model is compared with the experimental results of Wang et al. (1984) for the burning of heptane-hexadecane fuel with 0.7-0.3 initial liquid side mass fraction combination, the comparison is quite satisfactory considering the fact that the present model deals with spherically symmetric combustion whereas, Wang et al.

(1984) performed their experiment on freely falling droplets under natural convection conditions. Their experiment showed three periods, the two periods correspond to the preferential gasification of the two fuels and the third period corresponds to the short intermediate transition in between during which vigorous droplet heating takes place. The present model also exhibits three dominant zones, two $d^2 - law$ periods separated by one transition zone. But, this transition in case of Wang et al. (1984) is reported to be very sudden as against a gradual change or transition exhibited by the present model. The present model does not include the effect of thermal expansion for the liquid phase which may cause this deviation.

5.16 Contributions to Knowledge

i. The entire burning period is identified with six distinct zones.

ii. Duration and nature of the $d^2 - law$ periods (hence, the burning rate constants) and the transition in between are observed to be directly dependent upon the gas side mass fraction of the fuels and indirectly dependent upon the initial mass fraction as well as the volatility differential of the fuels.

iii. Transition from one $d^2 - law$ period to the other is seen to be gradual. It becomes sharper when \hat{D} high and also when the effect of surface regression is neglected.

iv. Quasi steady mode of burning (when the droplet composition hardly changes) is found to correspond to the second $d^2 - law$ period .

v. Flame initially move towards the droplet surface, then it moves away from the surface and finally, at the end, it comes back and vanishes into the droplet surface.

vi. Variable specific heat and gas phase dissociation lowers the flame temperature considerably.

5.17 Recommendations for Further Study

1. Variable property model should be incorporated to get more realistic results.

2. The present spherically symmetric model can be relaxed to include the effect of flow around the droplet. This can be done in two ways:

(i) The full Navier-Stoke's equations can be used for solving both the liquid and the gas phase flow situations. This will give us the complete picture regarding the the importance of both batch distillation limit and diffusion limit models.

(ii) A known low Reynolds number flow solution for the gas phase can be first assumed and then the present model can be extended to include the effect of internal circulation through spherical vortex model and see how this affects the droplet burning.

This will give us a clear picture regarding the relative importance of batch distillation and diffusion limit models.

3. The present adaptive grid generation technique automatically generates the grid spacing, but can not choose the time interval for the numerical solution on it's own. Error due to improper choice of the time interval selection can be included as an additional part of the adaptive grid generation process.

4. radiation loss is important and it can be included to get more realistic results.

5. micro-explosions can be looked into.

6. The effect of the shrinking coordinate on the study towards the end of droplet burning is quite significant and it demands special attention. This can be looked into for more accurate analysis.

7. Effect of convective terms arising in both the liquid and the gas phases on different parameters can be looked into in more details.

References

- Agafanova, F.A., Gurevich, M.A. and Paleev, I.I., 1958, "Theory of Burning of a Liquid Fuel Drop", *Soviet Physics - Thechnical Physics* , 2, p. 1689.
- Annamalai, K., Kuppu Rao, V. and Sreenath, A.V., 1971, *Combustion and Flame* , 16, p. 287.
- Annamalai, K., Ramalingam, S.C., 1987, "Group Combustion of Char/Carbon Particles", *Combustion and Flame* , 70, pp.307-332.
- Ayyaswamy, P.S., Sadhal, S.S. and Huang, L.J., 1990, "Effects of Internal Circulation on the Transport to a Moving Drop", *International Communications in Heat and Mass Transfer* , 17, pp. 689-702.
- Bilger, R.W., 1976, *Progress in Energy and Combustion Science* , 1, pp. 87-109.
- Bolstad, J.H., 1982, "An Adaptive Finite Difference Method for Hyperbolic Systems in one Space Dimension", Ph.D. Thesis, Standford University, CA.
- Brzustowski, T.A. and Natarajan, R., 1965, *Canadian Journal of Chemical Engineering* , 43, p. 10.
- Brzustowski, T.A. and Natarajan, R., 1966, "Combustion of Aniline Droplets at High Pressures", *Canadian Journal of Chemical Engineering* , 44, 194-201.
- Brzustowski, T.A., Twardus, E.M., Wojcicki, S. and Sobeisiak, A., 1979, "Interaction of Two Burning Fuel Droplets of Arbitrary Size", *AIAA Journal* , 17, 1234-1242.
- Burgoyne, J.H. and Cohen, L., 1954, *Proc. R. Soc. Lond.* , A 225, pp. 375-392.
- Burke, S.P. and Schuman, T.E.W., 1965, *First Symposium (International) on Combustion* , 1928, pp. 2-11. Combustion Institute.
- Chen, S.J. and Tong, A.Y., 1988, "Application of Elliptic Grid Generation Technique to the Solution of Hydrodynamics and Heat Transfer of Droplet Arrays of Intermediate Reynolds Numbers", *International Journal of Heat and Mass Transfer* , 31, pp. 1063-1072.
- Chervinsky, A., 1969, "Supercritical Burning of Liquid Droplets in Stagnant Environment", *AIAA Journal*, 7, pp. 1815-1817.

- Chervinsky, A., 1969a, *Israel J. of Tech.*, 7, p. 35.
- Chigier, N.A., 1976, "The Atomization and Burning of Liquid Fuel Sprays", *Progress in Energy and Combustion Science*, 2, pp. 97-114.
- Chigier, N.A., 1981, "Energy Combustion and Environment", McGraw Hill, New York.
- Chiu, H.H. and Liu, T.M., 1977, "Group Combustion of Liquid Droplets", *Combustion Science and Technology*, 17, pp. 127-142.
- Chiu, H.H., Kim, H.Y. and Croke, E.J., 1983, "Internal Group Combustion of Liquid Droplets" *Nineteenth Symposium (International) on Combustion*, Combustion Institute, pp. 971-980.
- Chung, S.H. and Law, C.K., 1984, "Importance of Dissociation Equilibrium and Variable Transport Properties on Estimation of Flame Temperature and Droplet Burning Rate", *Combustion and Flame*, 55, pp. 225-235.
- Crespo, A. and Linan, A., 1975, "Unsteady Effects in Droplet Evaporation and Combustion", *Combustion Science and Technology*, 11, pp. 9-18.
- Curtis, A.R., Powell, M.J. and Reid, J.K., 1974, "On the Estimation of Sparse Jacobian Matrices", *J. Inst. Math. Appl.* 13, pp. 117-119.
- Davis, S.F. and Flaherty, J.E., 1982, "An Adaptive Finite Element Method for Initial Boundary Value Problem for Partial Differential Equations", *SIAM J. SCI. STAT. COMPUT.*, 3, pp. 6-27.
- Deuflhard, P., 1974, "A Modified Newton Method for the Solution of Ill-Conditioned Systems of Nonlinear Equations with Application to Multiple shooting", *Numer. Math.*, 22, pp. 289-315.
- Dryer, F.L., "Water Addition to Practical Combustion Systems - Concepts and Applications", *Sixteenth Symposium (International) on Combustion*, Combustion Institute, Pa., pp. 279-295.
- Dwyer, H.A., Kee, R.J. and Sanders, B.R., 1980, "Adaptive Grid Methods in Fluid Mechanics and Heat Transfer", *AIAA J.*, 18, pp. 1205-1212.

- Dwyer, H.A., 1989, "Calculations of Droplet Dynamics in High Temperature Environment", *Progress in Energy and Combustion Science* , 15, pp. 131-158.
- Dwyer, H.A. and Sanders, B.R., 1984, "A Detailed Computation of unsteady Droplet Dynamics", *Twentieth Symposium (International) on Combustion* , Combustion Institute, pp. 1743-1749.
- Dwyer, H.A. and Sanders, B.R., 1986, "A Detailed Study of Burning Fuel Droplets", *Twenty First Symposium (International) on Combustion* , Combustion Institute.
- El-Kaissy, M.M. and Homsy, G.M., 1973, "A Theoretical Study of Pressure Drop and Transport in Packed Beds at Intermediate Reynolds Numbers", *Industrial and Engineering Chemistry Fundamentals*, 12, pp.82-88.
- Faeth, G.M., 1977, "Current Status of Droplet and Liquid Combustion", *Progress in Energy and Combustion Science* , 9, pp. 1-76.
- Faeth, G.M., 1987, "Mixing Transport and Combustion in Sprays", *Progress in Energy and Combustion Science* , 13, pp. 293-345.
- Faeth, G.M. and Lazar, R.S., 1971, "Bipropellant Droplet Combustion in the Vicinity of the Critical Point", *Thirteenth Symposium (International) on Combustion* , Combustion Institute, pp. 801-811.
- Faeth, G.M., 1970 *AIAA Paper A70-18141*.
- Fendell, F.E., Sprankle, M.I. and Dodson, D.S., 1966, "Thin-Flame Theory for a Fuel Droplet in Slow Viscous Flow", *Journal of Fluid Mechanics* , 26, 267-280.
- Friedman, M.H. and Churchill, S.W., 1965, *Chemical Engineering Progress Symposium Series* , Heat Transfer- Boston, American Institute of Chemical Engineering, 61, p. 1.
- Gakkhar, R.P. and Prakash, S., 1990, "Unsteady Vaporization of Fuel Droplets in a Convective Environment with Varying Ambient Conditions", *International Journal of Heat and Mass Transfer* , 33, pp. 1003-1012.
- Gelinas, R.J., Doss, S.K. and Miller, K., 1981, "The Moving Finite Element Method Application to General Partial Differential Equation with Multiple Large Gradients", *J. Comp.*

Phys. , 40, pp. 202-249.

Godsave, G. A. E., 1953, *Nature* 164, 708(1949); 171, 86(1953)

Godsave, G. A. E., 1953, "Studies of the Combustion of Drops in a Fuel Spray : The Burning of Single Drops of Fuel", *Fourth Symposium, (International) on Combustion, Combustion Institute* , Pittsburgh, 1953, pp. 818-830.

Godsave, G. A. E., 1951, "The Burning of Single Drops of Fuel", Parts 1 and 2 National Gas Turbine Establishment, Reports Nos. R66(1950), R87(1951), R88(1951).

Gogos, G. and Ayyaswamy, P.S., 1988, "A Model for the Evaporation of a Slowly Moving Droplet", *Combustion and Flame* , 74, pp. 111-129.

Gogos, G., Sadhal, S.S., Ayyaswamy, P.S. and Sundararajan, T., 1986, "Thin-Flame Theory of Combustion of a Moving Liquid Drop : Effects Due to Variable Density", *Journal of Fluid Mechanics* , 171, 121-144.

Goldsmith, M. and Penner, S.S., 1954, "On the Burning of Single Drops of Fuel in an Oxidising Atmosphere", *Jet Propulsion* , 24, pp. 245-251.

Happel, J., 1958, "Viscous Flow in a Multiparticle System : Slow Motion of Fluids Relative to Beds of Spherical Particles", *AIChE Journal* , 4, pp. 197-201.

Hardt, A.P. and Phung, P.V., 1973, "Propagation of Gasless Reactions in Solids- I. Analytical Study of Exothermic Intermetallic Reaction Rates", *Combustion and Flame* , 21, 77-89.

Haywood, R.J., Nafzigier, R. and Renksizbulut, M., 1989, "A Detailed Examination of Gas and Liquid Phase Transient Processes in Convective Droplet Evaporation", *Journal of Heat Transfer, Transactions of ASME* , 111, pp. 495-502.

Hindmarsh, A.C., 1977, "Solution of Block Tridiagonal System of Linear Equations", Lawrence Livermore Laboratory Report UCID-30150, Livermore, CA.

Hirschfelder, J.D., Curtiss, C.F. and Bird, R.B., 1954, "Molecular Theory of Gases and Liquids", John Wiley and Sons, New York.

Huang, L.J. and Ayyaswamy, P.S., 1990, "Evaporation of Moving Liquid Droplet : Solution

- for Intermediate Reynolds Number", *International Communications in Heat and Mass Transfer* , 17, pp. 27-38.
- Kassoy, D.R. and Williams, F.A., 1968a, "Effects of Chemical Kinetics on Near Equilibrium Combustion of Nonpremixed Systems", *Physics of Fluids* , 11, pp. 1343-1351.
- Kassoy, D.R. and Williams, F.A., 1968b, "Variable Property Effects on Liquid Droplet Combustion", *AIAA Journal* , 6, pp. 1961-1965.
- Kautsky, J. and Nichols, N.K., 1980, "Equidistributing Meshes with Constraints", *SIAM J. SCI. STAT. COMPUT.* , 1, pp. 499-511.
- Khalil, E.E. and Whitelaw, J.H., 1977, "Aerodynamic and Thermodynamic Characteristics of Kerosene Spray Flames", *sixteenth Symposium (International) on Combustion* , Combustion Institute, pp. 803-813.
- Kotake, S. and Okajaki, T., 1969, "Evaporation and Combustion of a Fuel Droplet", *International Journal of Heat and Mass Transfer* , 12, pp. 595-609.
- Krier, H. and Wronkiewicz, J.A., 1972, "Combustion of Single Droplets of Fuel", *Combustion and Flame* , 18, pp. 159-166.
- Kumagai, S. and Isoda, H., 1957, "New Aspects of Droplet Combustion", *Seventh Symposium (International) on Combustion* , Combustion Institute, pp. 523-531.
- Kumagai, S. and Isoda, H., 1957a, *6th Symposium (International) on Combustion* , Reinhold, New York, p. 726.
- Kumagai, S., Akai, T. and Okajima, S., 1971, "Free Fuel Droplets in a Freely Falling Chamber", *Thirteenth Symposium (International) on Combustion* , Combustion Institute, pp. 779-785.
- Kuo, K.K., 1986, *Principles of Combustion*, John Wiley & Sons, New York.
- Kuwabara, S., 1959, "The Forces Experienced by Randomly Distributed Parallel Circular Cylinders or Spheres in a Viscous Flow at a Small Reynolds Number", *Journal of Physical Society of Japan* , 14, pp. 527-532.
- Labowsky, M., 1976, "The Effect of Nearest Neighbouring Interactions on the Evaporation

Rate of Cloud Particles" *Chemical Engineering Science* , 31 : 803-813.

Labowsky, M., 1978, "A Formulation for Calculating the Evaporation Rates of Rapidly Evaporating Interacting Particles", *Combustion Science and Technology* , 18, pp. 145-151.

Labowsky, M., 1980a, "Transfer Rate Calculations for Compositionally Different Interacting Particles", *Chemical Engineering Science* , 35, pp. 1041-1048.

Labowsky, M., 1980b, "Calculation of Burning Rates of Interacting Fuel Droplets", *Combustion Science and Technology* , 22, pp. 217-226.

Labowsky, M. and Rosner, D.E., 1978, "Group Combustion of Droplets in Fuel Clouds I. Quasi-Steady Predictions", *Advances in Chemistry Series* , 166, Evaporation Combustion of Fuels, J.T. Zung, (Editor), pp. 63-79.

Landis, R.B. and Mills, A.F., 1974, "Effects of Internal Diffusional Resistance on the Vaporization of Binary Droplets", *Fifth International Conference* , Paper B7.9, Tokyo, Japan.

Lara-Urdaneja, P. and Sirignano, W.A., 1981, "Theory of Transient Multicomponent Droplet Vaporization in a Convective Field", *Eighteenth Symposium (International) on Combustion* , The Combustion Institute, Pittsburgh, pp.1365-1374.

Lasheras, J.C., Fernandez-Pello, A.C. and Dryer, F.L., 1979, "Initial Observations on the Free Droplet Combustion Characteristics of Water-in-Oil Emulsions", *Combustion Science and Technology* , 21, pp. 1-14.

Lasheras, J.C., Fernandez-Pello, A.C. and Dryer, F.L., 1980, "Experimental Observations on the Disruptive Combustion of Free Droplets of Multicomponent Fuels", *Combustion Science and Technology* , 22, pp. 195-209.

Lasheras, J.C., Fernandez-Pello, A.C. and Dryer, F.L., 1981, "On Disruptive Burning of Free Droplets Alcohol/n-Paraffin Solutions and Emulsions", *Eighteenth Symposium (International) on Combustion* , Combustion Institute, pp. 295-305.

Law, C.K., 1976, *Combustion and Flame* , 26, pp. 219-233.

Law, C.K., 1978a, "Internal Boiling and Superheating in Vaporizing Multicomponent

Droplets", *AIChE Journal* , 24, pp. 626-632.

Law, C.K., 1981, "On the Fire-Resistant Nature of Oil-Water Emulsion", *Fuel* , 60, pp. 998-999.

Law, C.K., 1981a, "Comments", *Eighteenth Symposium (International) on Combustion* . Combustion Institute, Pa., p. 359.

Law, C.K., 1982, "Recent Advances in Droplet Vaporization and Combustion", *Progress in Energy and Combustion Science* , 8, pp. 171-201.

Law, C.K. and Law, H.K., 1982, "D²-Law for Multicomponent Droplet Vaporization and Combustion", *AIAA Journal* , 20(4), pp.522-527.

Law, C.K. and Sirignano, W.A., 1977, "Unsteady Droplet Combustion with Droplet Heating II : Conduction Limit", 28, pp. 175-186.

Law, C.K. and Williams, F.A., 1972, "Kinetics and Convection in the Combustion of Alkane Droplets", *Combustion and Flame* , 19, pp. 393-405.

Law, C.K., Chung, H.K. and Srinivas, N., 1980, "Gas Phase Quasi-Steadiness and Vapour Accumulation Effects in Droplet Burning", *Combustion and Flame* , 38, pp. 173-198.

Law, C.K., Law, H.K. and Lee, C.H., 1979, "Combustion Characteristics of Coal Oil and Coal-Oil-Water Mixtures", *Energy* , 4, pp. 329-339.

Lee, A. and Law, C.K., 1991, "Gasification and Shell Characteristics in Slurry Droplet Burning", *Combustion and Flame* , 85, pp. 77-93.

Lorell, J., Wise, H., and Carr, R.E., 1956, "Steady State Burning of a Liquid Droplet : II Bipropellant Flame", *Journal of Chemical Physics* , 25, pp. 325-331.

Makino, A. and Law, C.K., 1988, "On the Controlling Parameter in the Gasification Behaviour of Multicomponent Fuels", *Combustion and Flame* , 73, pp. 331-336.

Margolis, S.B., 1983, "An Asymptotic Theory of Condensed Two Phase Flame Propagation", *SIAM J. Appl. Math.* , 43, pp. .

Mawid, M. and Aggarwal, S.K., 1991, "Analysis of Transient Combustion of a Multicomponent Liquid Fuel Droplet", *Combustion and Flame* , 84, pp. 197-209

- Mellor, R., Chigier, N.A. and Beer, J.M., 1970, "Pressure Jet Spray in Air Stream", *ASME* Paper 70-GT-101.
- Miller, K., and Miller, R., 1981, "Moving Finite Elements", *I, SIAM J. Numer. Anal.*, 18, pp.1019-1032.
- Miyaska, K. and Law, C.K., 1981, "Combustion of Strongly Interacting Linear Droplet Arrays", *Eighteenth Symposium (International) on Combustion*, Combustion Institute, pp. 631-645.
- Mizutani, Y. and Nakazima, A., 1973, *Combustion and Flame*, 20, pp. 343-350, 351-357.
- Mizutani, Y., Yasuma, G. and Katuski, M., 1977, "Stabilization of Spray Flames in a High Temperature Stream", *Sixteenth Symposium (International) on Combustion*, Combustion Institute, pp. 631-638.
- Natarajan, R., and Brzustowski, T.A., 1970, "Some New Observations on the Combustion of Hydrocarbon Droplets at Elevated Pressure", *Combustion Science and Technology*, 2, pp. 259-269.
- Niooka, T. and Sato, J., 1986, "Combustion and Micro-Explosion of Miscible Fuel Droplets Under High Pressure", *Twenty First Symposium (International) on Combustion*, Combustion Institute, pp. 623-631.
- Okazima, S. and Kumagai, S., 1975, "Further Investigation of Combustion of Free Droplets in a Freely Falling Chamber Including Moving Droplets", *Fifteenth Symposium (International) on Combustion*, Combustion Institute, pp. 401-407.
- Okazima, S. and Kumagai, S., 1982, *Nineteenth Symposium (International) on Combustion*, Combustion Institute, pp. 1021.
- Parks, J.M., Ablow, C.M. and Wise, H., 1966, *AIAA Journal*, 4, p. 1032.
- Penner, S.S., 1957, "Chemistry Problems in Jet Propulsion", Pergamon Press, New York.
- Pereyra, V. and Sewell, E.G., 1975, "Mesh Selection for Discrete Solution of Boundary Value Problems in Ordinary Differential Equations", *Numer. Math.*, 23, pp. 261-268.
- Peters, N. and Warnatz, J., 1982, "Numerical Methods in Laminar Flame Propagation",

Vieweg, wiesbaden.

Prakash, S. and Sirignano, W.A., 1978, "Liquid Droplet Heating with Internal Circulation", *International Journal of Heat and Mass Transfer* , 21, pp. 885-895.

Prakash, S. and Sirignano, W.A., 1980, "Theory of Convective Droplet vaporization with Unsteady Heat Transfer in the Circulating Liquid Phase", *International Journal of Heat and Mass Transfer* , 23, pp. 253-268.

Probert, R.P., 1946, "The Influence of Spray Particle Size and Distribution in the combustion of Oil Droplets", *Philosophical Magazine* , 37, pp.94-105.

Raghunandan, B.N. and Mukunda, H.S., 1977, "Problem of Liquid Droplet Combustion - A Re-examination", *Combustion and Flame* , 30, pp. 71-84

Ramachandran, S., Kleinstreuer, C. and Altwicker, E.R., 1987, "Mass Transfer to an Accelerating Multidrop System", *International Journal of heat and Mass Transfer* , 30, pp. 607-610.

Ramachandran, S., Kleinstreuer, C. and Wang, T.-Y., 1989, "Forced Convection Heat Transfer of Interacting Spheres", *Numerical Heat Transfer* , 15, pp. 471-487.

Ranz, W.E. and Marshall, Jr. W.R., 1952, "Evaporation from Drops", *Chemical Engineering* , 48, pp. 141-146 and 173-180.

Rao, V.C.V., 1992, "A Finite Element Study of Body-Fitting and Adaptive Grid Generation with Application to Flame Propagation Problems", Ph.D. Thesis submitted in Dept. of Mathematics, IIT Kanpur, India.

Ray, A.K. and Davis, E.J., 1980, "Heat and Mass Transfer with Multiple Particle Interactions Part I. Droplet Evaporation", *Chemical Engineering Communication* , 6, pp. 61-79.

Reid, R.C., Prausnitz, J.M. and Polling, P.E., 1988, "The Properties of Gases and Liquids", McGraw Hill, New York.

Reid, R.C., Prausnitz, J.M. and Sherwood, T.K., 1977, "The Properties of Gases and Liquids", McGraw Hill, New York.

Renkizbulut, M. and Haywood, R.I., 1988, "Transient Droplet Evaporation with Vari-

- able Properties and Internal Circulation at Intermediate Reynolds Number", *International Journal of Multiphase Flow* , 14, pp. 189-202.
- Renkizbulut, M. and Yuen, M.C., 1983, "Numerical Study of Droplet Evaporation in High Temperature Stream", *Journal of Heat Transfer, Transactions of ASME* , 105, pp. 389-397.
- Russel, R.D., 1979, "Mesh Selection Methods", Proc. Conference for Working Codes for Boundary Value Problems in ODE's, Childs, B. et al. , (eds), Lecture Notes in Computer Science 176, Springer-Verlag, New York.
- Ryan, W., Annamalai, K. and Carton, J., 1990, "Relation Between Group Combustion and Drop Array Studies", *Combustion and Flame* , 80, pp. 313-321
- Sadhal, S.S. and Ayyaswamy, P.S., 1983, "Flow Past a Liquid Drop with a Large Non-Uniform Radial Velocity", *Journal of Fluid Mechanics* , 133, pp.65-81.
- Samson, R., Bedeaux, D., Saxton, M.J. and Deautch, J.M., 1978, "Simple Model of Fuel Spray Burning I : Random Sprays", *Combustion and Flame* , 31, pp. 215-221
- Sangiovanni, J.J., 1978, "Model for the Nonsteady Ignition and Combustion of a Fuel Droplet", *Advances in Chemistry Series* , 166, Evaporation-Combustion of Fuels, J.T. Zung, (Editor), pp. 27-53.
- Sangiovanni, J.J. and Labowsky, M., 1982, "Burning Times of Linear Fuel Droplet Arrays; A Comparison of Experiment and Theory", *Combustion and Flame* , 47, pp. 15-30.
- Sanyal, D. and Sundararajan, T., *Int. J. Heat Mass Transfer* , V.35, No.5, pp. 1035-1048(1992).
- Shaw, B.D., 1990, "Studies of Influence of Liquid-Phase Species Diffusion on Spherically Symmetric Combustion of Miscible Binary Fuel Droplets", *Combustion and Flame* , 81, 277-288.
- Shaw, B.D. and Williams, F.A., 1990, "Theory of Influence of a Low-Volatility Soluble Impurity on Spherically Symmetric Combustion of Fuel Droplets", *Int. J. Heat Mass Transfer* , 33, No.2, pp.301-317.
- Sirignano, W.A., 1986, "The Spray Formulation of Spray Combustion Models : Resolutions

- Compared to Droplet Spacing", *Journal of Heat Transfer, Transactions of ASME* , 108, pp. 633-639.
- Shuen, J.S., 1988, "Numerical Study of the Interaction Between the Droplets at Intermediate Reynolds Number", *Journal of Propulsion and Power* , 4, pp. 481-489.
- Smooke, M.D., 1983, "An Error Estimate for the Modified Newton Method with Applications to the Solution of Nonlinear Two-Point Boundary value Problems", *J. Optim. Theory Appl.* , 39, pp. 489-511.
- Smooke, M.D., Koszykowski, M.L., 1986, " Fully Adaptive Solutions of One-Dimensional Mixed Initial-Boundary Value Problems with Applications Unstable Problems of Combustion ", *Siam J. SCI. STAT. COMPUT.*, 7, No.1, pp 301-321.
- Smooke, M.D., Mitchell, R.E. and Keyes, D.E., 1989, "Numerical Solution of Two-Dimension Axisymmetric Laminar Diffusion Flames", *Combust. Sci. and Tech.*, 67, pp 85-122.
- Spalding, D.B., 1950, *Fuel* , 29, 2,25.
- Spalding, D.B., 1953, "The Combustion of Liquid Fuels", *Fourth Symposium (International) on Combustion* , Combustion Institute, pp. 847-864.
- Spalding, D.B., 1959, "Theory of Particle Combustion at High Pressures", *ARS Journal* , 29, pp. 828-835.
- Suzuki, T. and Chiu, H.H., 1971, "Multi-Droplet Combustion of Liquid Propellants", *Nineteenth Symposium (International) on Combustion* , Combustion Institute, pp. 145-154.
- Tal, R. and Sirignano, W.A., 1982, "Cylindrical Cell Model for the Hydrodynamics of Particle Assemblages at Intermediate Reynolds Numbers", 28, pp. 233-237.
- Tal, R., Lee, D.N. and Sirignano, W.A., 1983, "Hydrodynamics and Heat Transfer in Sphere Assemblages - Cylindrical Cell Models", *International Journal of Heat and Mass Transfer* , 26, pp. 1265-1273.
- Tarifa, C.S., Perez Del Notario, P. and Moreno, F.G., 1962, *Eighteenth Symposium on Combustion* , Williams and Wilkins, Baltimore, p. 1035.
- Tishkoff, J.M., 1979, "A Model for the Effect of Droplet Interaction of Vaporization"

International Journal of Heat and Mass Transfer , 22, pp. 1407-1415.

Tong, A.Y. and Sirignano, W.A., 1982a, "Analytical Solution for Diffusion and Circulation in a Vaporizing Droplet", *Nineteenth Symposium (International) on Combustion* , Combustion Institute, pp.1007-1020

Tong, A.Y. and Sirignano, W.A., 1982b, "Transient Thermal Boundary Layer Heating of Droplets with Internal Circulation : Evaluation of assumptions", *Combustion Science and Technology* , 28, pp. 87-94.

Tong, A.Y. and Sirignano, W.A., 1983, *ASME-JSME Thermal Engineering Joint Conference* , Honolulu, Hawaii.

Tsai, J.S. and Sterling, A.M., 1990, "The Application of an Embedded Grid to the Solution of Heat and Momentum Transfer for Spheres in a Linear Array", *International Journal of Heat and Mass Transfer* , 33, pp. 2491-2502.

Umemura. A., Ogawa, S. and Okashima, N., 1981, "Analysis of the Interaction Between Two Burning Fuel Droplets with Different Sizes", *Combustion and Flame* , 43, pp. 111-119.

Vandormaal, J.P. and Raithby, G.D., 1984, "Enhancement of SIMPLEC Method for Predicting Incompressible Fluid Flow", *Numerical Heat Transfer* , 7, pp. 147-163.

Varshavskii. G.A., 1945, B.N.T.M.A.P., Moscow.

Varshavskii, G.A. and Germeier, E.M., 1967, *Combustion, Explosion and Shock Waves* , 3, p. 147.

Waldman, C.H., 1975, "Theory of Non-Steady Droplet Combustion", *Fifteenth Symposium (International) on Combustion* , Combustion Institute, pp. 429-441.

Wang, T.Y., 1989, "Approximate Analysis of interacting Spheres and Vaporizing Droplets", Ph.D. Thesis, North Carolina State University.

Wang, C.H., Liu, X.Q., and Law, C.K., 1984, "Combustion and Micro-Explosion of Freely falling Multicomponent Droplets", *Combustion and Flame* , 56, 175-197.

White, A.B., 1979, "On Selection of Equidistributing Meshes for Two-Point Boundary Value Problems", *SIAM J. Numer. Anal.* , 16, pp.472-502.

- Williams, A., 1973, "Combustion of Droplets of Liquid Fuels : A Review", *Combustion and Flame* , 21, 1-31.
- Williams, A., 1976a, "Combustion of Spray of Liquid Fuels", Elek Science, London.
- Williams, A., 1976b, "Fundamentals of Oil Combustion", *Progress in Energy and Combustion Science* , 2, pp. 167-179.
- Williams, F.A., 1960, *J. Chem. Phys.* , 33, p. 133.
- Williams, F.A., 1961, *Combustion and Flame* , 5, p. 207.
- Williams, F.A., 1965, "Combustion Theory", Addison-Wesley, Reading, MA.
- Williams, F.A., 1985, "Combustion Theory", Benjamin/Cummings Publishing Company California.
- Wise, H., Lorell, J. and Wood, B.J., 1955, "The Effects of Chemical and Physical Parameters on Burning Rate of a Liquid Droplet", *Fifth Symposium (International) on Combustion* , Combustion Institute, pp. 132-141.
- Wolfhard, H.G. and Parker, W.G., 1947, Royal Aircraft Establishment Report No. Chem.4
- Wolfhard, H.G. and Parker, W.G., 1949, *J. Inst. Pet.* , 35, p. 118.
- Zung, J.T., 1967, "The Cellular Model", *Journal of Chemical Physics* , 46, pp. 2064-2070

REFERENCES

- Agafanova, F.A., Gurevich, M.A. and Paleev, I.I., 1957, "Theory of Burning of a Liquid Fuel Drop", Soviet Physics - Tech. Physics, 2, p. 1689.
- Annamalai, K., Ramalingam, S., Dadah, T. and Chiu, D., 1988, "Group Combustion of Cylindrical Cloud of Char/Carbon Particles", Journal of Heat Transfer, Transactions of ASME, 110, pp. 190-200.
- Bellán, J. and Cuffel, R., 1983, "A Theory of Nondilute Spray Evaporation Based upon Multiple Droplet Interaction", Combustion and Flame, 51, pp. 55-67.
- Bellán, J. and Harstad, K., 1987a, "Analysis of Convective Evaporation of Nondilute Clusters of Drops", IJHMT, 30, pp. 125-136.
- Bellán, J. and Harstad, K., 1987b, "The Details of Convective Evaporation of Dense and Dilute Clusters of Drops", IJHMT, 30, pp. 1083-1093.
- Cook, D.H. and Law, C.K., 1978, "A Preliminary Study on the Utilization of Water-in-oil Emulsions in Diesel Engines", Combust. Sci. Tech., 18, pp. 217-221.
- Hayashi, S. and Kumagai, S., 1975, Fifteenth Symposium (International) on Combustion, pp. 445-452. The Combustion Institute, Pittsburgh.
- Hubbard, G., Denny, V.E. and Mills, A.F., 1975, "Droplet Evaporation: Effects of Transients and Variable Properties", IJHMT, 18, pp. 1003-1008.
- Jaiswal, A.K., 1990, "Modeling of Newtonian and Power Law Fluid Past Multi-Particle Assemblages by Finite Element Method", Ph. D. Thesis, IIT Kanpur, India.
- Lottes, S.A., 1989, "Unsteady Group Combustion", Ph.D. Thesis, University of Illinois at Chicago.
- Marberry, M., Ray, A.K. and Leung, K., 1984, "Effect of Particle Interactions of Burning Droplets", Combustion and Flame, 57, pp. 237-245.
- McCreath, C.G. and Chigier, N.A., 1973, "Liquid Spray Burning in the Wake of a Stabilizer Disk", Fourteenth Symposium (International) on Combustion, pp. 1355-1363. The Combustion Institute, Pittsburgh.
- Newbold, F.R. and Amundson, N.R., 1973, "A Model for Evaporation of a Multicomponent Droplet", AIChE J., 19, pp. 22-30.

Amachandran, S., Kleinstreuer, C. and Altwicker, E.R., 1985, "Coupled Two-phase Mass Transfer to Spherical Droplets", Canadian J. of Chemical Engg., 63, pp. 911-918.

wardus, E.M. and Brzustowski, T.A., 1977, "The Interaction Between Two Burning Fuel Droplets", Archiwum Termodynamiki i Spalania, Polish Academy of Science, 8, pp. 347-358.

Weatherford, W.D., Jr., Fodor, G.E., Naegeli, D.W., Owens, E. C., Wright, B.R. and Schaekel, F.W., 1979, "Army Fire Resident Diesel Fuel", SAE Tech. Paper Series, Paper No. 790926.

Values of Constants and Properties:

Value of universal gas constant (R_u) = 8.134 J/Mol-K.

Value of constants used in Arrhenius equation (2.76) are:

$A = 4 \times 10^{11}$; $\alpha = 0.0$; $E = 12.6 \times 10^4$ J/mol.

	heptane	decane	undecane	dodecan
Latent heat of evaporation in J/kg	$3.182_5 \times 10^5$	2.8×10^5	2.6×10^5	2.55×10^5
Density in kg/m ³	684	730	740	748
Boiling pt. in K	371	447	469	489
Molecular Wt.	100	142	156	170

For the gas phase:

Density (ρ) = 1.1614 kg/m³.

Binary diffusion coefficient (D) = 2.25×10^{-5} m²/s.

Specific heat (C_p) = 1.007×10^3 J/kg-K.

Thermal conductivity (λ) = 26.3×10^{-3} W/m-K.

For the liquid phase:

Binary diffusion coefficient (\hat{D}) = 5.0×10^{-9} m²/s.

Specific heat (\hat{C}_p) = 1.75×10^3 J/kg-K.

Thermal conductivity ($\hat{\lambda}$) = 0.1 W/m-K.

For the variable specific heat case, the data were taken from Penner (1957). Other references consulted for the property values are Reid et al. (1988) and Shaw (1990).

Date **123594**

This image shows a blank sheet of white paper with horizontal ruling lines. A single vertical line runs down the center of the page, creating two equal-width columns. The horizontal lines are evenly spaced and extend across the entire width of the paper. There is no handwriting or other markings on the page.